IECM Technical Documentation:

Pulverized Coal-Fired Power Plants and Air Pollution Controls

March 2019

IECM Technical Documentation:

Pulverized Coal-Fired Power Plants and Air Pollution Controls

---

Prepared by:

The Integrated Environmental Control Model Team
Department of Engineering and Public Policy
Carnegie Mellon University
Pittsburgh, PA 15213
www.iecm-online.com

For
U.S. Department of Energy
National Energy Technology Laboratory
P.O. Box 880

Compiled in March 2019

Contents

1. Introduction 1

2. Base Plant 2

2.1. Introduction 2
2.2. Nomenclature 2
2.3. Stream Properties and Composition 8
2.3.1. Fuel and Other Solid Streams 9
2.3.2. Air and Flue Gas Streams 12
2.3.3. Thermodynamic Data 14
2.4. Boiler Efficiency 17
2.5. Power Plant Economics 19
2.5.1. Base Plant Costs 19
2.5.2. Pollution Control Equipment Energy Penalties 20
2.5.3. Pollution Control Equipment Energy Credits 21
2.5.4. Total Pollution Control Cost 23
2.6. Key Financial Parameters 24
2.6.1. Fixed Charge Factor 24
2.6.2. Levelization Factor 27
2.6.3. Year-by-Year Revenue Requirement Analysis 27
2.6.4. Accumulated Funds Used During Construction 27
2.7. Capital Cost Models 28
2.8. Cost Data and Capital Cost Models 29
2.8.1. Regional Cost Factors 29
2.8.2. Effect of Plant Size 29
2.9. O&M Cost Models 32
2.10. A Numerical Example 33
2.10.1. Capital Costs 33
2.10.2. Fixed O&M Costs: 34
2.10.3. Variable O&M Costs: 34
2.10.4. Electricity Cost 35
2.11. Sensitivity Analysis 35
2.12. References 36

3. Retrofit Boiler NO_x Reduction 37

3.1. Introduction 37
3.1.1. NO_x Formation Types 37
3.1.2. NO_x Formation Chemistry 38
3.1.3. NO_x Emission Limits 38
3.1.4. NO_x Combustion Controls 38
3.1.5. Effects of Boiler Type 39
3.2. Low NO_x Burners 41
3.2.1. Process Overview 41
3.3. Overfire Air 43
3.3.1. Process Overview 43
3.4. Fuel Reburn 44

3.4.1. Process Overview 44
3.4.2. Process Chemistry 44
3.5. References 45

4. Selective Non-Catalytic Reduction 47

4.1. Introduction 47
4.2. Process Overview 47
4.3. Process Chemistry 49
4.3.1. Reducing Agents 49
4.3.2. Overall Reactions 50
4.4. Industry Experience with SNCR 51
4.5. SNCR Performance in Commercial Applications 52
4.6. Factors Affecting SNCR Performance 53
4.6.1. Normalized Stoichiometric Ratio (NSR) 53
4.6.2. Ammonia Slip 54
4.6.3. Flue Gas Injection Temperature 54
4.6.4. Flue Gas Residence Time 55
4.6.5. Uncontrolled NO_x Emissions 55
4.6.6. Boiler Load 55
4.6.7. Mixing of Flue Gas and Reagent 56
4.7. Modeling SNCR Performance for IECM 56
4.7.1. NO_x Reduction Under Typical Operating Conditions 57
4.7.2. Estimating NSR performance away from typical conditions 60
4.8. Mass and Energy Calculations 63
4.8.1. Urea Mass Flow 63
4.8.2. Water Flow to Boiler 63
4.8.3. Flue Gas Losses 63
4.8.4. Parasitic Power Consumption 64
4.9. SNCR Process Costs 64
4.9.1. SNCR Variable Operating Costs 64
4.9.2. SNCR Capital Costs 64
4.9.3. SNCR Fixed Operating & Maintenance Costs 67
4.10. Incorporating Uncertainty 67
4.10.1. NO_x Reduction Potential 67
4.10.2. Reagent Consumption 69
4.10.3. Uncertainties in Process Capital Costs 69
4.11. Sample Calculations 70
4.12. Conclusion 71
4.13. References 72

5. Selective Catalytic Reduction 74

5.1. Nomenclature 74
5.1.1. Performance Models 74
5.1.2. Cost Models 76
5.2. Introduction to SCR Technology 78
5.3. Process History and Development 78
5.4. Process Design 79
5.4.1. SCR Integration in the Power Plant 79
5.4.2. The SCR Process Area 81
5.5. Technical Overview 85
5.5.1. Process Chemistry 86
5.5.2. Catalyst Sizing 87
5.5.3. Catalyst Fouling and Poisoning 88
5.5.4. Catalyst Life 90

5.5.5. Catalyst Disposal 90
5.5.6. Impacts on Other Plant Components 90
5.5.7. SO_2 Oxidation 91
5.5.8. Ammonia 91
5.5.9. U.S. Outlook 93
5.6. Performance Models 93
5.6.1. Catalyst Requirement 93
5.6.2. Ammonia Requirement 101
5.6.3. SO_3 Oxidation Rate 101
5.6.4. Downstream Effects 101
5.6.5. Pressure Drop 103
5.6.6. Energy Penalties 103
5.6.7. Flue Gas Reheat for Tail-End SCR 104
5.7. SCR Capital Cost Model 106
5.7.1. Reactor Housing 106
5.7.2. Ammonia Handling and Injection 108
5.7.3. Ductwork 109
5.7.4. Air Preheater Modifications 110
5.7.5. Gas-Gas Heat Exchanger 112
5.7.6. ID Fan and Booster Fan Costs 112
5.7.7. Structural Support 113
5.7.8. Miscellaneous Other Direct Capital Costs 114
5.7.9. Total Direct Cost 114
5.7.10. Other Capital Costs 115
5.8. O&M Costs 116
5.8.1. Fixed Operating Costs 116
5.8.2. Variable Operating Costs 116
5.9. References 116

6. Air Preheater 119

7. Electrostatic Precipitator 124

7.1. Introduction 124
7.2. Background 124
7.3. ESP Performance Models 125
7.3.1. Ash Resistivity 125
7.3.2. Effective Migration Velocity 126
7.3.3. Default Ash Composition 128
7.4. ESP Cost Models 129
7.4.1. Capital Cost Models 129
7.4.2. O&M Cost Models 131
7.4.3. A Numerical Example 133
7.5. Analytica Model Code for Ash Resistivity 134
7.6. Coal and Ash Analysis 138
7.7. Regression Analysis for w_k 138
7.8. References 139

8. Fabric Filter 140

8.1. Introduction 140
8.2. Fabric Filters for Electric Utilities 140
8.3. Fabric Filter Design 140
8.4. Cost Models for Fabric Filters 142
8.4.1. Reverse Gas Systems 143
8.4.2. Pulse-Jet Systems 147

8.5. References 150

9. Flue Gas Desulfurization 152

9.1. Background to FGD Models 152
9.2. FGD Performance Models 152
9.2.1. Wet FGD Performance 153
9.2.2. Wet Limestone FGD Systems 160
9.2.3. Wet Lime FGD System 164
9.2.4. Spray Dryer Performance 165
9.2.5. Lime Spray Dryer System 170
9.3. FGD Cost Models 173
9.3.1. Capital Costs 173
9.3.2. The Methodological Approach 177
9.4. FGD Capital Cost Models 179
9.4.1. Wet Limestone with Forced Oxidation 179
9.4.2. Wet Limestone with Additives 180
9.4.3. Magnesium-Enhanced Lime System 182
9.4.4. Lime Spray Dryer 183
9.4.5. Sparing Philosophy 184
9.5. Fixed O&M Costs 185
9.6. Variable O&M Costs 186
9.6.1. Reagent Cost 186
9.6.2. Solid Waste Disposal Costs 187
9.6.3. Power Costs 187
9.6.4. Steam Costs 188
9.6.5. DBA Costs 188
9.6.6. Water Costs 189
9.7. A Numerical Example 189
9.7.1. Capital Cost 190
9.7.2. Fixed O&M Costs 191
9.7.3. Variable O&M Costs 191
9.7.4. Sparing Options 193
9.8. References 193

10. Carbon Injection 196

10.1. Background 196
10.2. Emission Control Options 196
10.3. Mercury Emission Controls 197
10.4. Evaluating Feasibility and Cost 197
10.5. The IECM Modeling Framework 198
10.5.1 Technology Performance Models 198
10.5.2 Technology Cost Models 199
10.5.3 Characterization of Uncertainties 199
10.5.4 User-Friendly Operation 199
10.6. Mercury Control Module 200
10.6.1 Performance Model 200
10.6.2 Mercury Emission Constraint 201
10.6.3 Baseline Mercury Removal 201
10.6.4 Activated Carbon Injection Model 202
10.6.5 Flue Gas Humidification Model 203
10.6.6 Illustrative Example 203
10.6.7 Uncertainty Considerations 205
10.6.8 Economic Model 206
10.6.9 Capital Cost Model 206

10.6.10 O&M Cost Model 207
10.6.11 Total Revenue Requirement 207
10.7. Conclusion 208
10.8. Acknowledgements 208
10.9. References 209

11. Region-Specific Cost Factors 210

11.1. Introduction 210
11.2. Research Method 210
11.3. Case Study 210
11.4. Reference 212

12. Appendix: Additional References 213

13. Glossary of Terms 215

List of Figures

Figure 2-2-1. Schematic Diagram of the Gaseous and Solid Streams in IECM 10

Figure 2-2-2 Air Preheater 19

Figure 3-1. Combustion and post-combustion NO_x control options (SCR = selective catalytic reduction; SNCR = selective non-catalytic combustion; FGD = flue gas desulfurization) 39

Figure 3-2. Cut-away view of a wall-fired and tangential-fired boiler. Coal input and air nozzle arrangement can be modified to enhance NO_x suppression. 40

Figure 3-3. "Staged" combustion in a low NO_x burner [DOE, 1996 #57] 41

Figure 3-4. Overfire air added to an existing low NO_x burner reduces NO_x formation to lower levels [DOE, 1996 #57]. 43

Figure 4-1. Process schematic for an SNCR system 48

Figure 4-2. Chemical kinetics simulations of variation of NO_x reduction and NH_3 slip with flue gas injection temperature. (NSR = 1.2, inlet NO_x = 0.6 lb/MBtu, O_2 = 4.5%, residence time = 0.5s) [Ciarlante, 1997 #37] 50

Figure 4-3. Variation of NH_3 slip and NO_x reduction with NSR (full load, inlet NO_x = 451 ppm) [Staudt, 1995 #54] 54

Figure 4-4. Differences in SNCR performance with SNCR design [Hunt, 1997 #48] 56

Figure 4-5. Variability of NO_x reduction estimates with boiler capacity 58

Figure 4-6. Variation of NO_x reduction with NSR for different capacity boilers. 58

Figure 4-7. Modeled typical NO_x reductions versus boiler capacity 59

Figure 4-8. Model NSR versus boiler capacity 60

Figure 4-9. Correlation between Δslip and $\overline{\text{redn}}$ 61

Figure 4-10. Correlation between NO_x reduction and NSR. 62

Figure 4-11. SNCR process capital cost estimates - low initial NO_x 65

Figure 4-12. SNCR process capital cost estimates - high initial NO_x 66

Figure 4-13. NO_x reduction estimates for low NO_x boilers 68

Figure 4-14. NO_x reduction estimates for high NO_x boilers 68

Figure 4-15. Variability of NSR at different NO_x reduction levels 69

Figure 5-1. Targeted and Actual Installed Retrofit SCR Capacity in Germany 79

Figure 5-2. Alternative Placements of SCR systems in Coal-Fired Power Plants 81

Figure 5-3. Schematic Diagram of SCR System 82

Figure 5-4. Diagram of SCR Reactor Housing with Downward Flue Gas Flow 83

Figure 5-5. Schematic Diagram of Tail-End SCR System 84

Figure 5-6. SCR Honeycomb Catalyst Monolith Designs 85

Figure 5-7. Regression Model of Space Velocity as a Function of NO_X Removal Efficiency and End-Mole Ratio 95

Figure 5-8. A typical Catalyst Activity Curve 97

Figure 5-9. An example Catalyst Activity Curve 98

Figure 5-10. Illustrative Example of Average Catalyst Activity for a Three Layer Catalyst 98

Figure 5-11. Illustrative Example of a Catalyst Addition and Replacement Scheme 99

Figure 5-12. Schematic of Gas-Gas Heat Exchanger Performance Model 105

Figure 5-13. Direct Capital Cost Model for SCR Reactor Housing 108

Figure 5-14. Direct Capital Cost Model for the Ammonia Handling and Injection System 109

Figure 5-15. Simplified Schematic of a Counter-Current Flow Heat Exchanger 111

Figure 5-16. Simplified Schematic of the Gas-Gas Heat Exchanger Employed in Cold-Side SCR Systems 113

Figure 6-1. Schematic Diagram of Air Preheater 119

Figure 9-1. Schematic Diagram of the Wet FGD Model 153

Figure 9-2. Flue Gas Specific Heat versus Exit Temperature 155

Figure 9-3. Enthalpy Difference between Saturated Steam and Saturated Water at 120°F 156

Figure 9-4. Saturation Pressure of Water versus Temperature 157

Figure 9-5. Evaporated Water versus Temperature 158

Figure 9-6. IECM performance model for Wet Limestone FGD (with Forced oxidation). Constant parameter value for this case are [SO_2]=1260 ppm, [Cl]= 32360 ppm, and [DBA]=0 ppm. 164

Figure 9-7. IECM performance model for Wet Limestone FGD (with Forced oxidation). Constant parameter value for this case are [SO_2]=1260 ppm, [Cl]= 32360 ppm, and ϕ =1.03. 164

Figure 9-8. IECM performance model for Wet Mg-Lime FGD 165

Figure 9-9. IECM performance model for Lime Spray Dryer. Constant parameter value for this case are [Cl]=0.4% wt., [ΔT]=28 F, and [SO_2]= 1260 ppm 172

Figure 9-10. IECM performance model for Lime Spray Dryer. Constant parameter value for this case are [Cl]=0.4% wt., [T]=300 F, and [SO_2]= 1260 ppm 172

Figure 9-11. IECM cost model for LSFO with ϕ = 1.03 180

Figure 9-12. IECM cost model for Wet Limestone FGD with 1500 ppm of DBA as additive 181

Figure 9-13. IECM cost model for Mg-enhanced Lime FGD with ϕ = 1.02 183

Figure 9-14. IECM cost model for Lime Spray Dryer for ϕ = 1.1 184

Figure 9-15. Fixed costs for all Wet Limestone FGD systems for 90% SO_2 removal, and default stoichiometry ϕ =1.03 186

Figure 9-16. Variable costs for all Wet Limestone FGD systems for 90% SO_2 removal, and default stoichiometry ϕ = 1.03 189

Figure 10-1. A hierarchy of models for policy analysis 197

Figure 10-2. Schematic diagram of the IECM technology types 198

Figure 10-3. Sample screens from the IECM graphical user interface 200

Figure 10-4. Mercury removal across an ESP for various operating temperatures (Eastern bituminous coal; 31% baseline mercury capture) 203

Figure 10-5. Carbon injection requirement as a function of water spray injection for the case study plant with 90% mercury removal 204

Figure 10-6. Carbon injection requirement (with humidification) as a function of coal type and control technology for 90% mercury removal 204

Figure 10-7. Uncertainty of activated carbon injection (base plant) 205

Figure 10-8. Uncertainty of activated carbon injection (base plant with retrofit SCR and FGD) 206

Figure 10-9. Deterministic results for a low-sulfur bituminous coal-fired plant (base case with retrofit technologies added). All costs in constant 1999 dollars. 208

Figure 11-1. Choose a Plant Location under Configure Session 211

Figure 11-2. Specify Allocations of PFC to Equipment and Materials under Set Parameters 211

Figure 11-3. Specify Site-Specific Cost Factors under Set Parameters 211

Figure 11-4. Display Cost Summary Under Get Results 212

List of Tables

Table 2-1. Standard Heat of Formation 15

Table 2-2. Heats of Reactions 16

Table 2-3. Constants for the Specific Heat Correlations 17

Table 2-4. Federal Tax Depreciation Schedule 26

Table 2-5. Process Areas for Base Plant 28

Table 2-6. Regional Cost Factors 29

Table 2-7. Reference Cases for PC Base Plant Costs 29

Table 2-8. Process Capital Costs for the Pittsburgh Coal (PA location) (M$ 1993) 30

Table 2-9. Scaling Exponent fi for Pittsburgh Coal 30

Table 2-10. Cost Estimates for 300 MW Plant by Coal Type (PA Location) (M$ 1993) 30

Table 2-11. Cost Estimates for Wyoming Coal (PA location) (M$ 1993) 31

Table 2-12. Scaling Exponents for Wyoming Coal 31

Table 2-13. Cost Estimates for Lignite Coal (M$ 1993) and Scaling Exponents 31

Table 2-14. Total Capital Requirement for Base Plant 31

Table 2-15. Process Area costs for Example Reference Plant (M$ 1993) 33

Table 2-16. Characteristics of U.S. Coals Used for Sensitivity Analysis 35

Table 3-1. Coal-Fired Boiler NOx Emission Limits, lb/106 Btu (1990 CAAA Title IV) 38

Table 3-2. NO_x Emissions from Coal-Fired Boilers in the U.S. 39

Table 4-1. Recent SNCR Experience on Electric Utility Boilers 51

Table 4-2. SNCR Experience on Large Capacity Boilers 52

Table 4-3. SNCR Performance of Commercial Urea-Based Systems on Coal-Fired Utility Boilers [Staudt, 1998 #55] 53

Table 4-4. SNCR NO_x Reduction Estimates 57

Table 4-5. Normalized Forms of Performance Variables 61

Table 4-6. Normalized Forms Used for Reduction - NSR Correlation 62

Table 4-7. Urea-Based SNCR Process Capital Costs 65

Table 4-8. Estimates Included in Capital Cost Model 66

Table 4-9. Sample Calculations 70

Table 7-1. Coal Resistivity 126

Table 7-2. Estimation of w_k 127

Table 7-3. Summary of Resistivity and w_k 128

Table 7-4. Default Ash Composition 128

Table 7-5. ESP Process Areas 129

Table 7-6. Experimental Design 129

Table 7-7. Capital Costs in $/kW, 1982 dollars 130

Table 7-8. Exponents for Equation (7-6) 130

Table 7-9. Total Capital Requirement 131

Table 7-10. O&M costs in 1990 $/kW-yr 132

Table 7-11. Parameters for Equation (7-9) 133

Table 7-12. Ultimate Analysis for Coals 138

Table 7-13. Ash Analysis for Coals 138

Table 8-1. Typical Fabric Filter Design Parameters 142

Table 8-2. Process Areas for Fabric Filter cost Models 142

Table 8-3. Range of Model Design Parameters 143

Table 8-4. Process Area Capital Costs Used for Scaling Parameter Estimation (1982 $/kW) 143

Table 8-5. Model Scaling Factors 144

Table 8-6. Total Capital Requirement 144

Table 8-7. Data Used for Scaling Parameter Estimation of O&M Costs ($/kW-yr) 145

Table 8-8. Design Parameters for Pulse-Jet Systems 147

Table 8-9. Exponents for Equation (8-4) 148

Table 8-10. Relative O&M costs Used for Scaling Factor Estimation (in $/kW-yr) 148

Table 9-1. Typical Values for SO_2 Removal and L/G. 162

Table 9-2. Stoichiometry and Alkalinity Approximations 162

Table 9-3. Inlet SO_2 Concentration.....163
Table 9-4. Calcium Chloride Accumulation.....163
Table 9-5. L/G for Mg-Lime.....165
Table 9-6. Reagent Stoichiometry.....171
Table 9-7. Effect of 40°F Approach Temperature to Saturation.....171
Table 9-8. Effect of 0.6% Calcium Chloride.....171
Table 9-9. Nomenclature for EPRI Cost Estimates.....173
Table 9-10. Cost Areas for Process Capital Breakdown (Source: EPRI).....174
Table 9-11. Criteria for Calculating Operating Costs.....176
Table 9-12. Description of Default Criteria used in the Model.....177
Table 9-13. PRCC Analysis for Limestone Forced Oxidation.....179
Table 9-14. Regression Coefficients for LSFO.....180
Table 9-15. PRCC analysis for Wet Limestone with Dibasic Acid.....180
Table 9-16. Regression Coefficients for Wet Limestone with DBA.....181
Table 9-17. PRCC Analysis for Mg-Lime.....182
Table 9-18. Regression Coefficients for Process Facilities Capital Cost.....182
Table 9-19. PRCC Analysis for Lime Spray Dryer.....183
Table 9-20. Regression Coefficients for Lime Spray Dryer.....184
Table 9-21. Regression Coefficients for Different Sparing Philosophies.....185
Table 9-22. Regression Coefficients for Power.....188
Table 9-23. Water Consumption for FGD Systems.....189
Table 9-24. IECM Operating Parameter Values.....190
Table 9-25. Example Calculation of Process Capital Costs (1990 $).....190
Table 9-26. Capital Cost Summary (1993 $).....191
Table 10-1. Power plant operations affecting mercury emissions.....196
Table 10-2. Summary of mercury in coal-fired power plants in 1999 (ICR data[10]).....201
Table 10-3. Baseline mercury removal for various plant configurations.....202
Table 10-4. Regression coefficients used in Equation (12) for eastern bituminous coal.....202

Table 10-5. Base case IECM input parameters used in the illustrative example 203

Table 10-6. Carbon injection system capital cost process areas 207

Table 10-7. O&M unit costs for the mercury module ($1999) 207

1. Introduction

The purpose of this contract is to develop and refine the Integrated Environmental Control Model (IECM) created and enhanced by Carnegie Mellon University (CMU) for the U.S. Department of Energy, Federal Energy Technology Center (U.S. DOE FETC) under contract Numbers DE-FG22-83PC60271 and DE-AC22-87PC79864.

In its current configuration, the IECM provides a capability to model various conventional and advanced processes for controlling air pollutant emissions from coal-fired power plants before, during, or after combustion. The principal purpose of the model is to calculate the performance, emissions, and cost of power plant configurations employing alternative environmental control methods. The model consists of various control technology modules, which may be integrated into a complete utility plant in any desired combination. In contrast to conventional deterministic models, the IECM offers the unique capability to assign probabilistic values to all model input parameters, and to obtain probabilistic outputs in the form of cumulative distribution functions indicating the likelihood of different costs and performance results.

The previous version of the IECM, implemented on a Macintosh computer and containing a number of software and model enhancements, was delivered to U.S. DOE FETC at the end of the previous contract in May 1991. The current contract continued the model development effort on the Macintosh to provide U.S. DOE FETC with improved model capabilities, including new software developments to facilitate model use and new technical capabilities for analysis of environmental control technologies and integrated environmental control systems involving pre-combustion, combustion, and post-combustion control methods. This new enhanced Macintosh version was delivered in May 1995. The most recent version of the IECM, implemented for a computer using the Windows operating system was delivered to U.S. DOE FETC at the end of the recent contract in May 1999. Although the model capabilities remained the same, the Windows environment provides a better user interface, improved performance, and stability.

Future work will consider additional technical capabilities such as boiler NO_x controls, gasifiers, and mercury control technologies. Although the current IECM model is capable of configuring a wide variety of power plant configurations, it is only capable of simulating one session at a time. Improved model capabilities being considered would expand this limitation to include (1) optimization of user-specified model parameters to meet a user-defined objective and (2) synthesis of user-specified technologies into an optimized flow sheet based on user-specified objectives. These enhancements have been effective and powerful tools with related DOE projects.

2. Base Plant

2.1. Introduction

This chapter summarizes new economic models developed for pulverized coal -fired power plants with subcritical steam cycles. The cost models described here apply to the "base power plant" without any of the environmental control options that are separately modeled in the IECM. While the purpose of the IECM is to model the cost and performance of emission control systems, costs for the base plant are also needed to properly account for pre-combustion control options that increase the cost of fuel, and affect the characteristics or performance of the base plant. Base plant costs are also needed to calculate the internal cost of electricity, which determines pollution control energy costs. Originally, a simple exponential scaling model was used in the IECM to relate the base plant cost to plant size. The new models described here provide additional parameters for estimating base plant cost variations with key emission control design parameters based on more recent cost data.

The new cost models relate the capital costs to process parameters and the costs of labor and materials. These models reflect the most recent EPRI cost estimates. The capital cost models developed have been disaggregated by process area. The main factors that affect the capital cost of the base plant are the plant size, the coal rank, and the geographic location of the plant. The capital cost models are anchored to the base capital cost for a specific unit size and are adjusted to other sizes using scaling factors based on cost data provided by EPRI (1993) for base plants of different sizes using different coal types. The variable O&M costs are calculated from the variable costs for fuel, water consumption and bottom ash disposal (from the furnace). The fixed O&M costs are based on maintenance and labor costs.

2.2. Nomenclature

English Symbols

a	Advalorem tax rate (fraction)
A_n	Annuity factor per year (fraction)
$A_{overhead}$	Overhead ash (fraction)
AC	Annual cost (M$/yr)
AFUDC	Accumulated funds used during construction (M$)
B	Rate of return for bonds in current dollars (fraction)
B_1	Booklife (years)
B_r	Rate of return for bonds in constant dollars (fraction)
Byp	Bypass (fraction)
C	Weighted cost of capital or return on investment (fraction)
C_{ash}	Carbon in collected ash (mass fraction)

C_{CO}	Carbon in fuel oxidized to carbon monoxide (fraction)
C_f	Capacity factor (fraction)
C_{idx}	Chemical Engineering Plant cost index for current year
$C_{idx,\#}$	Chemical Engineering Plant cost index for year #
c_k	Chemical cost for k^{th} level coal cleaning plant (78$/dry ton of cleaned coal)
$C_{Unburned}$	Unburned carbon (lb carbon/lb fuel)
$CC_{l,n}$	Levelized carrying charge per year (fraction)
CC_n	Carry charges per year (fraction)
$CC_{pv,n}$	Cumulative present value of carrying charges per year (fraction)
Cp	Heat capacity of fluid (Btu/°R)
Cp'	Specific heat (Btu/lb•mole °R)
$Cp_{\#,avg}$	Average heat capacity of flue gas at point # (Btu/°R)
CS	Rate of return for common stock in current dollars (fraction)
CS_r	Rate of return for common stock in constant dollars (fraction)
d	Temporary variable used in heat exchanger analysis (dimensionless)
D_b	Book depreciation per year including investment tax credit (fraction)
D_f	Fraction of capital cost financed by bonds
$D_{s,n}$	Depreciation schedule per year for tax purposes (fraction)
DC	Direct capital cost (M$)
DCC	Cost coefficient for cleaning equipment (78$/dry ton of raw coal)
dis	Nominal discount rate (fraction)
E	Weighted rate of return for preferred and common stock (fraction)
e_{boiler}	Excess air for boiler (fraction of stoichiometric air)
E_{cost}	Cost of electricity (mills/kWhr)
E_d	Energy needed for thermal drier (Btu/lb of dry coal)
E_{wetfgd}	Energy needed to reheat flue gas (Btu/hr)
e_f	Apparent escalation rate of variable and fuel costs (fraction)
e_i	Inflation rate (fraction)
e_k	Electricity cost for k^{th} level coal cleaning plant (78$/dry ton of cleaned coal)
e_{leak}	Leakage air across the air preheater (fraction of stoichiometric air)
e_r	Real escalation rate of variable and fuel costs (fraction)
EF_{NO2}	Emission factor for NO_x (lb equivalent of NO_2 per ton fuel)
ES	Emission standard (lb/million Btu into furnace)
f_k	Mass fraction of component k in fuel (fraction)
fs_i	Weight fraction of coal in stream i(fraction)
FCF	Fixed charge factor (fraction)
$h_j(T)$	Enthalpy of component j in flue gas at temperature, T (Btu/lb•mole)

Hhv	Higher heating value of fuel (Btu/lb)
Hhv_{natgas}	Higher heating value of natural gas (Btu/ft^3)
HR	Heat rate of power plant (Btu/kWhr)
HR_{cycle}	Gross cycle heat rate, includes the boiler efficiency (Btu/kWhr)
HR_{steam}	Steam cycle heat rate (Btu/kWhr)
HW_{idx}	Handy - Whitman electric utility cost index for current year
$HW_{idx,\#}$	Handy - Whitman electric utility cost index for year #
ICF	Indirect charge factor (fraction)
itc	Investment tax credit (fraction)
k	Temporary variable used in levelization factor (fraction)
L_i	Losses from category i (fraction)
LE	Latent heat of vaporization loss (Btu/lb fuel)
LHV	Lower heating value of coal (Btu/lb)
m'	Total moisture content of coal (fraction)
mi'	Inherent moisture content of coal (fraction)
ms'	Surface moisture content of coal (fraction)
$m_{\#,j}$	Pound moles of component j in gas at point # (lb•mole/lb fuel)
$\dot{m}_{\#_j}$	Molar flow rate of component j at point # (lb•mole/hr)
$\dot{M}_{\#_j}$	Mass flow rate of component j at point # (tons/hr)
MW_g	Gross electrical output of power plant (MW)
N	Years of construction (integer)
N_{NO}	Fraction of NO_x that is NO
NTU	Number of transfer units (dimensionless)
O_{comb}	Stoichiometric oxygen needed for combustion (lb•mole/lb fuel)
Ox	Oxidation of calcium sulfite to calcium sulfate (fraction)
P_{atm}	Atmospheric pressure (psia)
P_{fuel}	Price of fuel ($/ton)
P_g	Gauge pressure (inches of water)
PS	Rate of return for preferred stock in current dollars (fraction)
PS_f	Fraction of capital cost financed by preferred stock
PS_r	Rate of return for preferred stock in constant dollars (fraction)
PV_n	Present value factor per year
Q	Heat transfer (Btu/hr)
R_{H2O}	Moisture content of reagent (fraction)
R_{purity}	Purity of reagent (fraction)
RB_n	Remaining balance per year (fraction)

RD_n	Return on debt per year (fraction)
RE_n	Return on equity per year (fraction)
S_{ret}	Sulfur retained in bottom ash and fly ash streams (fraction)
S_{SO2}	Sulfur in fuel oxidized to sulfur dioxide (fraction)
SE_i	Sensible heat losses from category i (Btu/lb fuel)
t	Overall tax rate (fraction)
$t_{d,n}$	Deferred income tax per year (fraction)
t_f	Federal tax rate (fraction)
$t_{p,n}$	Taxes paid per year (fraction)
t_s	State tax rate (fraction)
$T_{\#}$	Temperature at point # (°R)
TDC	Direct capital cost (M$)
TCC	Total capital cost (M$/yr)
TCC_n	Total capital charges in a given year (current M$/yr)
TCE	Total cash expended (M$)
TPI	Total plant investment (M$)
TRR	Levelized total revenue requirement (M$/yr)
TRR_n	Total revenue requirement in a given year (current M$/yr)
TVC	Total variable cost without utilities (M$/yr)
TVC_n	Total variable cost in a given year (current M$/yr)
UA_{aph}	Overall heat transfer coefficient times the surface area for the air preheater (Btu/°R)
v_j	Volume fraction of component k (fraction)
VCLF	Levelization factor (fraction)
w_k	Water cost for k^{th} level coal cleaning plant (78$/dry ton of cleaned coal)
W	Water content (fraction)
W_{evp}	Evaporated water in scrubber (lb•mole/hr)
w'	Weight of water evaporated in thermal drier per pound of dry coal processed (fraction)
w'_e	Weight of water evaporated in thermal drier (tons/hr)
x_i	Electricity or steam consumption (fraction)
Y	Mass yield (fraction)
Y_i	Mass yield of the stream i in coal cleaning plant (fraction)
Yo_d	Ratio of coal mass exiting wash streams to coal mass exiting plant (fraction)

Greek Symbols

δ_i	Equals 0 if wash stream i is not thermally dried and 1 if it is thermally dried.
Δh	Enthalpy difference (Btu/lb•mole)
ΔT	Temperature difference (°F)
ε	Heat exchanger effectiveness (fraction)

η	Efficiency (fraction)
σ	Molar stoichiometry (fraction)
?	Specific humidity of air (mass of moisture per mass of dry air)

Subcategories for Losses

C	Losses from unburned and incomplete combustion of carbon
Gas	Sensible heat losses for dry flue gas
H_2O	Latent and sensible heat losses for moisture
R	Radiation losses
Unacc	Unaccounted losses

Subcategories for Combustion Air and Flue Gas Components

CO	Carbon monoxide
CO_2	Carbon dioxide
H_2O	Moisture
N_2	Nitrogen
NO	Nitrogen oxide
NO_2	Nitrogen dioxide
O_2	Oxygen
SO_2	Sulfur dioxide
SO_3	Sulfur trioxide

Subcategories for Fuel Components

Ash	Ash
C	Carbon
H	Hydrogen (monatomic)
H_2O	Moisture
N	Nitrogen (monatomic)
O	Oxygen (monatomic)

Subcategories for Natural Gas Components

CH_4	Methane
C_2H_6	Ethane
CO_2	Carbon dioxide
N_2	Nitrogen
O_2	Oxygen

Subcategories for Solid Stream Components

Ash	Ash
CaO	Lime
$CaCO_3$	Limestone
$CaSO_3$•.5H_2O	Hydrated calcium sulfite

$CaSO_4$	Calcium Sulfate
$CaSO_4 \cdot 2H_2O$	Hydrated calcium sulfate
H_2O	Water or Moisture
Misc	Miscellaneous

Subcategories for Stream Location

apho	Exiting air preheater on combustion air side
botash	Bottom ash stream
econo	Exiting the economizer
fdfan	Exiting forced draft fan
fg1	Located at point 1 in flue gas stream (see Figure 2-2-1)
fg2	Located at point 2 in flue gas stream (see Figure 2-2-1)
fg3	Located at point 3 in flue gas stream (see Figure 2-2-1)
fgaphi	Entering air preheater on flue gas side
fgapho	Exiting air preheater on flue gas side
fuel	Fuel stream
furn	In furnace after combustion
leak	Leakage across air preheater
stack	Entering stack
unc	"Uncorrected" flue gas temperature

Subcategories for Utility Consumption

c	Cooling system
f	Fans
misc	Miscellaneous
p	Pulverizers
sp	Steam pumps

Subcategories for Economic Variables

fuel	Fuel charges
non	Non fuel charges
util	Utility charges, i.e. steam and electricity consumption (M$/yr)
w/o cc	Without coal cleaning
w/o util	Without utility charges

Subcategories for FGD Variables

evp	Evaporated
max	Maximum
min	Minimum
reag	Reagent
rem	Removed

rh	Reheater
S	Sulfur or sulfur compound
sd	Spray dryer
sat	Saturation
sludge	Sludge exiting bottom of scrubber
SO_2	Sulfur dioxide
std	Based on emission standard
TSP	Total suspended particulates in flue gas

General Subcategories

aph	Air preheater
bp	Base power plant
c	Coal exiting the washing equipment
credit	Credit
d	Thermal drier
delta	Change between current and original
exit	Exiting device
ff	Fabric filter
in	Entering device
natgas	Natural gas
new	Current or modified
o	Final product of coal cleaning plant
orig	Original or without pollution control equipment
oil	Fuel oil
op	Overall power plant (including pollution control equipment)
out	Exiting device
p	Cleaning equipment in coal cleaning plant
pce	Pollution control equipment
ref	Refuse stream in coal cleaning plant
ROM	Run-of-mine coal
t	Overall coal cleaning plant
total	Sum or total

2.3. Stream Properties and Composition

This section describes how the IECM calculates the quantity and quality of solid and gaseous streams in fossil-fuel fired power plants. A schematic of the solid and gaseous streams for the base power plant is shown in Figure 2-2-1. These basic streams are always present in the model. As the plant is configured with pollution control equipment, additional streams are created and the equations defining the streams in Figure 2-2-1 may be modified.

The phrases in quotation marks in Figure 2-2-1 are the stream labels. They are used as variable subscripts in this documentation to show the variable location in the power plant. For example, the variable T_{fgaphi} refers the temperature of the flue gas at the air preheater inlet. The subscripts "fg1", "fg2" and "fg3" refer to locations downstream from the air preheater. Pollution control equipment is placed between these locations. For example, an ESP is placed between "fgapho" and "fg1". The variables at "fgapho" and "fg1" are respectively the inlet and outlet variables for the ESP. The equations for some variables at "fg1" are redefined to reflect the changes caused by the ESP. The following section describes in more detail the stream variables and their equations.

2.3.1. Fuel and Other Solid Streams

This section describes the fuel and other solid streams in the base power plant. The IECM tracks the following chemical compounds in most solid streams (tons per hour): final ash, lime, limestone, hydrated calcium sulfite, calcium sulfate, hydrated calcium sulfate, moisture and miscellaneous[1]. The total mass flow of any stream is the sum of these chemical compounds. For the fuel stream, the total mass flow rate is determined instead of the mass flow rates of the chemical components.

Oil or natural gas is added to coal in the IECM as boiler fuels. The model requires the following property variables for coal and oil:

Hhv	Higher heating value of the fuel (Btu/lb)
f_{Ash}	Ash content (mass fraction)
f_C	Carbon content (mass fraction)
f_H	Hydrogen content (mass fraction)
f_{H2O}	Moisture content (mass fraction)
f_N	Nitrogen content (mass fraction)
f_O	Oxygen content (mass fraction)
f_S	Sulfur content (mass fraction)

For coal and oil these variables define the ultimate analysis of the fuel. Natural gas analysis usually reports methane, ethane, carbon dioxide, nitrogen and oxygen content on a percent volume basis and the higher heating value in Btu per standard cubic foot. The standard temperature and pressure are 80°F and 30 inches of mercury respectively. Therefore, the input parameters for natural gas are:

Hhv_{natgas}	Higher heating value of the natural gas (Btu/ft$^{3)}$
v_{CH4}	Methane content (volume fraction)
v_{C2H6}	Ethane content (volume fraction)
v_{CO2}	Carbon dioxide content (volume fraction)
v_{N2}	Nitrogen content (volume fraction)
v_{O2}	Oxygen content (volume fraction)

[1] The exceptions are the fuel stream and some solid streams used by pollution control equipment. For example, a wet scrubber has a lime or limestone slurry, which only contains the reagent plus miscellaneous material.

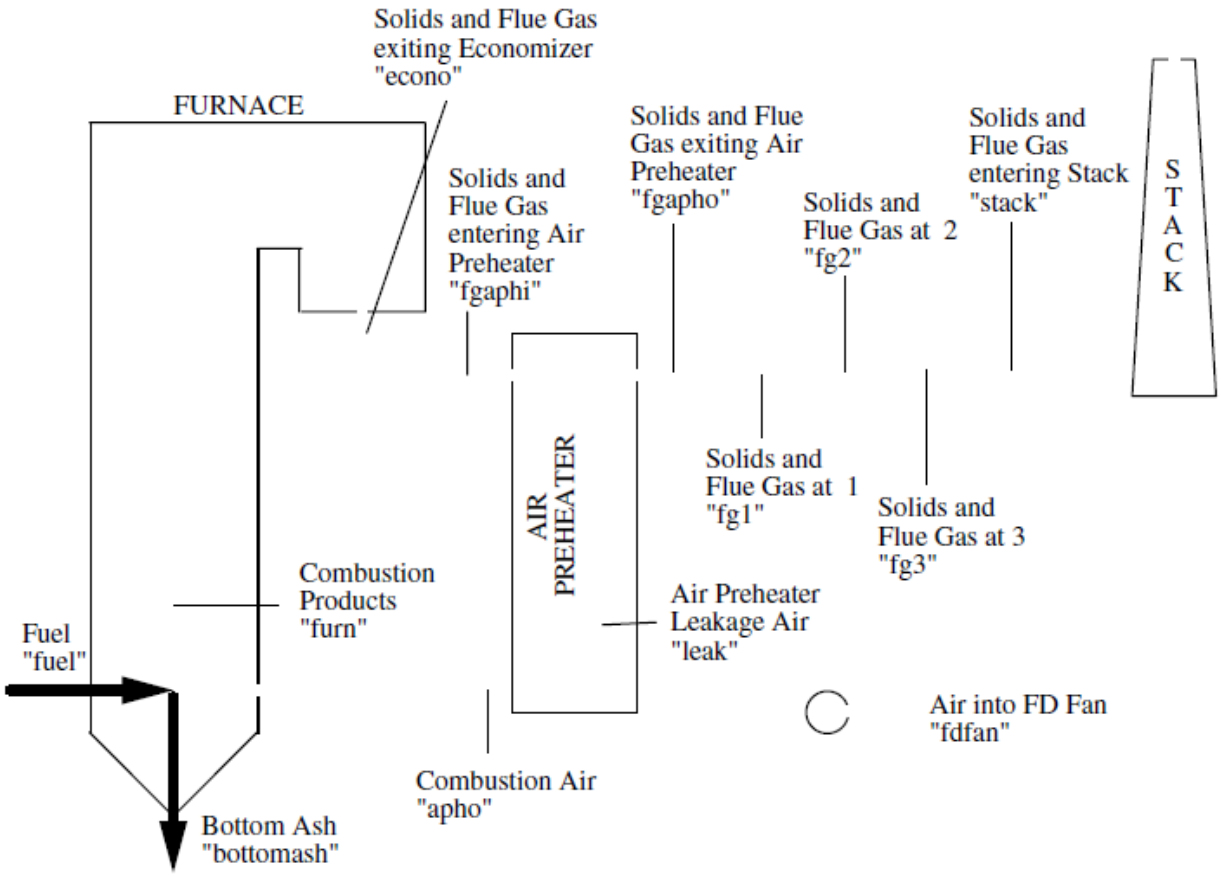

Figure 2-2-1. Schematic Diagram of the Gaseous and Solid Streams in IECM

Since the analysis of natural gas is not in elemental units, it has to be converted to the mass fraction of carbon, hydrogen, nitrogen, oxygen and sulfur. In addition, the higher value has to be converted to Btu per pound. Natural gas is assumed to behave as an ideal mixture, so volume fractions are equivalent to molar fractions. Therefore, the average molecular weight and density are estimated by[2]

$$\hat{M}_{natgas} = 16.04 v_{CH_4} + 30.07 v_{CH_4} + 44.01 v_{CO_2} + 28.01 v_{N_2} + 32.00 v_{O_2}$$

$$\rho_{natgas} = 0.04246 v_{CH_4} + 0.08029 v_{C_2H_6} + 0.1170 v_{CO_2} + 0.07439 v_{N_2} + 0.08461 v_{O_2}$$

The higher heating value on a mass basis can be determined by dividing the higher heating value on a volume basis by the density.

$$Hhv = \frac{Hhv_{natgas}}{\rho_{natgas}}$$

The mass fractions of carbon, hydrogen, nitrogen and oxygen are found by determining the mass of the individual components (i.e. carbon, hydrogen, etc.) and dividing by the average molecular weight. Since the natural gas is assumed to be free of ash, sulfur and moisture, these values are set to zero.

$$f_C = \frac{12.01 v_{CH_4} + 24.02 v_{C_2H_4} + 12.01 v_{CO_2}}{\hat{M}_{natgas}}$$

2 The values for the densities are from "Combustion: Fossil Power Systems" (3)

$$f_H = \frac{4.04v_{CH_4} + 6.06v_{C_2H_4}}{\hat{M}_{natgas}}$$

$$f_N = \frac{28.01v_{N_2}}{\hat{M}_{natgas}}$$

$$f_O = \frac{32.00v_{O_2} + 32.00v_{CO_2}}{\hat{M}_{natgas}}$$

$$f_{Ash} = f_S = f_{H_20} = 0$$

With the fuel characteristics it is possible to calculate the mass flow rates and composition of the gaseous and solid streams in the power plant. The mass flow rate of fuel must be calculated first.

The base power plant is sized to produce a specified amount of electricity, MW_g, which is the amount of electricity that the generators produce. The amount of fuel needed to produce the gross electric capacity, MW_g, depends upon the gross cycle heat rate, boiler efficiency and higher heating value of the fuel. It is determined by

$$M_{fuel} = \frac{MW_g \cdot HR_{cycle}}{2Hhv}$$

See Nomenclature for units of each variable.

where

$$HR_{cycle} = \frac{HR_{steam}}{\eta_{boiler}}$$

The gross electrical capacity, steam cycle heat rate and the higher heating value of the fuel are input parameters. The boiler efficiency is calculated and described in more detail in Section 2.4.

With the mass flow rate of fuel determined, it is now possible to determine the mass flow rates of the other solids streams in the power (e.g. the bottom ash or flyash). The solids produced by combustion are from three sources: ash in the fuel, sulfur retained in the ash and any unburned carbon. The mass from sulfur in the ash and the unburned carbon is accounted for in the variable $M_{furn,misc}$. The base power plant does not inject lime or limestone slurries into the flue gas stream. Therefore, mass flow rates of lime, limestone, calcium sulfate, hydrated calcium sulfate calcium sulfite and moisture are zero.

$$M_{furn,ash} = f_{Ash} M_{fuel}; M_{furn,Misc} = \left(f_S S_{ret} + f_C C_{Unburned}\right) M_{fuel}$$

$$M_{furn,k} = O \text{ for } k = CaO, CaCO_3, CaSO_3 \bullet O.5H_2O, CaSO_4 \bullet 2H_2O, H_2O$$

The unburned carbon is a solid entrained in the bottom ash and flyash streams. Utilities measure the fraction of carbon in their collected ash streams. This value is called the percent carbon in refuse and is used in the following formula to determine the amount of unburned carbon per pound of fuel.

$$C_{unburned} = f_{ash} \frac{C_{ash}}{1 - C_{ash}} \quad (2.1)$$

The solids produced by combustion can either exit the furnace with the flue gas or drop out the bottom of the furnace. The fraction that exists with the flue gas is the overhead ash fraction and is a function of the furnace design and coal rank. The bottom ash flow rate is determined by

$$\dot{M}_{botash,k} = \dot{M}_{furn,k}\left(1 - A_{overhead}\right) \text{ for all k}$$

The solids exiting the economizer is equal to the overhead ash fraction times the solids produced by combustion.

$$M_{econo,k} = M_{furn,k} A_{overhead} \text{ for all k}$$

For the base power plant, no pollution control equipment can change the mass flow rates of solids in the flue gas. The mass flow rates of solids at each location are the mass flow rate of solids at the previous location. When pollution control equipment is added the definitions of these variables change depending upon the specific choice of equipment.

$$M_{stack,k} = M_{fg3,k} = M_{fg2,k} = M_{fg1,k} = M_{fgapho,k} = M_{fgaphi,k} = M_{econo,k} \text{ for all k}$$

2.3.2. Air and Flue Gas Streams

This section describes the gaseous streams in the base power plant. The IECM tracks the following chemical compounds in all gaseous streams (lb•mole/lb fuel and lb•mole/hour): diatomic nitrogen, diatomic oxygen, moisture, carbon dioxide, carbon monoxide, sulfur dioxide, sulfur trioxide, nitrogen oxide and nitrogen dioxide. At every location in Figure 2-2-1, the IECM determines the gaseous stream flow rate in lb•mole/lb fuel and lb•mole/hour. The gaseous stream variables with units of lb•mole/lb fuel describe the gas stream created by the base power plant. They do not change as pollution control equipment is added. These variables are needed by different algorithms in the IECM for comparison with the base power plant[3]. The gaseous stream variables with units of lb•mole/hour describe the gas stream for the current power plant configuration.

The gas streams are assumed to act as ideal mixtures and obey the ideal gas law. Therefore, the total value of a stream property can be determined by summing the values of the property of the individual components. Since the gases obey the ideal gas law, the enthalpy is a function of temperature only. The enthalpy functions are described in more detail in Section 2.3.3. The total volumetric flow rate and enthalpy of a gaseous stream are determined by

$$\dot{V} = \frac{1545T}{144 * 60\left(P_{atm} + 0.036127P_g\right)_{j=1}} \sum_{j=1}^{9} \dot{m}_j$$

$$h(T) = \sum_{j=1}^{9} h_j(T)$$

The IECM assumes that dry air consists of 79% nitrogen and 21% oxygen. The specific humidity is an input parameter. The volumetric fraction of nitrogen, oxygen and moisture can be determined from

$$v_{N_2} = \frac{0.79}{1 - \frac{0.79 * 28.01 + 0.21 * 32.00}{18.02}\omega} = \frac{0.79}{1 + 1.601\omega}$$

$$v_{H_2O} = \frac{1.601\omega}{1 + 1.601\omega} \quad ; \quad v_{O_2} = \frac{0.21}{1 + 1.601\omega}$$

The amount of oxygen needed for stoichiometric combustion of the fuel is the sum of the oxygen needed to convert of carbon to carbon dioxide, hydrogen to water and sulfur to sulfur dioxide minus any oxygen in the fuel[4]. To minimize incomplete combustion losses, the combustion air entering the furnace is more than the stoichiometric air requirement. This additional air is called excess air and is an input parameter.

---

[3] The boiler efficiency algorithm uses the gaseous stream variables in units of lb•mole/lb fuel to prevent a cyclic dependency between the boiler efficiency and the mass flow rate of fuel.

[4] Equation corrected 2/9/2005

$$O_{comb} = \frac{f_C}{12.01} + \frac{1}{4} \times \frac{f_H}{1.01} + \frac{f_S}{32.06} - \frac{1}{2} \times \frac{f_O}{16.00}$$

$$m_{apho,N_2} = \frac{v_{N_2}(1+e_{boiler})O_{comb}}{v_{O_2}} \quad ; \quad m_{apho,H_2O} = \frac{v_{H_2O}(1+e_{boiler})O_{comb}}{v_{O_2}}$$

$$m_{apho,O_2} = (1+e_{boiler})O_{comb} \quad ; \quad m_{apho,j} = 0 \qquad \text{for j} = CO_2, CO, SO_2, SO_3, NO, NO_2$$

$$m_{apho,j} = 2000 M_{fuel} m_{apho,j}$$

The leakage air across the air preheater is based upon the stoichiometric air requirement and is an input parameter. The air entering the forced draft fans is the sum of the leakage air and the air entering the furnace.

$$m_{leak,N_2} = \frac{v_{N_2}(1+e_{leak})O_{comb}}{v_{O_2}} \quad ; \quad m_{leak,H_20} = \frac{v_{H_2O}(1+e_{leak})O_{comb}}{v_{O_2}}$$

$$m_{leak,O_2} = (1+e_{leak})O_{comb} \quad ; \quad m_{leak,j} = 0 \qquad \text{for j} = CO_2, CO, SO_2, SO_3, NO, NO_2$$

$$m_{leak,j} = 2000 M_{fuel} m_{leak,j}$$

$$m_{fdfan,j} = m_{apho,j} + m_{fdfan,j} \quad ; \quad m_{fdfan,j} = m_{apho,j} + m_{leak,j}$$

The products of combustion are determined by specifying extent of combustion for carbon, sulfur and nitrogen and an emission factor for NO_2. The carbon in the fuel can oxides to carbon monoxide or carbon dioxide or it can remain unburned. The amount of unburned carbon, $C_{Unburned}$, is determined with Equation (2.1). The amount of carbon monoxide is determined by the input parameter C_{CO}, the fraction of carbon that oxidizes to carbon monoxide. The sulfur in the fuel can oxidize to either sulfur dioxide or sulfur trioxide. It also can be captured in the ash. The amount sulfur retained in the ash is determined by the input parameter, S_{ret}. The amount of sulfur dioxide is determined by the input parameter S_{SO2}. The nitrogen in the fuel can remain unchanged or oxidize to nitrogen oxide or nitrogen dioxide. The amount of NO_x formed is controlled by the NO_2 emission factor. The units of the NO_2 emission factor for coal, oil and natural gas are pounds NO_2 per ton, pounds NO_2 per thousand gallons and pounds NO_2 per million cubic feet respectively. The NO_2 emission factor for oil is converted to pounds NO_2 per ton if the density of oil is 7.8 pounds per gallon (4). The fraction of NO_x that is nitrogen oxide is determined by the input parameter N_{NO}.

$$EF_{NO_2} = \frac{2000 EF_{oil}}{7.8*1000} = 0.2564 EF_{oil} \quad ; \quad EF_{NO_2} = \frac{2000 EF_{natgas}}{1{,}000{,}000 \rho_{natgas}} = \frac{2x10^{-3} EF_{natgas}}{\rho_{natgas}}$$

With these parameters, it is possible to find the combustion products from a molar balance of the air and the fuel entering the furnace.

$$m_{furn,N_2} = m_{apho,N_2} + \frac{f_N}{2*14.01} - \frac{EF_{NO_2}}{2*46.01*2000}$$

$$m_{furn,O_2} = M_{apho,O_2} + \frac{f_O}{2*16.00} - \frac{f_C(1-C_{unburned}-0.5C_{CO})}{12.1} - \frac{f_H}{4*1.01} - \frac{f_s(1-S_{ret})(1.5-0.5S_{SO_2})}{32.06} - \frac{EF_{NO_2}(1-0.5N_{NO})}{46.01*2000}$$

$$m_{furn,H_2O} = M_{apho,H_2O} + \frac{f_H}{2*1.01} + \frac{H_{H_2O}}{18.02}$$

$$m_{furn,CO_2} = m_{apho,CO_2} + \frac{f_C\left(1 - C_{unburned} - C_{CO}\right)}{12.01} \quad ; \quad m_{furn,CO} = m_{apho,CO} + \frac{f_C C_{CO}}{12.01}$$

$$m_{furn,SO_2} = m_{apho,SO_2} + \frac{f_S S_{SO_2}\left(1 - S_{ret}\right)}{32.06} \quad ; \quad m_{furn,SO_3} = m_{apho,SO_3} + \frac{f_S\left(1 - S_{SO_2}\right)\left(1 - S_{ret}\right)}{32.06}$$

$$m_{furn,NO} = m_{apho,NO} + \frac{EF_{NO_2} N_{NO}}{46.01 * 2000} \quad ; \quad m_{furn,NO_2} = m_{apho,NO_2} + \frac{EF_{NO_2}\left(1 - N_{NO}\right)}{46.01 * 2000}$$

$$m_{furn,j} = 2000 M_{fuel} m_{furn,j}$$

The flue gas flow rate remains the same until it exits the air preheater in the base power plant. At the air preheater, the leakage air is added to the flue gas. Pollution control equipment do not alter the flue gas flow rates after the air preheater in the base power plant. The molar flow rates of the gases at each location are defined to be the molar flow rate of the gases at the previous location. When pollution control equipment is added, the definitions of these variables will change depending upon the specific pollution control equipment added.

$$m_{fgaphi,j} = m_{econo,j} = m_{furn,j} \quad ; \quad m_{fgaphi,j} = m_{econo,j} = m_{furn,j}$$

$$m_{fgapho,j} = m_{fgaphi,j} = m_{leak,j} \quad ; \quad m_{fgapho,j} = m_{fgaphi,j} = m_{leak,j}$$

$$m_{stack,j} = m_{fg3,j} = m_{fg2,j} = m_{fg1,j} = m_{fgapho,j}$$

$$m_{stack,j} = m_{fg3,j} = m_{fg2,j} = m_{fg1,j} = m_{fgapho,j}$$

2.3.3. Thermodynamic Data

This section documents the thermodynamic data used in the IECM. This data includes the heats of reaction for chemical processes occurring in the copper oxide, NOXSO and sulfuric acid plant systems. All the data except the enthalpy for the alumina substrate is from Barin and Knacke (5) or Barin, Knacke and Kubaschewski (6). This data is from the SMC report (7). All the enthalpies are set to zero at 77°F and are assumed to be at a constant pressure. The heats of reaction and formation are calculated at this temperature. Although most data are shown to four significant digits, at least six significant digits were used to calculate the heats of reaction.[5] Table 2-1 shows the heats of formation for 18 species.

Table 2-2 shows the heats of reaction for 21 chemical reactions.

The enthalpy data for all the compounds is obtained by integrating polynomial correlations for the specific heat at constant pressure between 77°F and the specified temperature. The correlations are in cal/(g-mole °K), except the alumina substrate, and must be converted to Btu/(lb•mole °R). The polynomial correlations are shown below. The values of the constants for all the species are shown in Table 2-3.

$$Cp = A + Be^{-3}T + \frac{Ce^5}{T^2} + De^{-6}T^2 \qquad (2.2)$$

The correlation for the alumina substrate in J/(g-mole °K) is

$$Cp_{AL_2O_3} = Ae^2 + Be^{-3}T + \frac{Ce^2}{\sqrt{T}} + \frac{De^6}{T^2}$$

Integrating Equation (2.2) with respect to temperature and choosing 298.15°K as a reference temperature gives

5 All the original data are in metric units and had to be converted to English units.

$$h(T) = \int_{298.15}^{T_k} \left(A + Be^{-3}T + \frac{Ce^5}{T^2} + De^{-6}T^2 \right) dT$$

$$h(T_k) = AT_k + \frac{Be^{-3}T_k^2}{2} - \frac{Ce^5}{T_k} + \frac{De^{-6}T_k^2}{3} - \left(A298.15 + \frac{Be^{-3}298.15^2}{2} - \frac{Ce^5}{298.15} + \frac{De^{-6}298.15^3}{3} \right) \quad (2.3)$$

Next, evaluate Equation (2.3) and substitute H_{298} for the sum of the terms evaluate at 298.15°K. Converting this from cal/g-mole to Btu/lb•mole by multiplying by 1.8 gives

$$h(T_k) = 1.8AT_k + \frac{1.8Be^{-3}T_k^2}{2} - \frac{1.8Ce^5}{T_k} - \frac{1.8De^{-6}T_k^3}{3} - 1.8H_{298.15}$$

Yet the input temperature is still in degrees Kelvin and it is desirable to the temperature in degrees Rankine. Substituting $T_K = T_R/1.8$ gives

$$h(T_R) = \frac{1.8AT_R}{1.8} + \frac{1.8Be^{-3}T_R^2}{2*1.8^2} - \frac{1.8^2Ce^5}{T_R} - \frac{1.8De^{-6}T_R^3}{3*1.8^3} - 1.8H_{298.15}$$

Simplifying $h(T_R)$ yields

$$h(T_R) = AT_R + \frac{Be^{-3}T_R^2}{3.6} - \frac{3.24Ce^5}{T_R} - \frac{De^{-6}T_R^3}{9.72} - 1.8H_{298.15} \quad (2.4)$$

Equation (2.4) is used as a function for all the species except the alumina substrate, since its units are Btu/lb and the correlation for the specific heat has a different form. The final form of the enthalpy equation for the alumina substrate is

$$h_{AL_2O_3}(T_R) = 0.23901\left(Ae^2T_R + \frac{Be^3T_R}{3.6} + Ce^2\sqrt{7.2T_R} - \frac{3.24De^6}{T_R} - 1.8H_{298.15} \right)/102$$

The constant 0.23901 converts joules to calories. 102 is the molecular weight.

Table 2-1. Standard Heat of Formation

Species	H_o (77°F) Btu/lb•mole
CH_4	-32,180
CO	-47,560
CO_2	-169,300
COS	-61,020
Cu	0
CuO	-67,050
$CuSO_4$	-331,300
H_2	0
H_2O	-104,000
H_2S	-8820
N_2	0
NH_3	-19,760

NO	38,840
NO_2	14,240
O_2	0
S_2	55,350
SO_2	-127,700
SO_3	-170,300

Table 2-2. Heats of Reactions

Reaction	?H (77°F) Btu/lb•mole
$CH_4 + O_2 = CO_2 + 2H_2O$	-345,200
$CO + 0.5O_2 = CO_2$	-121,700
$COS + 1.5O_2 = CO_2 + SO_2$	-236,000
$COS + 1.85O_2 = CO_2 + 0.3SO_2 + 0.7SO_3$	-265,800
$Cu + 0.5O_2 = CuO$	-67,050
$CuO + 0.25CH_4 = Cu + 0.25CO_2 + 0.5H_2O$	-19,240
$CuO + CO = Cu + CO_2$	-54,680
$CuO + H_2 = Cu + H_2O$	-36,980
$CuO + SO_2 + 0.5O_2 = CuSO_4$	-136,500
$CuO + SO_3 = CuSO_4$	-93,940
$CuSO_4 + 0.5CH_4 = Cu + SO_2 + 0.5CO_2 + H_2O$	30,980
$CuSO_4 + 2CO = Cu + SO_2 + 2CO_2$	-39,910
$CuSO_4 + 2H_2 = Cu + SO_2 + 2H_2O$	-4500
$H_2 + 0.5O_2 = H_2O$	-104,000
$H_2S + 1.5O_2 = H_2O + SO_2$	-222,900
$H_2S + 1.85O_2 = H_2O + 0.3SO_2 + 0.7SO_3$	-261,500
$NO + NH_3 + 0.25O_2 = N_2 + 1.5H_2O$	-175,100
$NO_2 + 2NH_3 + 0.5O_2 = 1.5N_2 + 3H_2O$	-286,800
$S_2 + 2O_2 = 2SO_2$	-255,400
$S_2 + 2.7O_2 = 0.3*2*SO_2 + 0.7*2*SO_3$	-315,000
$SO_2 + 0.5O_2 = SO_3$	-42,570

Table 2-3. Constants for the Specific Heat Correlations

Species	A	B	C	D	H_0 Cal/g-mole	Temp. Range °K
CH_4	2.975	18.329	0.346	-4.303	1,547.6	298 – 2000
CO	6.790	0.980	-0.110	-	2,104.9	298 – 2500
CO_2	10.550	2.160	-2.040	-	3,925.7	298 – 2500
COS	11.330	2.180	-1.830	-	4,088.7	298 – 1800
Cu (s)	5.940	0.905	-0.332	-	1,922.6	298 – 1357
CuO (s)	10.476	4.007	-1.406	-	3,773.1	298 – 1359
$CuSO_4$ (s)	17.545	36.532	-2.942	-17.110	7,690.4	298 – 1078
H_2	6.520	0.780	0.120	-	1,938.4	298 – 3000
H_2O	7.170	2.560	0.080	-	2,224.7	298 – 2500
H_2S	7.020	3.680	-	-	2,256.6	298 – 1800
N_2	6.660	1.020	-	-	2,031.0	298 – 2500
NH_3	6.165	7.558	0.084	-	2,145.9	298 – 800
	12.601	2.500	-15.231	-	7,590.5[6]	800 – 2000
NO	6.616	1.778	-0.036	-0.342	2,060.6	298 – 3000
NO_2	8.529	5.475	-1.124	-1.514	3,149.9	298 – 1500
	12.848	0.305	-	-	5,440.5[7]	1500 -3000
O_2	7.160	1.000	-0.400	-	2,313.4	298 – 3000
S_2	8.720	0.160	-0.900	-	2,908.8	298 – 2000
SO_2	10.380	2.540	-1.420	-	3,684,0	298 – 1800
SO_3	13.658	6.536	-3.086	-1.847	4,972.4	298 – 2000
Al_2O_3 (s)[8]	1.534	1.968	-9.006	-2.031	20,804	298 – 1800

Note: all species are assumed to be gaseous, except where noted.

2.4. Boiler Efficiency

This section describes the algorithm used to calculate the boiler efficiency. The boiler efficiency is determined for a power plant without any pollution control equipment. This fixes the amount of fuel entering the furnace. Any changes in the energy efficiency of the boiler caused by pollution control equipment are considered by the energy credit algorithm. The air preheater is described in more detail in the next section. Yet, it is necessary to understand that the air preheater is divided into an ideal heat exchanger (i.e., no leakage) followed by a section where air leaks into the flue gas (see Figure 2-2-2). The uncorrected air preheater temperature, $T_{unc,orig}$, is the flue gas temperature after the heat exchanger.

The boiler efficiency in the IECM is based on the algorithm in "Steam/ Its Generation and Use", by Babcock and Wilcox (8) and "Combustion, Fossil Power Systems", by Combustion Engineering, Inc (9). The boiler efficiency is the energy absorbed by the steam cycle divided by the energy in the fuel. The energy that is not absorbed by the steam cycle is lost to the environment. These losses can be categorized into five areas:

6 Value of enthalpy at 800°K.

7 Value of enthalpy at 1,500°K.

8 Units of correlations J/(g-mole °K)

- sensible heat loss of the dry flue gas
- sensible and latent heat loss from water vapor
- unburned carbon and carbon monoxide
- radiation loss
- unaccounted losses

Therefore, the boiler efficiency is

$$\eta_{boiler} = 1 - L_{Gas} - L_{H_2O} - L_C - L_R - L_{Unacc}$$

The sensible heat loss of the dry flue gas is the energy that could be used if the dry flue gas were cooled to the inlet air temperature of the air preheater, $T_{fdfan,orig}$. The inlet fuel temperature is assumed to be the same as the combustion air. This energy loss in Btu per pound of fuel can be defined as

$$SE_{Gas} = \sum_{j=1}^{8} m_{fgap\ hi,j,orig} \left(h_j\left(T_{unc,orig}\right) - h_j\left(T_{fdfan,orig}\right) \right)$$

where j equals all the flue gas components except H_2O

This energy loss can be expressed as a fraction of the fuel's energy content by dividing it by the higher heating value.

$$L_{Gas} = \frac{SE_{Gas}}{Hhv}$$

The heat loss due to water vapor in the flue gas can be split into the latent heat of vaporization and the sensible heat loss. The latent heat loss is the energy that could be used if the water vapor in the flue gas was condensed. Every pound of water vapor that is condensed releases 1,040 Btu of energy. The water vapor in the flue gas is produced by the vaporization of moisture in the fuel and the combustion of hydrogen in the fuel. The latent heat loss can be calculated as follows:

$$LE = \left(f_{H_2O} + \frac{18.02 f_H}{2 * 1.01} \right) 1{,}040$$

The sensible heat loss due to water vapor is the energy that could be used if the water vapor could be cooled to the inlet air temperature, $T_{fdfan,orig}$. This energy loss can be calculated as follows:

$$SE_{H_2O} = M_{fgaphi,H_2O,orig} \left(h_{H_2O}\left(T_{unc,orig}\right) - h_{H_2O}\left(T_{fdfan,orig}\right) \right)$$

The total loss from moisture expressed as a fraction is the sum of the latent heat and sensible heat losses divided by the higher heating value of the fuel.

$$L_{H_2O} = \frac{\left(LE + SE_{H_2O}\right)}{Hhv}$$

Since the fuel's higher heating value is based on the complete oxidation of carbon to carbon dioxide, the boiler efficiency has to account for energy loss from unburned carbon and carbon monoxide. Pure carbon has a higher heating value of 14,100 Btu/lb. The energy lost per pound of unburned carbon is 14,100 Btu. For every pound of carbon converted to carbon monoxide, 9755 Btu of energy are lost. The total energy loss due to unburned carbon and carbon monoxide is

$$L_C = \left(12.01 * 9{,}755 m_{fgaphi,co} + 14{,}100 C_{unburned}\right) / Hhv$$

The loss from radiation exchange with the surroundings is estimated based on Figure 27 in reference (8) and Figure 6-5 in reference (9). Modern utility boilers usually have four water cooled walls and range in output from 800 to 6,000

million Btu per hour. Therefore, this curve was fitted to the following equation between 800 and 6,000 million Btu per hour:

$$LR = 0.0015 + \frac{6000}{MW_g HR_{steam}}$$

There are other minor losses that are not determined in this algorithm. An example of one of these losses is the sensible heat loss from the ash exiting the boiler. These losses and other miscellaneous tolerance errors are entered as an input parameter in L_{Unacc}.

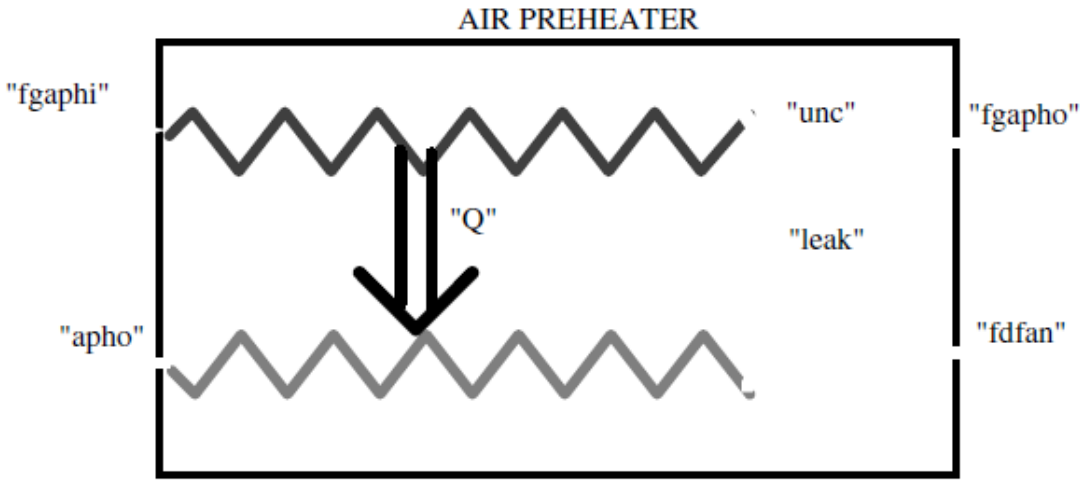

Figure 2-2-2 Air Preheater

2.5. Power Plant Economics

This section describes the economics of the base (original) power plant. Subsequent sections then describe how the pollution control equipment affects the economics of the base plant. The following section will describe how the economics changes when pollution control equipment is added. For purposes of cost estimate and internal consistency, the IECM effectively considers the power plant and pollution control equipment to be separate entities. The base power plant essentially consumes fuel and produces electricity and flue gas, while the pollution control equipment consumes some electricity and removes the pollutants from the flue gas.

2.5.1. Base Plant Costs

The base power plant uses electricity and steam for running pulverizers, steam cycle pumps, flue gas fans, cooling system and miscellaneous other equipment. These components represent internal utility (auxiliary power) consumption that reduces the amount of electricity that the power plant can sell to customers (including the pollution control equipment). The auxiliary power consumption reduces the electricity available for sale and increases the heat rate.

$$MW_{bp} = MW_g \left(1 - x_p - x_{sp} - x_f - x_c - x_{misc}\right)$$

$$HRbp = \frac{HRcycle}{1 - x_p - x_{sp} - x_f - x_c - x_{misc}}$$

The capital and operating cost of a power plant is based on the algorithms presented in Molberg (11). The direct and total capital costs are estimated as follows:

$$TDC_{bp} = 600\left(\frac{MW_{bp}}{1{,}000{,}000}\right)^{0.85} \frac{HW_{idx}}{HW_{idx,1988}}$$

$$TCC_{bp} = TDC_{bp}(1 + ICF)$$

The operating cost is divided into two categories: fuel cost and non-fuel cost. The non-fuel expenses include labor, maintenance, overhead, taxes, etc. The fuel cost depends on the fuel consumption and cost of fuel, while the non-fuel cost is proportional to the size of the power plant.

$$AC_{fuel} = 8766 x 10^{-6} C_f m_{fuel} P_{fuel}$$

$$AC_{non} = 8766 x 10^{-6} C_f 4.35 MW_{bp} \frac{C_{idx}}{C_{idx,1988}}$$

$$AC_{bp} = AC_{fuel} + AC_{non}$$

The total revenue requirement excluding any income from "selling" electricity to the pollution control equipment can be calculated by annualizing the total capital cost and levelizing the total operating and maintenance costs. The model does not explicitly charge the power plant for its own utility consumption. The main reason is that any charge to the power plant is collected by the power plant, so the net effect is zero. The price of electricity, E_{cost}, charged to the pollution control equipment can be set to any value by the model user (as is typically done in most economic analyses). However, the default is to use the marginal electricity cost based on the total revenue requirement of the base plant without utilities:

$$TRR_{w/o\,util,bp} = TCC_{bp} FCF + AC_{bp} VCLF \quad (2.5)$$

$$E_{cost} = \frac{TRR_{w/o\,util,bp} x 10^6}{8766 C_f MW_{bp}} \quad (2.6)$$

where 8766 is the average number of hours in a year (including leap years).

2.5.2. Pollution Control Equipment Energy Penalties

This section gives a brief overview of the economics of pollution control equipment and describes in detail how the pollution control equipment affects the economics of the base power plant. This section assumes that the pollution control equipment is a consumer of energy. The next section describes the effects when pollution control equipment *contributes* energy (e.g. from exothermic chemical reactions). How the capital and operating costs of specific pollution control equipment are determined is described in other chapters and is not covered in this section. Once the total capital and operating costs are determined for a specific pollution control equipment the total revenue requirement can be calculated.

$$TRR_{w/o\,util,pce,j} = TCC_{pce,j} FCF + AC_{pce,j} VCLF$$

However, this does not reflect the cost of electricity and steam consumption charged to the pollution control equipment by the power plant. The utility cost is the equivalent electricity consumption times the cost of electricity. Given the utility cost, the total revenue requirement can be determined. This total revenue requirement can be expressed in mills per kilowatt hour by divided it by the net electric capacity of the power plant.

$$AC_{util,pce,j} = 8766 C_f MW_{bp} x_{pce,j} E_{cost}$$

$$TRR_{pce,j} = TRR_{w/o\,util,pce,j} + AC_{util,pce,j}$$

$$E_{pce,j} = \frac{TRR_{pce,j} x10^6}{8766 C_f MW_{net}}$$

The electricity consumption of the pollution control equipment reduces the amount of electricity available for sale to external customers. Therefore, the net electric capacity is the gross capacity minus the internal consumption, including all pollution control equipment:

$$MW_{net} = MW_g \left(1 - x_p - x_{sp} - x_f - x_c - x_{misc} - \sum_{j=1}^{n} x_{pce,j} \right)$$

Since the pollution control equipment "pays" the base power plant for electricity consumption, these charges are income for the base power plant. The pollution control equipment utility costs appear as negative charges (i.e. income) in the base power plant utility cost. This procedure is a bookkeeping operation to change pollution control equipment for utility use:

$$AC_{util,bp} = -\sum_{j=1}^{n} AC_{util,pce,j}$$

The total revenue requirement including utility cost for the power plant can be calculated as the sum of the total revenue requirement without utilities plus the utility cost for the base power plant. The total revenue requirement can be divided by the net capacity to determine the cost of electricity including utility costs of the base power plant, E_{bp}. This cost of electricity, E_{bp}, will equal the price of electricity charged to the pollution control equipment, E_{cost}, if the price charged to the pollution control equipment is equal to the value determined by Equation (2.6).

$$TRR_{bp} = TRR_{w/o\ util,bp} + AC_{util,bp} \quad (2.7)$$

$$E_{bp} = \frac{TRR_{bp} x10^6}{8766 C_f MW_{net}} \quad (2.8)$$

2.5.3. Pollution Control Equipment Energy Credits

This section describes the changes in economics when pollution control equipment contributes energy that can be converted to electricity (as is true of an exothermic process that increases the potential heat input to the boiler). There are a variety of ways to treat this case. For the IECM, the pollution control equipment is assumed to sell the energy back to the power plant, that converts the additional energy into electricity for sale. Therefore, the revenue generated from the sale of energy to the power plant shows up as a credit in the operating costs for the pollution control equipment and a debit in the fuel cost of the power plant.

The power plant is considered to have two choices for treating this energy. Either it can reduce the amount of purchased fuel while the gross amount of electricity remains constant or it can "build" additional equipment to convert this energy into additional electricity (i.e., increase the gross plant size). The first choice requires an iterative solution since the energy generated by the pollution control equipment is a function of the fuel consumption of the power plant.[9] Because of the complexities of the IECM, it is not possible to solve this iterative problem explicitly.

[9] The energy generated by the pollution control equipment is based on the fuel flow rate into the power plant and the characteristics of the specific pollution control equipment. So, reducing the fuel flow rate into the power plant, changes the energy generated by the pollution control equipment, which changes the fuel flow rate. To accurately solve this problem requires an interactive solution, since it is not possible to *a priori* determine the appropriate fuel flow rate and energy from the pollution control equipment to produce a specific amount of electricity.

Instead, the IECM assumes the power plant builds additional equipment to convert the additional energy into electricity. Since the IECM models new power plants, the additional equipment is "built" simultaneously with the base power plant, yet is accounted separately in the economics. This approach allows a simpler solution. Or, the user simply can neglect the change in size since it is generally small and does not change the economics substantially. The additional equipment has capital and non-fuel operating costs, that are charged to the base power plant.

The equivalent electric capacity of this energy is needed to determine the charges and debits for energy generated by pollution control equipment. If the additional energy is in the form of heat captured by the air preheater, it is treated the same as the energy from coal. The additional energy is divided by the original heat rate. If the additional energy is in the form of steam, it is treated the same as energy in the steam cycle, so the additional energy is divided by the original heat rate times the boiler efficiency. With the equivalent electric capacity, the electric capacity of the power plant with and without pollution control equipment also can be determined.

$$MW_{credit} = \frac{Q_{aph,delta}}{HR_{orig}} + \frac{Q_{steam}}{\eta_{boiler} HR_{orig}}$$

$$MW_{bp,new} = MW_g \left(1 - x_p - x_{sp} - x_f - x_c - x_{misc}\right) + MW_{credit}$$

$$MW_{net} = MW_g \left(1 - x_p - x_{sp} - x_f - x_c - x_{misc} - \sum_{j=1}^{n} x_{pce,j}\right) + MW_{credit}$$

Multiplying the electric capacity by the heat rate and dividing by the higher heating value of the fuel gives the equivalent fuel consumption. The equivalent fuel consumption is multiplied by the cost of fuel to determine the revenue from the sale of the energy to the power plant. This revenue is credited to the operating cost of the pollution control equipment that generated the energy.

$$m_{fuel,credit} = \frac{MW_{credit} HR_{bp}}{2Hhv}$$

$$AC_{fuel,credit} = 8766 x 10^{-6} C_f M_{fuel,credit} P_{fuel}$$

$$AC_{pce,j} = AC_{w/o\ credit,pce,j} + AC_{fuel,credit}$$

Several base plant economic variables must be modified to account for the energy credit. The direct capital cost for the additional equipment is estimated to be proportional to the direct capital cost of the original power plant. Therefore, the direct capital cost is determined by

$$TDC_{bp} = 600 \left(1 + \frac{MW_{credit}}{MW_{bp}}\right) \left(\frac{MW_{bp}}{1{,}000{,}000}\right)^{0.85} \frac{HW_{idx}}{HW_{idx,1988}}$$

The non-fuel operating and maintenance costs are estimated to be proportional to the non-fuel operating and maintenance cost of the original power plant. The total operating cost for the base plant is

$$AC_{non} = 8766 x 10^{-6} C_f \, 4.35 \left(MW_{bp} + MW_{credit}\right) \frac{C_{idx}}{C_{idx,1988}}$$

$$AC_{bp} = AC_{fuel} + AC_{non} + AC_{fuel,credit}$$

The equations for the total revenue requirement, (2.7) and (2.5) and the cost of electricity of the base power plant, (2.8), do not change, but the equation for the default price of electricity charged to pollution control equipment, (2.6), does change:

$$E_{cost} = \frac{TRR_{w/o\ util,bp} x10^{6}}{8766 C_f MW_{bp,new}}$$

2.5.4. Total Pollution Control Cost

The total capital, operating, utility and revenue requirements for pollution control excluding coal cleaning can be determined by summing the values the pollution control equipment:

$$TCC_{total,pce} = \sum_{j=1}^{n} TCC_{pce,j} \quad ; \quad AC_{total,pce} = \sum_{j=1}^{n} AC_{pce,j}$$

$$TRR_{w/o\ util,total,pce} = \sum_{j=1}^{n} TRR_{w/o\ util,pce,j} \quad ; \quad AC_{util,total,pce} = \sum_{j=1}^{n} AC_{util,pce,j}$$

$$TRR_{total,pce} = \sum_{j=1}^{n} TRR_{pce,j} \quad ; \quad E_{total,pce} = \sum_{j=1}^{n} E_{pce,j}$$

The total capital, operating, utility and revenue requirements of the power plant are the sum of the base power plant and the total pollution control equipment.

$TCC_{total} = TCC_{bp} + TCC_{bptotal,pce}$

$AC_{total} = AC_{bp} + AC_{total,pce}$

$TRR_{w/o\ util,total} = TCC_{w/o\ util,bp} + TCC_{w/o\ util,total,pce}$

$AC_{util,total} = AC_{util,bp} + AC_{util,total,pce}$

$TRR_{total} = TCC_{bp} + TCC_{total,pce}$

$EC_{total} = EC_{bp} + EC_{total,pce}$

The total cost for pollution control including coal cleaning has to be determined by examining two identical power plant. One power plant uses cleaned coal, while the other does not. The total pollution control costs are calculated by subtracting the base plant costs for the plant that is not using cleaned coal from the total plant costs for the plant that is using cleaned coal. This procedure is necessary since the coal cleaning plant is assumed to be separate from the power plant. The capital and operating costs of the coal cleaning plant are added to the cost of raw coal, so delivered cost of coal to the power plant increases.

$TCC_{total,pce} = TCC_{total} - TCC_{bp,w/o\ cc}$

$AC_{total,pce} = AC_{total} - AC_{bp,w/o\ cc}$

$TRR_{w/o\ util,total,pce} = TCC_{w/o\ util,total} - TCC_{w/o\ util,bp,w/o\ cc}$

$AC_{util,total,pce} = AC_{util,total} - AC_{util,bp,w/o\ cc}$

$TRR_{total,pce} = TCC_{total} - TCC_{bp,w/o\ cc}$

$EC_{total,pce} = EC_{total} - EC_{bp,w/o\ cc}$

2.6. Key Financial Parameters

2.6.1. Fixed Charge Factor

The fixed charge factor is used to convert the future carrying charges of the plant investment into a uniform series of payments over the plant life. It is calculated based on the revenue requirement methodology presented in the EPRI Technical Assessment Guide (12, 13).

Revenue requirements consist of two main components, carrying charges (fixed charges) and expenses (operating costs). Carrying charges are related to the capital investment and are incurred despite how the plant is used. They consist of return on investment, book depreciation, income taxes, local property taxes and insurance. Expenses are related to the operation and maintenance of the plant and generally used within one year and generally consist of fuel, operating and maintenance costs.

Book depreciation is the annual charge to repay the original investment. A straight-line method is used in the IECM and it is assumed that the salvage value is equal to the cost of retiring the plant. The current tax laws allow for an investment tax credit. This credit is an immediate reduction in the income taxes for the year that the plant goes into services. The investment tax credit is normalized as opposed to "flow through" (these terms are explained later). Therefore, the book depreciation calculation is

$$D_b = \frac{1 - itc}{B_1}$$

Money to cover the total capital investment comes from the sale of bonds (known as debt financing) and the sale of common and preferred stock (equity financing). The ratio of debt financing to equity financing is generally around 50%. The return on debt and equity is the money a utility must pay to its investors for using their money. The weighted average of the return on debt and equity is often called the "return on investment", "cost of money" or the "weighted cost of capital". This return is based on the undepreciated investment or the remaining balance on the initial investment, that will be defined later in Equation (2.15). The annual rate of return on debt and equity is related to the inflation rate. The IECM assumes that the real rate of return or the return in the absence of inflation remains constant. Therefore, the rates of return are input parameters expressed in constant dollars and the nominal or current rates of returns are calculated with Equations (2.9), (2.10), (2.11). The weighted cost equity is shown in Equation (2.12), while the weighted cost of capital is shown in Equation (2.13).

$$B = (1 + e_i)(1 + B_r) - 1 \qquad (2.9)$$

$$CS = (1 + e_i)(1 + CS_r) - 1 \qquad (2.10)$$

$$PS = (1 + e_i)(1 + PS_r) - 1 \qquad (2.11)$$

$$B = \frac{PS\,PS_f + CS(1 - PS_f - D_f)}{1 - D_f} \qquad (2.12)$$

$$C = B\,D_f + E\,(1 - D_f) \qquad (2.13)$$

Income taxes are based on company profit within a given year. The profit is equal to the total revenue minus all the deductible expenditures. Income taxes consist of state and federal taxes, with state taxes being deductible for federal tax purposes. Therefore, the effective total tax rate is.

$$t = t_s + (1 - t_s)\,t_f$$

Federal tax laws also allow for an accelerated cost recovery or depreciation. This accelerated depreciation schedule, $D_{s,n}$ used for tax purposes is a 200% declining balance method over 15 years and is shown in

Table 2-4. It allows for a shorter recovery time and a greater deduction in the early years that the straight-line depreciation schedule.

Table 2-4. Federal Tax Depreciation Schedule

Year	Depreciation %	Year	Depreciation%
1	7.5	16	4.4
2	6.9	17	4.4
3	6.4	18	4.4
4	5.9	19	4.4
5	5.5	20	4.4
6	5.1	21	0
7	4.7	22	0
8	4.5	23	0
9	4.5	24	0
10	4.5	25	0
11	4.5	26	0
12	4.5	26	0
13	4.5	28	0
14	4.5	29	0
15	4.5	30	0

Deferred income tax is the difference between income tax actually paid and the income tax that would have been paid if a straight-line tax recovery schedule had been used, Equation (2.14). There are two methods of handling deferred taxes: "flow through" and "normalization". The flow through method pass the tax deferrals immediately to the rate payers or to the stockholders. The normalized method, which the IECM uses, accumulates the deferred taxes in a reserve account to pay for new investment items. The utility collects revenue as if a straight-line recovery schedule was used. The utility then has use of the funds until the tax obligation has to be paid in the later years of the booklife. The deferred income taxes and the investment tax credit are called tax preferences.

$$t_{d,n} = (D_{s,n} - 1/B_1)\, t \text{ for } n = 1, B_1 \qquad (2.14)$$

As mentioned earlier, the return on investment was based on the remaining balance. The remaining balance per year is the initial investment minus the book depreciation, deferred income tax per year and investment tax credit in the first year, Equation (2.15). The returns on debt and equity per year are shown in Equation (2.16) and (2.17). The taxes paid per year are shown in Equation (2.18). The year by year carrying charges is just the sum of the book depreciation, deferred taxes, return on debt, return on equity, income taxes paid and the advalorem tax, Equation (2.19).

$$RB_n = RB_{n-1} - D_b - t_{d,n-1} \qquad (2.15)$$

$$RD_n = RB_n\, D_f\, B \qquad (2.16)$$

$$RE_n = RB_n\, (1 - D_f)\, E \qquad (2.17)$$

$$t_{p,n} = \frac{t}{1-t}\left(D_b - D_{s,n} + t_{d,n} + RE_n\right) \qquad (2.18)$$

$$CC_n = D_b + t_{d,n} + RD_n + RE_n + t_{p,n} + a \text{ for } n = 1, B_1 \qquad (2.19)$$

$$RB_1 = 1 - itc$$

The discount rate used for present value calculations is related to the weighted cost of capital. The most common method used in the utility industry is a "before tax discount rate" that is equal to the weighted cost of capital. Some industries use an "after tax discount rate" that is equal to the weighted cost of capital less the tax rate times the return on debt. The IECM uses a "before tax discount rate", Equation (2.20). The present value factor of a future expense in a given year is given by Equation (2.21). It is assumed for present value calculations that all expenses are paid at the end of year. The annuity factor shown in Equation (2.22), calculates the present value of a uniform series of payments in the future, while the reciprocal of the annuity factor calculates an equivalent uniform annual amount for a single payment.

$$dis = C \tag{2.20}$$

$$PV_n = (1 + dis)^n \tag{2.21}$$

$$A_n = \frac{1 - PV_n}{dis} \tag{2.22}$$

The present value of future carrying charges is the sum of carrying charges times the present value factor, Equation (2.23). The levelized carrying charge converts the actual carrying charges that vary from year to year into a uniform payment for the tax life of the plant. The levelized carrying charge per year is just the cumulative present value of the carrying charge divided by the annuity, Equation (2.24). The levelized carrying charge for the last year of the book life is the fixed charge factor, Equation (2.25).

$$CC_{pv,n} = \sum_{m=1}^{n} CC_m PV_m \tag{2.23}$$

$$CC_{1,n} = \frac{CC_{pv,n}}{A_n} \tag{2.24}$$

$$FCF = CC_{1,B1} \tag{2.25}$$

2.6.2. Levelization Factor

The levelization algorithm is used to convert a series of future payments that have a uniform escalation rate into a uniform series of payments over the same period. The IECM assumes that the real escalation rate for expenses is constant, so the apparent escalation rate is calculated from Equation (2.26). The levelization factor is calculated with Equation (2.27). The total revenue requirement is calculated in Equation (2.28).

$$e_f = (1 + e_r)(1 + e_i) - 1 \tag{2.26}$$

$$L_n = \frac{k\left(1 - k^n\right)}{A_{B_1}(1 - k)} \quad \text{where } k = \frac{1 + e_f}{1 + dis} \tag{2.27}$$

$$TRR = TCC\ FCF + TVC\ L_{B1} \tag{2.28}$$

2.6.3. Year-by-Year Revenue Requirement Analysis

A year-by-year revenue requirement analysis is also available in the IECM. This method has the advantage of showing the revenue requirement in current dollars over the entire tax life. The total revenue requirement in a future year is the sum of the carrying charges and the operating expenses.

$$TCC_n = TCC\ CC$$

$$TVC_n = TVC\ (1 + e_f)^n$$

$$TRR_n = TCC_n + TVC_n$$

2.6.4. Accumulated Funds Used During Construction

The accumulated funds used during construction, AFUDC, or interest during construction is determined from the total plant cost, TPC. It is assumed that the equipment begins service at the beginning of January and that the construction takes place during the preceding years. Also the IECM determines the total plant cost in the same year dollars that the equipment begins services. The actual cashed expended for construction is assumed to be spent uniformly at the middle of each year during construction. Therefore, the total cash expended, TCE, in mixed year dollars, is found by de-escalating the total plant cost back in time.

$$\mathrm{TCE} = \frac{\mathrm{TPC}}{\mathrm{N}} \sum_{\mathrm{j}=1}^{\mathrm{N}} \frac{1}{(1+\mathrm{i})\mathrm{j}^{-0.5}}$$

After the money is spent, interest charges are accumulated as part of the AFUDC at a discount rate, dis. The discount rate is determined from Equation (2.20). Therefore, the total plant investment, TPI, is

$$\mathrm{TPE} = \frac{\mathrm{TPC}}{\mathrm{N}} \sum_{\mathrm{j}=\mathrm{i}}^{\mathrm{N}} \frac{(1+\mathrm{dis})^{\mathrm{j}-0.5}}{(1+\mathrm{i})^{\mathrm{j}-0.5}} = \frac{\mathrm{TPC}}{\mathrm{N}} \sum_{\mathrm{j}=1}^{\mathrm{N}} \left(\frac{1+\mathrm{dis}}{1+\mathrm{i}}\right)^{\mathrm{j}-0.5}$$

The AFUDC is the difference between the total plant investment and the total cash expended.

AFUDC = TPI - TCE

2.7. Capital Cost Models

The three main factors that affect the capital cost of a base plant are its capacity, in MW, (also referred to as size), the coal type, and the location of the plant. The capacity of the plant determines the size of the (boiler) furnace and hence the capital cost. For a given capacity, the heating value and the ash content of the coal influence the dimensions of the furnace and ash handling equipment, also affecting capital cost.

The mathematical model used to describe the sensitivity of the capital cost models to parameter variations is normalized against the cost for a reference base case. The effect of coal type is treated discretely using coal rank (bituminous, sub-bituminous, or lignite) as another cost-related parameter. The cost models for each coal rank are disaggregated by process area and are parameterized to scale with size for each coal type. Table 2-5 provides a description of the process areas for the base power plants.

Table 2-5. Process Areas for Base Plant

Process Area	Description
10	Steam Generator
20	Turbine Island
30	Coal Handling
40	Ash Handling
50	Water Treatment
60	Auxiliaries

The general form of the capital cost model *for a given coal type* is shown below:

$$\frac{PC_i}{PC_i^{/}} = \left(\frac{MW}{MW^{/}}\right)^{f_i} \qquad (2\text{-}1)$$

where

i process area

PC_i process area capital (M$)

$PC_i^{/}$ reference base case process area capital (M$)

MW plant size (MW)

$MW^{/}$ reference case plant size

f_i scaling exponent, dependent on coal rank.

The cost models presented below provide the value for the scaling exponent, f_i, for each coal type.

2.8. Cost Data and Capital Cost Models

The cost data used for model development is based on a cost study conducted by EPRI (1993) that evaluated the capital costs of pulverized coal (PC) fired power plants using supercritical and subcritical steam cycles. Since most commercial U.S. plants employ subcritical steam cycles, this chapter has excluded the study of supercritical and other advanced steam cycle designs. The EPRI data have also been adjusted to remove the cost elements for systems or equipment that are modeled separately in the IECM, such as flue gas desulfurization systems.

The first subsection provides a brief discussion of the regional factors used for normalization when comparing costs of plants at different locations. The second subsection provides the derived cost models for the IECM showing the effect of varying unit size and coal type on the cost of PC plants with subcritical steam cycles.

2.8.1. Regional Cost Factors

The location of a plant influences a number of cost parameters such as the labor wage rates, labor productivity, bulk material costs, and uniform building codes which differ across states. Regional factors from the EPRI TAG manual (1993) have been used to provide aggregate factors for six different regions of the U.S. These are shown in Table 2-6.

Table 2-6. Regional Cost Factors

EPRI Region (Reference Location)	Factor
Northeast (PA)	1.0
Southeast (GA)	0.87
E/W Central (WI)	0.97
West Central (MO)	1.03
South Central (TX)	0.84
West (UT)	0.92

Note: The Northeast location (PA) is treated as the reference case.

In order to compare the effect of unit size or coal type on plant cost, cost estimates need to be normalized to a common reference. In the following sections, all cost numbers are presented normalized to the Northeast reference. To get costs for any other location, the cost estimates presented in this chapter should be multiplied by the appropriate regional factor.

2.8.2. Effect of Plant Size

Two coal types were considered for the EPRI base case studies to examine the effect of plant size — a bituminous Pittsburgh seam coal and a sub-bituminous Wyoming coal from the Powder River Basin. An overview of the base case studies is shown in Table 2-7.

Note that all costs in this chapter are in 1993 dollars. The costs for the 600 MW case are based on two 300 MW units.

Table 2-7. Reference Cases for PC Base Plant Costs

Case Name	Size (MW, net)	State Location	Coal Name
B1	200	PA	Pittsburgh
B2	300	PA	Pittsburgh
B3	400	PA	Pittsburgh
B4	500	PA	Pittsburgh
B5	600	PA	Pittsburgh

B6	200	WI	Wyoming
B7	300	TX	Wyoming
B8	500	WI	Wyoming
B9	600	WI	Wyoming

The process capital cost estimates (EPRI 1993) for each coal type are presented separately. We first present the cost data and evaluate the scaling exponent for Pittsburgh coal and then for Wyoming coal. Cost studies for size sensitivity of lignite coals were not available, thus, the scaling components used for lignite are the values derived for sub-bituminous coals.

The cost estimates for Pittsburgh coal disaggregated by process area are shown in Table 2-8. Note that M$ denotes millions of 1993 dollars.

Table 2-8. Process Capital Costs for the Pittsburgh Coal (PA location) (M$ 1993)

Case Name (MW)	Area 10	Area 20	Area 30	Area 40	Area 50	Area 60
B1 (200)	80.81	60.51	29.86	10.17	6.036	22.1
B2 (300)	112.6	82.97	39.81	12.04	7.646	30.31
B3 (400)	143.3	104.4	49.07	13.61	9.084	38.15
B4 (500)	172.9	124.9	57.73	14.97	10.38	45.61
B5 (600)	208.3	153.5	66.95	20.25	12.86	56.07

The 300 MW plant (case B2) is used as the reference base plant and the cost for other sizes is scaled against these process area base costs. The scaling exponents are derived by solving Equation (2-1) for f_i , for each of the cases shown in Table 2-7. The scaling exponents derived from the sensitivity studies are shown in Table 2-9.

Table 2-9. Scaling Exponent fi for Pittsburgh Coal

Size (MW)	Area 10	Area 20	Area 30	Area 40	Area 50	Area 60
200	0.8174	0.7785	0.709	0.4159	0.5831	0.7785
400	0.84	0.8	0.727	0.4265	0.5992	0.8
500	0.84	0.8	0.7277	0.4269	0.5993	0.8
Average (< 500)	0.82	0.79	0.72	0.42	0.59	0.79
> 600	0.8875	0.8875	0.75	0.75	0.75	0.8875

Notice that the average value for the scaling component is computed only over the 200-500 MW range. The 600 MW plant consists of two units of 300 MW each, so the scaling component for sizes 600 and greater is treated separately. Since sensitivity studies for other bituminous coals are not available, *these scaling factors are used for all bituminous coals*. Note however, that the actual base cost (M$) for a 300 MW plant varies slightly for each bituminous coal type as shown in Table 2-10.

Table 2-10. Cost Estimates for 300 MW Plant by Coal Type (PA Location) (M$ 1993)

	Pgh	Ill# 6	KY	Utah	WV
Area 10	112.6	115.1	105.3	113.6	111.7
Area 20	82.97	81.37	74.21	82.65	81.37
Area 30	39.81	45.91	39.28	43.79	39.58
Area 40	12.04	15.55	13.24	14.43	11.91
Area 50	7.646	7.58	7.239	7.482	7.579

Area 60	30.31	30.04	28.73	29.66	30.04

The cost data for Wyoming sub-bituminous coal is presented next with similar scaling exponents derived for the cost model. The cost data disaggregated by process area is presented in Table 2-11. Note that since the plants corresponding to these cases are in different regions of the U.S., the cost numbers have been normalized to an equivalent plant in PA (the reference location) using the regional location factors shown earlier in Table 2-5.

Table 2-11. Cost Estimates for Wyoming Coal (PA location) (M$ 1993)

Size	Area 10	Area 20	Area 30	Area 40	Area 50	Area 60
200	87.28	59.34	43.74	11.07	5.957	21.91
300	114.5	74.73	56.35	12.66	7.326	29.04
500	186.7	122.4	84.56	16.29	10.25	45.21
600	224.9	150.5	98.06	22.03	12.69	55.58

Since the cost data for the 200, 500 and 600 MW size plants are for the same location (see Table 2-6) we use the 200 MW size plant (instead of the location-adjusted 300 MW plant) as the reference case. The scaling exponents for the Wyoming sub-bituminous coal are provided in Table 2-12.

Table 2-12. Scaling Exponents for Wyoming Coal

Size	Area 10	Area 20	Area 30	Area 40	Area 50	Area 60
300	0.6686	0.5685	0.6249	0.3319	0.5104	0.6944
500	0.83	0.7905	0.7194	0.422	0.5923	0.7905
Average (< 500)	0.75	0.67	0.67	0.37	0.56	0.74
600	0.8616	0.8473	0.7349	0.6267	0.6885	0.8473

Once again, the average value for the scaling component is computed only over the 200-500 MW range. The 600 MW plant consists of two units of 300 MW, so the scaling component for sizes 600 MW and greater is treated separately. *These scaling factors are used for all sub-bituminous coals.*

Cost estimates for different unit sizes for lignite coals were not provided in the EPRI study, therefore, it was not possible to calculate the scaling exponents for lignite coals. Instead, the scaling exponents derived for sub-bituminous coals were used for lignite coals (lignite boilers are more similar to sub-bituminous than to bituminous units). Table 2-13 provides the capital cost estimates for a 300 MW base plant (i.e., assumed to be located in PA) using Texas lignite. The scaling factors for each process area, based on Table 2-12, are also provided.

Table 2-13. Cost Estimates for Lignite Coal (M$ 1993) and Scaling Exponents

Size	Area 10	Area 20	Area 30	Area 40	Area 50	Area 60
300	131.1	74.73	73.22	23.53	7.32	29.04
Average (< 500)	0.75	0.67	0.67	0.37	0.56	0.74

The total capital requirement for a PC base plant is calculated as shown in Table 2-14. This includes the direct process capital costs and indirect costs associated with base power plants.

Table 2-14. Total Capital Requirement for Base Plant

Component	Cost
Process Area Capital	
Steam Generator	PC_{10}
Turbine Island	PC_{20}

Coal Handling	PC_{30}
Ash Handling	PC_{40}
Water Treatment	PC_{50}
Auxiliaries	PC_{60}
Total Process Capital	$PC=PC_{10}+PC_{20}+PC_{30}+PC_{40}+PC_{50}+PC_{60}$
General Facilities*	0.10 PC
Eng. & Home Office Fees*	0.064 PC
Process Contingency*	0.003 PC
Project Contingency*	0.1167 PC
Total Plant Cost*	TPC=1.284 PC
Total Plant Investment (including AFUDC)*	TPI=1.103 TPC‡
Preproduction Cost*	0.02 TPI
Inventory Capital*	0.00034 TPI
Royalty*	0.00045 TPI
Total Capital Requirement*	TCR=1.00279 TPI
* These items show the model default values for indirect cost factors. The IECM allows these factors to be changed by the user. ‡ Based on a 4.1% cost escalation, 9.2% interest rate and 5 years construction.	

2.9. O&M Cost Models

The O&M costs for the base power plant consists of fixed costs and variable costs. The fixed operating cost consists of labor, maintenance labor, material, and administrative labor. A mathematical model for the fixed cost is provided by Equation (2-2).

$$\begin{aligned} FOM &= FOM_{labor} + FOM_{maint} + FOM_{admin} \\ FOM_{labor} &= labor \times N_{labor} \times 40 \text{ (hrs/week)} \times 52 \text{ (weeks/yr)} \\ FOM_{maint} &= 0.02 \times C_{10} + 0.013 \times C_{20} + 0.026 \times C_{30} \\ &\quad + 0.046 \times C_{40} + 0.013 \times C_{50} + 0.013 \times C_{60} \\ FOM_{admin} &= 0.07 \times (FOM_{labor} + FOM_{maint}) \end{aligned} \qquad (2\text{-}2)$$

where,

FOM = fixed operating and maintenance cost, M$/yr

FOM_{labor} = operating labor, M$/yr

FOM_{maint} = maintenance material costs, M$/yr (coefficients based on EPRI TAG). 35% of these costs are allocated to maintenance labor and the rest to maintenance material.

FOM_{admin} = administrative costs (assumed to be 7% of total labor costs) M$/yr.

C_i = total plant cost for process area i based on default values in Table 2-13. This gives Ci = 1.284 PCi, i = (10,20,30,40, 50,60)

N = total number of laborers (at 40 hrs/week), (default 60)

labor = labor rate ($/hr), (default 23.4)

The variable costs include the fuel cost, water costs (used for the steam cycle), and bottom ash disposal cost. The fuel cost is based on the rate of coal use which, in turn, depends on the size of the plant. The ash disposal cost is proportional to the bottom ash generated. The variable operating and maintenance cost is given by:

$$\begin{aligned} VOM &= VOM_{coal} + VOM_{water} + VOM_{ash} \\ VOM_{coal} &= C_{coal} \times M_{coal} \times H_{yr} \\ VOM_{water} &= C_{water} \times M_{water} \times MW_{yr} \\ VOM_{ash} &= C_{ash} \times M_{ash} \times H_{yr} \end{aligned} \qquad (2\text{-}3)$$

Where

H_{yr}	=	cf x 8760[10], operating hours per year
MW_{yr}	=	H_{yr} x MW, MW operating hours per year
cf	=	capacity factor, fraction
VOM	=	variable operating costs, M$/yr
VOM_{coal}	=	fuel (coal) costs, M$/yr
VOM_{water}	=	water consumption costs, M$/yr
VOM_{ash}	=	ash disposal costs, M$/yr
M_{coal}	=	coal consumption, tons/hr
M_{water}	=	water consumption, gallons/MWh (default = 1000)
M_{ash}	=	bottom ash disposed, tons/hr
C_{coal}	=	as-delivered coal cost, $/ton
C_{ash}	=	bottom ash disposal cost, $/ton, (default 10.24)
C_{water}	=	water cost, $/gallon, (default = 0.7 per 1000 gallons)

2.10. A Numerical Example

The capital and O&M costs of a PC power plant of size 450 MW (net) operating at a 65% capacity factor using Illinois #6 bituminous coal have been estimated. The location of the plant is assumed to be in Kenosha, WI. The reference 300 MW base case cost for Illinois coal disaggregated by process area for the reference location of PA is provided in row 1 (from Table 2-6). The cost of locating in WI is shown in row 2 of Table 2-15 and is derived by multiplying the process area cost for the 300 MW base case by the scaling factor, 0.97, found in Table 2-5.

Table 2-15. Process Area costs for Example Reference Plant (M$ 1993)

	Area 10	Area 20	Area 30	Area 40	Area 50	Area 60
300 (PA)	115.1	81.37	45.91	15.55	7.58	30.4
300 (WI)	111.7	78.93	44.54	15.08	7.35	29.14

2.10.1. Capital Costs

The scaleup in capital costs due to an increase in size from 300 MW to 450 MW would be calculated using the following template from Equation (2-1).

$$PC_i = PC_i^{/} \times \left(\frac{MW}{MW^{/}} \right)^{f_i}$$

For each process area, the base case process capital $PC_i^{/}$ for a 300 MW plant is shown in row 2 of Table 2-15 above. The scaling exponent for each process area is provided in Table 2-8 row 4 (bituminous coals). The process capital cost for each process area for a 450 MW plant would be calculates as shown:

[10] 8760 is the total number of hours in a year (24x365)

$$\text{Total Process Capital (PC)} = \sum \text{PC}_i = 391.49 \text{ M\$}$$

$$\text{General Facilities (GFC)} = 0.10 \times 391.49 = 39.15 \text{ M\$}$$

$$\text{Eng. \& Home Office (EHO)} = 0.064 \times 391.49 = 25.06 \text{ M\$}$$

$$\text{Process Contingency } (C_{proc}) = 0.003 \times 391.49 = 1.17 \text{ M\$}$$

$$\text{Project Contingency } (C_{proj}) = 0.1167 \times 391.49 = 45.69 \text{ M\$}$$

$$\text{Total Plant Cost (TPC)} = \sum \left(\text{PC} + \text{GFC} + \text{EHO} + C_{proc} + C_{proj}\right) = 502.56 \text{ M\$}$$

$$\text{Total Plant Investment (TPI)} = 1.03 \times 502.56 = 554.32 \text{ M\$}$$

$$\text{Preproduction Costs} = 0.02 \times \text{TPI} = 11.09 \text{ M\$}$$

$$\text{Inventory Capital} = 0.00034 \times \text{TPI} = 0.19 \text{ M\$}$$

$$\text{Royalty} = 0.00045 \times \text{TPI} = 0.25 \text{ M\$}$$

$$\text{Total Capital Requirement} = 565.85 \text{ M\$} = 1256 \text{ \$/kW}$$

2.10.2. Fixed O&M Costs:

The fixed O&M costs are calculated using Equation (2-2). The formulae from Equation (2-2) reproduced here with appropriate numeric values. Text is provided in brackets next to each number to explain the source of these numbers. Note that the total plant cost for each process area (denoted by C_i) is calculated as $C_i = 1.284\ PC_i$.

$$\begin{aligned}
\text{FOM}_{labor} &= \text{labor } (23.4 \text{ \$/hr}) \times N_{labor} \text{ (60 laborers)} \\
&\quad \times 40 \text{ (hrs/week)} \times 52 \text{ (weeks/yr)} \\
&= 2.92 \text{ M\$/yr} \\
\text{FOM}_{maint} &= 0.02 \times 199.9\ (C_{10}) + 0.013 \times 139.6\ (C_{20}) \\
&\quad + 0.026 \times 76.6\ (C_{30}) + 0.046 \times 22.96\ (C_{40}) \\
&\quad + 0.013 \times 11.99\ (C_{50}) + 0.013 \times 51.5\ (C_{60}) \\
&= 9.69 \text{ M\$/yr} \\
\text{FOM}_{admin} &= 0.07 \times (2.92\ (\text{FOM}_{labor}) + 9.689\ (\text{FOM}_{maint})) = 0.88 \text{ M\$/yr} \\
\text{FOM} &= 2.92\ (\text{FOM}_{labor}) + 9.69\ (\text{FOM}_{maint}) + 0.88\ (\text{FOM}_{admin}) \\
&= 13.49 \text{ M\$/yr}
\end{aligned}$$

2.10.3. Variable O&M Costs:

The variable O&M costs are calculated using Equation (2-3). The formulae from Equation (2-3) reproduced here with appropriate numeric values. Text is provided in brackets next to each number to explain the source of these numbers. Some of the variables such as coal consumption and bottom ash disposed are calculated using the IECM and provided as inputs to the model presented here. This is denoted by (IECM) in brackets.

$$VOM_{coal} = 35.75\{C_{coal}\ \$/\text{ton}\} \times 219.3\{M_{coal}\ \text{ton/hr}\}$$
$$\times 5694\{H_{yr}\ \text{IECM}\}$$
$$= 44.68\ \text{M\$/yr}$$

$$\text{VOM}_{\text{water}} = 7 \times 10^{-4}\{C_{water}\ \$/\text{gallon}\} \times 10^{3}\{M_{water}\ \text{gallon/Mwh}\}$$
$$\times 450 \times 5694\{MW_{yr}\ \text{IECM}\}$$
$$= 1.79\ \text{M\$/yr}$$

$$\text{VOM}_{\text{ash}} = 9.36\{C_{ash}\ \$/\text{ton}\} \times 8.83\{M_{ash}\ \text{tons/hr}\}$$
$$\times 5694\{H_{yr}\ \text{IECM}\}$$
$$= 0.47\ \text{M\$/yr}$$

$$VOM = 44.68\{VOM_{coal}\} + 1.79\{\text{VOM}_{\text{water}}\} + 0.47\{\text{VOM}_{\text{ash}}\}$$

2.10.4. Electricity Cost

The cost of electricity is calculated by levelizing the total capital requirement (TCR) and the total (fixed + variable) O&M costs on a per kWh basis. This done by using a fixed charge factor (fcf) for levelizing the TCR by assuming a 30-year life cycle of a power plant, and an O&M levelization factor (vclf). The algorithms for calculating these levelization factors are incorporated in IECM and the numbers used for the example here are based on the IECM. The calculation for cost of electricity is shown below:

$$\text{E}_{\text{cost}}\ (\text{mills/kWh}) = (\text{fcf} \times \text{TCR} + \text{vclf} \times \text{O \& M})/\text{MW}_{\text{yr}}$$
$$= (0.0877 \times 391.5 + 1.0 \times 60.4) \times 10^{6}/(450 \times 0.65 \times 8760)$$
$$\approx 44\ \text{mills/kWh}$$

2.11. Sensitivity Analysis

The base plant cost models have been parametrized by cost and coal rank. The models can be applied to examine the effects of coal rank on total capital requirement (normalized in $/kW) for six U.S. coals (Table 2-16) and total levelized electricity cost (in mills/kWh) for a base plant with no environmental controls.

Table 2-16. Characteristics of U.S. Coals Used for Sensitivity Analysis

	App.MS	App.LS	Ill#6	WPCU	WPRB	NDL
HHV (Btu/lb)	13260	13080	10900	11240	8340	6020
Carbon (%)	73.81	73.87	61.22	64.20	48.18	35.04
Hydrogen (%)	4.88	4.75	4.20	4.60	3.31	2.68
Oxygen (%)	5.41	6.27	6.02	5.80	11.87	11.31
Chlorine (%)	0.07	0.06	0.17	0.01	0.01	0.09
Sulfur (%)	2.13	0.66	3.25	0.58	0.37	1.16
Nitrogen (%)	1.42	1.46	1.16	1.16	0.70	0.77
Ash (%)	7.23	10.08	11.00	11.00	5.32	15.92

Moisture (%)	5.05	5.79	13.00	7.54	30.24	33.03
Cost ($/ton)	32.07	36.94	29.49	27.18	12.46	12.22

2.12. References

Electric Power Research Institute (1993). Cost Studies for Pulverized Coal-Fired Power Plants. Data provided by Dr. C. McGowin.

Electric Power Research Institute (1993). TAG Technical Assessment Guide, Vol. 1: Electricity Supply - (Revision 7)

3. Retrofit Boiler NO_x Reduction

3.1. Introduction

This chapter discusses boiler combustion modifications to reduce NO_x emissions from a fossil-fuel power plant. These technologies are designed to reduce emissions of oxides of nitrogen (NO and NO_2, collectively referred to as NO_x) from existing or new coal-fired utility boilers. Although modifications can also be made to oil and natural gas utility boilers, they are not directly considered here.

NO_x control is accomplished by two different methods, namely combustion controls and post-combustion controls. Combustion controls are considered in this chapter and focus particularly on modern low-NO_x burners (LNB), overfire air (OFA), and natural gas reburn. These technologies are considered separately and in combination with each other. Separate performance and economics are presented as a function of various boiler types: wall fired, tangentially fired, and cyclone fired.

3.1.1. NO_x Formation Types

NO_x is formed during combustion as a result of the interaction of chemical and physical processes in the furnace. A large majority of the NO_x formed during the combustion process is the result of two oxidation mechanisms:

1. Thermal NO_x – reaction of nitrogen in the combustion air with excess oxygen. This occurs particularly in the high-temperature, post-flame region of the combustion process.
2. Fuel NO_x – reaction of nitrogen that is chemically bound in the coal. This process is believed to occur very quickly.

In addition, minor amounts of NO_x are formed through complex interaction of molecular nitrogen with hydrocarbons in an early phase of the flame front; this is referred to as prompt NO_x. Prompt NO_x is reduced to N_2 in the boiler. Due to the small effect of prompt NO_x, it is not considered in this report.

Thermal NO_x generally represents about 20 - 50% of the total and the balance attributable to fuel NO_x. The amount of thermal NO_x formed is dependent mainly upon the level of excess O_2 in the combustion zone and the combustion temperature.

The quantity of NO_x formed depends primarily on temperature, time, turbulence, and coal volatility. Fuel NO_x is formed from nitrogen present in both volatile matter and char[11]. Reactive, gas-phase nitrogen species are produced as volatile matter evolves during combustion. As a result, NO_x emissions from coal-fired boilers can be dependent upon the volatility of the coal. Where greater amounts of oxygen are available as the volatile matter evolves, greater amounts of NO_x result.

Combustion modifications are designed to delay the mixing of fuel and air during the initial stages of combustion, thereby reducing temperature and initial turbulence, which minimizes NO_x formation. These modifications are accomplished without compromising safety and combustion efficiency.

[11] Char is the product of coal devolatilization. It consists mainly of unburned carbon, a small amount of high molecular weight hydrocarbons, and ash.

3.1.2. NO_x Formation Chemistry

During combustion, coal particles are heated and pyrolyze. Volatile matter (VM) evolves from the coal and burns homogeneously in the gas phase within a relatively short period of time (on the order of 10 milliseconds), while the char burns heterogeneously and much less rapidly. In the gas phase, the nitrogen will form reactive cyanogens (HCN, CN), oxycyanogens (OCN, HNCO), and amine species (NH_3, NH, N). The fate of these reactive species is strongly dependent on local oxygen concentration. In an uncontrolled combustion system – where these volatiles burn in an oxygen-rich environment – a high conversion to NO_x results. Under fuel-rich conditions characteristic of low NO_x operations, however, these reactive species can be reduced to N_2.

3.1.3. NO_x Emission Limits

NO_x emissions have been linked to acid rain, photochemical smog, and tropospheric ozone (the greenhouse effect). This has lead to the establishment of regulatory measures and development of NO_x reduction technologies. NO_x emissions are now regulated under the provisions of the Clean Air Act, particularly the Clean Air Act Amendments (CAAA) of 1990. These regulations are a function of the boiler type, as shown in Table 3-1.

Table 3-1. Coal-Fired Boiler NOx Emission Limits, lb/106 Btu (1990 CAAA Title IV)

Boiler Type	Phase I: 1996-2000	Phase II: 2000 +
Group 1 Boilers		
Dry Bottom Wall-Fired	0.50	0.45
Tangentially Fired	0.45	0.38
Group 2 Boilers		
Wet Bottom Wall-Fired	NA	0.86
Cyclone-Fired	NA	0.94
Vertically Fired	NA	0.80
Cell Burner	NA	0.68
Fluidized Bed	NA	0.29

3.1.4. NO_x Combustion Controls

Control of NO_x emissions can be achieved by the following methods:

- combustion controls
- post-combustion controls
- a combination of combustion and post-combustion controls

Post-combustion controls include hot-side and cold-side selective catalytic reduction (SCR), selective non-catalytic reduction (SNCR), and combined NO_x/SO_2 technologies (e.g., copper oxide or NOXSO). These are shown on the top and the right side of Figure 3-1. SCR and combined NO_x/SO_x technologies are described elsewhere [Berkenpas, 1999 #58]. The SNCR technology is described in Chapter 4.

Combustion controls include low NO_x burners, overfire air, and reburning (coal, oil or natural gas). The left side of Figure 3-1 shows these technologies. These can be implemented separately or in combination to reach a desired level of NO_x removal in the combustion zone. These are described in more detail in the following sections.

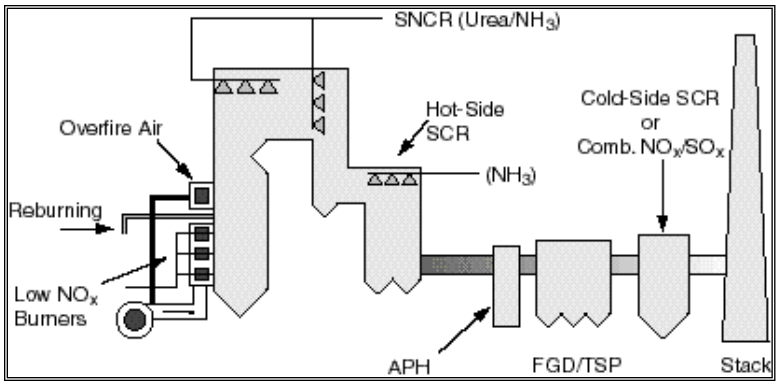

Figure 3-1. Combustion and post-combustion NO_x control options (SCR = selective catalytic reduction; SNCR = selective non-catalytic combustion; FGD = flue gas desulfurization)

3.1.5. Effects of Boiler Type

There are a large variety of boiler types used to burn coal. Table 3-2 summarizes the NO_x emissions from coal-fired utility plants in the U.S. prior to CAAA of 1990, categorized by boiler type. This chapter only considers three most prominent: wall, tangential, and cyclone. Figure 3-2 shows a schematic cut-away view of the burner and inlet air nozzle arrangement for wall and tangential boilers.

Table 3-2. NO_x Emissions from Coal-Fired Boilers in the U.S.

Boiler Type	No. of Boilers	Capacity, GWe	% of Total Capacity	NO_x Emission (% of Total)
Dry Bottom Wall-Fired	411	120.7	36.9	35.8
Wet Bottom Wall-Fired	39	8.6	2.6	4.6
Tangentially Fired	423	138.3	42.3	34.2
Cyclone Fired	89	27.6	8.5	12.2
Vertically Fired	33	4.8	1.5	1.7
Cell Burner	36	24.1	7.4	11.3
Fluidized Bed	5	0.7	0.2	0.1
Other	27	1.9	0.6	0.1
Total	**1063**	**326.7**	**100.0**	**100.0**

The key operating conditions of each boiler type includes excess O_2 level, pulverizer selection, burner tilt (tangential-fired boilers), load and duty cycle, water-wall slag conditions. Other factors that affect NO_x formation are the distribution of air and coal among the burners, burner settings, and the primary air-to-coal ratio.

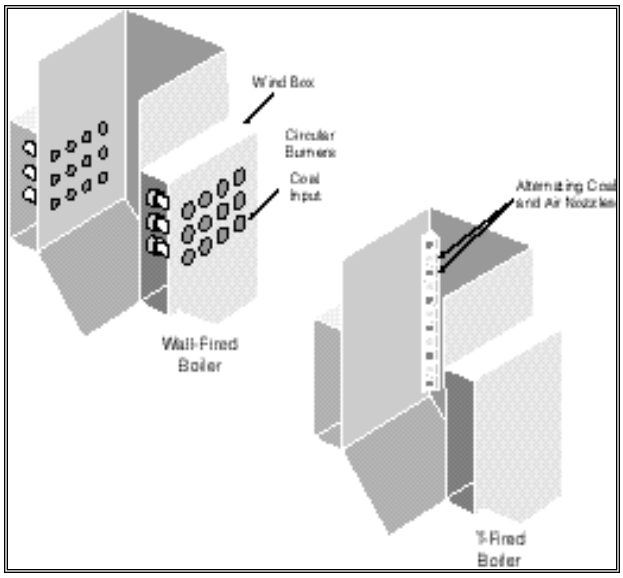

Figure 3-2. Cut-away view of a wall-fired and tangential-fired boiler. Coal input and air nozzle arrangement can be modified to enhance NO_x suppression.

3.1.5.1. Wall-Fired

Wall-fired boilers most commonly use circular burners, in which each burner nozzle is surrounded by water tubes. A wall-fired boiler is shown in Figure 3-2. Cell burners are a variant of the circular burners and are treated as wall-fired boilers in this report. Cell burners represent two or three circular burners grouped closely together, the cell surrounded by water tubes.

Burners for conventional wall-fired boilers impart substantial swirl to the combustion air to promote rapid, turbulent mixing of the coal with the primary and secondary air. This produces an intense, turbulent flame, with consequent high levels of NO_x formation. Wall-fired boilers put into service after enactment of the 1971 NSPS include first-generation LNBs and OFA, and increased furnace sizes.

3.1.5.2. Tangential

Tangential boilers in the United States are manufactured exclusively by ABB C-E. Their design is fundamentally different from that of wall-fired boilers, and typically lead to lower NO_x emissions in uncontrolled boilers.

Tangential boilers consist of a vertical array of coal nozzles and air ports mounted in each corner of the furnace as shown in Figure 3-2. These nozzles inject stratified layers of air and fuel into relatively low-turbulence areas of the furnace. In operation, coal and air are directed axially into the furnace (no swirl is imparted) and tangent to an imaginary circle, causing the majority of the combustion to occur in a swirling fireball in the center of the furnace away from the injection point. This creates a fuel-rich region in an overall fuel-lean environment, igniting it before the layers are mixed in the highly turbulent center fireball.

Axial introduction of coal and air into the furnace in combination with the combustion in the center of the furnace reduces the intensity of mixing. This results in the increase in the fraction of nitrogen that is devolatilized under fuel-rich conditions. The resulting lower temperature created and diminished turbulence lead to inherently lower NO_x formation than is the case in wall-fired burners.

3.2. Low NO_x Burners

3.2.1. Process Overview

Low NO_x burners are designed to "stage" combustion. Local staging in wall-fired boilers is accomplished using LNBs. The principle of LNB operation involves decreasing the amount of air introduced into the primary combustion zone. This creates a fuel-rich reducing environment and lowers the temperature. Both conditions generally suppress NO_x formation. Auxiliary air required for complete burnout of the combustibles is added after the primary combustion zone, where the temperature is sufficiently low that additional NO_x formation is minimized. The stages are shown in Figure 3-3.

- Staging (i.e., delaying) the mixing of coal and air to limit oxygen availability during the initial stages of combustion, thereby inhibiting fuel NO_x formation
- Directing secondary air to mix with the products of initial combustion at a location near the flame boundary where temperatures are below approximately 2800°F, thereby inhibiting thermal NO_x formation

LNB typically reduce NO_x by 30-55%. This typically is not sufficient to meet regulatory constraints. Thus, other advanced stage combustion technologies are used in addition to LNB to reduce NO_x further. Advanced staging can be accomplished in either of two ways: air staging (OFA) or fuel staging. Fuel staging, typically called reburning, is discussed in the "Fuel Reburn" section below. OFA can be employed alone or in combination with LNBs on wall-fired boilers; on tangential-fired boilers it is expected to be an integral component of all combustion NO_x control retrofits.

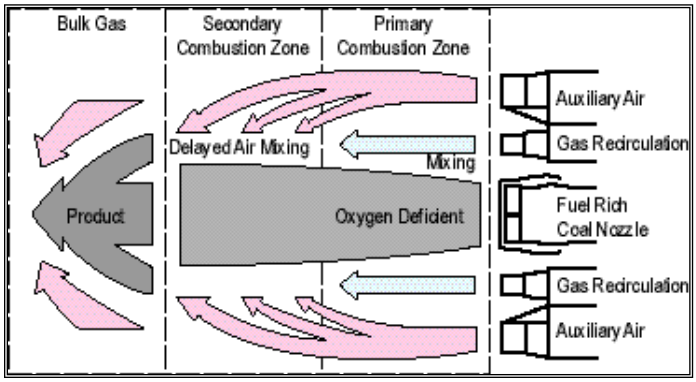

Figure 3-3. "Staged" combustion in a low NO_x burner [DOE, 1996 #57]

Operation of LNBs with reduced air in the primary combustion zone can lead to an increase in unburned carbon (also referred to as loss on ignition or LOI), increased slagging in the combustion zone, and accelerated corrosion of boiler tubes. These result in economic losses and performance loss of electrostatic precipitators (ESP). To counteract these tendencies, several steps can be taken:

- Increase the coal fineness
- Adjust the air/fuel distribution
- Adjust the arrangement of the burners
- Coat the boiler tubes with corrosion-resistant materials

Application of retrofit combustion NO_x controls will require boiler equipment modifications and, in some cases, changes in combustion system operation. Modifications to key plant auxiliary systems — coal and air supply, I&C, and ignition and fame scanning — and changes in their operation are not explicitly required but may also be necessary, especially to offset potential combustion NO_x control system impacts on plant O&M.[12]

[12] See Section 7, "Potential Combustion NO_x Control Impacts on Plant O&M and the Environment."

3.2.1.1. Wall-fired Boiler Retrofits

Burner staging with LNBs in wall-fired boilers can be viewed as being accomplished in two steps: primary combustion and secondary combustion. This staging is usually accomplished locally within the burner. Primary combustion occurs in an oxygen-deficient environment (local stoichiometry $\leq$ 1.0) near the burner throat; secondary combustion occurs in a higher oxygen environment (local stoichiometry > 1.0) farther from the burner throat but still within the flame envelope.

Figure 3-3 schematically illustrates these various zones. Improved secondary air registers, and often a higher axial air flow component, are designed into these burners to accomplish the accurate control and thorough mixing of coal and air necessary for effective staging. A coal nozzle that splits the coal stream into several separate jets is sometimes included to accelerate coal devolatilization and, therefore, increase the degree of devolatilization that occurs in an oxygen deficient environment. This approach is in contrast to conventional burners, which incorporate a high swirl to promote rapid mixing of the coal-primary air and the secondary air in an intense flame close to the burner throat. Rapid, turbulent mixing typically results in a very stable flame. However, it also produces high NO_x emissions.

Nine suppliers are currently known to offer combustion NO_x control equipment for wall-fired boilers in the United States. Babcock and Wilcox, Foster-Wheeler, and Reley are domestic suppliers of both wall-fired boilers and combustion NO_x control systems for these boilers.

Retrofit combustion NO_x controls on wall-fired boilers are expected to be accomplished primarily using LNBs with or without OFA. Operating alone, LNBs have achieved NO_x reductions up to 60%.

3.2.1.2. Tangential-fired Boiler Retrofits

Retrofits to tangential boilers consists of installing air and coal inlet nozzles in various configurations that change the way in which coal, primary air, secondary air, and OFA are injected into the boiler. These arrangements are generally referred to as low-NO_x concentric firing systems (LNCFS). Southern Company Services, Inc. has demonstrated three distinct variations of LNCFS [DOE, 1996 #57].

Coal/air nozzle modifications on tangential-fired boilers are physically analogous to LNBs in that they stage combustion within the flame, but they have not achieved NO_x reductions equivalent to LNBs.

Coal/air nozzle modifications involve the redesign or resizing of coal and/or air nozzles in tangential-fired boilers. Modifications are often manufacturer specific and can include concentric firing system, coal nozzle clustering, and flame holders employed separately or in combination.

In effect, concentric firing creates a lateral staging of the combustion process by aiming a fraction of the combustion air (i.e., changing the "auxiliary air" to "offset air") away from the fuel jets towards the furnace wall, thereby separating the walls from the central fireball with a layer of air. This layer of air reduces impingement of molten ash on furnace tubes. Further, by maintaining a high oxygen content at the tube surface, it reduces ash deposition and corrosion potential. An increase in heat transfer in the furnace radiant zone and a reduction in furnace outlet gas temperature also generally occur.

3.2.1.3. Capital Cost Factors

A primary determinant of process capital costs for retrofit combustion NO_x controls is the desired level of NO_x reduction and subsequently, the NO_x control technology selected — especially OFA on wall-fired boilers or separated OFA on tangential-fired boilers. Differences in control system design and engineering approaches from supplier to supplier influence these costs, as does the extent to which potential plant O&M impacts may be offset by system design. A variety of site-specific boiler design factors and the condition of the boiler and related combustion system equipment also can affect process capital costs. If the costs associated with any one of these factors are extreme, or if several of these factors apply, total retrofit costs can easily move outside the project range (i.e., beyond $7 to $25/kW). Primary among these factors are:

- Boiler size
- Boiler age
- Furnace configuration
- Windbox design and condition

- Physical interference
- Number of burners/elevations

3.3. Overfire Air

3.3.1. Process Overview

Under circumstances where NO_x emissions exceed desired levels despite the use of LNBs, it may be necessary to more deeply stage the combustion. This is accomplished by introducing the remaining air required for combustion through separate ports at higher elevations in the boiler as shown in Figure 3-4. Temperatures in this location will be lower, thus limiting production of additional NO_x even further than with LNBs [EPA, 1996 #8].

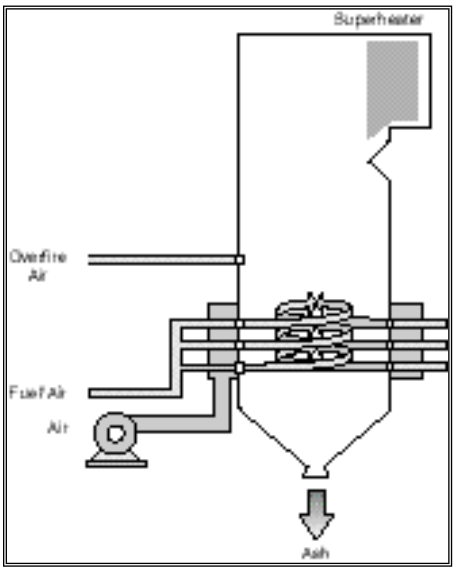

Figure 3-4. Overfire air added to an existing low NO_x burner reduces NO_x formation to lower levels [DOE, 1996 #57]

With OFA, a portion of the secondary air is diverted to injection ports (wall-fired boilers) or compartments (tangential-fired boilers) located above the primary combustion zone, thereby reducing available oxygen in the primary combustion zone. The percent of total combustion air diverted to OFA ports/compartments, and the overall furnace excess O_2 level, determine furnace stoichiometry. In practice, OFA quantities range from 10 to 25% of total combustion air. LNB and OFA are often combined together to increase the overall NO_x reduction to 40-60% [DOE, 1996 #57].

OFA flow and excess oxygen vary with boiler load. As a result, furnace stoichiometry and thus NO_x reductions vary over the operating range of the boiler. In all cases, sufficient air is added to ensure safe boiler operation and maximum combustion efficiency.

OFA effectiveness is primarily dependent on:

- **Placement of OFA ports/compartments**. Optimum placement of OFA ports/compartments is determined by available upper furnace residence time, available physical space for installation, and potential structural impediments and other components (e.g., soot blowers, steam headers, downcomers, and observation doors).
- **Coal properties**. Reactivity (as it affects UBC), slagging characteristics, and corrosion potential are the most important coal properties affecting OFA performance. A higher amount of OFA can be applied with more-reactive coals and with coals that exhibit low slagging and corrosion potential. Slagging and corrosion can be avoided or minimized with application of concentric firing system on tangential-fired boilers and water-wall protection systems on wall-fired boilers.

- **OFA flow penetration**. Sufficient OFA flow penetration into the furnace is necessary to achieve adequate mixing of the OFA with furnace gases. OFA flow penetration depends on the location, number, and design of the OFA ports/compartments.

In addition to these factors, a variety of others — including the configuration of existing windbox and secondary air ducts, furnace stoichiometry, and heat absorption patterns — can affect OFA effectiveness.

Applied in combination with OFA, concentric firing can work to counter-act potential slagging and corrosion problems resulting from staged combustion, thereby allowing for higher amounts of OFA or extending OFA application to a wider range of coals. The amount of main windbox air designed to pass through the concentric firing system nozzles depends on the amount of combustion staging required and the properties of the coal fired.

3.4. Fuel Reburn

3.4.1. Process Overview

Reburn is a NO_x reduction process that consists of reducing the fuel flow of coal into the main combustion zone and addition of an equal heat input of coal, oil, or natural gas above the main combustion zone (see Figure 3-1). Gas reburn can reduce the NO_x emissions by as much as 55-60% [EPA, 1996 #8]. Reburn can be used with any existing or new burners of any type (wall, cell, tangential, or cyclone).

The majority of the fuel is burned in the primary combustion zone at or near stoichiometric conditions. The additional fuel (coal, oil, or natural gas) injected burns in another zone higher in the boiler with additional air. Most reburn applications divert between 10 and 20% of the total heat throughput to the upper furnace. A reducing condition exists in this reburn zone. Some of the NO_x already formed is therefore reduced or converted back to molecular nitrogen. Thus, reburning decomposes NO_x once it is formed.

The reburn process can be applied to nearly any boiler type and size. The amount of NO_x reduced depends on the conditions in the main combustion and reburn zones. Specifically, the temperatures, residence time, and furnace flow patterns are important in determining the effectiveness of the process. NO_x reduction performance improves as the reburn residence time increases.

Reburn as a technology has several benefits when compared to LNB or OFA [EPA, 1996 #8]:

- Works with virtually any hydrocarbon fuel
- Minor impacts to boiler operation
- Minimal boiler retrofit capital cost
- Operational flexibility
- Reduced emissions of air toxics, SO_2, and ash
- Compliance flexibility

The only disadvantage is the uncertainty in the supply, transportation and availability of natural gas at the plant site.

3.4.2. Process Chemistry

The composition of the flue gas changes above the combustion zone in the boiler where the reburn fuel is injected into the hot flue gas. The most significant change is the combustion of the reburn fuel. It has been shown that complex reactions take place in the reburn zone, producing several radicals[ref]. Because these formations are not entirely understood, a simplified combustion equation is used in the IECM. This is shown in Equation 3-1.

$$CH_4 + 2O_2 \rightarrow CO_2 + 2H_2O \qquad (3\text{-}1)$$

Using this chemical reaction, the composition of the flue gas exiting the reburn zone can be determined from a molar balance as shown below.

$$\dot{m}_{rb,exit,j} = \dot{m}_{rb,in,j} \text{ for } j = CO_2, CO, HCl, SO_2, SO_3 \quad (3\text{-}2)$$

3.5. References

'Reducing Emissions of Nitrogen Oxides via Low-NO_x Burner Technologies'. Clean Coal Technology, Topical Report No. 5. September, 1996. U.S. DOE, Federal Energy Technology Center.

4. Selective Non-Catalytic Reduction

4.1. Introduction

Selective Non-Catalytic Reduction (SNCR) is a post-combustion method of reducing emissions of oxides of nitrogen (NO_x) used on fossil fuel fired power-generating systems, such as boilers, combustion turbines and internal combustion engines. It employs a strong reducing agent to react with the NO_x formed during the combustion process to reduce it to nitrogen gas. In commercial applications, NO_x reductions have ranged from 15% to over 60% with ammonia slip below 10 ppm by volume, at a cost of $750 - 1500/ton of NO_x removed. This document describes the use of SNCR on coal-fired electric utility boilers and describes models developed to predict the costs and performance of such systems.

4.2. Process Overview

Figure 4-1 shows a process schematic for a typical SNCR application on a steam boiler. The system is relatively simple, requiring equipment only for reagent storage, transport, injection, and I&C (instrumentation and controls). An aqueous solution of urea, $CO(NH_2)_2$, is the reagent most commonly used. In a typical application, urea is brought to the site in 7000-gallon trailers. From there, it is transported to a control and mixing panel, where it is diluted to a 15 - 20% solution. Then, a metered quantity is injected in the upper furnace and convective sections of the boiler through a series of injection nozzles and lances. The quantity of reagent injected is typically set so that the mole ratio of nitrogen in the reagent to NO in the flue gas is greater than unity. On entering the boiler, the urea droplets vaporize and the urea then decomposes to form NH, NH_2 and HCNO radicals, which react with the NO_x to reduce it to N_2. Adjusting the dilution level of the urea mixture controls the rate of vaporization and decomposition. The principal by-products of the SNCR process are H_2O, CO_2, N_2O and NH_3. N_2O is an intermediate product formed during the NO_x reduction process. NH_3 is formed from unreacted reagent.

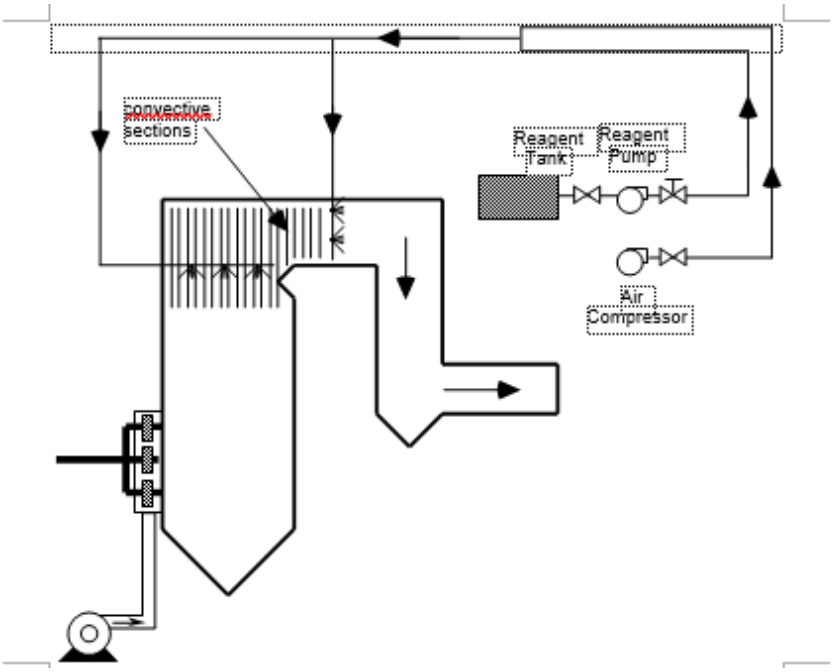

Figure 4-1. Process schematic for an SNCR system

Some SNCR systems use anhydrous (NH_3) or aqueous (NH_4OH) forms of ammonia as reagent. In the U.S., urea has been used as the reagent in all but one commercial installation [Staudt, 1998 #55]. Urea is the preferred reagent because of safety and ease of handling considerations and because urea-based SNCR systems are less complicated to design and operate than their ammonia-based counterparts. Sometimes, trace amounts of proprietary chemicals are also added in an attempt to improve SNCR performance. Urea reacts with NO_x over a slightly broader and higher temperature range than ammonia, making it easier to locate appropriate temperature windows in utility boilers.

Urea is injected into the furnace as an aqueous solution. Since its vapor pressure is lower than that of water, it is not completely released into the furnace gases until the droplets evaporate, leading to better mixing of the reagent with the flue gases. Ammonia, on the other hand, has a much higher vapor pressure than water. Therefore, when an aqueous solution of ammonia is injected into the flue gas, the ammonia rapidly volatilizes off from the reagent droplets. The ammonia gas, having a lower density and less momentum than the droplets, cannot penetrate the flue gas flow field. Therefore, ammonia SNCR systems on electric utility boilers require complex injection systems and high-energy blowers to achieve good reagent distribution. These systems thus have higher capital costs. Some SNCR systems use large amounts of compressed air to impart greater momentum to the reagent for improved mixing. Such systems are called high-energy systems because of the higher parasitic energy consumption associated with compressed air use. Applications that do not use compressed air are referred to as low-energy systems.

Multiple injector locations are required to maintain adequate SNCR performance across the entire load range. Successful SNCR operation requires injecting the reagent into the flue gas within a particular temperature window (1600 - 2000 F). Since the physical location of this temperature window shifts from the convective sections towards the upper furnace as boiler load decreases, multiple injector locations are necessary to ensure that the flue gas temperature at injection location is optimal.

Two types of injectors are most commonly used in industry. The first kind is wall-mounted single-nozzle injectors, placed along the front and side walls of the upper furnace. These injectors do not penetrate into the furnace. The second kind is multiple-nozzle lance injectors that penetrate into the furnace and are generally installed in the convective sections of the boiler. Because the lance injector can deliver the reagent across the depth of the furnace, it results in more uniform mixing of the reagent with the flue gas. However, because it is operating in a 2000° F environment, it must be cooled and is more complex to design.

4.3. Process Chemistry

The SNCR process involves injecting ammonia or urea into the boiler flue gas. The ammonia or urea reagent react with NO_x in the flue gas to produce intermediate reducing agents and eventually N_2 and water.

4.3.1. Reducing Agents

NO_x reduction takes place through the conversion of NO_x to nitrogenous intermediates, which under certain conditions are then further reduced to N_2, rather than being oxidized back to NO_x. The reducing agents are amine (NH, NH_2) and cyanuric nitrogen (HNCO) radicals, formed from the ammonia or urea introduced into the combustion zone. A detailed exposition of nitrogen chemistry in the combustion zone can be found in [Miller, 1989 #10]. The major routes of NO_x reduction and formation in the SNCR process are described below:

When urea-based reagents are used, the urea dissociates into ammonia and isocyanuric acid (HNCO) above about 500 K (440 F):

$$M_{econo,k} = M_{furn,k} A_{overhead} \text{ for all k} \quad (4\text{-}1)$$

At temperatures above 600 K (620 F), ammonia dissociates into amine free radicals by the following reaction steps:

$$NH_3 \rightarrow NH_2 + H \quad (4\text{-}2)$$

$$NH_2 \rightarrow NH + H \quad (4\text{-}3)$$

The radicals then reduce NO in the following steps:

$$NH_2 + NO \rightarrow N_2H + OH \quad (4\text{-}4)$$

$$NH_2 + NO \rightarrow N_2 + H + OH \quad (4\text{-}5)$$

A competing reaction is oxidation of other intermediate nitrogenous compounds formed back to NO_x, namely:

$$HNO + OH \rightarrow NO + H_2O \quad (4\text{-}6)$$

The net amount of NO_x reduced to N_2 through the amine free radical strongly depends on temperature. In the temperature range of interest, specifically 900K to 1350 K (1160 - 1970 F), the rates of reactions shown in Equations (4-4), (4-5), and (4-6) are comparable. At low temperatures, the reduction steps shown in Equations (4-4) and (4-5) have slightly higher reaction rates, resulting in a net reduction of NO_x. At higher temperatures, the oxidation reaction is favored. The change in dominance of formation or reduction reactions with temperature results in a bell-shaped curve of the variation of NO_x reduction with temperature. At lower temperatures, the reduction reactions shown in Equations (4-4) and (4-5) are dominant and NO_x reduction increases with temperature. At about 1250 K (1790 F), NO_x formation from the reaction described by Equation (4-6) becomes significant, and NO_x reduction begins to fall off.

The amount of ammonia slip observed also depends on injection temperature. At higher temperatures, any unreacted amine radicals are oxidized to NO_x. Therefore, NH_3 slip monotonically decreases with injection temperature. The variation of NO_x reduction and NH_3 slip with temperature for a typical SNCR application is illustrated in Figure 4-2. The curves were generated from a numerical computer simulation that considers several hundred elementary reaction steps [Ciarlante, 1997 #37]. Each point on this graph is generated by modeling the chemical kinetics of the reaction process at the specified flue gas temperatures, assuming a reaction time of 0.5 seconds.

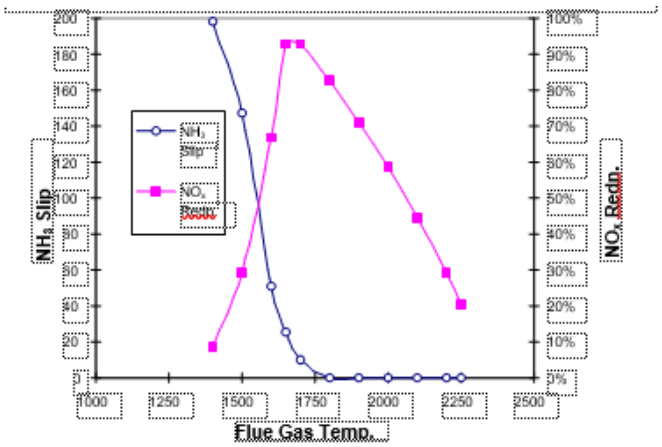

Figure 4-2. Chemical kinetics simulations of variation of NO_x reduction and NH_3 slip with flue gas injection temperature. (NSR = 1.2, inlet NO_x = 0.6 lb/MBtu, O_2 = 4.5%, residence time = 0.5s) [Ciarlante, 1997 #37]

The HNCO reaction pathways are:

$$O_{comb} = \frac{f_C}{12.01} = \frac{f_H}{1.01} + \frac{f_S}{32.06} - \frac{f_O}{16.00} \quad (4\text{-}7)$$

$$NCO + O \rightarrow NO + CO \quad (4\text{-}8)$$

$$NCO + NO \rightarrow N_2O + CO \quad (4\text{-}9)$$

$$N_2O + M \rightarrow N_2 + O + M \quad (4\text{-}10)$$

The NCO radical results in both formation and destruction of NO via the competing reactions shown in Equations (4-8) and (4-9). Some of the N_2O formed via Equation (4-9) does not decompose, resulting in N_2O emissions when urea is used as the reagent.

With urea, a similar temperature effect is observed as with ammonia, but with a temperature window that is slightly wider and 50° K (100° F) higher.

Additional details of SNCR chemistry can be found in several sources [Jodal, 1990 #49; Siebbers, 1990 #53]. A comprehensive fluid dynamics (CFD) model to simulate SNCR performance that incorporates the global kinetic rates of the principal reactions relevant to the SNCR process is described in [Chen, 1997 #36].

4.3.2. Overall Reactions

The overall chemistry of the NO_x reduction equations depends on the reagent type and the temperature. Typical reactions for reducing NO_x in a hot-side SCR or by the lower temperature copper oxide (CuO) process do not apply to the SNCR process. The SCR and CuO reactions consider O_2 as the oxidizing agent in the flue gas stream. For the SNCR process, NO is a more effective oxidizing agent than O_2 [EPA, 1994 #56].

4.3.2.1. Ammonia

The following overall mechanism should ideally govern the reduction of NO_x at the optimal temperature in the SNCR (1750 ? 90F) when ammonia is used as the reagent:

$$4NH_3 + 6NO \rightarrow 5N_2 + 6H_2O \quad (4\text{-}11)$$

If the ammonia is not injected into the optimum temperature zone of the boiler or mixed effectively with the flue gas, the following reactions dominates the reaction shown in Equation (4-11):

$$4NH_3 + 4NO + O_2 \rightarrow 4N_2 + 6H_2O \quad (4\text{-}12)$$

$$4NH_3 + 5O_2 \rightarrow 4NO + 6H_2O \quad (4\text{-}13)$$

$$4NH_3 + 3O_2 \rightarrow 2N_2 + 6H_2O \quad (4\text{-}14)$$

Equation (4-12) is generally accepted as the operating reaction with ammonia in the SNCR.

4.3.2.2. Urea

The following overall mechanism predominates at the optimal temperature in the SNCR (1750 ? 90F) when urea is used as the reagent:

$$2CO(NH_2)_2 + 4NO + O_2 \rightarrow 4N_2 + 2CO_2 + 4H_2O \quad (4\text{-}15)$$

This equation assumes that one mole of urea reacts with two moles of NO. However, in practice a higher stoichiometric ratio is used to achieve the desired NO_x removal. Any excess or unreacted urea decomposes by the following reaction:

$$6CO(NH_2)_2 + 3O_2 \rightarrow 2N_2 + 6CO_2 + 8NH_3 \quad (4\text{-}16)$$

4.4. Industry Experience with SNCR

SNCR is a mature NO_x reduction technology that has been used on a commercial scale for several years. In the U.S., there is more commercial experience (24 boiler-years) with SNCR on coal-fired facilities than with selective catalytic reduction (SCR) or reburning [Staudt, 1998 #55]. Commercial and full-scale demonstration projects are documented in several sources including [EPRI, 1993 #44; EPRIb, 1997 #45; Eddings, 1998 #39]. However, industry experience has generally been limited to smaller boilers (<200 MW), and primarily to those firing oil or gas. Recent commercial applications or demonstration projects on coal or residual fuel oil in the United States are tabulated in Table 4-1 [Colburn, 1996 #38; EPRIb, 1997 #45]. Very recently, demonstration programs to evaluate the use of SNCR on coal-fired boilers of larger capacity have been undertaken in the U.S. They are summarized in Table 4-2.

Table 4-1. Recent SNCR Experience on Electric Utility Boilers

Utility Name	Plant Name	Boiler Type	Boiler Capacity (MW)	Fuel	SNCR Supply	Reag.	Comm. Date
New England Power	Salem Harbor 1, 2 & 3	Wall	2 x 85 and 185	Bit Coal 0.7%S	Nalco	Urea	1993
Eastern Utilities	Somerset	PC	112	Coal 0.7%S	Nalco	Urea	1994
Public Serv. Electric and Gas	Mercer 1 & 2	PC wet bottom, twin furnace	2 x 321	Bit Coal 0.8% S	Nalco	Urea	1993
Delmarva Power and Light	Edge Moor 3	NA	80	Coal 07%S	Nalco	Urea	1996
PA Electric	Seward 5	Tangential	150	Bit Coal 1.5% S	Nalco	Urea	1995
Atlantic Electric	B. L. England 1 &2	Cyclone	2 x 138	Bit Coal 2.4% S	Nalco	Urea	1994
Public Serv. of New Hampshire	Merrimack 1	Cyclone	120	Bit Coal 1.5%S	Noell, Inc	NH_4OH	1995

Connecticut Light & Power	Norwalk Harbor	Tangential	2 x 170	Residual Fuel Oil	NA	NA	NA
WI Electric Power	Valley 4	Wall	70	Bit Coal	Nalco	Urea	1992
Public Service of Colorado	Arapahoe 4	Roof	100	Bit, Sub Coal	Noell, Inc	NH_4OH	1993
North American Chemical	Trona 1 & 2	NA	2 x 75	Bit Coal	Nalco	Urea	1989
Nebraska Public Power	Shendon 1	Cyclone	105	Bit, Sub Coal	Nebraska PPD	NH_3	1996

Overseas, SNCR has been used on coal-fired boilers for several years in Europe. However, most of the experience has been on units firing brown coal. These boilers have longer residence times in the SNCR operating temperature window than do U.S. boilers, which are designed for firing bituminous or sub-bituminous coals.

Table 4-2. SNCR Experience on Large Capacity Boilers

Utility	Plant Name	Boiler Type	Boiler Capacity (MW)	SNCR Supplier	Notes
American Electric Power[13]	Cardinal 1	Wall - dry bottom PC	600	Nalco	Demo installed in 1998
PSE&G[14]	Hudson	NA	620	NA	Commercial contract in place
Connectiv[2]	Indian Point	NA	450	NA	Commercial contract in place
Georgia Power Co.[15]	Hammond 4	Wall - PC	500	Nalco	Demo. completed
Georgia Power Co.[3]	Wansley 1	Tangential - twin furnace	880	Nalco	Demo completed

4.5. SNCR Performance in Commercial Applications

In commercial applications on coal-fired boilers, SNCR has typically achieved NO_x reductions of approximately 40%, with an NH_3 slip of less than 10 ppm. Performance data for commercial U.S. utility systems are tabulated in Table 4-3. Note that these results have been reported at full load operation, with the boiler and SNCR system operating under the supervision of system optimization experts. Long-term performance results should be expected to be inferior to these results.

[13] [Malone, 1998 #50]
[14] [Staudt, 1998 #55]
[15] [Eddings, 1998 #39]

Table 4-3. SNCR Performance of Commercial Urea-Based Systems on Coal-Fired Utility Boilers [Staudt, 1998 #55]

Plant Name	Boiler Capacity (MW)	Baseline NO_x (lb/MBtu)	Outlet NO_x (lb/MBtu)	NO_x Red. (%)	NH_3 Slip (ppm)
Salem Harbor 1, 2 and 3	85 85 185	0.42 0.60 0.43	0.30 0.30 0.30	30 50 30	<10 <10 <10
Somerset	112	0.50 - 0.92	0.35	24 - 62	<5
Mercer 1&2	2 x 321	1.6 - 1.8	1.2	25 - 33	<5
Edge Moor 3	80	0.70	0.40	45	<5
Seward 5[16]	150	0.75	0.51	32	<2
B.L. England, Units 1&2	138 138	1.31 1.40	.90 .90	31 36	<5 <5

At the present time, there is no commercial experience with SNCR on utility boilers larger than 320 MW. Further, because the 320 MW units have split furnaces, the application of SNCR on these units is equivalent to its use on two 160 MW units.

An analysis conducted for TVA's Paradise Units 1 & 2 (650 MW cyclone-fired boilers) concluded that a 15 - 20% NO_x reduction would be achieved with an ammonia slip of under 2 ppm and a 40+% reduction could be obtained if the ammonia slip could be 5 - 10 ppm. Another study evaluating the use on Southern Company's Hammond #4, a 500 MW wall-fired boiler equipped with low- NO_x burners and overfire air, concluded that a 28% NO_x reduction could be obtained with a 2 ppm ammonia slip. Both analyses were conducted through the use of CFD and chemical kinetics simulations of the SNCR process on this boiler [Staudt, 1998 #55].

4.6. Factors Affecting SNCR Performance

The performance of an SNCR system depends on several factors that depend on the operating and design parameters of both the SNCR system and the boiler. An understanding of the effects of these factors will assist in developing models to explain observed differences in the performance.

4.6.1. Normalized Stoichiometric Ratio (NSR)

The overall reactions between urea and NO and ammonia and NO can be written as:

$$NH_3 + NO \rightarrow N_2 + H_2O \qquad (4\text{-}17)$$

$$CO(NH_2)_2 + 2NO \rightarrow 2N_2 + H_2O + CO_2 \qquad (4\text{-}18)$$

For the overall reaction, the ideal stoichiometric ratio of reagent to NO_x is 1.0 for ammonia and 0.5 for urea. The normalized stoichiometric ratio (NSR) is the actual stoichiometric ratio used for a particular application normalized by the ideal stoichiometric ratio. That is,

$$\text{NSR} = \frac{\text{actual stoichiometric ratio}}{\text{ideal stoichiometric ratio}} \qquad (4\text{-}19)$$

NSR is the standard method used to report the amount of reagent used.

There are several pathways competing with the reactions shown in Equations (4-17) and (4-18) for consumption of the reagent. Some of these pathways actually result in the formation of additional NO_x. Therefore, even under perfectly

[16] Seward was designed for a 0.45 lb/MBtu target. However, NO_x reduction is limited due to air heater fouling which occurs when ammonia slip exceeds 2 ppm.

mixed conditions, an NSR of 1.0 results in NO_x reductions significantly less than 100%. To compensate for competing destruction pathways and imperfect mixing, an NSR greater than unity is generally used in practice.

With increased NSR, NO_x reduction increases because chemical kinetic rates of the global reactions shown in Equations (4-17) and (4-18) increase with increased reagent concentrations. However, as the NSR increases, the amount of reagent that is unreacted also increases, resulting in higher NH_3 slip emissions. Reagent utilization, defined as the fraction of reagent that reacts with NO_x to reduce it to N_2, also decreases with increasing NSR, which in turn results in increasing marginal costs of removal. However, for commercial applications, limiting NH_3 slip to a tolerable level is the prime consideration in fixing the NSR used, which in turn limits the NO_x reductions achieved. The variation of NO_x reduction and NH_3 slip as a function of NSR on a 112 MW coal-fired boiler is shown in Figure 4-3. The trends are typical of those observed in SNCR applications.

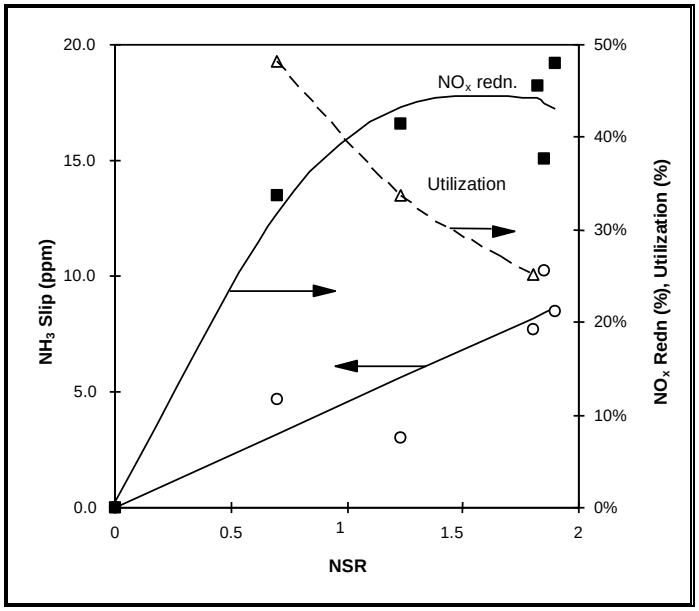

Figure 4-3. Variation of NH_3 slip and NO_x reduction with NSR (full load, inlet NO_x = 451 ppm) [Staudt, 1995 #54]

4.6.2. Ammonia Slip

Ammonia slip is a by-product of the SNCR process. It can result in several operational problems including:

- air heater plugging - the NH_3 reacts with sulfur trioxide in the flue gas to form ammonium hydrogen sulfate. This is a sticky substance that causes the flyash to bind together, plugging the air heater. This is also a common problem with SCR systems.
- flyash salability - high amounts of NH_3 slip result in higher levels of NH_3 concentration in the flyash. Most buyers of flyash require NH_3 levels to be below certain limits.
- air quality concerns – NH_3 is identified as a hazardous air pollutant in the 1990 Clean Air Act Amendments.

In order to mitigate the effects of ammonia slip, the maximum allowable slip is generally limited to 5 - 10 ppm by volume for most commercial applications. For a given SNCR application, the level of slip depends primarily on the NSR used. Hence, a tighter slip level requires operation at a lower NSR, resulting in lower NO_x reductions.

4.6.3. Flue Gas Injection Temperature

As seen from Figure 4-2, NO_x reductions with SNCR are maximum when the injection temperature is about 1600 F. However, at this temperature, NH_3 slip is generally excessive in commercial applications. Even when the NSR is below unity, local reagent-rich pockets are formed because of incomplete mixing, where the local NSR might be 2 or greater. These pockets result in excessive NH_3 emissions. Therefore, in commercial practice, the SNCR is operated in a region where flue gas temperatures are above 1600 F. If the reagent is injected into a region that is too cold, NH_3 and N_2O

emissions rapidly increase. Injection into a region that is too hot reduces process effectiveness because the reaction rate of oxidation of the reagent to NO becomes significant.

Flue gas temperatures are fixed by boiler design and operating conditions. Therefore, an SNCR system has to be designed appropriately to ensure that injectors are placed at locations where the flue gas temperatures will be optimal across the desired load range and range of operating conditions.

4.6.4. Flue Gas Residence Time

Reduction of NO_x using SNCR is kinetics-limited. Therefore, longer flue gas residence times within the reaction temperature window will result in greater NO_x reduction and lower NH_3 and N_2O emissions.

Residence times are primarily a function of boiler design and load; changes in boiler operating conditions or fuel will only have a minor effect. Therefore, furnace design will affect the potential amount of NO_x reductions possible at a particular boiler.

4.6.5. Uncontrolled NO_x Emissions

NO_x reduction, expressed as a fraction of initial NO_x levels, is higher when the inlet concentration of NO_x for the SNCR process is higher, *all other factors remaining constant* [Hofmann, 1993 #28; Rini, 1993 #52]. This is because of several factors:

- higher NO_x concentrations result in faster chemical kinetics
- at higher inlet NO_x concentrations, the temperature window for SNCR NO_x reduction reactions is wider, resulting in greater NO_x reductions (on a percentage basis), and,
- SNCR cannot reduce NO_x concentrations below a critical NO_x level, which depends on temperature. Therefore, in applications where the inlet NO_x levels are low, the NO_x reduction, expressed as a percentage, will be low.

In practice, combustion modification methods used to reduce NO_x emissions (which will result in reduced inlet NO_x concentrations for the SNCR system) can also change other process parameters, such as flue gas temperature at the reagent injection point. The overall effect of these changes can be negative or positive on the performance of the SNCR system. At one installation, SNCR NO_x reduction actually increased after low-NO_x burners were installed [Hunt, 1993 #47]. Even though the combustion modification resulted in lower inlet NO_x for the SNCR process, the favorable changes in flue gas temperature more than compensated for any loss in performance due to lower NO_x levels.

4.6.6. Boiler Load

As boiler load changes, the flue gas temperature at different locations in the boiler and residence time in the temperature range of interest for the SNCR process changes. Performance at partial loads depends greatly on the ability of the SNCR system to inject reagent into the flue gas at the optimal temperature. In well-designed SNCR systems, this goal is usually achieved through the use of multiple injector locations. For such systems, NO_x reduction and chemical utilization increase and NH_3 slip decreases with decreasing load because of increased residence times. However, for SNCR systems that lack the flexibility to alter injection location, performance generally deteriorates as load drops. This is because the injection location that was optimal at full load is now too cold for part load operation, resulting in excessive NH_3 slip. To reduce the NH_3 slip to acceptable levels, such systems have to be derated by decreasing the NSR at partial loads, which in turn results in lower NO_x reduction.

To illustrate how differences in SNCR system design affect performance, particularly at partial load, the variation in NO_x reduction with boiler load of an original and modified SNCR system installed on a 110 MW roof-fired boiler burning low-sulfur bituminous coal is plotted in Figure 4-4 [Hunt, 1997 #48]. The original system only used a single level of injectors, and its performance is labeled as "single-level injectors." As seen from Figure 4-4, while NO_x reduction was satisfactory at high loads, it dropped to 11% at mid-load. Further, the original system could not be used at lower loads because of excessive levels of ammonia slip. Part-load performance was very poor because the flue gas temperatures at the injector location were too low for proper SNCR performance.

To improve part-load performance, the system was modified by installing an additional level of injectors upstream of the original injectors, where flue gas temperatures would be higher at low loads. The new injectors were only used at loads

below 80 MW. Retractable lance-type injectors were used so that they could be removed from the furnace at higher loads to prevent damage to the lances. The NO_x reductions of the modified system are identified as "multiple-level retractable injectors" in Figure 4-4. As seen from the figure, SNCR performance at part-load operation was significantly improved and the highest NO_x reductions are now obtained at part-load.

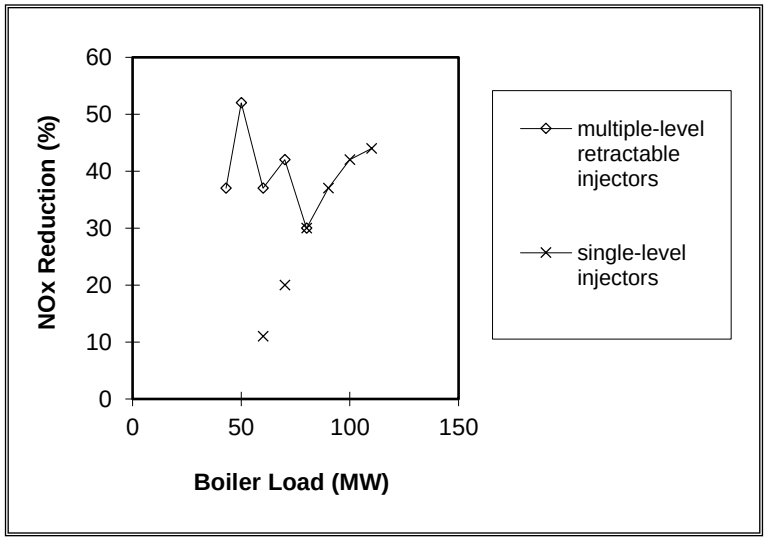

Figure 4-4. Differences in SNCR performance with SNCR design [Hunt, 1997 #48]

4.6.7. Mixing of Flue Gas and Reagent

If the reagent does not mix properly with the flue gas, there will be pockets of flue gas where the NSR is below and above the average NSR. Because NO_x reduction is a concave function of NSR, while NH_3 slip is a convex function of NSR, this will result in lower NO_x reductions and higher NH_3 slip than if the flue gas and reagent were properly mixed. It is generally easier to achieve good mixing in smaller boilers, because the flow cross-sections are smaller, making it possible to achieve good mixing simply with the use of wall injectors. Therefore, NO_x reductions achievable generally tend to be higher for smaller boilers than for larger boilers.

4.7. Modeling SNCR Performance for IECM

The IECM is designed to estimate the performance of environmental control technologies averaged over a time scale of the order of years. Although SNCR performance does depend on load, we neglect this dependency in the IECM model for the following reasons:

- For most applications, annual NO_x emissions calculated using the full load NO_x reduction as a proxy for reductions at all loads will approximately equal NO_x emissions calculated using load-specific NO_x reductions.
- The dependency of NO_x reduction with load is very boiler specific. Maximum NO_x reduction can be at full, partial or low load, depending on the specifics of the SNCR design, flue gas temperature and flow field at different boiler loads. Therefore, estimating the variation of NO_x reduction across the load range requires a significant amount of technical detail specific to the particular SNCR application. The IECM is designed to screen potential environmental control technologies. At this stage in the decision-making process, such details are unlikely to be available.

SNCR performance is characterized by three interdependent variables – NO_x reduction, NSR, and NH_3 slip. “SNCR Performance in Commercial Applications” on page 52 provides a description of how different boiler design and operating parameters affect the performance of an SNCR system. Except for NSR and NH_3 slip, these parameters can only be quantified by an extensive and detailed furnace flow and temperature mapping effort coupled with 3-dimensional computational fluid dynamic modeling. Such data will not be available at the technology screening level that IECM is designed for. Therefore, we adopt a two-part approach to estimating NO_x reduction using SNCR. First, we develop estimates of reductions typically achievable at commercial installations at full load using proxies for boiler design

parameters, namely, boiler capacity and uncontrolled NO_x emissions. Then, we develop a correlation to estimate how NO_x reduction would change from the nominal value, because of changes in NSR and allowable NH_3 slip.

4.7.1. NO_x Reduction Under Typical Operating Conditions

We define typical operating conditions as full load operation and NH_3 slip limited to 10 ppm. Estimates of typical SNCR reductions have been developed by several organizations, including the Utilities Air Regulatory Group (UARG), the Institute of Clean Air Companies (ICAC), the Northeast States Coordinated Air Use Management (NESCAUM), and the United States Environmental Protection Agency (EPA). Their modeling efforts have been motivated primarily by EPA's decision to develop legislation to control NO_x emissions in the OTAG (Ozone Transport Air Group) regions. NO_x reduction estimates are summarized in Table 4-4 below.

The estimates of NO_x reduction versus boiler capacity are shown in Figure 4-5. In this report, all boiler and plant sizes refer to *gross* megawatts (MWg). Estimates for boilers having high levels of uncontrolled NO_x emissions (greater than 0.50 lbs/ MBtu) are plotted using filled symbols and solid lines, and for boilers with low NO_x levels (less than 0.50 lbs/ MBtu) are plotted using open symbols and broken lines. As seen from the figure, these estimates are in good agreement for small-capacity boilers, but there is considerable divergence at larger capacity.

Table 4-4. SNCR NO_x Reduction Estimates

Source	NO_x Reduction	Factors Considered
NESCAUM [Staudt, 1998 #55]	40%	Methodology focuses primarily on SNCR estimates for 200 MW boilers.
U.S. EPA [EPAa, 1998 #40]	35 - 40%	Initial uncontrolled NO_x -- lower reduction for high initial NO_x and vice-versa.
UARG [EPAb, 1998 #41]	21 - 36%	Initial uncontrolled NO_x boiler capacity -- higher reduction for smaller capacity and vice-versa.

The EPA estimate is based on the average performance of small boilers (100-200 MW), and therefore is not applicable to boilers of larger capacity. NESCAUM has not provided any explicit basis for its estimate. It appears to be based on the high end of reported reductions for small capacity boilers and on computer simulations for NO_x reductions on larger boilers [Staudt, 1998 #55].

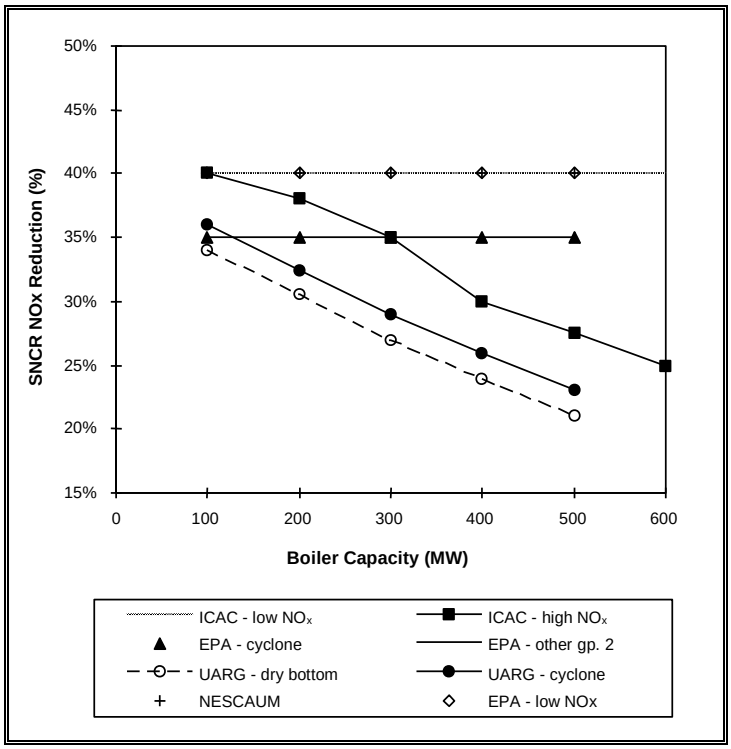

Figure 4-5. Variability of NO_x reduction estimates with boiler capacity

Note: Both ICAC - low NO_x, NESCAUM and EPA - low NO_x estimates are coincident. EPA - cyclone and EPA - other group 2 estimates are also coincident.

The UARG and ICAC high NO_x case reduction estimates decrease with increasing boiler capacity. The decrease in NO_x reduction is based on operating at successively lower NSR at higher boiler capacities. This is evident from Figure 4-6, in which variation of NO_x reduction is plotted against operating NSR. Each point in the graph represents the operation of a boiler of a particular capacity. Points along any given trendline represent boilers of different capacities, with capacity decreasing with increasing NSR.

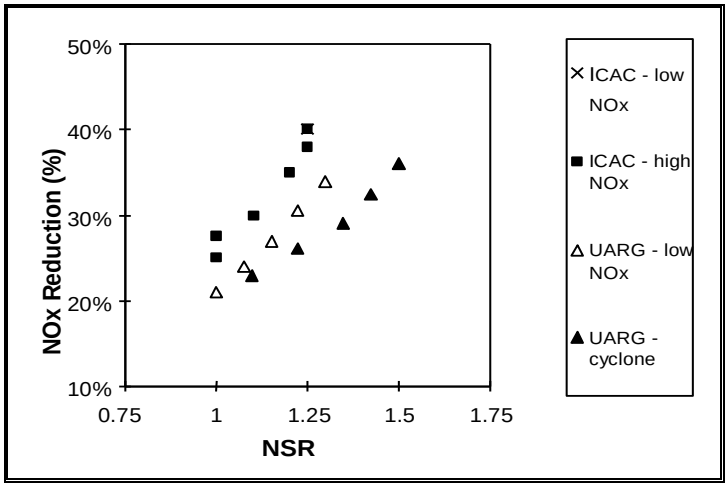

Figure 4-6. Variation of NO_x reduction with NSR for different capacity boilers.

Note: ICAC - low NO_x is a single point and is coincident with the uppermost point of the ICAC -high NO_x plot.

As boiler capacity increases, the flue gas flow cross-section area increases and it becomes increasingly difficult to ensure proper mixing of reagent and flue gas. Mixing difficulties are aggravated in high uncontrolled NO_x applications, since a greater quantity of reagent has to be injected into the boiler per unit of flue gas. Inadequate mixing leads to increased NH_3 slip levels. The standard method of reducing slip in such situations is to operate at reduced NSR, which also results in lower NO_x reduction. Test results of the demonstration programs conducted on large units (Hammond, 500 MW, and Wansley, 880 MW) suggest that NH_3 slip is excessive at the NSR and NO_x reduction levels typical for smaller boilers [Eddings, 1998 #39]. Since ICAC and UARG consider technological limitations of the SNCR system on larger capacity boilers in developing their performance estimates, we use their estimates as our basis.

The ICAC and UARG estimates are provided for high and low uncontrolled NO_x conditions. The former applies to boilers such as cyclones, cell-burners, and wet-bottomed boilers. The latter estimate applies to boilers such as dry-bottomed tangential and wall-fired boilers. We average the NSR and NO_x reductions predicted by ICAC and UARG, and use these values as estimates for typical operating conditions for high and low NO_x boilers. These estimates are presented in Figure 4-7 and Figure 4-8.

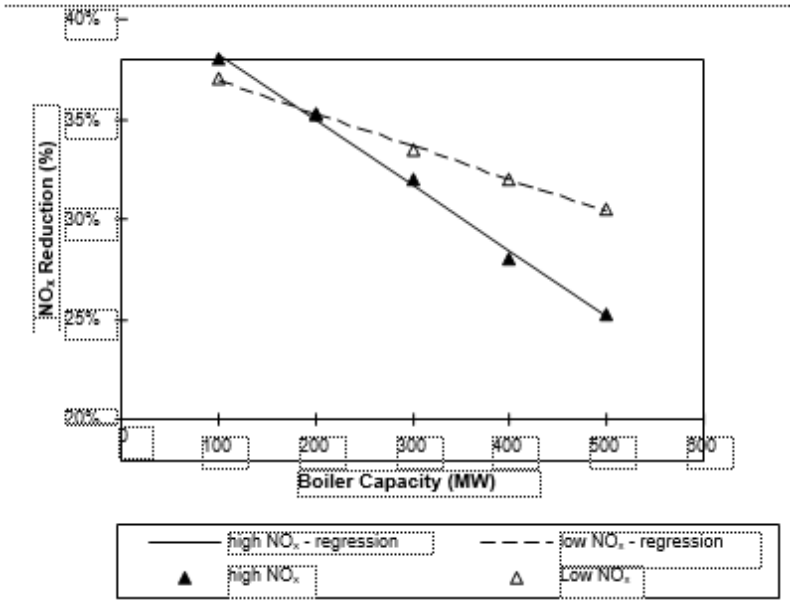

Figure 4-7. Modeled typical NO_x reductions versus boiler capacity

The correlation for the low NO_x case is:

$$\text{reduction} = 0.38525 - 1.625x10^{-4}\,\text{MW} \qquad (4\text{-}20)$$

$R^2 = 0.99$

and for the high NO_x case is:

$$\text{reduction} = 0.41525 - 3.275x10^{-4}\,\text{MW} \qquad (4\text{-}21)$$

$R^2 = 0.99$

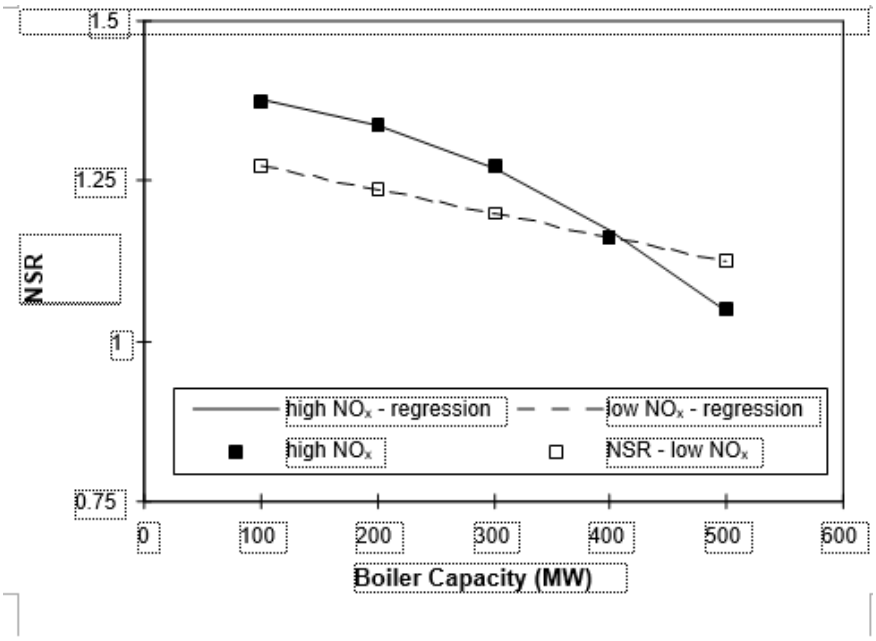

Figure 4-8. Model NSR versus boiler capacity

The correlation for the low NO_x case is:

$$NSR = 1.3125 - 3.75x10^{-4} MW \quad (4\text{-}22)$$

$R^2 = 1$

and for the high NO_x case is:

$$NSR = 1.3871 - 3.5327x10^{-5} MW - 1.433x10^{-6}(MW)^2 \quad (4\text{-}23)$$

$R^2 = 0.99$

Therefore, the algorithm to estimate typical reductions is:

1. Specify the boiler capacity
2. Specify the boiler type, (i.e., uncontrolled NOx emission)
3. Estimate typical NOx reductions using correlations represented in Equations (4-20) and (4-21)
4. Estimate the NSR using correlations represented in Equations (4-22) and (4-23)

It should be noted that UARG is most conservative and ICAC most optimistic about SNCR performance. For a given application, UARG typically estimates the highest reagent consumption, highest capital cost and lowest NO_x reduction; the ICAC estimates are generally the lowest for reagent consumption and capital cost, and highest for NO_x reduction. These differences may reflect the different perspectives of electric utility companies (UARG) and equipment manufacturers (ICAC). We attempt to remove or mitigate any systematic biases by averaging the estimates provided by different organizations.

4.7.2. Estimating NSR performance away from typical conditions

The above section provides an algorithm to predict NO_x reductions and NSR when the SNCR system is operated at typical operating conditions, namely, full load and an NH_3 slip limit of 10 ppm. How does performance change away from typical operating conditions?

Reducing the level of allowable slip will require operating at lower NSR, which in turn will result in lower reduction. To estimate the change in reduction, we develop a correlation between normalized forms of reduction and slip. The normalized forms are listed in Table 4-5.

Table 4-5. Normalized Forms of Performance Variables

Variable	Normalized Form	Definition
NH_3 slip	Δslip	reported slip - 10ppm
NO_x reduction	$\overline{\text{redn}}$	$\frac{\text{reported redn} - \text{redn}_{10}}{\text{redn}_{10}}$ redn_{10} is the reduction @10 ppm slip

We develop the variables in this manner to eliminate NO_x reduction effects idiosyncratic to the particular SNCR application. This correlation was developed using test data from several test programs [Hofmann, 1993 #28; Hunt, 1993 #47], and is presented in Figure 4-9. Consider the point (11,0.21) at the extreme left of Figure 4-9. The interpretation of this point is as follows: when the slip increased by 11 ppm from design (i.e., a slip of 21 ppm), the NO_x reduction increases to 121% of what it was at a slip of 10 ppm. For example, if the NO_x reduction was 40% at 10 ppm, at 21 ppm it would be 1.21 x 40% = 48.4%. Note that a negative Δslip corresponds to a reported slip of less than 10 ppm and a Δslip of -10ppm would imply a reported slip of zero ppm.

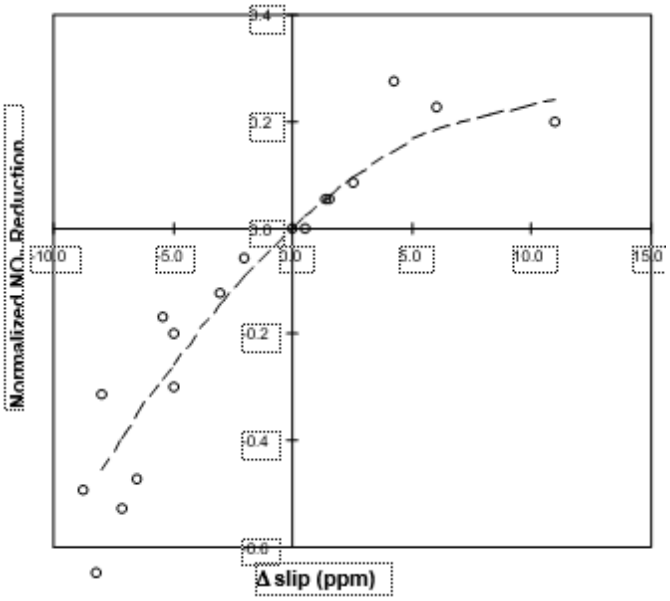

Figure 4-9. Correlation between Δslip and $\overline{\text{redn}}$

The equation for the correlation is:

$$\overline{redn} = (0.042195)(\Delta slip) - (0.001835)(\Delta slip)^2 \qquad (4\text{-}24)$$

$R^2 = 0.89$

When using this correlation to estimate reduction at a slip level other than 10 ppm, we use the value of redn_{10} predicted by Equations (4-20) or (4-21) as the normalizing factor for NO_x reduction. Using this correlation, changes in NO_x reduction because of a change in the allowable slip can be estimated. Note that this correlation is only valid for Δslip between -8 and 8 ppm, which should cover most operating conditions of practical interest. Also, the use of this correlation is predicated on the assumption that changes in slip and NO_x reduction are brought about only by changes in

NSR. This correlation does not consider other factors, such as changes in mixing or flue gas temperature distribution that can result in lowered NO_x reduction and higher slip, even if the NSR remains unchanged.

Next, the change in NSR corresponding to this change in NO_x reduction is estimated by developing a correlation between normalized forms of NO_x reduction and NSR. The forms and their definitions are given in Table 4-6.

Table 4-6. Normalized Forms Used for Reduction - NSR Correlation

Variable	Normalized Form	Definition
NSR	$\overline{NSR}$	$\frac{reported\ NSR - NSR_{typ}}{NSR_{typ}}$ NSR_{typ} is the typical operating NSR
NO_x reduction	$\overline{redn}$	$\frac{reported\ redn - redn_{typ}}{redn_{typ}}$ $redn_{typ}$ is the reduction @ average NSR.

The average NSR of 1.04 was chosen as NSR_{typ} to normalize the NSR data. Again, we define the variables in this manner to eliminate NO_x reduction effects idiosyncratic to the particular SNCR application. This correlation too was developed using test data from several test programs [Hofmann, 1993 #28; Hunt, 1993 #47], and is presented in Figure 4-10. Consider the point (0.18,0.85). The interpretation of this point is as follows: when NO_x reduction increases by 18% of its value when the NSR is 1.04, urea consumption increases by 85% from when the SNCR operated at typical NSR levels. For example, if the NO_x reduction were 40% at an NSR of 1.04, then increasing NO_x reduction by 0.18 x 40% = 7.2%, increases the NSR by 0.85 x 1.04 = 0.884.

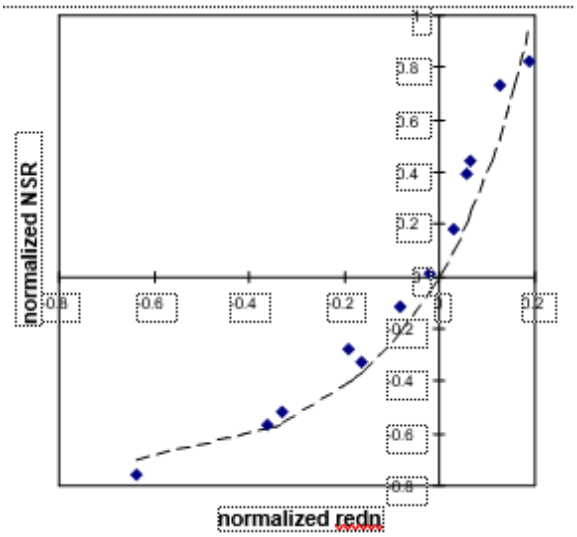

Figure 4-10. Correlation between NO_x reduction and NSR.

The correlation equation is:

$$\overline{NSR} = 0.425356 \times \left[e^{(\overline{redn}+1)^{2.172}} - e^{1} \right] \qquad (4\text{-}25)$$

$R^2 = 0.94$

Once the $\overline{NSR}$ is calculated, the new NSR can be calculated by using the value of operating NSR calculated from Equations (4-22) or (4-23) as NSR_{typ}. An exponential form has been chosen to ensure that the slope of the normalized form of NSR versus NO_x reduction is continuously increasing, as would be expected in all SNCR operations.

4.8. Mass and Energy Calculations

This section presents calculations of the relevant mass flow rates and energy consumption that are subsequently used to calculate SNCR operating costs.

4.8.1. Urea Mass Flow

Urea consumption is calculated from the NSR and uncontrolled NO_x flow.

$$M_{urea} = NSR \times NO_{xi} \times Q \times \frac{60}{46} \times \frac{1}{2} \times \frac{1}{2000} \quad (4\text{-}26)$$

where,

M_{urea} urea mass flow rate (tons/h)

NO_{xi} initial uncontrolled NO_x emissions (lb/MBtu)

Q boiler heat input (MBtu/h)

60/46 conversion factor of ratio of molecular weights of NO_2 and urea

1/2 stoichiometric reaction ratio of urea and NO_2

1/2000 conversion factor for (tons/lb)

4.8.2. Water Flow to Boiler

Urea is generally diluted to a 15 - 20% solution before injection into the boiler. The water injected with the urea results in added flue gas losses.

$$M_{water} = M_{urea} \times \frac{(1-r)}{r} \quad (4\text{-}27)$$

where,

M_{water} mass flow rate of water into boiler (tons/h)

M_{urea} mass flow rate of urea (tons/h)

r urea concentration in reagent when injected into the boiler (expressed as a fraction)

4.8.3. Flue Gas Losses

The flue gas loss associated with the use of SNCR is the sensible and latent heat losses associated with water entering the boiler at room temperature and leaving the boiler as steam, at the flue gas exit temperature.

$$Q_{loss} = 0.002 M_{water} \left[1040 + 0.38(T_{exit} - T_{inlet})\right] \quad (4\text{-}28)$$

where

Q_{loss} increase in flue gas losses (MBtu/h)

M_{water} mass flow rate of water into boiler (tons/h)

1,040 latent heat of evaporation (Btu/lb)

0.38	specific heat of steam (Btu/lb F)
T_{exit}	flue gas temperature at air heater exit (F)
T_{inlet}	combustion air temperature at air heater inlet (F)
0.002	conversion factor to account for (lbs/ton) and (MBtu/Btu)

4.8.4. Parasitic Power Consumption

The SNCR system typically uses electricity for urea tank heaters, mixers and reagent pumps. Based on information presented in different sources [Colburn, 1996 #38; Staudt, 1998 #55], we assume that the parasitic power consumption is a constant 50 kW. Since the parasitic consumption is very small compared to the typical output of an electric utility power plant, we do not attempt to refine this estimate by examining its dependence on boiler or SNCR design and process parameters.

4.9. SNCR Process Costs

This section describes the capital and operating costs associated with the SNCR process. Note that like the performance models, the cost models too are applicable only for urea-based SNCR systems used on coal-fired boilers. The costs are discussed in order of their typical contribution to the total levelized cost of operation.

4.9.1. SNCR Variable Operating Costs

The cost of reagent is the principal cost of operating an SNCR system. As will be seen later, it typically constitutes 60 - 80% of the total levelized cost. Other variable costs include flue gas losses and parasitic power consumption, described in the previous section.

$$VC = \left[(P_{urea} M_{urea}) + (P_{fuel} Q_{loss}) + (P_{elec} * \text{parasitic power})\right](CF)(8766) \qquad (4\text{-}29)$$

where

VC	variable operating costs ($/yr)
P_{urea}	price of urea ($/ton)
P_{fuel}	fuel price ($/MBtu)
P_{elec}	electricity price ($/kWh)
CF	capacity factor (fraction)
8,766	conversion factor (hours/year)

4.9.2. SNCR Capital Costs

Published data on SNCR capital costs are available only for small and medium capacity boilers, and are summarized in Table 4-7 [Staudt, 1998 #55]. While these costs are not identified as constant or current dollars, since most of these projects were recently completed, they can be assumed to be constant 1995 dollars.

Table 4-7. Urea-Based SNCR Process Capital Costs

Plant	Boiler Capacity (MW)	Furnace Type	Capital Costs ($/kWg)
Salem Harbor 1, 2 and 3	85 85 185	Wall - dry Wall - dry Wall - dry	15 18 15
Somerset	112	Tang. - dry	15 - 16
Mercer 1 & 2[a]	321 321	Wall - dry Wall - dry	14 14
Seward 5	150	Tang. - dry	23b
B. L. England, Units 1, 2 & 3	138 138 160	Cyclone – wet Cyclone – wet Tang. - dry	15.4 12.5 9.4

[a] Mercer units are split furnaces, hence their economies of scale are comparable to installation on 160 MW units

Since capital cost data for larger capacity units are not available, we adopt an approach similar to that used for estimating SNCR performance, namely, using cost estimates provided by different organizations. Capital cost estimates for high and low- NO_x boilers as a function of boiler capacity are plotted in Figure 4-11 and Figure 4-12 respectively. In both plots, capital costs are reported in real 1995 dollars.

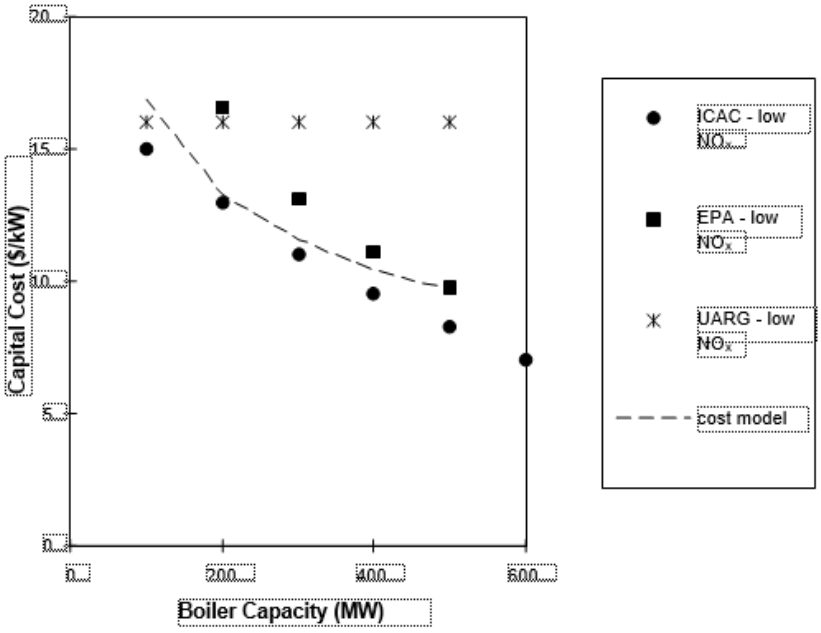

Figure 4-11. SNCR process capital cost estimates - low initial NO_x

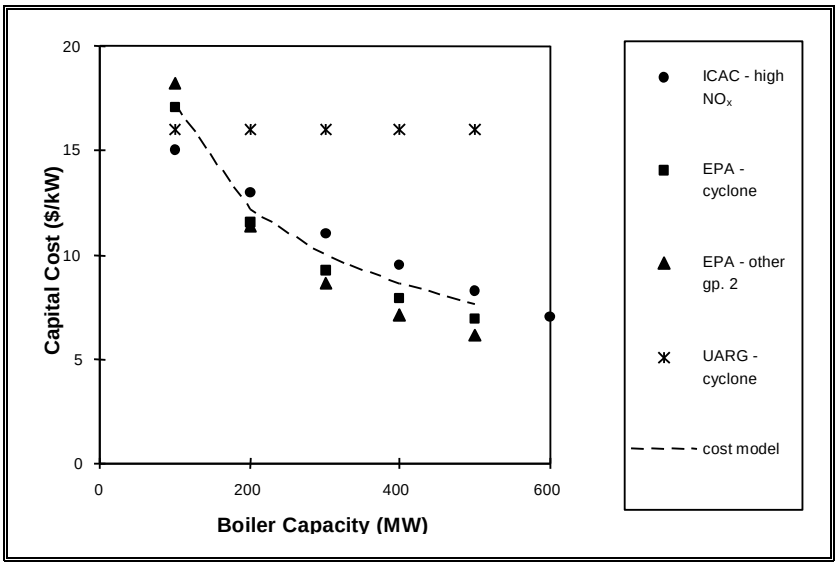

Figure 4-12. SNCR process capital cost estimates - high initial NO_x

The UARG estimates ignore economies of scale. Their uniform cost estimate of $16/kW is based on the average capital costs of SNCR installations on small capacity (100 - 200 MW) boilers. They justify ignoring economies of scale by assuming that added complexity of injectors required for larger installations will cancel out any other costs savings. However, injector cost is only a fraction of total cost for small capacity installations, and significant economies of scale can be expected in other components of the SNCR capital cost, such as urea storage and distribution systems, control systems and the engineering, design and installation costs.

To develop capital cost estimates, we selectively average estimates reported by ICAC, UARG and EPA. The estimates included at each boiler capacity are shown in Table 4-8, and the regression models developed using these estimates for high and low initial NO_x conditions are shown in Figure 4-11 and Figure 4-12 respectively.

Table 4-8. Estimates Included in Capital Cost Model

Boiler Capacity (MW)	ICAC	UARG	EPA
100	Yes	Yes	Yes (only for high NO_x case)
200	Yes	Yes	Yes
300 – 500	Yes	No	Yes

The correlation equation for the low initial NO_x case is:

$$\text{Capital Cost} = 82.97(\text{MW})^{-0.3454} \qquad (4\text{-}30)$$

$R^2 = 0.86$

and for the low initial NO_x case is:

$$\text{Capital Cost} = 173.1(\text{MW})^{-0.5013} \qquad (4\text{-}31)$$

$R^2 = 0.96$

where

Capital Cost = SNCR capital cost, real 1995 dollars per gross kilowatt ($/kWg)

MW = boiler capacity (MWg)

4.9.3. SNCR Fixed Operating & Maintenance Costs

Studies of eight power plants suggest that plant labor increases by only 8 man-hours per week for SNCR maintenance and inspection. Other fixed operating costs will include items such as periodic maintenance of the SNCR process equipment. NESCAUM has estimated fixed operating costs to be $50,000 per SNCR unit, and invariant with boiler capacity [Staudt, 1998 #55]. Other organizations have estimated the fixed operating costs as 1.5% of process capital costs [EPAa, 1998 #40; EPAb, 1998 #41; EPAc, 1998 #42; EPAd, 1998 #43]. We use the latter approach since fixed operating costs of environmental control technologies generally increase with size, and process capital costs can serve as a suitable proxy for size. Since fixed (O&M) operating and maintenance costs are a small fraction of the total levelized operating cost, we do not attempt to further refine our estimate.

$$FOC = 0.015 \times CC \qquad (4\text{-}32)$$

where

FOC = fixed O&M costs - constant 1995 dollars ($/year)

CC = capital costs ($)

4.10. Incorporating Uncertainty

The SNCR cost and performance model described so far is deterministic. However, as suggested by the wide variations in performance and cost estimates presented by different organizations for the same SNCR application, there is considerable uncertainty in these estimates, particularly for applications to larger capacity boilers. In this section, we present means for characterizing key uncertainties in the model's predictions.

It should be noted that this probability distributions presented are subjective estimates since no data is available on the commercial application of SNCR to boilers of capacity larger than about 200 MW. We have assumed a triangular distribution to represent our beliefs that the deterministic estimate is the most likely estimate, and because the support of this distribution is bounded. Further, the cumulative density function of a triangular distribution can be expressed in closed form, which facilitates subsequent numerical probabilistic simulations.

4.10.1. NO_x Reduction Potential

NO_x reduction estimates for low and high NO_x boilers in plotted in Figure 4-13 and Figure 4-14 respectively for different boiler capacities. The solid straight line shows the deterministic NO_x reduction estimate developed earlier. Estimates developed by other organizations that was averaged to develop this estimate is shown as filled symbols; estimates not used are shown as "+" and "x" symbols.

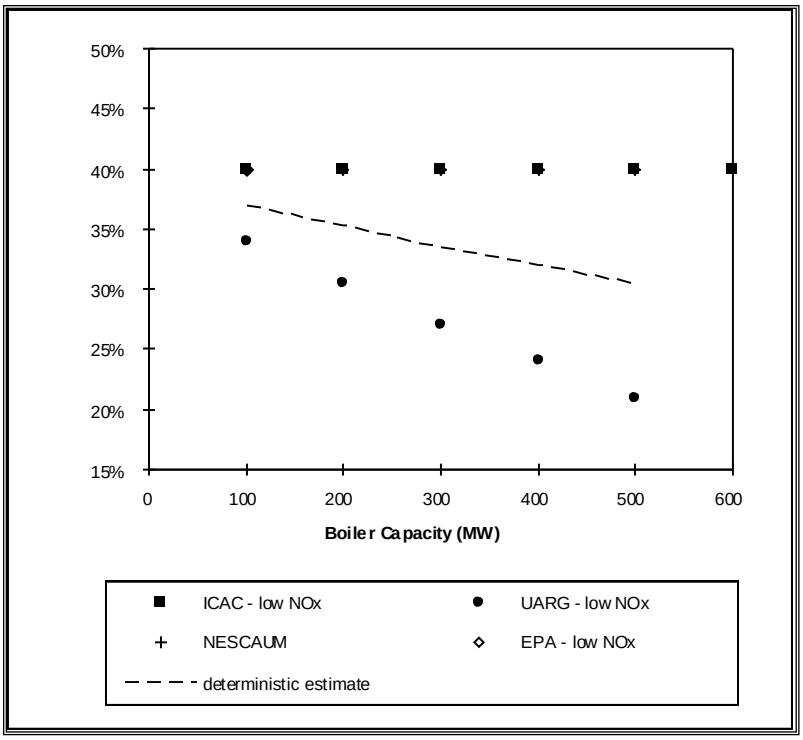

Figure 4-13. NO_x reduction estimates for low NO_x boilers

Note: ICAC, NESCAUM and EPA data points are coincident.

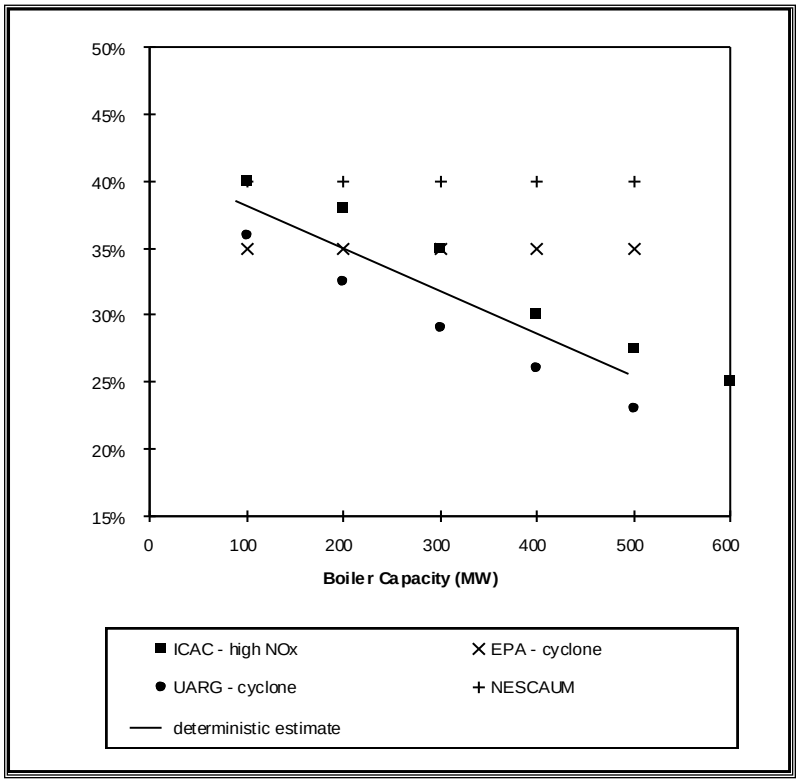

Figure 4-14. NO_x reduction estimates for high NO_x boilers

We assume that NO_x reductions at a given boiler capacity have a symmetric triangular distribution, centered at the deterministic estimate, with 95% of the probability mass contained between the minimum and maximum estimates used to develop the deterministic estimate for that particular boiler capacity. As can be inferred from Figure 4-13, the bounds on the estimate for NOx reduction grows with the level of NOx reduction. Accordingly, for the low NOx case, we incorporate the uncertainty by multiplying the typical value by a factor that has a symmetric triangular distribution with a mode of 1.0, a minimum of 0.71, and a maximum of 1.29.

For high NO_x boilers, as seen from Figure 4-14, the variability is invariant with reduction or boiler capacity. Accordingly, we model the uncertainty by adding to the deterministic model prediction a factor which has a symmetric triangular distribution with a mode of 0.0, a minimum of -0.06, and a maximum of +0.06.

4.10.2. Reagent Consumption

Uncertainties in this parameter are captured through variations in NSR. We consider two sources of uncertainty in NSR:

1. Uncertainty in the actual NO_x reductions achieved versus predicted. This source of uncertainty is described in the previous section. If NO_x reductions are higher than estimated by the deterministic model, NSR will also be higher, and vice-versa. This source of uncertainty can be viewed as caused by uncertainty of the capability of the SNCR process. This deviation in NSR from the deterministically predicted value is estimated from the deviation of NO_x reduction from the deterministically estimated value and the NSR-reduction correlations developed. The methodology will be explained later.
2. Uncertainty in reagent utilization. This represents uncertainty in how efficiently reagent will react with NO_x to form N_2. The NSR versus MW correlations and the correction to NSR made above assume that reagent utilization will be at typical levels. Measured levels of NSR are plotted versus NO_x reduction in Figure 4-15, using the same data used earlier to develop the correlation between NSR and NO_x. As is apparent from the figure, NSR levels increase with increasing NO_x reduction, and the variability in NSR also increases with increased NO_x reduction. Combining these two observations, we see that the variability can be modeled to be directly proportional to the nominal level of NSR. Accordingly, we incorporate the variability in NSR values by multiplying the typical value by a factor that has a symmetric triangular distribution with a mode of 1.0, a minimum of 0.75, and a maximum of 1.25.

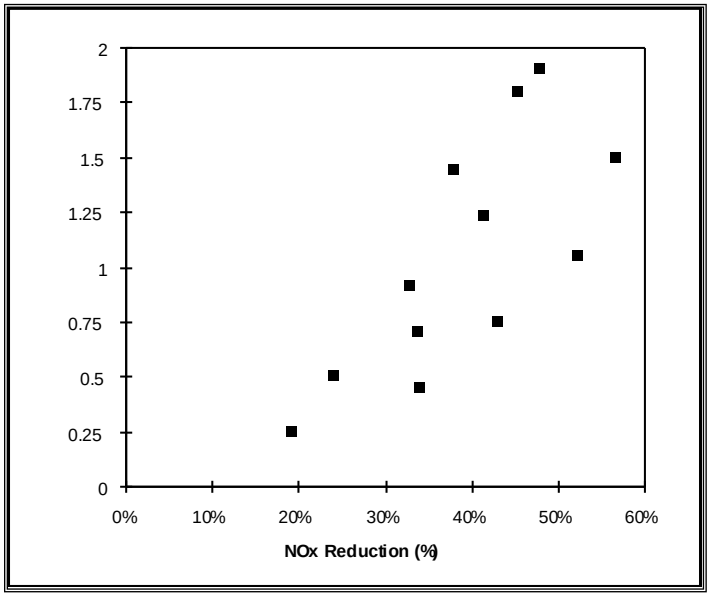

Figure 4-15. Variability of NSR at different NO_x reduction levels

4.10.3. Uncertainties in Process Capital Costs

Process capital costs reported from different sources for low and high NO_x boilers are plotted against boiler considerable variability was found in the cost estimates provided by different organizations. Restricting our attention to only those

estimates considered when developing the deterministic model, we see that the upper and lower bounds of these estimates are somewhat parallel to the deterministic model line. We assume that 95% of the probability mass is contained between these bounds, and model the uncertainty by adding to the deterministic model a factor which has a symmetric triangular distribution with a mode of 0.0, a minimum of -1.08, and a maximum of +1.08.

4.11. Sample Calculations

Estimates of performance and cost of several different SNCR systems using the models described in this report are presented in Table 4-9.

Table 4-9. Sample Calculations

Model Inputs					
SNCR Performance Inputs					
Boiler Capacity	MW	200	200	500	500
Heat Input	MBtu/h	2000	2000	2000	2000
Capacity Factor		0.7	0.7	0.7	0.7
Uncontrolled NO_x	lb/MBtu	0.9	0.9	0.9	0.45
Allowable Slip	ppm	10	2	10	4
Urea Concentration in Reagent		0.2	0.2	0.2	0.2
Preheated Flue Gas Exit Temp	F	350	350	350	350
Preheated Comb. Air Inlet Temp	F	100	100	100	100
Cost Inputs					
Capacity Factor		0.7	0.7	0.7	0.7
Capital Recovery Factor	1/yr	0.1	0.1	0.1	0.1
Urea Price	$/ton	300	300	300	300
Fuel Price	$/MBtu	1.5	1.5	1.5	1.5
Electricity Price	$/kW	0.03	0.03	0.03	0.03

Performance Calculations					
Use high NO_x correlations?		No	No	No	No
NO_x reduction predicted at typical operating conditions		35%	35%	25%	30%
NSR predicted at typical operating conditions		1.32	1.32	1.01	1.13
Δslip		0.0	-8.0	0.0	-6.0
Normalized NO_x redn. - result from slip adjustment & input for NSR calculation		0.00	-0.46	0.00	-0.32
Final NO_x reduction		35%	19%	25%	21%
Normalized NSR		0.00	-0.64	0.00	-0.55
Final NSR		1.32	0.48	1.01	0.51
Utilization		26%	40%	25%	41%
Mass Flow Calculations					
Urea	Tons/h	0.78	0.28	0.59	0.15

Water	Tons/h	3.11	1.12	2.37	0.59
Energy Calculations					
Flue gas loss	MBtu/h	7.05	2.54	5.39	1.35
Parasitic power consumption	KWh/h	50.00	50.00	50.00	50.00
Cost Calculations					
Urea	M$/yr	1.43	0.51	1.09	0.27
Fuel	$/yr	28,584	10,280	21,852	5,457
Electricity	$/yr	9,204	9,204	9,204	9,204
Total Variable Operating Costs	M$/yr	1.47	0.533	1.12	0.29
Unit Capital Cost	$/kW	12.2	12.2	7.7	9.7
Total Capital Cost	M$	2.43	2.43	3.84	4.85
Levelized capital cost	M$/yr	0.24	0.24	0.38	0.48
Fixed Operating Costs	$/yr	36,468	36,468	57,592	72,737
Total Annual Costs	$/yr	1,746,576	813,085	1,565,189	845,164
Levelized NO_x removal costs	$/ton	904	772	1,127	1,479
Levelized Cost Breakup					
Urea		82%	63%	70%	32%
Fuel		2%	1%	1%	1%
Electricity		1%	1%	1%	1%
Levelized capital cost		14%	30%	25%	57%
Fixed Operating Costs		2%	4%	4%	9%

Model predictions for a range of boilers and operating conditions are presented in Table 4-9. Although we have not explicitly modeled reagent utilization, we see from the table that the model provides correct trends for this process variable, with utilization decreasing with increased levels of NSR or NO_x reduction. Also, we see that the costs of NO_x removal predicted are within the range reported in published literature.

In developing the SNCR cost models, an emphasis was placed on accurately predicting the cost of reagent consumption since it is the largest cost item for most applications. It is only in certain applications, such as SNCR use on large boilers with low slip limits, that capital costs become a significant component of total levelized cost. However, for such applications, levelized NO_x control costs using SNCR are also high and SNCR is unlikely to be the NO_x control technology of commercial choice.

4.12. Conclusion

In this report, we have developed models to estimate the performance and cost of commercial SNCR systems for NO_x reduction on electric-utility coal-fired boilers. These models are applicable to both pulverized coal and wet bottom boilers. No attempt has been made to model fluidized bed boilers, or boilers using other coal combustion technologies.

These models are empirical or semi-empirical in nature, since predicting SNCR performance and cost from first principles is beyond the scope of the IECM modeling framework. An emphasis has been placed on attempting to predict SNCR process parameters accurately in regions of commercial interest. Accordingly, we have restricted the capacity range of boilers modeled to 100 - 600 MW, and the range of NH_3 slip limits to 2 - 18 ppm.

The models presented here are intended for screening and preliminary analyses. Estimating the performance and cost of using an SNCR system at a particular site at the accuracy level required for a commercial contract will continue to require site-specific engineering feasibility study and detailed temperature and velocity measurements of the flue gas conditions in the upper furnace.

4.13. References

Chen, W., et al. (1997). 'Derivation and application of a global SNCR model in maximizing NO_x reduction'. EPRI-DOE-EPA Combined Utility Air Pollutant Control Symposium, Washington, DC. August 25 -29. Electric Power Research Institute, Palo Alto, CA.

Ciarlante, V. and Romero, C. (1997). 'Design and characterization of urea-based SNCR system for a utility boiler'. EPRI-DOE-EPA Combined Utility Air Pollutant Control Symposium, Washington, DC. August 25-29. Electric Power Research Institute, Palo Alto, CA.

Colburn, K. (1996). *Control Technologies and Options Workshop*. Ozone Transport Assessment Group. April 11.

Eddings, E., et al. (1998). 'Assessment of SNCR Performance on Large Coal-Fired Utility Boilers'. 1998 Conference on Selective Catalytic and Non-Catalytic Reduction for NO_x Control, Pittsburgh, PA. May 21 - 22. U.S. DOE, Federal Energy Technology Center.

EPAa (1998). Attachment A: EPA's assumptions for selective non-catalytic reduction to high-NO_x boilers. http://www.epa.gov/capi/otag/rnd3atta.html

EPAb (1998). *Attachment B: UARG's SNCR and SCR cost evaluation*. http://www.epa.gov/capi/otag/rnd3attb.html

EPAc (1998). Attachment C: ICIC's alternative assumptions for SCR, SNCR and hybrid costs and performance. http://www.epa.gov/capi/otag/rnd3attc.html

EPAd (1998). Using the Integrated Planning Model to estimate the costs of NO_x control strategies on electric power generation in OTAG's Round 3 analysis. http://www.epa.gov/capi/otag/rnd3NO_x.html

EPRI (1993). Retrofit NO_x Controls for Coal-Fired Utility Boilers. A Technology Assessment Guide for Meeting Requirements of the 1990 Clean Air Act Amendments. Electric Power Research Institute, Palo Alto, CA. TR-102906.

EPRIb (1997). *Retrofit* NO_x *Controls for Coal-Fired Utility Boilers - 1996 Update Addendum*. Electric Power Research Institute, Palo Alto, CA. TR-102906. May.

Hofmann, J., et al. (1993). 'Post combustion NO_x control for coal-fired utility boilers'. 1993 Joint Symposium on Stationary Combustion NO_x Controls, Miami Beach, FL. May 24 - 27. Electric Power Research Institute, Palo Alto, CA.

Hunt, T., et al. (1997). 'Using retractable lances to maximize SNCR performance'. EPRI-DOE-EPA Combined Utility Air Pollutant Control Symposium, Washington, DC. August 25 - 29. Electric Power Research Institute, Palo Alto, CA.

Hunt, T., et al. (1993). 'Selective non-catalytic operating experience using both urea and ammonia'. 1993 Joint Symposium on Stationary Combustion NO_x Controls, Miami Beach, FL. May 24 - 27. Electric Power Research Institute, Palo Alto, CA.

Jodal, M., et al. (1990). 'Pilot-scale experiments with ammonia and urea as reductants in selective non-catalytic reduction of nitric oxide'. Twenty-third symposium (International) on Combustion, The Combustion Institute.

Malone, P., et al. (1998). 'Cardinal Unit 1 Large Scale Selective Non-Catalytic Reduction Demonstration Project'. 1998 Conference on Selective Catalytic and Non-Catalytic Reduction for NO_x Control, Pittsburgh, PA. May 21 - 22. U.S. DOE, Federal Energy Technology Center.

Miller, J. A. and Bowman, C. T. (1989). 'Mechanism and modeling of nitrogen chemistry in combustion.' *Prog. Energy Combustion Science* **15**:

Rini, M. J., et al. (1993). 'Evaluating the SNCR process for tangentially-fired boilers'. 1993 Joint Symposium on Stationary Combustion NO_x Controls, Miami Beach, FL. May 24 - 27. Electric Power Research Institute, Palo Alto, CA.

Siebbers, D. L. and Caton, J. A. (1990). 'Removal of nitric oxide from exhaust gas with cyanuric acid.' *Combustion and Flame* **79**:

Staudt (1995). 'Commercial applications of urea SNCR for NO_x RACT compliance on a 112-MWe pulverized coal boiler'. EPRI/EPA 1995 Symposium on Stationary Combustion NO_x Control, Kansas City, MO. May. Electric Power Research Institute, Palo Alto, CA.

Staudt, J. (1998). Status report on NO_x control technologies and cost effectiveness for utility boilers. NESCAUM, Boston, MA. June.

5. Selective Catalytic Reduction

5.1. Nomenclature

5.1.1. Performance Models

5.1.1.1. English Letter Symbols

a = Constant

A_c = Catalyst area, ft^2

A_{min} = Minimum catalyst activity level

A_{inc} = Incremental catalyst activity subject to exponential decay ($1-A_{min}$)

AV = Area velocity, ft/hr

c_f = Annual plant capacity factor, fraction of year

C = Constant representing catalyst activity for a given operating condition (e.g., temperature, inlet NO_x concentration) with NH_3/NO_x ratio equal to 1.0

$\vec{C}_i$ = Vector of concentrations of trace species in stream i, ppmw

$C_{NH3,hc}$ = Concentration of ammonia in "high concentration" wash water, mg/l

$C_{NH3,k}$ = Concentration of ammonia in "low concentration" wash water, mg/l

C_r = Ratio of catalyst activities for two catalysts.

E_a = Activation energy

E_i = Energy penalty for system i, MW

f_{FGD} = Fraction of gas-gas heat exchanger pressure drop that is normally associated with FGD flue gas reheat.

f_{hc} = Fraction of ammonia deposited on air preheater surfaces removed in high concentration wash water.

f_i = Generic correction factor

F_1 = Fraction of flue gas exiting FGD system that leaks across gas-gas heat exchanger in tail-end SCR system

f_{NH_3} = Fraction of ammonia slip partitioned to fate i (e.g., "dep"=deposition on air preheater surfaces, "abs"=absorbed by flyash, "out"=emitted with flue gas)

f_{ox} = Fraction of SO_2 oxidized to SO_3 in the SCR reactor.

f_r = Ratio of correction factors for linear velocity and temperature

G_{FG}	=	Flue gas volumetric flow rate, ft^3/hr at standard conditions
G_{scr}	=	Flue gas volumetric flow rate in the SCR system, ft^3/min
$H_i(T_j)$	=	Enthalpy of gas i at temperature j, Btu/lbmole
H_r	=	Ratio of catalyst layer heights
HR_g	=	Gross plant heat rate, Btu/kWh
HR_s	=	Steam cycle heat rate, Btu/kWh
k	=	Reaction rate constant. Also interpreted as catalyst "activity."
L_C	=	Catalyst life, years
m	=	End-mole ratio
m_i	=	Mass flow rate of species i, lb/hr
M_i	=	Molar flow rate of species i, lbmole/hr
N_C	=	Number of active catalyst layers
$N_{C,a}$	=	Number of active catalyst layers replaced each year, yr^1
$N_{C,r}$	=	Number of active catalyst layers replaced at each replacement interval
N_I	=	Number of active catalyst layers installed initially
N_R	=	Number of reserve catalyst layers installed at end of first catalyst replacement interval
n_d	=	Number of dummy catalyst layers
Q_r	=	Ratio of flue gas flow rates
p_i	=	Partition factor within a partition factor matrix for trace species i
$\mathbf{P}_{i\square j}$	=	Partition factor matrix for partitioning of trace species from stream i to stream j.
r_e	=	Exit molar ratio of NH_3 to NO_x at SCR reactor outlet.
r_{ea}	=	Ratio of air to stoichiometric requirement (excess air ratio).
R	=	Universal gas constant
R_A	=	Ratio of ammonia to nitrogen oxides, molar basis
R_g	=	Geometric ratio, ft^2/ft^3
R_S	=	Ratio of steam-to-ammonia, molar basis
S_r	=	Ratio of reactor cross-section areas
SV	=	Catalyst space velocity, 1/hr
SV_{ref}	=	Reference catalyst space velocity, 1/hr
t	=	Time, seconds
t_r	=	Catalyst replacement interval, hours
T	=	Temperature
V_c	=	Total catalyst volume, ft^3
$V_{c,i}$	=	Initially installed catalyst volume, ft^3
$V_{c,a}$	=	Volume of catalyst replaced each year, ft^3/yr
$V_{c,r}$	=	Volume of catalyst replaced at each replacement interval, ft^3/interval
$[NH_3]_{out}$	=	Ammonia slip, ppm

[x] = Concentration of species x, molar basis

5.1.1.2. Greek Letter Symbols

b_r = Ratio of fractions of reactor plugging

DH_r = Heat of reaction, Btu/lbmole reactant

DP_i = Pressure drop for component i

$?_{NO_X}$ = NO_X removal efficiency, fraction

$?_a$ = Time constant for catalyst activity decay.

5.1.1.3. Subscripts

cat = Catalyst

DB = Duct burner

duct = Ducting

dum = Dummy catalyst

FG = Flue gas

FGD = Flue gas desulfurization

GGH = Gas-gas heat exchanger

i = In

NG = Natural gas

o = Out

org = Organics

scr = Selective catalytic reduction

stm = Steam

tr = Trace species

WW = Wash water

5.1.2. Cost Models

c_f = Plant capacity factor (fraction of the year at full load)

C_{ProcC} = Cost of project contingencies, $1,000

$DC_{aph,mod}$ = Direct capital cost of air preheater modifications, $1,000

DC_{BF} = Direct capital cost of the booster fan for cold-side SCR, $1,000

DC_D = Direct capital cost of ductwork, $1,000

$DC_{D,CS}$ = Direct capital cost of ductwork for a cold-side SCR system, $1,000

DC_{DB} = Direct cost of duct burners for a cold-side SCR system, $1,000

DC_{GGH} = Direct capital cost of the gas-gas heat exchanger for cold-side SCR, $1,000

DC_{misc} = Direct capital cost of miscellaneous items, $1,000

DC_{NH_3} = Direct capital cost of the ammonia injection systems, $1,000

DC_R = Direct capital cost of reactors, $1,000

$EC_{ID,dif}$	=	Electricity consumption associated with SCR flue gas pressure drop, kWh
E_{scr}	=	Electricity requirement for SCR, kW
$f_{D,CS}$	=	Factor for cold-side SCR duct costs
f_{IC}	=	Factor for inventory capital costs (0.005 of non-catalyst direct costs)
f_{PP}	=	Factor for preproduction costs (0.02 of TPI)
$f_{projC,i}$	=	Project contingency factors for each process area.
$G°_{fg}$	=	Flue gas volumetric flow rate, referenced to a standard temperature (32°F) and pressure (1 atm), ft^3/hr
G_{fg}	=	Flue gas volumetric flow rate, at actual temperature and pressure, ft^3/hr
HHV_{NG}	=	Higher heating value of natural gas, Btu/lb
m_{fg}	=	Mass flow rate of flue gas, lb/hr.
m_{NG}	=	Mass flow rate of natural gas, lb/hr
$m_{NH_3 i}$	=	Mass flow rate of ammonia injected into the flue gas, lb/hr
$m_{NH_3 A,i}$	=	Molar flow rate of ammonia injected into the SCR system, lbmole/hr
M_{steam}	=	Molar flow rate of steam required for ammonia injection, lbmole/hr
MW_{fg}	=	Equivalent molecular weight of flue gas, lb/lbmole
N_{act}	=	Number of active catalyst layers at plant startup
N_{sp}	=	Number of spare catalyst layers at plant startup
$N_{R,TOT}$	=	Total number of reactor housings
$N_{T,aph}$	=	Total number of air preheaters
$N_{T,DB}$	=	Total number of duct burners
$N_{T,GGH}$	=	Total number of Gas-Gas Heat Exchangers
$P°_{fg}$	=	Reference pressure of the flue gas at standard conditions, 1 atm
PCI	=	*Chemical Engineering* Plant Cost Index. For Dec. 1989, PCI = 357.3
$\dot{Q}_{fg}$	=	Flue gas volumetric flow rate, actual ft^3/min
Q_{NG}	=	Heating value of natural gas used in duct burners, Btu/hr
R	=	Ideal Gas Constant, 0.730 $(fte^3$ atm)/(lbmole °R)
$SV°_{act}$	=	Active catalyst space velocity, referenced to a flue gas temperature of 32°F,1/hr
$T_{a,i}$	=	Temperature of air entering a heat exchanger, °R
$T_{a,o}$	=	Temperature of air exiting a heat exchanger, °R
$T°_{fg}$	=	Reference temperature of the flue gas at standard conditions, 32°F
$T_{fg,i}$	=	Temperature of flue gas entering a heat exchanger, °R
$T_{fg,o}$	=	Temperature of flue gas exiting a heat exchanger, °R
UA	=	Product of universal heat transfer coefficient and heat exchanger surface area, Btu/°R
UC_{cat}	=	Unit cost of catalyst, $\$/ft^3$
UC_{elec}	=	Unit cost of electricity, \$/kWh
UC_L	=	Unit cost of labor, \$/hour

$m_{NH_3 i}$ = Unit cost of ammonia, $/ton

UC_{steam} = Unit cost of steam, $/1,000 lb

$V_{C,A}$ = Volume of catalyst replaced annually, ft^3/yr

V_{TOT} = Total volume of the catalyst, including active and spare layers, ft^3

5.2. Introduction to SCR Technology

Selective catalytic reduction (SCR) is a process for the post-combustion removal of NO_x from the flue gas of fossil-fuel-fired power plants. SCR is capable of NO_x reduction efficiencies of up to 80 or 90 percent. SCR technology has been applied for treatment of flue gases from a variety of emission sources, including natural gas- and oil-fired gas turbines, process steam boilers in refineries, and coal-fired power plants. SCR applications to coal-fired power plants have occurred in Japan and Germany. Full-scale SCR systems have not been applied to coal-fired power plants in the U.S., although there have been small-scale demonstration projects.

Increasingly strict NO_x control requirements are being imposed by various state and local regulatory agencies in the U.S. These requirements may lead to U.S. SCR applications, particularly for plants burning low sulfur coals (Robie et al., 1991). Furthermore, implicit in Title IV of the 1990 Clean Air Act Amendment is a national NO_x emission reduction of 2 million tons per year. Thus, there may be other incentives to adapt SCR technology more generally to U.S. coal-fired power plants with varying coal sulfur contents. However, concern remains over the applicability of SCR technology to U.S. plants burning high sulfur coals or coals with significantly different fly ash characteristics than those burned in Germany and Japan. There is also concern regarding the application of SCR to peaking units due to potential startup and shutdown problems (Lowe et al., 1991).

5.3. Process History and Development

SCR was invented and patented in the U.S. in 1959. It was used originally in industrial applications. In the 1970s, SCR was first applied in Japan for control of NO_x emissions from power plants. Japan was the first country to make widespread use of this technology in response to national emission standards for NO_x. In Japan, SCR has been applied to gas, oil, and coal-fired power plants. There were over 200 commercial SCR systems operating on all types of sources in Japan in 1985. The Japanese SCR systems tend to run at moderate NO_x removal efficiencies of 40 to 60 percent (Gouker and Brundrett, 1991). By 1990, a total of 40 systems had been installed on 10,852 MW of coal-fired power plants (Lowe et al., 1991).

Germany currently imposes more stringent NO_x emission standards than Japan. To meet the emission requirements, SCR has been adopted and applied to many coal-fired power plants. SCR will be required as a retrofit technology on a total of 37,500 MW of existing capacity. As of 1989, SCR had been applied in 70 pilot plants and 28 full scale retrofit installations, with the latter totaling 7,470 MW of hard coal-fired capacity (Schönbucher, 1989). By 1990, more than 23,000 MW of capacity were fitted with SCR systems (Gouker and Brundrett, 1991). These plants typically burn low sulfur coals (0.8 to 1.5 percent sulfur) with 0.1 to 0.3 percent chlorine. SCR has been retrofitted to power plants with both wet and dry bottom boilers, with variations on the location of the SCR system. As of 1989, 18 installations involve placement of the SCR system between the economizer and air preheater, while the remaining involve "low dust" or "tail-end" placement of the SCR downstream of the FGD system. Two of the high-dust retrofits involve wet bottom boilers (Schönbucher, 1989). In 1991, 129 systems were reported to have been installed on a total of 30,625 MW of coal-fired capacity (Lowe et al., 1991). The recent German progress in installing retrofit SCR systems is shown graphically in Figure 5-1.

The process environment for SCR in Germany is typically more demanding than that in Japan, with the requirement for higher NO_x removal with higher flue gas sulfur and ash loadings (Gouker and Brundrett, 1991). In both Japan and Germany, the SCR systems are not operated during startup or shutdown (Lowe et al., 1991).

SCR is being applied in the U.S. for NO_x control of natural gas and oil-fired gas turbine-based power generation systems. In 1990 SCR was installed at a total of 110 gas turbine units totaling 3,600 MW (May et al., 1991). While the operating environment for these systems is not as demanding as for coal-fired power plant applications, some of these applications do provide experience with systems firing sulfur-bearing fuels that encounter problems analogous to those anticipated in

coal-based applications. In particular, ammonium salt formation and downstream effects have been studied (Johnson et al., 1990).

Recently, a number of U.S. projects for coal-fired applications of SCR technology have been initiated. These include, for example, a U.S. Department of Energy Clean Coal Program funded demonstration of SCR at Gulf Power Company's Plant Crist (DOE, 1992). SCR systems have also been permitted for two coal-fired cogeneration plants to be built in New Jersey (Fickett, 1993).

Since the 1970s, the cost of SCR has dropped substantially. For example, the levelized cost of SCR dropped by a factor of 3 in Japan within a 6-year period, while in recent years costs in Germany have dropped by an additional factor of 2. These improvements are due in part to the international competition among catalyst suppliers. SCR catalysts are available from manufacturers in Japan, Germany, and the U.S. U.S. manufacturers, such as Grace, expect improvements in catalysts to continue, resulting in potential further drops in capital and operating costs. For example, Grace is testing a new catalyst design that is expected to lead to a 50 percent increase in catalyst activity while also increasing catalyst life (Gouker and Brundrett, 1991).

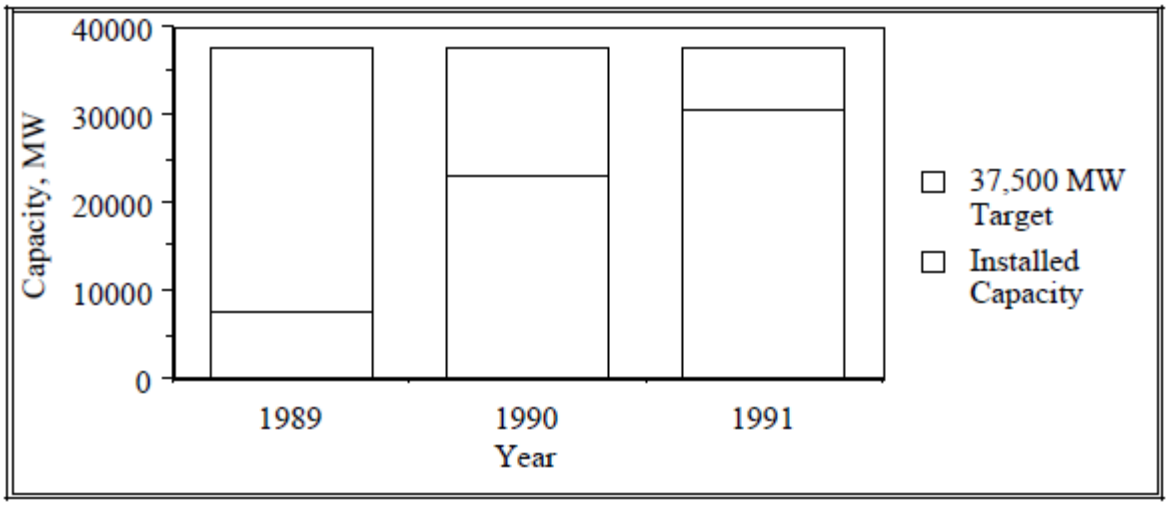

Figure 5-1. Targeted and Actual Installed Retrofit SCR Capacity in Germany

SCR has not yet been used commercially on coal-fired power plants in the U.S. The experience in Germany, which includes boiler types similar to those in the U.S., provides useful data for predicting SCR performance and cost in the U.S. However, U.S. coals, such as eastern bituminous coals, typically have a higher sulfur content than that of German coals. In addition, fly ash compositions may vary significantly. These differences lead to concerns about maintenance of catalyst activity and potential difficulties downstream of SCR reactors, such as deposition of ammonia salts.

The German experience is particularly useful for U.S. planners because German SCR systems are subject to a more relevant range of flue gas conditions than typical Japanese systems. For example, slagging wet bottom boilers produce different flue gas and flyash characteristics that can significantly affect catalyst performance (Offen et al., 1987).

5.4. Process Design

The general design considerations for the SCR NO_x control technology for coal-fired power plants are described here. These include the placement of the SCR system in a power plant, and a description of equipment associated with the SCR process area.

5.4.1. SCR Integration in the Power Plant

The SCR system can be located in several places in the coal-fired power plant flue gas stream (Schönbucher, 1989; Behrens et al., 1991). A key limitation of SCR systems is the operating temperature requirement. The operating

temperature window for SCR systems is typically from approximately 550 to 750°F. Several possible locations are illustrated in Figure 5-2. These are:

1. "Hot-side" and "high-dust" SCR, with the reactor located between the economizer and the air preheater. In this configuration, shown in Figure 5-2 (a), the SCR is located upstream of a cold-side ESP and, hence, is subject to a high fly ash or "dust" loading. At full-load, the economizer outlet temperature is typically around 700°F. An economizer bypass is required to supply hot gas to the SCR during part-load operating conditions, in order to maintain the proper reaction temperatures (Lowe et al., 1991).
2. "Hot-side, low-dust" SCR, which features placement of the SCR system downstream of a hot-side ESP and upstream of the air preheater and FGD systems. This configuration has been employed in some Japanese coal-fired power plants, such as Takehara Power Station Unit 1 in Hiroshima (Behrens et al., 1991). This configuration has the advantage of minimizing the fly ash loading to the SCR catalyst, which leads to degradation in catalyst performance.
3. "Cold-side" or "Tail-end" placement of the SCR system downstream of the air preheater, particulate collector, and FGD system. This system minimizes the effects that flue gas contaminants have on SCR catalyst design and operation, but requires a gas-gas flue gas heat exchanger and duct burners to bring the flue gas up to reaction temperature (Lowe et al., 1991).

The most common configurations envisioned for U.S. power plants are the hot-side high-dust and post-FGD tail-end systems (Robie et al., 1991), with high-dust systems predominating. These are the two most common configurations employed in German coal-fired power plants retrofitted with SCR.

Recent German experience indicates increasing acceptance for tail-end systems. Prior to 1987, the number of high-dust installations was twice that of tail-end installation. But since 1987, the number of tail-end installations has been slightly greater. The tail-end systems have tended to be installed on smaller plants, however, and account for about one-third of total installed capacity. They have been preferred for wet bottom boiler applications (Lowe et al., 1991).

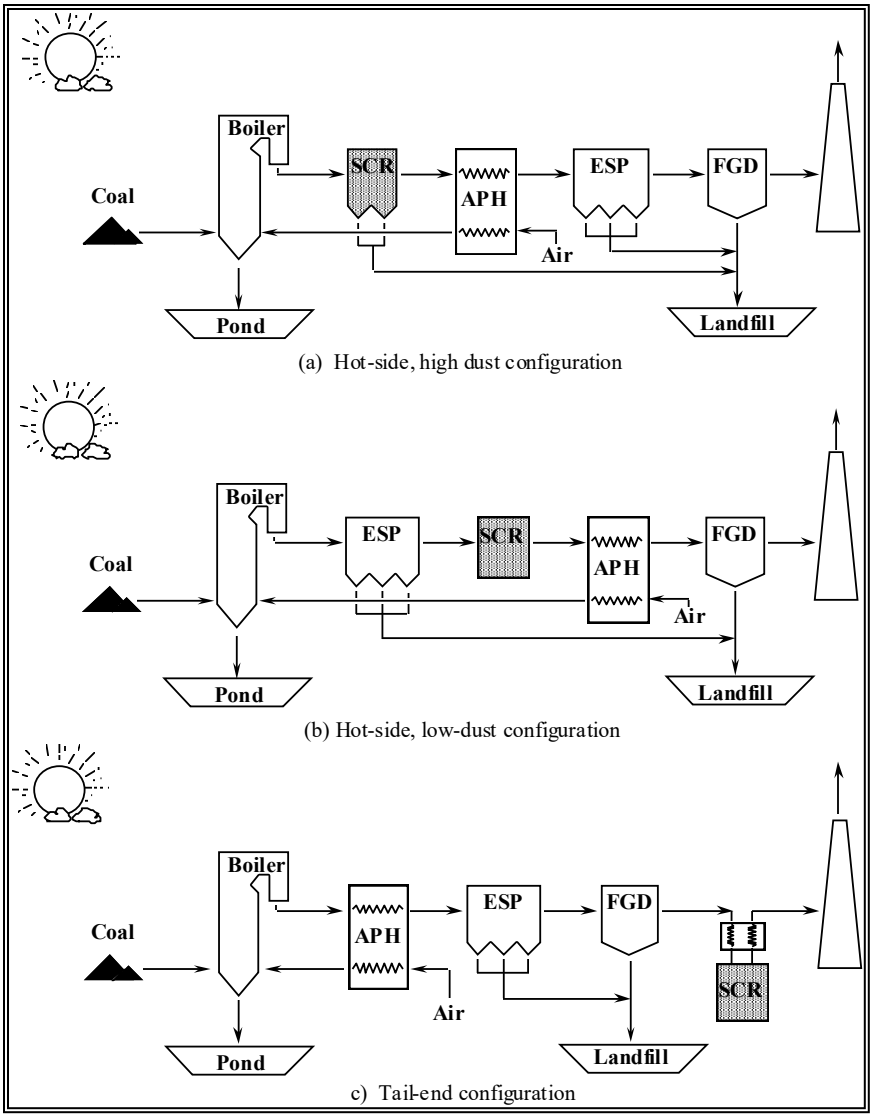

Figure 5-2. Alternative Placements of SCR systems in Coal-Fired Power Plants

In many evaluations, tail-end SCR systems have been charged with the full cost of flue gas reheat, even though a portion of the reheat would be necessary to maintain stack buoyancy for flue gas exiting the FGD system. Similarly, in comparing hot-side and tail-end systems, the significant efficiency penalty for the high-dust system when operating at part load, due to the need for economizer bypass, must be considered (Lowe et al., 1991).

5.4.2. The SCR Process Area

A schematic of the SCR System is given in Figure 5-3. The schematic assumes an SCR location in the hot-side, high-dust configuration. Ammonia is injected into the flue gas upstream of the SCR reactor vessel. The ammonia/flue gas mixture enters a reactor vessel, containing SCR catalyst. The catalyst promotes the reaction of ammonia and NO_x to form nitrogen and water vapor. Products of the SCR reactions may form ammonium sulfate or bisulfate, which can deposit on downstream equipment. Additional air preheater water washing is expected to be required to remove such deposits.

The SCR system consists primarily of a reactor housing containing catalyst material, an ammonia storage and handling system, an ammonia injection system, and a control system. In additional, air preheater wash water pretreatment may be required to remove ammonia from the wastewater.

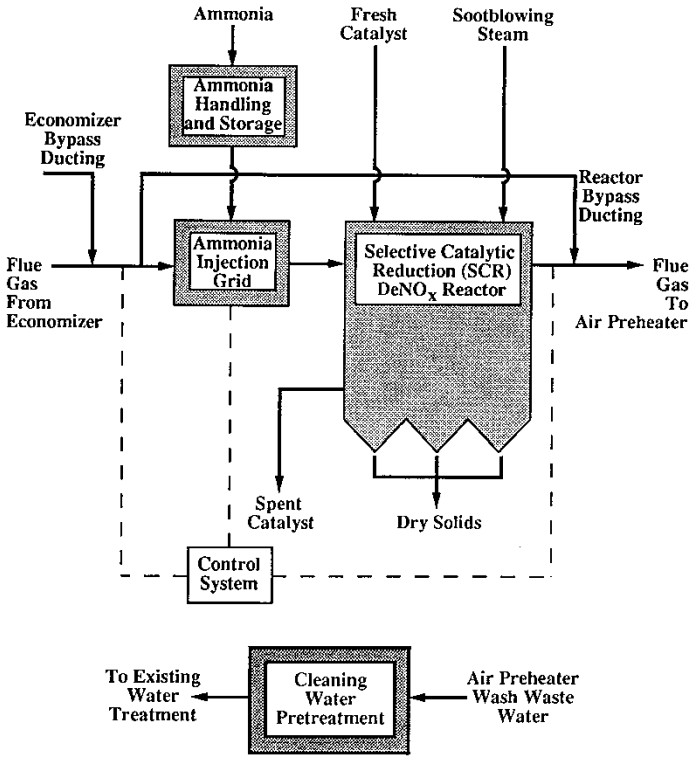

Figure 5-3. Schematic Diagram of SCR System

A more detailed schematic of the SCR reactor housing is shown in Figure 5-4. SCR design philosophy has evolved over the last 20 years due to the accumulation of operating experience in Japan and Germany. Based on Japanese experiences, both vendors and users of SCR technology have identified the following key design considerations for hot-side SCR systems (Lowe et al., 1991):

- Vertical downward flue gas flow to prevent ash accumulation and to allow ash drop out.
- Linear gas velocities of 16-20 ft/sec at maximum continuous rating to prevent ash accumulation. Higher velocities would be expected to increase catalyst erosion.
- Use of grid shaped catalyst with channel spacing (pitch) of 7 to 7.5 mm to allow passage of dust and prevent ash accumulation and erosion.
- Elimination of catalyst seams along the gas flow direction to prevent ash accumulation and erosion.
- Use of a "sacrificial" or dummy initial stage to prevent ash accumulation and erosion in downstream active catalyst layers.
- Removal of deposited ash using intermittent vacuuming or soot-blowing.
- Reliable ammonia feed control, including part load operation.
- Adequate ammonia feed distribution across the cross-sectional flue gas flow area.
- Flue gas ducting and guide vane designs that ensure good mixing of the flue gas and ammonia feed.

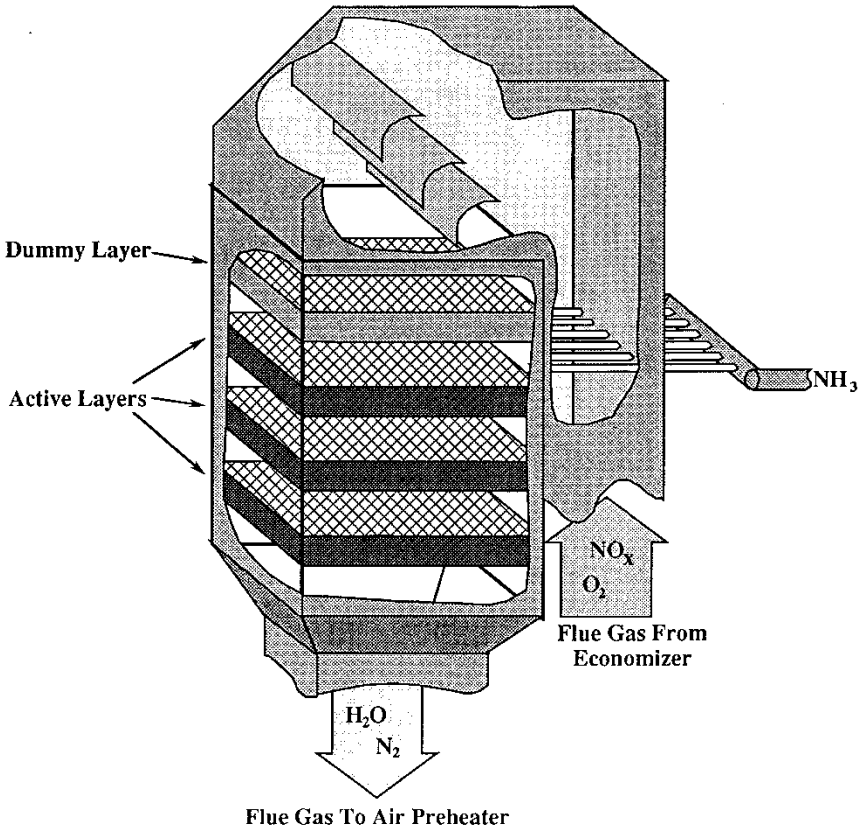

Figure 5-4. Diagram of SCR Reactor Housing with Downward Flue Gas Flow

A tail-end SCR system is illustrated in Figure 5-5 to show the configuration of the gas-gas heat exchanger and duct burner. The flue gas exiting the FGD system must be heated from approximately 130°F to a reaction temperature of approximately 625°F. The flue gas exiting the SCR can be cooled to a stack temperature near 225°F. Flue gas from the FGD system is preheating with flue gas exiting the SCR system in a heat exchanger. The SCR inlet flue gas is then heated to reaction temperature using a duct burner.

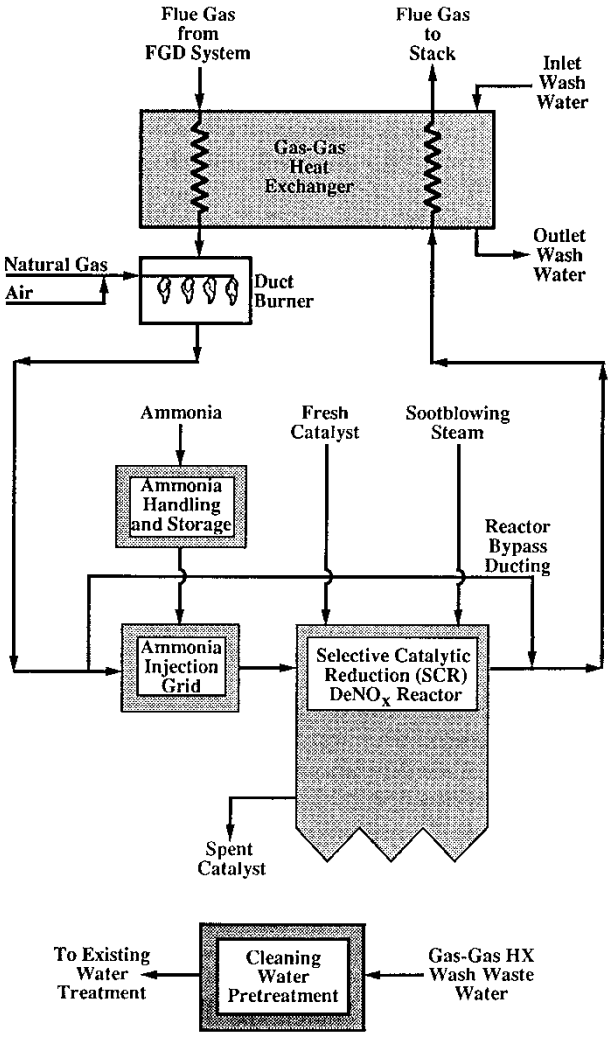

Figure 5-5. Schematic Diagram of Tail-End SCR System

5.4.2.1. Catalyst

SCR catalysts typically consist of a ceramic honeycomb substrate, a metal "carrier" and active components dispersed by the carrier on the honeycomb surfaces. A typical carrier is titanium dioxide (TiO_2). Vanadium pentoxide (V_2O_5) and tungsten trioxide (WO_3) are commonly used as active components for hot-side SCR applications (Schönbucher, 1989). WO_3 provides thermal and mechanical stability to the catalyst (Behrens et al., 1991). Catalysts based on titanium dioxide are best suited for operating temperatures of 280 to 400°C (536 to 752°F) (Schönbucher, 1989). At lower temperatures, catalyst activity drops substantially. At higher temperatures, catalyst material phase transition occurs, which causes irreversible activity loss (Bauer and Spendle, 1984). Catalysts using activated carbon may be employed for lower temperature applications near 100°C (212°F) (Schönbucher, 1989). The actual catalyst formulations which are offered commercially are closely held propriety information.

A key innovation from Japanese development of SCR technology has been the switch from noble metal oxides to base metal oxides for use as catalyst carrier materials, which has reduced many of the major problems associated with oil- and gas-fired flue gas applications. For coal applications, Japanese catalyst development also focused on improving catalyst geometry. To avoid plugging and erosion, parallel flow honeycomb and plate catalysts were developed. By the early 1980s, ceramic honeycomb and plate configurations have been developed that provide high surface areas while reducing the tendency for flyash plugging. In recent years, research has focused on understanding the deactivation mechanisms of SCR catalyst, particularly due to alkalis and trace metals such as arsenic (Gouker and Brundrett, 1991).

V_2O_5 is the component which controls the reactivity of the catalyst. However, it also catalyzes the conversion of SO_2 to SO_3 (Behrens et al., 1991), which may lead to opacity, ammonium salt deposition, or acid condensation problems downstream. For high-sulfur coal applications, the amount of V_2O_5 is minimized by homogeneous distribution throughout the catalyst. To obtain NO_x reduction, properly mixed ammonia and NO_x must enter micropores in the catalyst, which are the active sites for the reactions which consume NO_x.

The catalyst is typically installed in a reactor housing in three layers, with provision for a dummy layer for flow straightening and distribution. In some designs, provision is also made for a fourth active catalyst layer. In these cases, the initial catalyst charge consists of three active layers. When catalyst activity drops to the design value, a fourth active layer is added. Then the four layers are changed out periodically to maintain overall catalyst activity. Catalyst modules may be loaded and unloaded from the reactor housing using a fork-lift track assembly and/or rollers (e.g., Behrens et al., 1991)

Ceramic, homogeneous, honeycombed catalyst elements approximately 6 inches square can be extruded to a length of about 39 inches (Behrens et al., 1991). SCR systems subject to high-dust loadings often include a dummy honeycomb or leading edge to control catalyst erosion (Lowe et al., 1991). Catalyst honeycomb design depends on the location of the SCR system in the power plant. For high-dust systems, catalysts with a large pitch (spacing within honeycomb cells) are employed, to allow passage of fly ash. For low dust systems, smaller pitch catalysts can be used (Schönbucher, 1989). These catalyst designs are illustrated in Figure 5-6.

5.4.2.2. Ammonia Handling

In Germany, strict safety standards have been applied to the shipment and handling of ammonia. Shipments by truck are not permitted if they are larger than 500 liters. Thus, anhydrous ammonia is shipped primarily by rail. A 15–30-day supply is typically stored at the plant in two double wall tanks. Double walled piping is also typically employed. The ammonia is diluted to an 8 percent mixture prior to introduction to the flue gas. The ammonia is vaporized in German facilities using warm water. In many U.S. gas turbine installations, electrical heating is used (Lowe et al., 1991).

5.5. Technical Overview

This section presents a detailed technical overview of SCR NO_x control technology for coal-fired power plants, with particular focus on the effects of flue gas components on catalyst performance and the effects of the SCR system on the power plant.

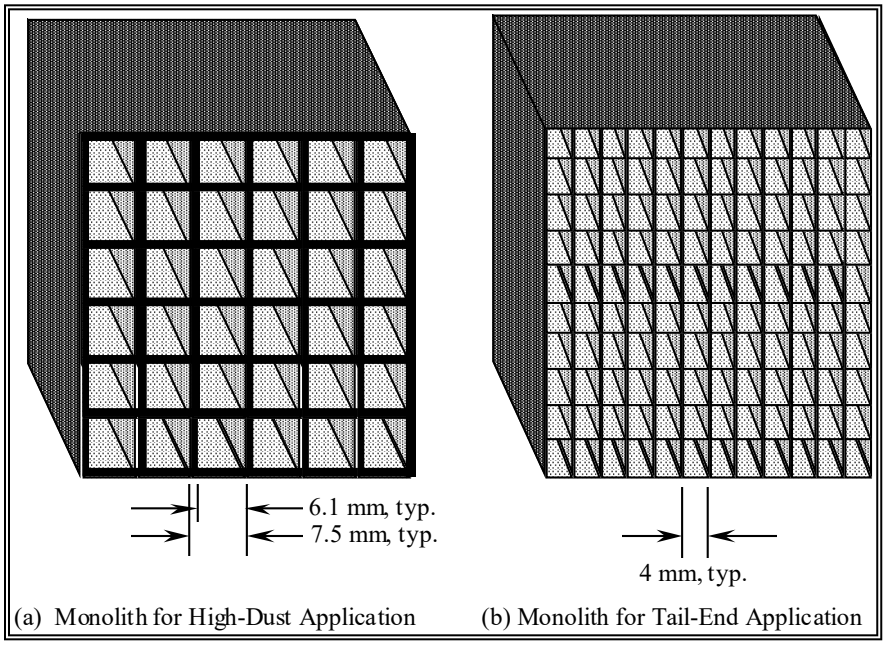

Figure 5-6. SCR Honeycomb Catalyst Monolith Designs

5.5.1. Process Chemistry

Nitrogen oxides in the flue gas are removed by reduction of NO_x by ammonia to nitrogen and water. The reduction occurs in the presence of a catalyst. Ammonia is injected in the flue gas upstream of the catalyst, as illustrated in Figure 5-3.

The principal reactions are:

$$4NH_3 + 6NO \rightarrow 5N_2 + 6H_2O$$

$$8NH_3 + 6NO_2 \rightarrow 7N_2 + 12H_2O$$

$$4NH_3 + 4NO + O_2 \rightarrow 4N_2 + 6H_2O \qquad (5\text{-}1)$$

$$4NH_3 + 2NO_2 + O_2 \rightarrow 3N_2 + 6H_2O$$

Of these reactions, Equation (5-1) is usually the most important. There is usually sufficient oxygen in the flue gas as a reactant. In addition, typically 90 to 95 percent of nitrogen oxides in the flue gas are in the form of NO.

Another overall reaction that may occur in the SCR unit is (Anderson and Billings, 1991):

$$2NH_3 + NO + NO_2 \rightarrow 2N_2 + 3H_2O \qquad (5\text{-}2)$$

The implication of the above reaction is that a molar ratio of ammonia to NO_x of 1:1 is sufficient to remove both NO and NO_2 when the NO/NO_2 mixture contains more than 50 percent NO.

Another important reaction occurring in the SCR reactor is the oxidation of sulfur dioxide:

$$2SO_2 + O_2 \rightarrow 2SO_3$$

Typically, 0.5 to 2 percent of the sulfur dioxide entering the SCR reactor is oxidized to sulfur trioxide (e.g., Bauer and Spendle, 1984). The resulting increased levels of sulfur trioxide at the SCR outlet increases the acid dewpoint of the flue gas, thus increasing the potential for sulfuric acid condensation on downstream components at temperatures of less than about 350°F. Sulfur trioxide may react with water vapor to form sulfuric acid (Johnson et al., 1990):

$$SO_{3(g)} + H_2O_{(g)} \leftrightarrow H_2SO_{4(g,l)}$$

where subscripts (g), (l), and (s) represent gas, liquid, and solid phases, respectively.

Unreacted ammonia exiting the SCR system ("ammonia slip") can react with sulfur trioxide to form compounds such as ammonium bisulfate and ammonium sulfate that deposit on downstream equipment. These compounds may result in plugging and corrosion. The key reactions for the formation of ammonium sulfate and bisulfate are (Johnson et al., 1990):

$$NH_{3(g)} + SO_{3(g)} + H_2O_{(g)} \leftrightarrow NH_4HSO_{4(l.,s)}$$

$$2NH_{3(g)} + SO_{3(g)} + H_2O_{(g)} \leftrightarrow (NH_4)_2SO_{4(l,s)} \qquad (5\text{-}3)$$

The formation of ammonium bisulfate (Equation (5-3)) is more sensitive to sulfur trioxide concentration than to ammonia concentration (Lowe et al., 1991).

As the flue gas cools in downstream equipment, the sulfuric acid may also react with ammonia to form condensate products (Johnson et al., 1990):

$$NH_{3(g)} + H_2SO_{4(g)} \leftrightarrow NH_4HSO_{4(l,s)}$$

$$2NH_{3(g)} + H_2SO_{4(g)} \leftrightarrow (NH_4)_2SO_{4(l,s)}$$

Reducing the ammonia slip and reducing the formation of sulfur trioxide can minimize the formation of ammonium bisulfate and other ammonia salts.

The key design considerations for SCR are the NO_x removal efficiency, the ammonia slip, and the SO_2 oxidation rate. While larger catalyst volumes allow higher NO_x removal efficiencies and/or lower ammonia slip, they tend to increase the oxidation of SO_2. Furthermore, large catalyst volumes significantly increase the capital and annual costs of SCR.

5.5.2. Catalyst Sizing

A key performance issue associated with SCR systems is the required catalyst volume and the catalyst replacement schedule. One parameter often used to measure catalyst volume is the space velocity, which is given by:

$$SV = G_{FG} / V_c$$

An alternative parameter is the area velocity, which is given by:

$$AV = G_{FG} / V_c$$

The relationship between the space velocity and area velocity depends on the "geometric ratio" of the catalyst, which is the unit surface area per unit volume of the catalyst.

$$R_g = \frac{A_c}{V_c}$$

For honeycomb monolith catalysts, the important design parameter that determines the geometric ratio is the "pitch," or spacing between the hollow cells through which the flue gas passes. As described earlier, the catalyst pitch depends primarily on the dust loading in the flue gas. Larger pitches are needed to accommodate high-dust loadings, resulting in a lower geometric ratio. Current catalysts for high-dust application typically have a pitch of around 7.5 mm, with a wall thickness of 1.4 mm and a channel thickness of 6.1 mm. For tail-end applications, pitches of around 4 mm are typical. For gas-fired applications, pitches of 3 mm are reported using ceramic plate-type catalysts. Catalyst using thin metal substrates may have a pitch as low as 0.2 mm for clean flue gas applications (Gouker and Brundrett, 1991).

The space velocity is commonly used to describe the catalyst requirement. However, both the space velocity and area ratio, or the space and area velocities, are needed in order to specify both the catalyst volume and the catalyst area in contact with the flue gas. For example, a high-dust SCR system typically requires a smaller space velocity (more catalyst) than a low-dust system, due primarily to the lower area ratio of the high-dust catalyst designs.

The space velocity is a function of the desired NO_x removal efficiency and the required ammonia slip. For example, one EPRI paper suggests a maximum space velocity of 2,500/hr for a NO_x reduction efficiency of 80 percent and an ammonia slip of 5 ppm (Damon et al., 1987).

Based on German experience, typical space velocities for high-dust SCR systems with honeycomb catalysts of about 7 mm pitch are 2,000 to 3,000/hr, whereas for tail-end systems employing honeycomb catalysts with pitches of approximately 4 mm space velocities are 4,000 to 6,500/hr. Thus, 50 to 60 percent smaller catalyst volumes per unit flue gas flow can be installed on tail-end systems for equivalent NO_x removal performance. However, the flue gas volumetric flow rate may be higher for tail-end systems than for high-dust systems, partially offsetting this advantage (Lowe et al., 1991).

The actual required catalyst volume for a given application depends on a number of site-specific factors. The amount of plugging or catalyst poisoning will determine the effective catalyst activity. The activity will decrease with operating time. Therefore, the initial catalyst volume must be large enough so that at the end of the design life there is sufficient active catalyst to maintain design performance levels.

Most SCR designs have a three-layer catalyst. Although most U.S. SCR studies assume that all catalyst layers are changed out simultaneously, most Japanese and German designs are based on periodic replacement of only one catalyst layer at a time. Therefore, at any given time, there may be three layers with differing lengths of service and differing activity levels. In determining the initial catalyst charge, it is necessary to account for the loss of catalyst activity at the design point in the catalyst replacement scheme. For a three-layer catalyst, the design point is the fourth catalyst change out.

To determine the catalyst activity at the design point, it is necessary to estimate the loss of catalyst activity as a function of time. Catalyst activity loss is a function of the catalyst formulation and geometry, the operating conditions associated with the flue gas, including temperature and composition, and the loading and composition of the fly ash. Recent papers, such as those presented at the 1991 Symposium on Stationary NO_x Control, provide examples of catalyst activity loss curves for specific power plant applications in Germany (e.g., Behrens et al., 1991; Gouker and Brundrett, 1991; Maier and Dahl, 1991).

5.5.3. Catalyst Fouling and Poisoning

Commercial operating experience in both Germany and Japan have provided insight into the mechanisms for catalyst fouling and poisoning. For coal-fired power plant applications, the primary cause of loss of catalyst activity was attributed to interactions between the catalyst and the flyash. As summarized by Gouker and Brundrett (1991), flyash has several effects on the catalyst, including:

- Fouling: Sub-micron ash particles may accumulate on the surfaces of the catalyst, and block the pores of the catalyst. This fouling or masking prevents NO_X and ammonia from reaching active catalyst sites, thereby reducing the effective catalyst surface area. This leads to a reduction in the performance of the catalyst.
- Plugging: Bulk plugging of the catalyst occurs when large accumulations of dust occur. Dust plugging may occur, for example, when large pieces of flyash on upstream equipment "flake" off. Wire screens located upstream of the catalyst help to break up these flakes. Soot blowing may also be required periodically to remove the flakes from the catalyst.
- Poisoning: Alkali metals from flyash are a source of catalyst poisoning. Water soluble alkali salts may be leached onto the catalyst due to moisture present on fly ash during startup or shutdown of the SCR unit. Alkali salts have been shown to form inactive complexes with vanadium and tungsten in laboratory studies.
- Erosion: Erosion problems may arise due to flue gas flow distribution problems. Flow straightening vanes and dummy "catalyst" layers have been employed in many installations to reduce this type of problem.

5.5.3.1. Japanese and German Experience

Due to improvements in catalyst technology, catalysts in Germany are not experiencing as much loss of activity as initially predicted based on Japanese high-dust, coal-fired applications (Gouker and Brundrett, 1991).

Behrens et al. (1991) report that the typical levels of potential catalyst poisons in the flyash of Ruhr coal have "not appeared to significantly accelerate catalyst deterioration" of the hot-side high-dust SCR unit at the Reuter West power station. These contaminant levels include 4 to 5 percent K_2O, 6.3 percent of CaO, 1.5 percent of MgO, and 0.6 percent of P_2O_5. However, data reported by them does indicate that catalyst activity decreased to 65 percent of the level of the fresh catalyst after 30,000 hours.

At the Aichi 40 MW coal-fired boiler burning low sulfur coal, a hot-side high-dust SCR arrangement is employed. The catalyst has experienced low deterioration. After 30,000 hours of operating, the catalyst activity is 75 percent of the fresh catalyst. The primary cause of deactivation is reported to be the deposition of CaSi on the catalyst surface (Behrens et al., 1991).

While arsenic is commonly cited as the most significant catalyst poison, small sticky dust particles can cause more serious deactivation than arsenic. Furthermore, in some cases, SCR fires due to dust accumulations have occurred in Japan (Lowe et al., 1991).

German experience with SCR catalyst indicates that catalyst "lifetimes" of 3 to 4 years are possible and typical for high-dust systems. For tail-end systems, some operators report no measurable catalyst degradation, and expect to achieve up to 80,000 operating hours on a single catalyst charge. Japanese experience on clean flue gases has been similar (Lowe et al., 1991).

In many German wet bottom boilers, fly ash is recirculated to the boiler in order to slag the ash. Arsenic tends to concentrate preferentially in the fly ash during this process by 10 to 100 times compared to cases where no fly ash recirculation is used. A study of 14 wet bottom plants indicates that the actual arsenic concentration obtained in the flue gas is not monotonically proportional to the coal arsenic concentration, but may depend also on the calcium content of the flyash. Calcium oxide in the fly ash tends to produce arsenic, leading to higher arsenic concentrations in the fly ash

and lower gaseous arsenic concentrations in the flue gas. This reduces the effect of arsenic as a catalyst poison. However, calcium can also "blind" the catalyst, if it does not react with arsenic (or perhaps other species). Hence, for flue gases where arsenic is not present, Japanese experience has been that fly ash calcium oxide contents of less than 1 percent permit long catalyst lives (e.g., 38,000 hours) while higher calcium contents of 5 to 8 percent result in shorter lives of less than 25,000 hours. For high sulfur coals that yield a gypsum ($CaSO_4 \cdot 2H_2O$) component in the fly ash, the deactivation of catalyst is less pronounced (Lowe et al., 1991).

5.5.3.2. Laboratory Studies of Poisons

A laboratory study by Chen et al. (1990) examined the effect of several catalyst poisons on a laboratory-manufactured sample of 5 percent V_2O_2 catalyst on a TiO_2 carrier. Both catalyst pellets and a ceramic substrate honeycomb catalyst were evaluated. The specific catalyst poisons that were evaluated include five alkali oxides (Li_2O, Na_2O, K_2O, Rb_2O, and Cs_2O) and four additional compounds CaO, PbO, P_2O_5, and As_2O_3. In the experimental work, maximum catalyst activity was observed in the 200 to 300°C (392 to 572°F) temperature range. Commercial catalysts also include WO_3 as a component, which allows increased catalyst activity at higher temperatures of 300 to 400°C (572 to 752°F).

U.S. coals, and especially eastern bituminous coals, contain relatively high concentrations of alkali metals. Thus, the effects of alkali and alkaline earth metal oxides on catalyst are important in these applications. Catalyst activity was shown to decrease as the amount of alkali metal dopant was increased in the laboratory tests. The strength ordering of the alkali oxide poisons corresponds to their basicity, with Cs_2O having the most pronounced effect. The deactivation may occur due to acid-base reactions forming alkali-vanadium compounds (e.g., $NaVO_3$). The poisoning due to CaO is weaker than that of the alkali metals. The basicity of CaO is also weaker than the weakest alkali oxide tested, Li_2O. Lead oxide, although a strong poison for automobile catalytic converters, is less important than the top three alkali metal oxides in deactivating the catalyst.

Although arsenic is often cited as the major catalyst poison concern, the experimental results of Chen et al. (1990) indicate that As_2O_3 is a substantially weaker catalyst poison than the alkali metal oxides Na_2O, K_2O, Rb_2O, and Cs_2O. P_2O_5 was also found to be a relatively weak poison.

However, the poisoning effect of both As_2O_3 and P_2O_5 are temperature dependent, with increased catalyst deactivation at lower temperatures. P_2O_5 poisoning leads to the formation of phosphate on the catalyst surface, which changes the catalyst surface active properties, and the blockage of surface area and pores. In spite of its relatively low poisoning activity, As_2O_3 may be a more notable poison because it is often found in gaseous form, whereas many of the potentially stronger alkali metal oxides are contained in the molten coal ash.

SO_2 entering the SCR reactor is a precursor to the formation of SO_3, ammonium sulfates, and sulfuric acid. Under certain conditions, ammonium sulfate may deposit on the catalyst, leading to catalyst deactivation. However, SO_2 alone has shown a promoting effect on catalyst activity. Formation of surface sulfates on the catalyst may promote the acidity of the surface. The work of Chen indicates that poisoning is associated with increasing basicity of the catalyst due to other contaminants.

Chloride species may have either poisoning or promoting effects on the catalyst. The poisoning effects of chlorides are much weaker than those of the corresponding oxides of the same metals (e.g., NaCl and Na_2O). In fact, the chlorine atom has a promoting effect, while the alkali metal atom has a poisoning effect, with a net poisoning for NaCl and KCl. KCl is a stronger poison than NaCl, analogous to the metal oxide K_2O being stronger than Na_2O.

HCl appears to react with ammonia to form NH_4Cl, which consumes ammonia and reduces ammonia available for NO_x conversion. It also deposits on the catalyst at temperatures below 340°C (644°F). HCl also appears to react with lower vanadium oxides, which are formed by reduction with ammonia, to form VCl_4 and VCl_2, which are red-brown and green liquids, respectively. Some chlorides, such as Cu_2Cl, act as an SCR catalyst, which may be attributable to its acidity.

In a later study, Chen et al. (1991) also added WO_3 to the catalyst formulation, yielding catalyst samples more representative of commercial offerings. They performed a set of tests with the same poisons as described above. WO_3 was found to improve catalyst activity and the resistance of catalyst to poisoning. However, similar qualitative results were obtained. Alkali compounds had the most pronounced effect in proportion to their basicity. Lead, arsenic, and phosphorous were also found to be weaker poisons than the strong alkali compounds tested. The addition of SO_2 decreased the activity of the WO_3 formulation catalyst, although when doped with alkali activity increased. Similar results were obtained for chloride related effects. In cases where vanadium chlorides form, catalyst activity will decrease.

The results of both studies (Chen et al., 1990; Chen et al., 1991) were not intended to identify the interactive simultaneous effects of multiple catalyst poisons in combination with masking or plugging, such as would occur in an actual flue gas. The purpose was to identify purely chemical mechanisms for catalyst poisoning to provide insight into actual deactivation mechanisms. Deactivation studies on actual flue gas slip streams will be conducted as part of a cooperative pilot plant program between EPRI and selected utilities (Flora et al., 1991).

5.5.4. Catalyst Life

Catalyst "life" is often reported as the number of operating hours between complete replacement of all catalyst in an SCR reactor. In many papers, catalyst life is described as if it is a property of the catalyst. However, it is actually a design variable. For example, there are trade-offs between catalyst life, space velocity, and catalyst replacement scheduling. In actual installations in Germany and Japan, the catalyst is installed in multiple layers and only one layer is replaced at a time according to a schedule.

In earlier EPRI-sponsored studies (e.g., Bauer and Spendle, 1984), the implicit assumption was that all catalyst would be replaced simultaneously at the end of a specified time interval. This leads to unnecessarily high operating costs. Japanese catalyst vendors and German SCR operators have both reported on the economic benefits of phased catalyst replacement schemes (e.g., Appendix B of Bauer and Spendle, 1984).

In a recent EPRI study, Robie et al. (1991) assume that a catalyst life of four years will be realized for U.S. coal-fired high-dust applications. They also assume the same life for tail-end applications even though there are clear differences in operating environments for the two cases. This type of assumption may unnecessarily penalize the tail-end configuration when in fact the major benefit of this configuration is a decrease in catalyst activity loss over time.

5.5.5. Catalyst Disposal

In Japan and Germany, spent catalyst is returned to the manufacturer. In Japan, catalyst manufacturers have not found it economical to regenerate the catalyst, and the catalyst is often simply disposed of (Lowe et al., 1991). It is likely that spent catalyst would be classified as a hazardous waste in the U.S.

5.5.6. Impacts on Other Plant Components

SCR has effects on other components of the power plant, particularly for high-dust designs. According to Robie et al. (1991), the main impacts are on the boiler, air heater, and induced draft fan. Other components affected are the FGD process, FGD reheat system, waste disposal system, and water treatment system. These impacts are summarized below.

- Air Preheater. Air preheater modifications are required due to the deposition of ammonium sulfates and bisulfates. Heat transfer surfaces must be replaced with heavier gauge metal and, in some cases, modified design surfaces. Additional water wash capability is required for air preheater cleaning. High pressure soot blowers are also required at both the hot and cold ends of the air preheater. Air preheater leakage may increase.
- Boiler. Loss of thermal efficiency results from air preheater modifications and, at part load operation, from an economizer bypass, which is required to maintain the reaction temperature in the SCR unit.
- Induced Draft Fan. In a new plant, a larger ID fan is required to overcome the pressure drop in the SCR reactor and any other incremental pressure drops associated with downstream effects. This pressure drop may be up to 11 inches of water.
- Forced Draft Fan. The forced draft fan for the combustion inlet air to the air preheater will have a higher mass flow rate due to increased air preheater air leakage.
- Stack. The increase in the SO_3 concentration of the flue gas could result in increased opacity of the flue gas plume if the SO_3 is not removed in the FGD system. Acid condensation would also be a potential source of concern.
- ESP. Because of the lower operating pressure of the ESP due to the pressure drop of the SCR system, higher flue gas temperature, and increased flue gas mass flow due to air preheater leakage and gases introduced for ammonia injection, the ESP will be required to handle a higher volumetric flow rate. In a new plant, therefore, a

larger ESP will be required. The ESP may require additional reinforcement due to the lower, and negative, operating pressure. Although the SO_3 content of the flue gas will increase, the beneficial effect of this on ESP performance may be offset by the increase in flue gas temperature. Ammonium salt precipitation in the fly ash could improve agglomeration and reduce reentrainment.

- Ash Disposal/Reuse. Ammonia compounds contained in fly ash material decompose and release ammonia at elevated pH. Even at lower pH, ammonia fixation with alkaline species could result in an ammonia odor problem. Flyash containing ammonia compounds may not be suitable for use in cement manufacturing.
- Water Treatment. Water treatment in addition to typical plant waste water treatment is required to covert nitrogen species in the air preheater wash water to free nitrogen.
- FGD/Reheat. Because of the higher flue gas inlet temperature and mass flow rate, there will be an increase in the water evaporation rate for wet limestone systems. In addition, steam would be required for reheat. The FGD liquor recirculation rate may need to be increased to maintain the same SO_2 removal efficiency. Alternatively, reheat can be accomplished using flue gas duct burners.
- Auxiliary Power Consumption. The net plant output will be decreased by the electricity required to operate SCR process equipment. In addition, during times of soot blowing, the plant efficiency will be decreased slightly due to the use of process steam. Steam is also used for ammonia vaporization, and dilution air for ammonia injection is taken from the discharge of the primary air fans.

The effects of the tail-end SCR system are not as significant as for the high-dust configuration. The tail-end SCR will result in auxiliary power consumption, flue gas pressure drop, water washing of the reheat gas/gas heat exchanger and associated wash water treatment, increased requirement to eliminate mist carryover from the FGD system, and stack effects due to increased SO_3 concentration and higher stack temperatures. In addition, a duct burner may be required. Sootblowers and ash collection hoppers are not required for the SCR system in the tail-end configuration. In the tail-end configurations, separate dedicated dilution air fans are used for ammonia injection (Robie et al., 1991).

For tail-end systems, the leakage rate of the gas-gas heat exchanger used for reheat has been reported to be as high as 7 percent in German facilities. Such leakage allows untreated flue gas to leak into the treated gas prior to stack discharge, thereby effectively bypassing the SCR system.

5.5.7. SO_2 Oxidation

In the U.S., flue gases have typically higher SO_2 and SO_3 concentrations than experienced in Japan and Germany due to the predominance of high sulfur coals in many regions of the country. The oxidation of SO_2 leads to downstream effects such as ammonium sulfate and bisulfate formation and acid condensations as previously described. Sulfur trioxide and sulfuric acid formed downstream of the SCR can also lead to attack of duct liners. The formation of these condensates and deposits depends critically on the presence of ammonia and sulfur trioxide in the flue gas. However, to minimize this type of problem in U.S. applications may require optimization of catalysts for specific U.S. markets (Lowe et al., 1991).

According to data reported by Bauer and Spendle (1984), SO_2 oxidation is primarily a function of catalyst formulation, space velocity, and operating temperature.

5.5.8. Ammonia

A portion of the ammonia injected into the SCR system may pass through the reactor unchanged. Ammonia in the flue gas may react chemically or physically with other constituents of the flue gas, including fly ash. This may lead to maintenance and operational problems. Several key concerns are discussed further.

5.5.8.1. Ammonia Injection

In commercial SCR systems, a critical design issue is the injection of ammonia into the flue gas upstream of the SCR reactor. A key difficulty in ammonia injection is obtaining a uniform mixture of ammonia in the flue gas. Failure to achieve proper ammonia injection and mixing can lead to channeling of ammonia through the SCR system, resulting in high levels of ammonia slip through the SCR reactor and to downstream components in the flue gas path.

Obtaining a uniform distribution of the injected ammonia in the flue gas upstream of the SCR catalyst is often difficult. Flue gas flow modeling and flow straightening devices are often needed to understand and achieve proper flow distribution. Ammonia injection systems typically consist of 30 to 40 injection points per square meter. These injection nozzles are controlled either singly or in groups of several, and the flow of ammonia through them can be optimized to achieve a reasonably uniform ammonia distribution (±10-30 percent) in the flue gas. However, dust deposits on or around the nozzles can lead to plugging of some or alteration of the flue gas flow pattern. Thus, the flow patterns may change over time and require periodic checking and adjustment (Lowe et al., 1991).

5.5.8.2. Ammonia Retention in Catalyst

Some SCR catalysts may retain ammonia during operation. The ammonia is then released during transients or shut downs. This desorption process may take up to eight hours, based on currently known experience. The ammonia injection rate during low temperature operation should be adjusted to compensate for offgasing of ammonia from the catalyst to maintain ammonia slip within tolerable levels. Because of the absorption/desorption phenomena, changes in NO_x emissions may lag changes in the ammonia injection rate by 30 minutes (Lowe et al., 1991).

Control problems under load swing conditions, exacerbated by the time-lag phenomena, remain an issue, particularly for potential U.S. high sulfur coal applications (Lowe et al., 1991).

5.5.8.3. Effects on Air Preheater

The most common effect of ammonia slip that is discussed in the literature is the deposition of ammonium sulfates on downstream equipment. However, commercial operation has not always substantiated this concern. For example, in the Takehara Power Station Unit 1, featuring hot-side SCR downstream of a hot side ESP, no additional air preheater washings have been necessary during 34,000 hours of SCR operation. The SCR operates at 80 percent removal efficiency with a NO_x loading of 300 ppm. The lack of plugging of the air preheater by ammonium salts, even in spite of SCR inlet SO_2 concentrations of 1,000 to 1,500 ppm, is attributed to low NH_3 slip levels. These have been 0.2 ppm or less. SO_3 conversion was typically 0.08 to 0.21 percent (Behrens et al., 1991).

The high-dust hot-side SCR system in the Reuter West power station in Berlin, Germany has operated over 15,000 hours on coals with sulfur contents up to 1.2 percent. The typical NO_x removal efficiency is 85 percent with an ammonia slip of 1.5 ppmvd and an SO_2 conversion rate to SO_3 of about 0.5 percent (Behrens et al., 1991). No plugging of the air preheater is reported and no washing of the air preheater has been necessary since SCR startup. The SCR catalyst layers receive a weekly sootblowing.

In one German power plant, Neckar (1989) reports that approximately 5 percent of the ammonia leaving the SCR system is deposited as an ammonium salt in the air preheater, with typically about 50 percent of the ammonia absorbed onto fly ash. The ammonium salts are easily soluble in water, and can be washed. As water washing in the air preheater proceeds, the concentration of ammonia in the exiting water stream decreases. Wash water with a high ammonia concentration must be treated to remove the ammonia prior to entering the regular plant wastewater treatment system. Neckar suggests that the initial wash water with a high ammonia concentration can be pretreated separately from the larger volume of water with a low ammonia concentration, which may be suitable for direct feed to the existing waste water treatment plant.

In pilot plant testing of an SCR system, Shiomoto and Muzio (1986) report that ammonia entering the preheater tends to deposit on air preheater surfaces as solid ammonium compounds or to be absorbed onto fly ash. Furthermore, SO_3 in the flue gas is consumed in the formation of ammonium sulfate or bisulfate, and also was absorbed onto fly ash. The investigators report that essentially all of the gaseous SO_3 entering the air preheater during testing was removed from the flue gas.

The effects of deposits include fouling of heat transfer surfaces and increase of pressure drop in flue gas paths. These types of effects may be more pronounced during process upsets (Lowe et al., 1991).

5.5.8.4. Ammonia Absorption by Flyash

Another concern regarding ammonia slip has emerged in Germany. German experience has been that the typical Japanese criteria of 5 ppm maximum ammonia slip is often not stringent enough to permit commercial use of fly ash as a byproduct. Therefore, in many German installations ammonia slip must be limited to 3 or even 1 ppm (Lowe et al.,

1991). Schönbucher (1989) reports that ammonia slip must be limited to 2 ppm to produce a byproduct fly ash acceptable to the cement industry.

Although ammonia does not alter the physical properties of concrete made from fly ash, ammonia captured in the fly ash is released during concrete mixing and may result in a noticeable odor. For ammonia concentrations of less than 60 mg per kg of fly ash, the odor is not noticeable. For the Altback/Deizisau power station Unit 5 in Germany, it appears that 20 to 80 percent of the ammonia slip is captured in the fly ash, with a mean value near 50 percent (Neckar, 1989).

Experimental studies by Shiomoto and Muzio (1986) indicate that most of the ammonia leaving the SCR system exits as a gas, with very little in the form of solid compounds or absorbed by fly ash. However, a portion of the gaseous ammonia is absorbed by flyash downstream of the SCR reactor, with higher ammonia partial pressures leading to increased absorption.

5.5.8.5. Ammonia Slip and Tail-End Systems

For tail-end systems, ammonia slip is not a significant concern because of the low concentration of sulfur in the flue gas. Therefore, the constraints on catalyst performance are less severe, allowing potentially greater degradation in catalyst activity (and associated increase in ammonia slip) before replacement is required. Ammonia slip constraints for tail-end systems are typically imposed by air emissions regulations, as opposed to downstream process requirements. Ammonia slip as large as 20 to 30 ppm is not expected to lead to operational problems in tail-end systems. Ammonia odor and plumes become noticeable when the ammonia concentration exceeds 50 ppm (Lowe et al., 1991). Ammonium salt deposition is expected to occur in the gas-gas heat exchanger used for flue gas reheat in tail-end SCR systems. Thus, heat exchanger water washing is also required in this case.

5.5.9. U.S. Outlook

Because the German and Japanese experiences cannot be directly applied to U.S. applications, EPRI and others are involved in pilot testing of SCR systems on selected slipstreams, analogous to the German testing of over 70 SCR pilot systems. These tests will provide additional data regarding cost and technical feasibility of SCR applied to plants firing domestic medium and high sulfur coals. EPRI will conduct as many as 14 separate tests (Lowe et al., 1991).

In the short term, low-dust tail-end SCR systems hold the most promise of reliable performance for high sulfur coal applications. This type of system would avoid the potentially excessive rate of air preheater fouling and catalyst deactivation that might otherwise be experienced in a high-dust configuration in high sulfur service (Lowe et al., 1991).

There are 105 operating cyclone units in the U.S. totaling over 26,000 MW. These are high NO_x emission technologies which are not easily amenable to combustion NO_x control. The typical NO_x emission rates for these units ranges from 0.8 to 1.8 lb/MMBtu, corresponding to flue gas concentrations of 500 to 1,100 ppm. Many of these units are also located in the Midwestern U.S., which is the major source of utility acid rain emissions. Thus, these boilers would appear to be a prime target for application of tail-end SCR systems (Lowe et al., 1991).

5.6. Performance Models

In this section, analytical performance models of SCR systems are presented. These include performance models for high-dust, hot-side and tail-end, low-dust SCR systems. For the hot-side system, downstream effects on the power plant air preheater are modeled. For the tail-end system, a gas-gas heat exchanger and duct burner used for flue gas reheat are modeled.

5.6.1. Catalyst Requirement

The catalyst requirement is a complex function of the physical and chemical properties of the catalyst, catalyst geometry, catalyst replacement philosophy, reaction temperature, flue gas volumetric flow rate, flue gas characteristics such as NO_x concentration, ash concentration, ash composition, SO_2 concentration, gaseous poisonous species concentration (e.g., As_2O_3), the desired NO_x removal efficiency, allowable flue gas pressure drop, and the desired ammonia slip. The latter in turn affects downstream precipitation of solids, such as ammonium sulfate and bisulfate, and, hence, affects air preheater design in hot-side SCR systems.

Although a catalyst requirement model ideally would be sensitive to all of the above factors, insufficient data are available to support the development of such a model. For example, the interactive poisoning effects of multiple flyash constituents is not well-understood. Therefore, the approach taken here is to develop a model of intermediate detail that captures the key functional dependencies between catalyst requirement and process conditions. The model is based on empirical and design assumptions supplied by the user and power plant performance parameters calculated from the power plant performance model.

A number of theoretical models were reviewed as a possible basis for model development. In most cases, these models were not adopted directly here, but were used to identify key functional dependencies that could be modeled based on empirical data.

5.6.1.1. Factors Affecting Catalyst Requirement

In a report prepared by Shiomoto and Muzio (1986), there is an appendix containing comments by Kawasaki Heavy Industries, a Japanese manufacturer of SCR systems. KHI presents the development of a simplified equation for estimating catalyst space velocities based on NO_x removal efficiency, ammonia slip, linear velocity, reaction temperature, and catalyst activity. The functional form of this equation is a basis for the performance model developed here.

The simplest model of an SCR system for the purpose of determining catalyst requirement is based on a rate model for the chemical reaction of NO with NH_3, which is the predominate reaction occurring in the SCR reactor. Under the condition of an NH_3/NO_x molar ratio of 1.0, pilot plant testing in Japan has shown that a first order reaction occurs:

$$\frac{d[NO_x]}{dt} = -k[NO_x]$$

Integration of this equation yields the following relation between flue gas residence time in the catalyst and NO_x removal efficiency:

$$t = \frac{-\ln(1-\eta_{NO_x})}{k}$$

The catalyst space velocity is related to flue gas residence time in the catalyst by the following:

$$SV\ (1/hr) = \frac{3{,}600\ \text{sec}/hr}{t\ (\text{sec})}$$

Therefore, the catalyst space velocity is given by:

$$SV = \frac{3600\ \text{k}}{-\ln(1-\eta_{\text{NO}_x})} \qquad (5\text{-}4)$$

The rate constant, k, corresponds to the so-called catalyst "activity." The catalyst activity is a complex function of catalyst geometry, chemical formulation, and operating conditions.

In the typical case where the NH_3/NO_x molar ratio is less than 1.0, the apparent catalyst activity will be less than the actual catalyst activity. This is because the reaction between NH_3 and NO_x is 1:1, while for molar ratios of less than 1, the active sites populated with ammonia molecules are fewer than the active sites sought by NO_x molecules. This is not a limitation of the catalyst, but rather a limitation due to the scarcity of NH_3.

To adjust for this phenomena, KHI developed an empirical correction factor based on the "end-mole ratio," which is the NH_3/NO_x molar ratio at the SCR reactor exit. The end-mole ratio is the molar ratio of ammonia slip to unreacted NO_x. Thus, Equation (5-4) becomes:

$$SV = \frac{3600\ \text{C}\ (r_e)_a}{-\ln(1-\eta_{NO_x})} \qquad (5\text{-}5)$$

The value of the exponent "a" is obtained empirically from test data obtained for constant conditions except for changes in NO_x removal efficiency and end-mole ratio. Data plotted by KHI suggest that a typical value of "a" is 0.3.

Equation (5-5) was used as the basis for a regression model for space velocity based on design data provided by KHI in an earlier SCR design study published by EPRI (Bauer and Spendle, 1984). The purpose of the regression model was to determine the adequacy of the simplified model of Equation (5-5) for use in an SCR performance model. The results are shown graphically in Figure 5-7.

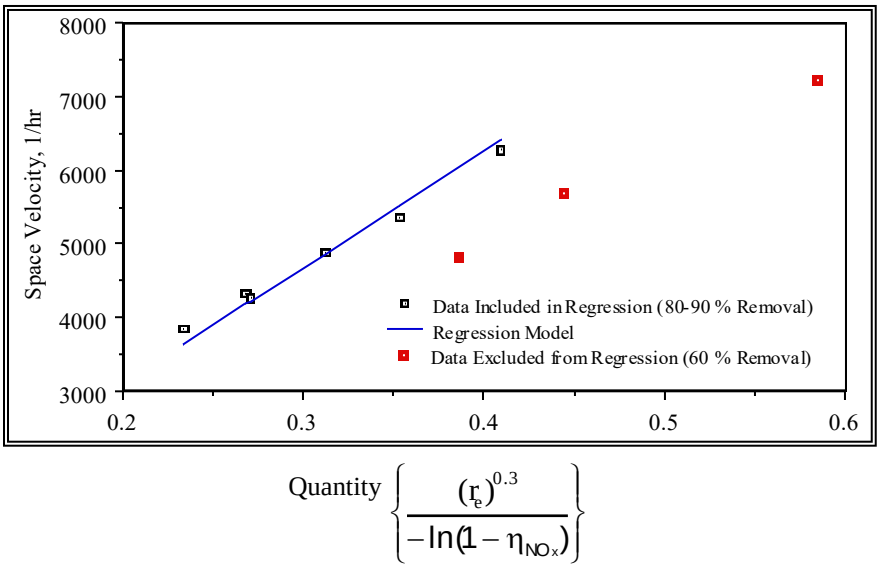

Figure 5-7. Regression Model of Space Velocity as a Function of NO_X Removal Efficiency and End-Mole Ratio

The regression analysis indicated that Equation (5-5) was valid for estimating space velocities for NO_x removal efficiencies of 80 and 90 percent, with varying end-mole ratios. However, the model could not also be applied simultaneously to the data for 60 percent NO_x removal. The results here suggest that the catalyst activities differ for the two sets of data. Bauer and Spendle (1984) do not report the design details, such as linear velocity; therefore, it is possible that design conditions were not the same for the two sets of data. Thus, it appears that the simple model of Equation (5-5) is a reasonable basis for correcting space velocity for differences in NO_x removal efficiency and end-mole ratio when all other factors are held constant.

To compare catalysts under different operating conditions, KHI suggests the following model:

$$\frac{\ln(1-\eta_2)}{\ln(1-\eta_1)} = C_r H_r \beta_r f_r W_r Q_r \left(\frac{m_2}{m_1}\right)^{0.3} \qquad (5\text{-}6)$$

From Equation (5-6), the performance of a specific catalyst may be estimated based on ratios of key performance parameters, assuming a reference catalyst. This formulation suggests that space velocity can be estimated based on a reference catalyst using multiplicative correction factors to adjust for differences in operating conditions.

Other models are possible, such as that reported by Chen et al. (1991). The NO_x removal efficiency is estimated in this model based on detailed design information regarding the SCR catalyst, including catalyst geometry, film mass transfer coefficient, effective diffusivity, and reaction rate constant. However, data to support this detailed model are often not reported in published literature.

5.6.1.2. Model Form

The modeling approach adopted here is to assume a reference catalyst and to apply a series of multiplicative correction factors to adjust space velocity for different design conditions. The general formulation is:

$$SV = SV_{ref} \prod_{i=1}^{4} f_i$$

Each correction factor, f_i, is a ratio that reflects the difference in space velocity from the reference to design conditions due to differences in certain design parameters. If the reference and design conditions are the same, these correction factors have a value of unity. A total of four correction factors have been developed, based on: (1) NO_x removal efficiency; (2) end-mole ratio; (3) catalyst activity; and (4) reaction temperature.

Default reference conditions are included in the model. The reference parameters required include space velocity, NO_x removal efficiency, NO_x inlet concentration, ammonia slip concentration, a catalyst activity curve, a catalyst life, and an operating temperature.

NO_x Removal Efficiency

The correction factor for NO_x removal efficiency is based on the model formulation suggested by KHI. This correction factor is:

$$f_1 = f_{eff} = \frac{\ln(1-\eta_{ref})}{\ln(1-\eta)}$$

As the NO_x removal efficiency increases, the catalyst space velocity decreases, leading to a larger catalyst volume.

For tail-end SCR, a portion of the flue gas exiting the FGD system leaks across the gas-gas heat exchanger used for flue gas reheat. Therefore, a portion of the NO_x in the flue gas will also pass across the heat exchanger and into the stack gas. Because of this, the NO_x removal efficiency in the SCR unit must be increased to compensate for the NO_x that bypasses the SCR system due to leakage. The required NO_x removal efficiency for the SCR system is calculated based on the overall NO_x removal efficiency required and the flue gas leakage rate across the gas-gas heat exchanger:

$$\eta = \frac{\eta_{overall}}{(1 - f_i)}$$

To satisfy this equation, the following constraint must be met:

$$\eta_{overall} + f_i \leq 1$$

This model assumes no additional NO_x formation in the duct burner.

End-Mole Ratio

The correction factor for end-mole ratio is based on the design ammonia slip, the design inlet NO_x concentration, and the design NO_x removal efficiency. The end-mole ratio is given by:

$$r_e = \frac{[NH_3]_{out}}{[NO_x]_{in}(1-\eta)}$$

The correction factor for end-mole ratio is given by:

$$f_2 = f_{r_e} = \left(\frac{r_e}{r_{e,ref}} \right)^{0.3}$$

Catalyst Activity

Experimental and commercial SCR operating data indicate that catalyst activity decreases with time, due to physical and chemical changes to the catalyst as previously discussed. The actual rate of catalyst activity deterioration depends on the operating conditions for the SCR reactor, and is usually not constant with time. Typically, there is an initial period of relative rapid catalyst deactivation, followed by a period of gradual activity change. A typical catalyst activity curve is shown schematically in Figure 5-8.

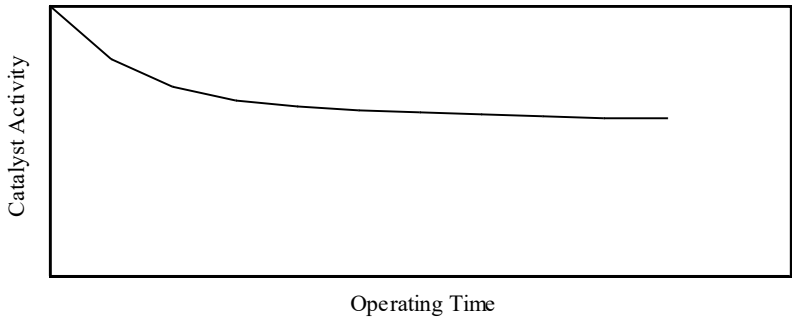

Figure 5-8. A typical Catalyst Activity Curve

Schönbucher (1989) presents several curves for catalyst activity as a function of time for high-dust and tail-end SCR systems. For wet-bottom boilers with high-dust SCR, catalyst activity loss may range from 25 to 45 percent during the first 2,000 hours of operation, with less rapid changes during subsequent operation. For other applications, such as tail-end systems on wet or dry bottom boilers, catalyst activity loss is slight (e.g., 5 percent) over 10,000 hours of operation and appears to decrease at a relatively constant rate.

To model catalyst activity loss, a simple function is employed to represent the catalyst activity curve. The purpose of this function is to provide a reasonable representation of the qualitative properties of catalyst activity loss for most cases. This function features two components: a minimum activity level and an exponential decay from the initial activity to the minimum activity levels. The initial activity is assumed to have a value of unity, while subsequent activity levels are relative to the initial activity.

$$A(t) = A_{\min} + A_{inc}\left\{\exp\left(-\frac{t}{\tau_a}\right)\right\} \qquad (5\text{-}7)$$

where:

$$A_{\min} + A_{inc} = 1$$

A model user specifies the minimum activity level, A_{min}, which determines the incremental initial catalyst activity, A_{inc}, that is subject to exponential decay. By also specifying one data point on the activity curve (an activity level $A(t_1)$ at time t_1), the activity decay time constant, t_a, can be estimated:

$$\tau_a = -\frac{t_1}{\ln\left(\frac{A(t_1) - A_{\min}}{A_{inc}}\right)}$$

For example, suppose we have a catalyst with a long-term activity level of 75 percent of the initial value, and for which the measured activity after 8,000 hours was 85 percent of the initial activity. Then:

$$A_{\min} = 0.75$$

$$A_{inc} = 1 - A_{\min} = 0.25$$

$$\tau_a = -\frac{t_1}{\ln\left(\frac{A(t_1) - A_{\min}}{A_{inc}}\right)} = -\frac{8{,}000}{\ln\left(\frac{0.85 - 0.75}{0.25}\right)} = 8{,}730$$

and:

$$A(t) = 0.75 + 0.25\left\{\exp\left(-\frac{t}{8{,}730}\right)\right\}$$

This example is shown graphically in Figure 5-9. In addition, a case in which the minimum activity level is assumed to be zero is also shown, to illustrate the flexibility of Equation (5-7) for representing catalyst activity curves.

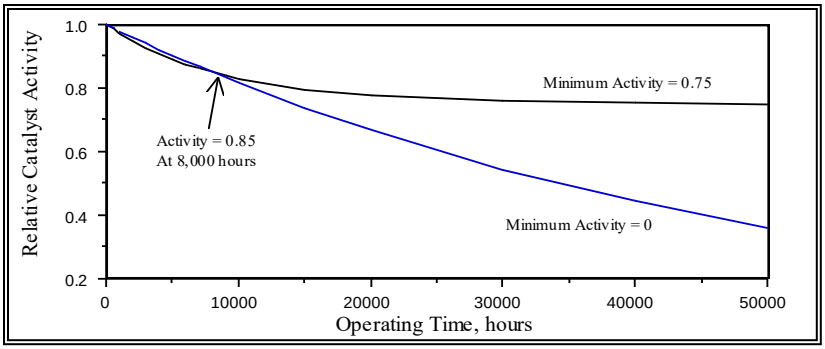

Figure 5-9. An example Catalyst Activity Curve

In typical SCR systems, multiple catalyst layers are employed. Furthermore, these catalyst layers are generally not replaced simultaneously. The overall catalyst relative activity in the case of multiple layers is the average of the individual catalyst layer relative activities (e.g., Nakabayashi and Abe, 1987). If we have N_c identical catalyst layers, and if each layer has been on-line for t_i hours at time t, then the average catalyst relative activity at any time t is given by:

$$A_{avg}(t) = \frac{1}{N_c}\sum_{i=1}^{N_c} A(t_i) \qquad (5\text{-}8)$$

However, we are usually interested in the activity at the design point of the catalyst, which corresponds to the activity level at the end of a catalyst layer replacement cycle. If we have N_c identical catalyst layers that are replaced one-at-a-time every t_r hours, the catalyst relative activity at the design point is:

$$A_{des} = \frac{1}{N_c}\sum_{i=1}^{N_c} A(i \cdot t_r) \qquad (5\text{-}9)$$

The implications of Equations (5-8) and (5-9) are illustrated in Figure 5-10. In this figure, the instantaneous average catalyst activity of a three-layer catalyst is illustrated for two cases. The first case, shown in a solid line, assumes that one catalyst layer is replaced every 10,000 hours, with a total time between complete catalyst replacements of 30,000 hours. The second case, shown as a dotted line, assumes that all catalyst layers are replaced simultaneously every 20,000 hours. For this particular illustrative case study, the design activity levels of both schemes are approximately the same. However, it is clear that by replacing individual layers sequentially, rather than simultaneously, the effective catalyst "life" is increased for a given volume of catalyst. In the illustrative example, catalyst life is 50 percent greater for the sequential replacement scheme compared to the simultaneous replacement scheme.

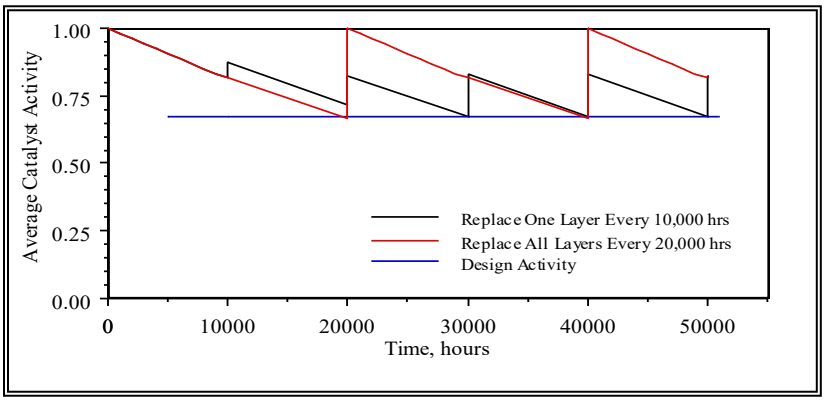

Figure 5-10. Illustrative Example of Average Catalyst Activity for a Three Layer Catalyst

In the more general case, sequential replacement schemes may lead to larger initial catalyst volumes in order to achieve the same design activity as a simultaneous replacement scheme. For example, if we simultaneously replace all three catalyst layers in the illustrative problem every 10,000 hours, the design activity level would be approximately 80 percent. To achieve this design activity level with a sequential replacement scheme of one layer every 10,000 hours, the initial catalyst charge would need to be 20 percent larger, which increases capital costs. However, the annual costs associated with catalyst replacement would be reduced by 60 percent, because in the sequential scheme the same amount of catalyst is replaced in 24,000 hours as is required every 10,000 hours in the simultaneous replacement scheme. Thus, selection of a catalyst "life" design value involves trade-offs between capital and annual costs.

Another catalyst charging and replacement scheme involves using an initial charge less than the ultimate design catalyst quantity. For example, three catalyst layers might be used initially, with a fourth layer added at a later time. Then, the four catalyst layers are replaced sequentially similar to the previous case. This example is shown in Figure 5-11. The example has a design relative activity slightly less than that of the case in Figure 5-10, which implies that a larger overall catalyst volume is required to achieve the same actual design activity. However, the initial catalyst charge and the periodic catalyst replacement rate are nearly 20 percent less than that for the previous case. This system achieves a better utilization of catalyst. However, a disadvantage of this approach is an increased flue gas pressure drop across the reactor at the design point, due to the requirement for approximately 10 percent additional total catalyst charge compared to the previous case.

For the purpose of estimating a catalyst space velocity based on a reference data point, recall from Equation (5-4) that space velocity is directly proportional to catalyst activity. Therefore, the correction factor for space velocity due to differences in catalyst activity and catalyst replacement schedules is given by:

$$f_3 = f_A = \frac{A_{des}}{A(t_{ref})}$$

The design activity is calculated using Equation (5-9) based on the total number of layers to be included in the steady-state catalyst charge (i.e. including layers added to the initial charge at a later time). The reference activity level is estimated assuming that the entire catalyst charge is replace simultaneously at time t_{ref}.

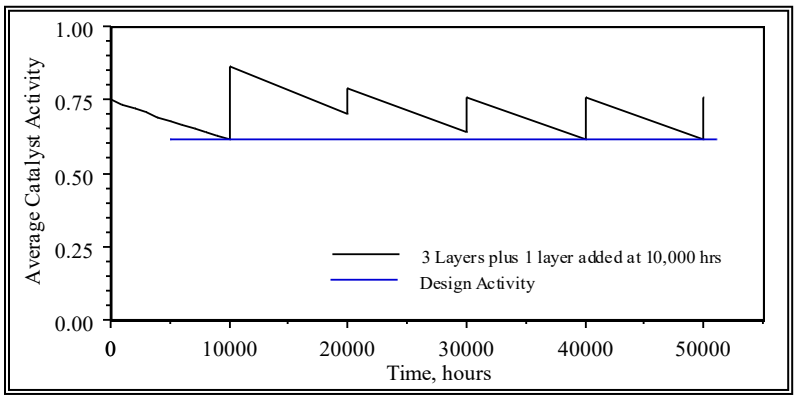

Figure 5-11. Illustrative Example of a Catalyst Addition and Replacement Scheme

Temperature

A temperature correction is assumed based on the Arrhenius relation for the reaction rate constant, which is given by:

$$k = k_o \exp\left(\frac{-E_a}{RT}\right)$$

A regression analysis using data from Bauer and Spendle (1984) was done to determine a value for the quantity E_a/R for use in the performance model. This was accomplished by rewriting Equation (5-5) as:

$$C = k_o \exp\left(\frac{-E_a}{RT}\right) = \frac{-\ln(1-\eta_{NO_x})(SV)}{3600(r_e)^a}$$

The quantity C was calculated using data presented in graphical form for NO_x removal efficiency as a function of temperature for a given ammonia slip, space velocity, and inlet NO_x concentration. From the regression analysis, the quantity E_a/R was estimated to be 7180, with an R^2 of 0.77 for 18 data points. Thus, the correction factor to adjust space velocity for differences in temperature is given by:

$$f_4 = f_T = \frac{\exp\left(\frac{-7180}{T}\right)}{\exp\left(\frac{-7180}{T_{ref}}\right)}$$

Initial and Annual Catalyst Volume Requirement

The SCR catalyst requirement is calculated based on the space velocity and flue gas volumetric flow rate. In cases where there are no later additions of catalyst layers, the catalyst volume is constant throughout the life of the plant. However, some designs assume that a new catalyst layer is added after some time period. In this case, the space velocity will decrease when the new layer is added. Thus, the total number of active catalyst layers may consist of catalyst layers existing at plant start-up and additional reserve layers added afterwards:

$$N_C = N_I + N_R$$

The initial catalyst volume is given by:

$$V_{c,i} = \frac{G_{FG}}{SV}\left(\frac{N_I}{N_C}\right)$$

The total catalyst volume is similarly given by:

$$V_c = \frac{G_{FG}}{SV}$$

The annual catalyst replacement rate depends in part on the catalyst design. In some studies, it is assumed that all catalyst layers are replaced simultaneously, while others assumed a phased approach to catalyst layer replacement. The number of catalyst layers replaced at the end of each replacement interval is given by:

$$N_{c,r} = 1 \text{ or } N_c$$

If only one layer is replaced at a time, then $N_{C,r}$ equals one. If all layers are replaced simultaneously, it equals the total number of layers in the catalyst. The number of layers replaced per year is:

$$N_{C,a} = \frac{N_{C,r}(8{,}760\ hr/yr)c_f}{t_r}$$

Thus, the catalyst volume replaced per year is:

$$V_{C,a} = V_C\left(\frac{N_{C,a}}{N_C}\right)$$

The catalyst "life" can be calculated based on the catalyst layer replacement interval and the number of layers replaced at the end of each interval:

$$L_C = \frac{(N_C/N_{C,r})t_r}{(8{,}760\ hr/yr)c_f}$$

In the case where all catalyst layers are replaced simultaneously, the catalyst life is the same as the catalyst replacement interval. Of course, the total volume of catalyst associated with each replacement scheme will differ.

5.6.2. Ammonia Requirement

The ammonia requirement is primarily a function of NO_x removal efficiency and the ammonia slip. The ammonia slip depends on the catalyst formulation and space velocity. However, it is treated here as a model input because insufficient data are currently available to develop a model of ammonia slip as a function of other variables. For each mole of NO and NO_2 that reacts in the SCR system, one mole of NH_3 is required (see Equations (5-1) and (5-2)). An excess amount of ammonia is required due to limitations related to diffusion of ammonia and NO_x to the catalyst's active sites. Typically, this excess ammonia leaves the SCR system unreacted. Thus, given a specified NO_x removal efficiency and ammonia slip, the molar ratio of ammonia to inlet NO_x is given by:

$$R_A = \eta + \frac{[NH_3]_{out}}{[NO_x]_{in}}$$

The ammonia mass flow requirement is then given by:

$$M_{NH3,in} = R_A \cdot M_{NOx,in}$$

Ammonia is stored as a liquid. Many design studies assume that the ammonia is vaporized by mixing it with steam prior to injection into the flue gas. A typical minimum ratio of steam to ammonia is approximately 8, based on the use of medium pressure saturated steam. However, for safety reasons, ammonia dilution to 5 volume percent may be required, leading to a requirement for a steam-to-ammonia ratio of 19. The steam requirement for ammonia injection is given by:

$$M_{steam} = R_s \cdot M_{NH3,in}$$

5.6.3. SO_3 Oxidation Rate

A portion of the SO_2 in the flue gas entering the SCR reactor is oxidized to SO_3. The percentage of SO_2 oxidized depends primarily on the reaction temperature, catalyst space velocity, and catalyst formulation. Regression analysis was used to develop two models representative of catalysts formulation for high sulfur and low sulfur operating environments. Data for both of these analyses were obtained from Bauer and Spendle (1984). For the high sulfur catalyst, which would be employed in high-dust hot-side applications, the fraction of SO_2 oxidized to SO_3, based on 31 data points, is given by:

$$f_{ox} = 2.38 \times 10^{-13} \cdot SV^{-1.06} \cdot (T - 460)^{5.03}$$

For the low sulfur catalyst, which would be employed in tail-end applications, the following regression model based on 26 data points gives the fraction:

$$f_{ox} = 1.05 \times 10^{-13} \cdot SV^{-0.996} \cdot (T - 460)^{5.05}$$

The coefficient of determination, R^2, for both of these regression models exceeds 0.99. SO_2 oxidation increases as space velocity decreases and as temperature increases.

5.6.4. Downstream Effects

Ammonia slip and SO_3 exiting the SCR system can combine to form ammonium sulfate and bisulfate, as previously discussed. Also, ammonia may be captured by fly ash prior to collection in the ESP. These downstream effects are of concern primarily for the hot-side SCR applications.

5.6.4.1. Air Preheater

The formation of ammonium salts is treated here empirically. Of primary concern is the amount of ammonia associated with ammonium salts deposited in the air preheater. The fraction of ammonia slip that is deposited as ammonium salts in the air preheater is treated as a parameter in the model, rather than as a calculated variable. The fraction of ammonia that

is absorbed onto flyash is also a parameter in the model. The remaining portion of the ammonia slip is assumed to exit the plant with the flue gas leaving the stack. The ammonia partitioning coefficients must satisfy the following condition:

$$f_{NH3,dep} + f_{NH3,abs} + f_{NH3,out} = 1$$

The molar flow rate of ammonia that is deposited as a solid in the air preheater is given by:

$$M_{NH3,dep} = f_{NH3,dep} \cdot \frac{[NH_3]_{out}}{[NO_x]_{in}} \cdot M_{NOx,in}$$

Similarly, the molar flows of ammonia absorbed by fly ash and emitted at the stack are given by:

$$M_{NH3,abs} = f_{NH3,abs} \cdot \frac{[NH_3]_{out}}{[NO_x]_{in}} \cdot M_{NOx,in}$$

$$M_{NH3,out} = f_{NH3,out} \cdot \frac{[NH_3]_{out}}{[NO_x]_{in}} \cdot M_{NOx,in}$$

The ammonia that deposits in the air preheater is removed periodically using water washing. As discussed by Neckar (1989), the concentration of ammonia in the wash water leaving the preheater is initially high, and then gradually decreases. The waste water from the washing may be separated into high and low ammonia concentration streams, with the high ammonia concentration stream requiring denitrification pretreatment before entering the regular plant waste water treatment system. The model includes provision for specifying the average ammonia concentration of the high concentration fraction of the spent waste water, as well as the portion of the deposited ammonia that is removed by this portion of the water. The model also includes a parameter for the ammonia concentration in the "low concentration" wastewater. These parameters are used to estimate the air preheater wash water requirement, with the concentrations specified in units of mg/l. The "high concentration" wash water requirement, in gallons/hour, is given by:

$$m_{wash,hc} = \frac{M_{NH3,dep} \cdot f_{hc}}{4.90141 \times 10^{-7} \cdot C_{NH3,hc}}$$

and the low concentration wash water requirement is given similarly by:

$$m_{wash,lc} = \frac{M_{NH3,dep} \cdot (1 - f_{hc})}{4.90141 \times 10^{-7} \cdot C_{NH3,lc}}$$

For tail-end SCR systems, the downstream effects are modeled similarly to those for hot-side systems. The partitioning of ammonia between ammonium salt deposition, ammonia absorbed onto fly ash, and ammonia retained in gaseous form will differ from the hot-side case. However, the gas-gas heat exchanger used for flue gas reheat will be subject to ammonia salt deposition and will require water washing. The spent wash water will require denitrification pretreatment prior to entering the plant waste water treatment system.

5.6.4.2. Catalyst Sootblowing

Catalyst sootblowing is required to remove ash that may mask or plug the catalyst. A sootblowing design by Bauer and Spendle (1984) is used as a basis to develop a model of the sootblowing steam requirement. The design basis includes steam sootblowing employing multiple sootblower sets. Bauer and Spendle report that the predicted steam requirement is 13,400 lb/hr for a total of approximately one hour per day, or an average of 31 lbmole/hr. There is no indication in the report that the steam requirement is a function of catalyst size, although such a relationship seems plausible. For example, Bauer and Spendle consider catalyst volumes ranging from 10,000 to 30,000 ft^3 but apparently assume the same sootblowing steam requirement for all cases. It is assumed here that the steam requirement reported by Bauer and Spendle is typical of the base case catalyst design, which for the high-dust configuration had a catalyst volume of 16,146 ft^3. Furthermore, the steam requirement is assumed to scale with catalyst volume, used here as a measure of catalyst size:

$$M_{soot} = 31\left(\frac{SV}{16{,}146\ \text{ft}^3}\right)$$

This model does not account for any differences in catalyst masking or fouling rates associated with flue gas or fly ash characteristics.

5.6.5. Pressure Drop

The flue gas pressure drop associated with the SCR system includes pressure drops across: (1) ductwork and ammonia injection grid; (2) dummy catalyst layers for erosion control; (3) active catalyst layers; and (4) air preheater due to buildup of deposits. Each of these sources of pressure drop are treated as input parameters in the model. The total pressure drop, in inches of water, across the SCR system is:

$$\Delta P_{scr} = n \cdot \Delta P_{cat} + n_d \cdot \Delta P_{dum} + \Delta P_{duct} + \Delta P_{aph,inc}$$

An additional consideration for hot-side SCR systems is the effect of the reduction in flue gas side pressure on the air leakage through the air preheater. For hot-side SCR systems, a nominal increase in the leakage rate of 10 percent is assumed. This is a model input parameter.

For tail-end systems, which are downstream of the air preheater, there is no incremental pressure drop associated with solids deposition in the air preheater. However, there is a pressure drop associated with flue gas reheating. Therefore, the pressure drop for the gas-gas heat exchanger used for reheat must be included. This pressure drop must be shared between the SCR system and the FGD system, for which reheat is often required also. Thus, a new parameter is introduced which represents the fraction of the gas-gas heat exchanger pressure drop that is solely attributable to the SCR system.

$$\Delta P_{scr} = n \cdot \Delta P_{cat} + n_d \cdot \Delta P_{dum} + \Delta P_{duct} + \Delta P_{GGH}\,(1 - f_{FGD})$$

The pressure drop term for ducting includes any pressure drop associated with the duct burner. These values must be specified as model inputs.

5.6.6. Energy Penalties

The energy penalties for the SCR system include electricity and steam consumption. The largest source of energy use is the incremental electricity required by the induced draft fan to overcome the flue gas pressure drops associated with the SCR system. In addition, electricity is required for the ammonia injection system, primary to compress vaporized ammonia for injection into the flue gas. Steam is consumed for ammonia vaporization and injection and for sootblowing in the SCR reactor. The steam consumption is converted to an equivalent electricity energy penalty based on the difference in enthalpy between the steam and water at standard conditions, the mass flow of steam used, and the steam cycle heat rate.

The energy penalty associated with operation of the induced draft fan to overcome the SCR flue gas pressure drop is given by:

$$E_{scr,fan} = \left(1.38 \times 10^{-6}\ \frac{MW}{cfm \cdot in\ H_2O}\right) G_{scr,in}\quad P_{scr}$$

The fan equation here assumes a fan efficiency of 85 percent. This equation also represents the energy penalty associated with a forced draft booster fan used in tail-end SCR systems.

The energy penalty associated with ammonia compression is calculated assuming a 100 psi differential compression with an 85 percent compression efficiency:

$$E_{scr,NH_3} = \left(3.47 \times 10^{-5}\ \frac{MW}{lb/hr}\right) \cdot \left(\frac{17.03 lb}{lbmole}\right) \cdot M_{NH_3,in}$$

The energy penalty for steam use in the SCR system is calculated based on the steam mass flows, the enthalpy added to the steam by the steam cycle, and the steam cycle heat rate:

$$E_{scr,steam} = \frac{(M_{steam} + M_{soot})\left(\frac{18lb}{lbmole}\right)\left(\frac{1{,}000\ \text{BTU}}{\text{lb}}\right)\left(\frac{MW}{1{,}000\ \text{kW}}\right)}{HR_s}$$

The total energy penalty for the high-dust SCR system is:

$$E_{scr} = E_{scr,fan} + E_{scr,NH_3} + E_{scr,steam}$$

For the tail-end SCR system, natural gas used to fire the duct burner represents an additional energy loss. Natural gas is a fuel that could be used to generate electricity. Therefore, the energy penalty is calculated based upon the gross plant heat rate to estimate the equivalent electricity energy penalty associated with natural gas firing:

$$E_{scr,NG} = \frac{m_{NG} HHV_{NG}\left(\frac{MW}{1{,}000\ \text{kW}}\right)}{HR_g}$$

The total energy penalty for the tail-end SCR system is:

$$E_{scr} = E_{scr,fan} + E_{scr,NH_3} + E_{scr,steam} + E_{NG}$$

5.6.7. Flue Gas Reheat for Tail-End SCR

For the tail-end SCR system, the temperature of the flue gas exiting the FGD system must be raised to the reaction temperature required by the SCR system. Furthermore, the temperature of the gas exiting the SCR system can be reduce prior to entering the stack. Therefore, a gas-gas heat exchanger (GGHX) and a duct burner are employed for heating and cooling the flue gas, as shown in Figure 5-12.

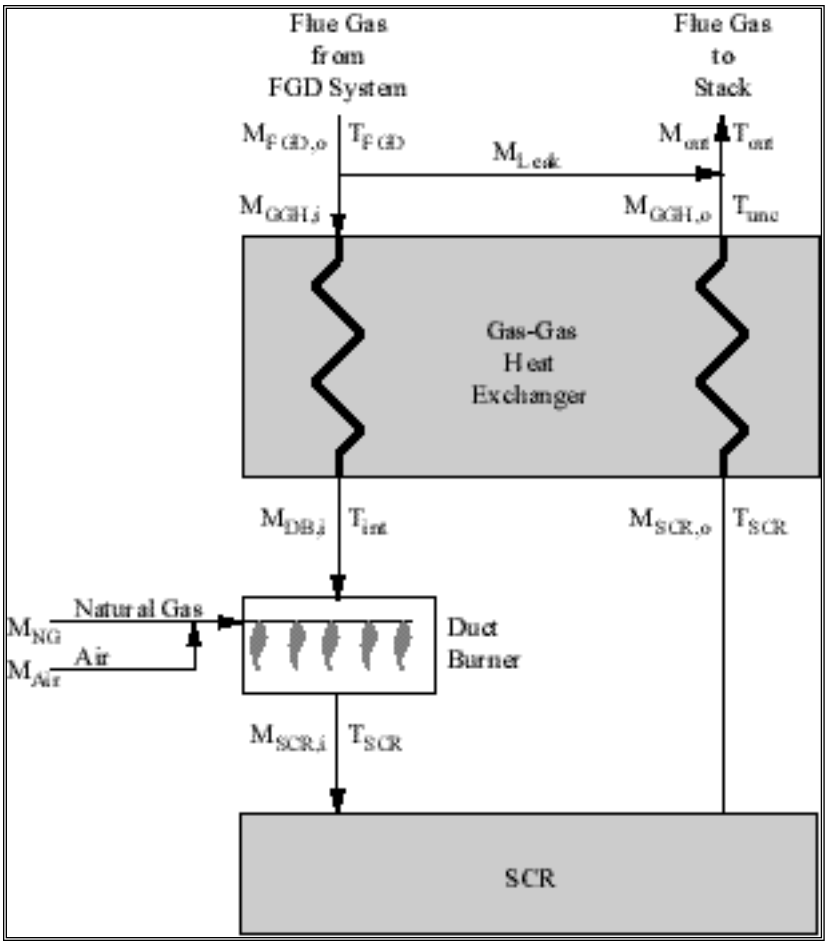

Figure 5-12. Schematic of Gas-Gas Heat Exchanger Performance Model

Typically, a Ljungstrum type heat exchanger would be used for the flue gas reheat and cooling system. A portion of the higher-pressure flue gas entering from the FGD system will leak into the flue gas stream exiting the heat exchanger to the stack. Therefore, an air leakage stream is modeled. For simplicity, it is assumed that the leakage flue gas is at the FGD system exit temperature. The flue gas leakage mass flow is estimated based on a leakage fraction as follows:

$$M_{leak} = f_l M_{FGD,o}$$

and the flue gas fraction entering the GGHX is given by:

$$M_{GGH,i} = (1 - f_l) M_{FGD,o}$$

In the GGHX, the untreated flue gas is heated from the FGD exit temperature to an intermediate temperature by cooling the treated flue gas exiting the SCR system. The heat transferred across the heat exchanger is given by:

$$Q_{GGH} = M_{GGH,i}(h_{fg}(T_{\text{int}}) - h_{fg}(T_{FGD}))$$

In the SCR computer model, the enthalpy of the flue gas is estimated using regression models for the enthalpy of each flue gas constituent at the given temperature.

The untreated flue gas must be heated an additional amount to reach the SCR reaction temperature. This additional heating is accomplished by use of a duct burner, which also introduces additional mass streams to the flue gas. The mass balance equation is:

$$m_{SCR,i} = m_{DB,i} + m_{NG} + m_{air}$$

Assuming that natural gas consists only of methane, the combustion reaction is:

$$CH_4 + 2(1+r_{ea})O_2 + 7.52(1+r_{ea})N_2 \rightarrow CO_2 + 2H_2O + r_{ea}O_2 + 7.52(1+r_{ea})N_2$$

For each pound of methane consumed, 3.6 pounds of air are consumed at stoichiometric conditions. If excess air is also considered, the air mass flow is then given by:

$$m_{air} = 3.6(1 + r_{ea})m_{NG}$$

The energy balance equation for the duct burner may be written as:

$$m_{scr,i}h_{fg}(T_{SCR}) = m_{DB,i}H_{fg}(T_{\text{int}}) + m_{NG}h_{NG}(T_{NG}) + 3.6(1+r_{ea})m_{NG}h_{air}(T_{air}) + m_{NG}\Delta H_r$$

The heat of reaction for methane is 345,700 Btu/lbmole. In Equation (5-10), all variables are specified except for the natural gas mass flow rate. Therefore, this equation can be used to solve for the natural gas requirement:

$$m_{NG} = \frac{m_{SCR,i}h_{fg}(T_{SCR}) - m_{DB,i}h_{fg}(T_{\text{int}})}{h_{NG}(T_{NG}) + 3.6(1+r_{ea})h_{air}(T_{air})v + \Delta H_r} \qquad (5\text{-}10)$$

In the SCR system, ammonia and steam are added to the flue gas, and the flue gas composition changes due to chemical reactions occurring in the reactor vessel. The SCR exit temperature is assumed to be the same as the inlet temperature. The flue gas exiting the SCR unit is cooled in the GGHX. The uncorrected temperature of the treated flue gas exiting the GGHX is estimated from the following relationship:

$$h_{fg}(T_{unc}) = h_{fg}(T_{SCR}) - \frac{Q_{GGH}}{m_{GGH,o}}$$

This equation is solved using an iterative technique to determine the flue gas temperature.

The treated flue gas from the SCR system is mixed with the flue gas leaking across the GGHX prior to entering the stack. The flue gas temperature entering the stack, corrected for the thermal mixing with the leakage air, is estimated using the following equation:

$$h_{fg}(T_{out}) = \frac{m_{GGH,o}h_{fg}(T_{unc}) + m_{leak}h_{fg}(T_{FGD})}{m_{out}}$$

where:

$$m_{out} = m_{GGH,o} + m_{leak}$$

5.7. SCR Capital Cost Model

The major equipment cost items for hot-side SCR systems include: (1) reactor housing; (2) catalyst; (3) ammonia storage and injection; (4) ductwork; (5) air preheater modifications; (6) induced draft fan modifications; (7) ash handling; and (8) water treatment. Additional costs may be incurred for flow modeling to properly design the ammonia injection system. For a tail-end system, there are no costs associated with air preheater modifications or ash handling. However, there are additional costs associated with the gas-gas heat exchanger and duct-burner used for flue gas reheat.

5.7.1. Reactor Housing

A reactor housing cost model was developed by Frey (1988). This model was later incorporated into the Integrated Air Pollution Control System (IAPCS) Version 4.0 computer program (Maibodi et al., 1990). The model was based on a statistical analysis of data from TVA (Maxwell and Humphries, 1985). The reactor housing costs include carbon steel

reactor vessel with six inches of mineral wool insulation, vessel internals and supports, steam sootblowers, reactor crane and hoist, installation labor, foundations, structures, piping, and electrical equipment. The costs for the reactor housing exclude catalyst. The direct capital cost for the reactor housing is given by:

$$DC_R(1982) = 145{,}800 + 316.9\left(\frac{V_{TOT}}{N_{TOT}}\right)$$

This model was based on regression analysis of 12 data points and has a coefficient of determination (R^2) of 0.998. The catalyst volume per housing ranged from 5,000 to 17,000 ft^3.

A similar analysis was done for data reported by EPRI (Bauer and Spendle, 1984). A total of 18 cost estimates were reported with catalyst volumes ranging from roughly 4,000 to 14,000 ft^3. However, the nature of the model was substantially different from the TVA model. It appears that the TVA model is predicated on the assumption of a simple linear relationship between reactor cost and catalyst volume. The EPRI data indicate a non-linear relationship, in which larger volumes yield a substantial economy of scale.

A more recent EPRI study is used here as a basis for developing a reactor cost model (Robie and Ireland, 1991). A total of 14 cost estimates are reported. However, two of these are for oil-fired power plants. All of the remaining 12 data points are for coal-fired power plants. The two oil-fired SCR applications appear to have substantially higher costs than for the coal-fired systems of similar catalyst volume; however, the basis for the difference is not reported. Of the dozen data points for coal-fired systems, one value is a duplicate. Therefore, 11 data points were used to develop a regression model of reactor housing cost versus total catalyst volume. The reactor housing includes flanged gas inlet and outlet, a single vertical downflow reactor, casing, ash hoppers, structural supports for catalyst modules, rectifying plate, baffles, turning vanes, walkways, stairs, monorails, hoists, and sootblowers. The catalyst volume includes both active and spare catalyst layers.

Robie and Ireland (1991) did not report the actual catalyst volumes for all 11 data points used in the regression model. Therefore, the catalyst volume was estimated based on the reported flue gas mass flow and flue gas molecular weight (which were used to calculated flue gas volumetric flow rate), active catalyst space velocity, and the ratio of the number of active plus spare catalyst layers to the number of active layers. Thus, the estimated total catalyst volume is given by:

$$V_{TOT} = \left(\frac{G^o_{fg}}{SV^o_{act}}\right)\left(\frac{N_{act} + N_{sp}}{N_{act}}\right)$$

where:

$$G^o_{fg} = \frac{\left(\frac{m_{fg}}{MW_{fg}}\right) \mathrm{R}\, \mathrm{T}^{\mathrm{o}}_{fg}}{P^o_{fg}}$$

The space velocity is referenced to a standard temperature and pressure, which in this case is 32 °F and 1 atm. Therefore, the flue gas volumetric flow rate is calculated at standard temperature and pressure. The active catalyst space velocity is adjusted based on the ratio of total to active catalyst layers for the purpose of determining the total catalyst volume for the reactor housing. For the cases where the actual catalyst volumes were reported, these estimates were often in very close agreement and never diverged by more than five percent.

The cost data reported by Robie and Ireland (1991) are based on subcontract costs for the process area to which additional costs have been added. These additional costs are not documented or discussed in the EPRI report, but appear to have been applied consistently for every cost reactor cost estimate. They may reflect installation and integration costs not covered by the subcontract costs. The multiplier for these additional costs is a function of whether the SCR is for a new or retrofit application. The multipliers are substantially larger for retrofit applications, presumably reflecting site access difficulty and congestion impeding equipment installation. All reactor housing costs were normalized to a new plant basis for purposes of the regression analysis. This was done by estimating the multiplier between subcontractor cost and total direct cost for a new plant based on the two case studies for a new installation. The direct costs for the remaining cases were then estimated on a new installation basis by multiplying the subcontract costs with the new installation direct cost factor. The relationship between direct cost and the catalyst volume per reactor housing was evaluated using regression analysis.

The resulting regression model for the direct cost of the reactor housing is:

$$DC_R = 18.65\, N_{R,TOT} \left(\frac{V_{TOT}}{N_{R,TOT}} \right)^{0.489} \left(\frac{PCI}{357.3} \right)$$

This model has a coefficient of determination (R^2) of 0.94 and a standard error of $169,000. The regression model is shown graphically in Figure 5-13. The costs are reported in December 1989 dollars, but may be adjusted to other years using the *Chemical Engineering* Plant Cost Index.

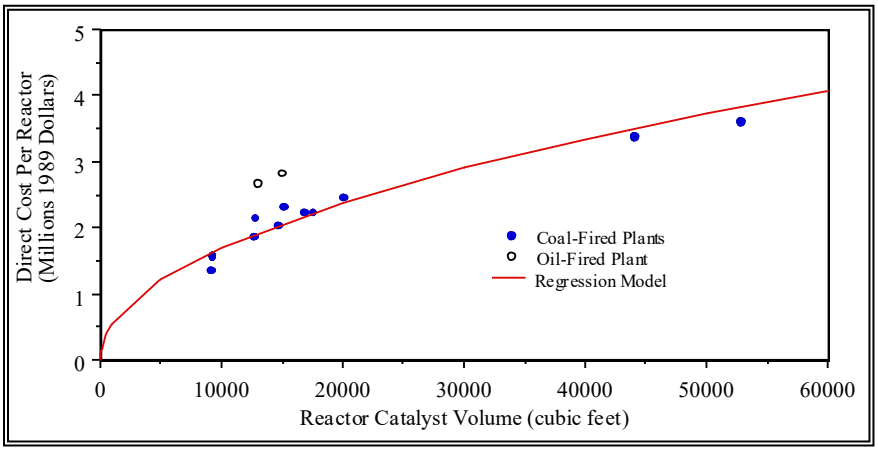

Figure 5-13. Direct Capital Cost Model for SCR Reactor Housing

From a statistical perspective, this regression model has significant limitations. The high coefficient of determination is influenced by the wide separation between two groups of data points. One set of data points are clustered for space velocities ranging from 10,000 to 20,000 cubic feet, whereas two other data points are close to 50,000 cubic feet. There is considerable scatter among the data points within the first cluster. However, because of the lack of reported detail regarding catalyst volumes and installation costs, it is not possible to reconcile these differences. Furthermore, there is no reported basis for the difference in values between the oil-fired and coal-fired data points. The oil-fired data points were excluded from the regression analysis, but are shown in Figure 5-13 for comparative purposes.

The regression model is satisfactory in representing the expected trend for SCR reactor housing cost. It is expected that there should be an economy of scale for increasing reactor housing size, and that the key measure of size is the total catalyst volume (including both active and spare catalyst layers).

5.7.2. Ammonia Handling and Injection

The direct cost for the ammonia injection process area was estimated based on analysis of eight data points taken from Robie and Ireland (1991). Six duplicate data points contained in their report were excluded from the statistical analysis. The ammonia unloading, storage, and supply system includes a horizontal bullet storage vessel with seven-days' supply capacity, an ammonia vaporizer, ammonia and dilution air mixer, ammonia injection grid, dilution air ductwork and dampers, and truck unloading station. The latter includes vapor recovery compressors, water deluge system, and transfer piping. The dilution air requirement is 20 parts air to one part ammonia. The regression model for ammonia process area direct costs is:

$$DC_{NH_3} = 50.8\, (m_{NH_{3,i}})^{0.482} \left(\frac{PCI}{357.3} \right)$$

This model has a coefficient of determination (R^2) of 0.87 and a standard error of $285,000. The regression model is shown graphically in Figure 5-14. Also shown in the figure is a regression model developed from data reported in an earlier EPRI report (Bauer and Spendle, 1984). The newer model yields costs that are lower than the previous model by a factor of approximately two. The reasons for the difference are not immediately clear. The earlier report used generally more conservative assumptions, reflecting higher levels of uncertainty perceived at that time for this technology.

Like the reactor housing direct cost model, the coefficient of determination for the ammonia injection system direct cost model benefits from the separation between clusters of data points. In this case, however, there is only one data point at the high end of the range of values for the predictive variable, ammonia flow rate. However, the model is satisfactory in reflecting economies of scale for larger sized systems.

5.7.3. Ductwork

Ductwork costs are considered both for hot-side and tail-end SCR applications.

5.7.3.1. Hot-Side SCR Applications

For a new hot-side SCR application, the ductwork associated with the SCR process includes economizer bypass ducts, economizer outlet duct, SCR inlet duct, SCR inlet control dampers, SCR outlet duct, SCR air preheater inlet plenum, various expansion joints in the ductwork, and dampers associated with the economizer bypass and air preheater cross-over ducting. Of the six major case studies reported by Robie and Ireland (1991), only two are for a new coal-fired power plant with hot-side SCR. Although these two case studies include five separate performance and cost estimates based on sensitivity analysis of key SCR performance characteristics, they are predicated on just two flue gas flow rates. Therefore, three of these estimates are duplicates. Because only two data points are available from this study to estimate duct costs as a function of flue gas flow, regression modeling was not employed to develop a direct cost model. Instead, a capacity-exponent model of direct cost versus flue gas volume flow rate was assumed as an appropriate function form. This formulation reflects the expected increase in cost that is associated with increases in flue gas volume flow rates. However, it implies that duct runs would be similar for differently sized systems. The parameters of this model, which include a multiplicative constant and an exponential coefficient, were estimated from the two data points. The resulting model is:

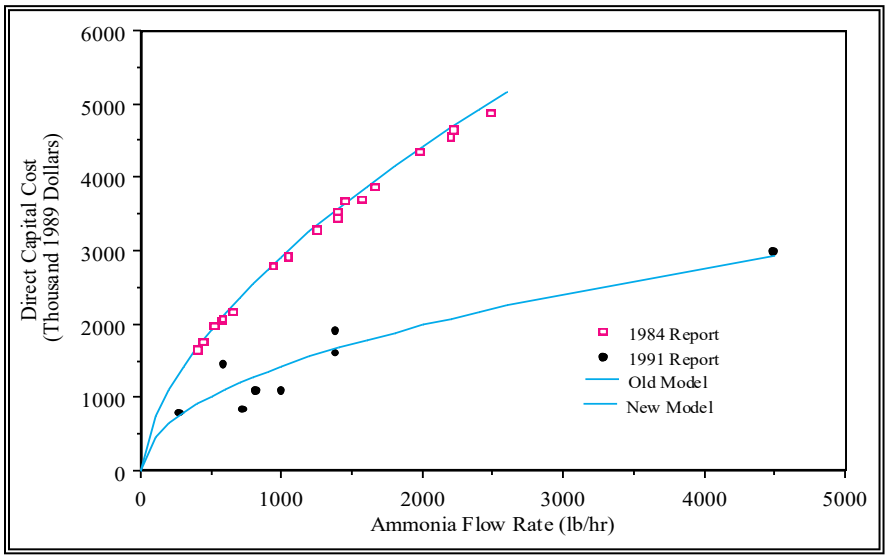

Figure 5-14. Direct Capital Cost Model for the Ammonia Handling and Injection System

$$DC_D = 14.2(G_{fg})^{0.7}\left(\frac{PCI}{357.3}\right)$$

The two data points used to estimate the parameters of this model are for flue gas flow rates of 3,026 and 2,713 macfm and direct costs of $4.44 and $4.10 million, respectively. This is a relative narrow range of values, but the resulting exponential scaling factor of 0.7 is consistent with scaling factors used in a variety of chemical engineering cost models.

5.7.3.2. Tail-End SCR Applications

For an SCR in the cold-side application, there are additional duct costs associated with the gas-gas heat exchanger. There are two data points available for estimating these costs. One is for a gas-gas heat exchanger system which has 5.6 percent

gas leakage. The second is for a system with no leakage. In this latter case, there is a higher gas flow rate through the SCR system, thereby leading to increased duct costs. Because of the scarcity of data points, the costs for these two cases are estimated as a multiplier of the costs for ductwork for a hot-side SCR application. The general equation is:

$$DC_{D,CS} = f_{D,CS}\,14.2(G_{fg})^{0.7}\left(\frac{PCI}{357.3}\right)$$

where $f_{D,CS}$ is 1.90 for a GGH with 5.6 percent air leakage, and 2.15 for a GGH with no air leakage.

5.7.4. Air Preheater Modifications

For hot-side SCR systems, a potentially significant concern is the deposition of ammonia-based compounds on downstream components. Unreacted ammonia exiting the SCR system ("ammonia slip") can react with sulfur trioxide present in the flue gas to form compounds such as ammonium bisulfate and ammonium sulfate that deposit on downstream equipment. These compounds may result in plugging and corrosion. The condensation of these compounds is most likely to occur on the cold and intermediate temperature heat transfer surfaces of the air preheater. In anticipation of deleterious effects, EPRI and others have recommended that air preheaters designed for use with SCR system be constructed with lower gauge (thicker) material, different geometries (e.g., combining intermediate and cold baskets of a conventional Ljungstrom air preheater into a single unit, to minimize seams where corrosion might occur), different materials, and larger motors, structure, and foundation to accommodate the larger weight of these modifications. Furthermore, more stringent provisions are made for soot blowing and water washing of the air preheater to remove the ammonia salts and any associated buildups at regular intervals. To enable an on-line water washing capability, crossover ducts and dampers are required. The changes in air preheater geometry and the effects of fouling can increase gas flow pressure drops. This in turn may increase gas leakage rates between the combustion air and flue gas sides of the heat exchanger.

Therefore, to accommodate the potential impacts of SCR systems on air preheater performance, a number of modifications are included in the design bases. Thicker material is used for the cold and intermediate heat transfer surfaces, in the region of the preheater where ammonia salt deposition is most likely. Furthermore, a corten steel alloy is used instead of carbon steel. A smoother heat transfer surface is used to aid in removing ammonia salts, but at the expense of reduced heat transfer and, hence, large heat transfer surface area. A larger motor is provided for the rotating Ljungstrom heat exchanger. Because of the additional weight of the heat exchanger, additional foundation and structural steel expense is incurred. High pressure steam sootblowers are installed in the cold-end of the heat exchanger. Water wash spray nozzles are also employed for on-line washing. Because of the increased heat transfer surface, there is a larger flue gas pressure drop which results, in turn, in a higher air leakage rate across the air preheater.

The costs of the major portions of the air preheater modifications, such as the increase in the heat transfer surface area and the associated increase in costs for special materials and increased structural support, are proportional to the size of the air preheater. Therefore, a cost model was developed for which the key parameter is a measure of the size of the air preheater.

For a counter-current heat exchanger (see Figure 5-15), the heat transfer is given by:

$$q_{aph} = U_{aph} A_{aph} \Delta T_{LM,aph}$$

where

$$\Delta T_{LM,aph} = \frac{(T_{fg,i} - T_{a,o}) - (T_{fg,o} - T_{a,i})}{\ln\left(\frac{T_{fg,i} - T_{a,o}}{T_{fg,o} - T_{a,i}}\right)}$$

is the log-mean temperature difference (LMTD). The product of the universal heat transfer coefficient, U, and the heat exchanger surface area, A, is assumed here to be constant for an air preheater before and after modification for use with SCR. Prior to modification, the air preheater has a higher heat transfer coefficient and a lower surface area than after modification. However, the heat exchanger is designed in either case to accommodate the same inlet and outlet conditions and, hence, the same LMTD. The product UA is calculated based on the known flue gas and air inlet and

outlet temperatures, the flue gas molar flow rate, and the average specific heat of flue gas. A typical value for the latter is 7.9 Btu/(lbmole-°R). Thus,

$$(UA)_{aph} = \frac{q_{aph}}{\Delta T_{LM,aph}} \qquad (5\text{-}11)$$

$$q_{aph} = M_{fg} c_{p,fg} (T_{fg,o} - T_{fg,i})$$

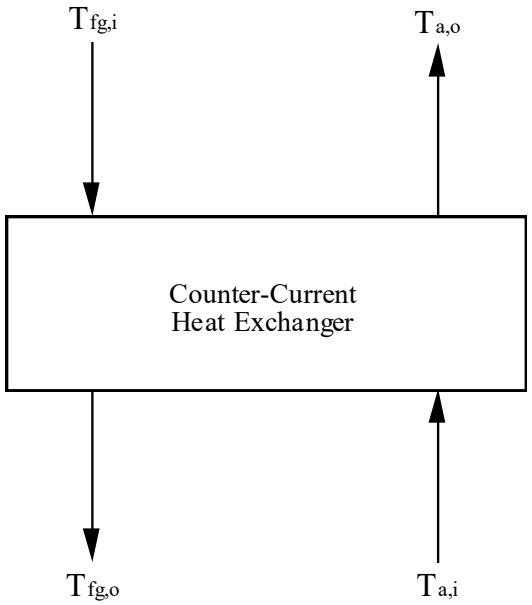

Figure 5-15. Simplified Schematic of a Counter-Current Flow Heat Exchanger

There are only two data points from the EPRI study which are directly relevant to estimating a reference basis for the product UA. These are the two cases involving installation of a new SCR system involving Ljungstrom air preheaters (Cases 1.0 and 2.0 in the EPRI report). Other cases reported are for modifications to shell and tube heat exchangers or for retrofit modification to Ljungstrom heat exchangers.

For the first case (Case 1.0), the inlet and outlet air temperatures are not given. The amount of heat transfer is estimated based on the flue gas cooling from 725°F to 270°F. Assuming an inlet air temperature of 80°F, and accounting for air leakage across the air preheater, the boiler air outlet temperature is estimated to be approximately 600°F. Using these values, the LMTD is estimated to be 155°F and the amount of heat transferred through the heat exchanger is 680 million Btu/hr. Therefore, the UA product in this case is 4.4 x 10^6 Btu/°F. Using a similar approach for Case 2.0 yields a UA product of 2.3 x 10^6. In this latter case, the reported primary air temperature (air preheater air-side outlet temperature) is inconsistent with the amount of heat transfer obtained from flue gas cooling, assuming an inlet air temperature of 80°F. Therefore, an independently calculated value of approximately 510°F was used.

The costs of air preheater modifications for the two cases are $1.37 million and $0.81 million, respectively (in December 1989 dollars). Assuming that the cost of the modification is proportional the UA product, then from these two cost estimates the following capacity-exponent cost model is obtained:

$$DC_{aph,\mathrm{mod}} = 1370\ \mathrm{N}_{T,aph} \left(\frac{UA_{T,aph}}{4.4x10^6\ N_{T,aph}} \right)^{0.8} \left(\frac{PCI}{357.3} \right)$$

While this model is based on only two data points, it nonetheless appears to provide a qualitatively reasonable relationship between air preheater modification costs based on the size of the air preheater. The model suggests a modest economy of scale for modifications to larger air preheaters.

5.7.5. Gas-Gas Heat Exchanger

The cost model for the gas-gas heat exchanger (GGH) used for cold-side SCR applications was developed in a manner similar to that for air preheater modifications. The GGH is a Ljungstrom heat exchanger, and typically there is one GGH per SCR reactor. Thus, in a typical 500 MW power plant, there would be two GGHs.

A simplified schematic of the GGH is shown in Figure 5-16. Gas exiting the flue gas desulfurization (FGD) system is heated by counter-current heat exchange with high temperature gas exiting the SCR reactor. The "untreated" gas entering the SCR system is heated by a duct burner.

There is only one case study in the EPRI report by Robie and Ireland which deals with a cold-side SCR. The UA product described in Equation (5-11) is assumed here as the key measure of heat exchanger size. Based on reported gas temperatures and flow rates, and correcting for gas leakage through the heat exchanger, the direct cost model is:

$$DC_{GGH} = 9100\, N_{T,GGH} \left(\frac{UA_{T,GGH}}{4.4x10^{6}\, N_{T,GGH}} \right)^{0.8} \left(\frac{PCI}{357.3} \right) \qquad (5\text{-}12)$$

This model is based on a GGH design with 5.6 percent gas leakage, on a mass basis. For a system with no leakage, multiply the cost given in Equation (5-12) by a factor of 2.4.

The cost of the duct burner is proportional to the amount of natural gas required to raise the flue gas temperature. The duct burners include combustion air fans, process controls, and a flame safeguard system. The capacity of the duct burners is expressed based on the heating value of the natural gas. The direct cost is given by:

$$DC_{DB} = 264\, N_{T,DB} \left(\frac{Q_{NG}}{90\ \mathrm{N_{T,DB}}} \right)^{0.6} \left(\frac{PCI}{357.3} \right)$$

where

$$Q_{NG} = \frac{m_{NG}\, HHV_{NG}}{10^{6}}$$

5.7.6. ID Fan and Booster Fan Costs

For a new SCR installation, the ID fans must be sized to deal with the increased flue gas pressure drop resulting from the additional ductwork and the SCR reactor. Typically, the increase in flue gas pressure drop is approximately 11 inches of water. The size of an ID fan and motor is proportional both to the flue gas flow rate and to the pressure drop. Therefore, the cost of the ID fan modifications is assumed here to be proportional to the difference in flue gas energy requirement necessary to overcome the flue gas pressure drop. This energy requirement is given by:

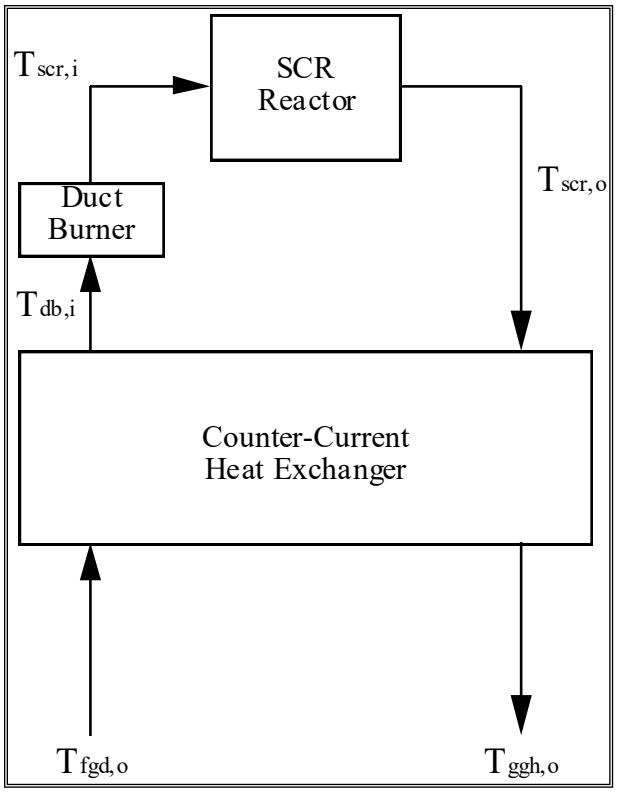

Figure 5-16. Simplified Schematic of the Gas-Gas Heat Exchanger Employed in Cold-Side SCR Systems

$$EC_{ID,dif} = \frac{\dot{Q}_{fg}\ \Delta P_{SCR}}{8{,}512\ \eta_{fan}} \qquad (5\text{-}13)$$

The fan efficiency is typically 85 percent. The cost of the ID fan differential is:

$$DC_{ID,dif} = 180\left(\frac{EC_{ID,dif}}{4{,}600}\right)^{0.6}\left(\frac{PCI}{357.3}\right)$$

In the case of a cold-side SCR system, a booster fan is required to overcome the flue gas pressure drop throughout the GGH and SCR components. Typically, the pressure drop across the cold-side system is approximately 14.5 inches of water. Thus, using Equation (5-13) to estimate the energy requirement as a function of the actual flue gas volumetric flow rate and the pressure drop, the cost of a cold-side SCR system booster fan is given by:

$$DC_{BF} = 810\ N_{T,BF}\left(\frac{EC_{BF}}{3{,}000\ \mathrm{N}_{\mathrm{T,BF}}}\right)^{0.6}\left(\frac{PCI}{357.3}\right)$$

There is typically one booster fan per SCR reactor train.

5.7.7. Structural Support

The basis for the SCR cost estimates developed by Robie and Ireland (1991) include a separate cost for structural support. While the definition of this process area is lacking, it appears to be related primarily to the SCR reactor housing, ductwork, and air preheater. In the case of a cold-side SCR system, the structural cost is related to the gas-gas heat exchanger, rather than the air preheater. As part of the data analysis, the structural cost was expressed as a percentage of the direct costs for the reactor housing, ductwork, and air preheater modifications for hot-side applications, and as a

percentage of the direct costs for the reactor housing, ductwork, and gas-gas heat exchanger costs for cold-side applications. Of the 14 data points from the EPRI study, 12 of them yielded structural costs as a relatively narrow range of percentages of the appropriate direct costs. The mean value was 18.7 percent, with a range from 16.2 to 20.8 percent and a standard deviation of 1.4 percent. For one retrofit case with a high site congestion, the structural costs were 50 percent of the other selected direct costs. For a new SCR hot-side application, the structural costs are estimated as:

$$DC_s = f_s(DC_R + DC_D + DC_{APH})$$

and for a cold-side application the structural costs are estimated as:

$$DC_s = f_s(DC_R + DC_D + DC_{GGH})$$

where f_s has a mean value of 0.187. For a retrofit application, a value of f_s of as high as 0.5 may be appropriate.

5.7.8. Miscellaneous Other Direct Capital Costs

Other capital costs may be incurred for ash handling addition, water treatment addition, and flow modeling for a hot-side SCR system. For a cold-side system, costs are incurred for water treatment and flow modeling.

Flow modeling costs are similar for all systems and typically represent a flat fee for designing the ammonia injection system to assure proper mixing of ammonia and flue gas. The value used in the EPRI study was $100,000.

Ash handling addition is required for hot side systems to remove ash deposited in the bottom of the SCR reactor to existing ash piping or to an ash silo. This cost is small compared to the costs of reactors, ammonia injection, heat exchangers, and fans. Here, it is assumed to have a value of approximately $150,000 for a 550 MW power plant.

For hot-side applications, there is additional waste water burden associated with soot-blowing and water washing in the SCR system. In the cold-side system, additional equipment is required to collect GGH wastewater. For hot-side systems, the additional cost associated with water treatment are less than $150,000. For cold-side systems, they are approximately $500,000. These numbers are representative of a typical 550 MW power plant.

The direct cost for miscellaneous expenses of flow modeling, ash handling addition, and water treatment addition for a hot-side SCR system are:

$$DC_{misc} = \left\{100 + 300\left(\frac{MW_e}{550}\right)^{0.6}\right\}\left(\frac{PCI}{357.3}\right)$$

For a cold-side SCR system, the direct cost is:

$$DC_{misc,CS} = \left\{100 + 650\left(\frac{MW_e}{550}\right)^{0.6}\right\}\left(\frac{PCI}{357.3}\right)$$

5.7.9. Total Direct Cost

The total direct cost is the sum of all of the direct costs. The cost of the initial catalyst charge is also included here in the total direct cost, because it is such a large and integral part of the SCR system. One component of the direct cost not estimated in any of the above sections is the cost of general facilities associated with the SCR process area. Based on the estimates reported by Robie and Ireland, it appears that general facilities cost is approximately 4 percent of the sum of all other direct costs. The total direct cost for the hot-side SCR system is therefore:

$$TDC_{HS} = (1 + f_{GF})\left(V_{act}UC_{cat} + \sum_{i=1}^{7} DC_i\right)$$

where there are seven direct cost components (reactor housing, ammonia injection, ductwork, air preheater modifications, ID fan differential, structural, and miscellaneous).

For a cold-side system, the total direct cost is given by:

$$TDC_{CS} = (1 + f_{GF})\left(V_{act}UC_{cat} + \sum_{i=1}^{8} DC_i\right)$$

where there are eight direct cost components (reactor housing, ammonia injection system, ductwork, gas-gas heat exchanger, duct burner, booster fan, structural, and miscellaneous).

5.7.10. Other Capital Costs

Other capital costs include various indirect capital costs, as well as preproduction costs associated with startup and inventory costs associated with providing initial stocks of chemicals and fuels.

Engineering and home office fees are typically estimated as a percentage of the total direct cost. In this case, a value of 10 percent is assumed as the default.

$$C_{EHO} = f_{EHO}TDC$$

Project contingency costs are also approximately 10 percent, as assumed by Robie and Ireland. Usually, project contingency is assigned as a multiplier of the total direct cost (e.g., EPRI, 1986). For example:

$$C_{\mathrm{Pr}ojC} = f_{\mathrm{Pr}ojC}TDC$$

Process contingency costs are typically evaluated separately for each process area. The total process contingency is given by:

$$C_{\mathrm{Pr}ocC} = \sum_i f_{\mathrm{Pr}ojC}DC_i$$

Typical values of the process contingency are: five percent for reactor, catalyst, structural support, and fans; ten percent for ammonia storage, ductwork, air preheater modifications, and gas-gas heat exchanger; fifteen percent for water treatment addition, and twenty percent for ash handling addition.

The total plant cost, or overnight construction cost, is given by:

$$TPC = TDC + C_{EHO} + C_{\mathrm{Pr}ojC} + C_{\mathrm{Pr}ocC}$$

An allowance for funds during construction (AFDC) is calculated based on the TPC as a function of the amount of time it would take to construct an SCR system. An 18-month construction period for a new plant is assumed. Methods for computing the AFDC are documented elsewhere (e.g., EPRI, 1986) and are not repeated here. The total plant investment (TPI) represents the sum of the total plant cost and the AFDC.

The final measure of capital cost is the total capital requirement (TCR). The TCR includes the total plant investment plus costs for royalties, startup costs, and initial inventories of feedstocks. In this case, no costs are assumed for royalties. Preproduction costs typically include one month of both fixed and variable operating costs and two percent of total plant investment. In the case of an SCR system, by far the largest portion of the preproduction (startup) costs are represented by the two percent multiplier on TPI. Inventory capital is estimated as 0.5 percent of total process capital excluding catalyst. The costs for initial catalysts and chemicals is zero. The SCR catalyst is included in the process capital costs. Thus, for an SCR system, the total capital requirement is:

$$TCR = (1 + f_{PP})TPI + f_{IC}\sum_i DC_i$$

5.8. O&M Costs

The annual costs for SCR systems include fixed and variable operating costs. Fixed operating costs include operating labor, maintenance labor and materials, and overhead costs associated with administrative and support labor. Variable operating costs include consumables, such as ammonia and catalyst replacement. Costs for steam and electricity consumed from within the plant may also be estimated.

5.8.1. Fixed Operating Costs

The fixed operating costs are predicated on 4 hours of labor per day per SCR reactor train for operating labor, and 8 hours of labor per day per SCR train for maintenance labor. Maintenance materials are estimated as one percent of the total process capital cost, excluding catalyst. Administrative and support labor is estimated as 30 percent of operating and maintenance labor costs. Therefore, the total fixed operating cost is given by:

$$FOC = 1.3\,(4+8)\,365\,\mathrm{N}_{\mathrm{T,R}} UC_L + 0.01\sum_i DC_i$$

A typical labor rate would be $22/hour for a Midwest location.

5.8.2. Variable Operating Costs

The major component of the variable operating cost is for catalyst replacement. The analytical models for estimating catalyst replacement are reported by Frey (1993) and are not repeated here. Similarly, the ammonia mass flow requirement, the steam requirement for ammonia injection, and the electricity consumption for the SCR systems are also reported by Frey (1993).

Therefore, the total variable operating cost for the SCR system may be estimated as:

$$VOC = V_{C,a} UC_{cat} + 8{,}760 c_f \left[\left(\frac{M_{NH_3,A,i}}{117.6} \right) UC_{NH_3} + \left(\frac{18 M_{steam}}{1{,}000} \right) UC_{steam} + E_{scr} UC_{elec} \right]$$

The unit cost for catalyst is highly variable. Robie and Ireland (1991) used a value of $660/ft^3, but noted that at the time of their study, catalyst costs in Europe were as low as $330/ft^3. The unit cost of ammonia is typically $150/ton. The unit cost of steam is approximately $3.00/1,000 lb. The cost of power is often assumed to be 5 cents per kWh.

5.9. References

Anderson, C. M., and J. A. Billings. "Simple Calculation Measures NH_3 Slip for Cogeneration Units," *Power Engineering*, April 1991, pp. 42-44.

Balling, L., and D. Hein. "DeNO_x Catalytic Converters for Various Types of Furnaces and Fuels--Development, Testing, and Operation," in 1989 Symposium on Stationary Combustion Nitrogen Oxide Control, Volume 2. Electric Power Research Institute. Palo Alto, California. Report No. GS-6423. July 1989. pp. 7A-27 to 7A-40.

Bauer, T.K., and R.G. Spendle (1984), "Selective Catalytic Reduction for Coal-Fired Power Plants: Feasibility and Economics," CS-3603, Electric Power Research Institute, Palo Alto, CA, October.

Behrens, E. S., S. Ikeda, T. Yamashita, G. Mittelbach, and M. Yanai. "SCR Operating Experience on Coal-Fired Boilers and Recent Progress," presented at the 1991 Symposium on Stationary Combustion Nitrogen Oxide Control, Washington, DC, March 25-28, 1991.

Chen, J. P., M. A. Buzanowski, R.T. Yang, and J.E. Chicanowicz, "Deactivation of the Vanadia Catalyst in the Selective Catalytic Reduction Process," *JAWMA* 40(10):1403-1409 (December 1990).

Chen, J., R.T. Yang, and J.E. Chicanowicz. "Poisoning of SCR Catalysts," presented at the 1991 Symposium on Stationary Combustion Nitrogen Oxide Control, Washington, DC, March 25-28, 1991.

CMU (1993), "Development of the Integrated Environmental Control Model: Performance Models of Selective Catalytic Reduction (SCR) NO_x Control Systems," Quarterly Progress Report prepared by Carnegie Mellon University for U.S. Department of Energy, June 1993.

EPA. Integrated Air Pollution Control System, Version 4.0, Volume 2: Technical Documentation Manual.

EPRI (1986). TAG - Technical Assessment Guide. Vol 1. P-4463-SR. Electric Power Research Institute. Palo Alto, CA. December.

Fickett, K.L., "Clean Coal-NO_x for the 21st Century: Managing Permit Risk with Selective Catalytic Reduction (SCR) Technology," Paper 43a presented at the AIChE 1993 Summer National Meeting, Seattle, WA, August 14-18, 1993.

Flora, H., J. Barkely, G. Janik, B. Marker, and J.E. Chicanowicz, "Status of 1 MW SCR Pilot Plant Tests at Tennessee Valley Authority and New York State Electric and Gas," presented at the 1991 Symposium on Stationary Combustion Nitrogen Oxide Control, Washington, DC, March 25-28, 1991.

Frey, H. C. (1988), "Selective Catalytic Reduction Cost Algorithm for the Advanced Utility Simulation Model", Technical Memorandum to J. A. Martinez, Radian Corporation, July 8.

Gouker, T.R., and C.P. Brundrett. "SCR Catalyst Developments for the U.S. Market," presented at the 1991 Symposium on Stationary Combustion Nitrogen Oxide Control, Washington, DC, March 25-28, 1991.

Johnson, K.L., G.S. Shareef, and P.A. May. Evaluation of Oil-Fired Gas Turbine Selective Catalytic Reduction (SCR) NO_x Control. Prepared by Radian Corporation for the Gas Research Institute and Electric Power Research Institute. EPRI Report No. GS-7056. December 1990.

Koppius-Odink, J.M., et al. "The First DE-NO_x Installation in the Netherlands: A Demonstration Project at Epon-Nijmegen Power Station," in 1989 Symposium on Stationary Combustion Nitrogen Oxide Control, Volume 2. Electric Power Research Institute. Palo Alto, California. Report No. GS-6423. July 1989. pp. 6A-57 to 6A-83.

Kuroda, H., et al. "Recent Developments in the SCR System and Its Operational Experience," in 1989 Symposium on Stationary Combustion Nitrogen Oxide Control, Volume 2. Electric Power Research Institute. Palo Alto, California. Report No. GS-6423. July 1989. pp. 6A-39 to 6A-55.

Lowe, P.A., W. Ellison, and M. Perlsweig (1991), "Understanding the German and Japanese Coal-Fired SCR Experience," presented at the 1991 Symposium on Stationary Combustion Nitrogen Oxide Control, Washington, DC, March 25-28, 1991.

Maibodi, M., A. L. Blackard, and R. J. Page (1990), "Integrated Air Pollution Control System Version 4.0, Volume 2: Technical Documentation Manual," Prepared by Radian Corporation for U.S. Environmental Protection Agency, EPA-600/7-90-022b, December.

Maier, H., and P. Dahl, "Operating Experience With Tail-End and High-Dust Denox-Technics at the Power Plant of Heilbronn," presented at the 1991 Symposium on Stationary Combustion Nitrogen Oxide Control, Washington, DC, March 25-28, 1991.

Maxwell, J. D., and L.R. Humphries (1985), "Economics of Nitrogen Oxides, Sulfur Oxides, and Ash Control Systems for Coal-Fired Utility Power Plants," Prepared for U.S. Environmental Protection Agency, EPA-600/7-85-006, February.

May, P.A., L.M. Campbell, and K.L. Johnson. "Environmental and Economic Evaluation of Gas Turbine SCR NO_x Control," presented at the 1991 Symposium on Stationary Combustion Nitrogen Oxide Control, Washington, DC, March 25-28, 1991.

Mori, T., and N. Shimizu. "Operating Experience of SCR Systems at EPDC's Coal-Fired Power Station," in 1989 Symposium on Stationary Combustion Nitrogen Oxide Control, Volume 2. Electric Power Research Institute. Palo Alto, California. Report No. GS-6423. July 1989. pp. 6A-85 to 6A-104.

Nakabayashi, Y., and R. Abe, "Current Status of SCR in Japan," in 1987 Symposium on Stationary Combustion Nitrogen Oxide Control, Volume 2. Electric Power Research Institute. Palo Alto, California. Report No. CS-5361. August 1987. pp. 25-1 to 25-29

Necker, I.P. "Experience Gained by Neckarwerke from Operation of SCR DeNO$_x$ Units," in 1989 Symposium on Stationary Combustion Nitrogen Oxide Control, Volume 2. Electric Power Research Institute. Palo Alto, California. Report No. GS-6423. July 1989. pp. 6A-19 to 6A-38.

Novak, M., and H.G. Rych. "Design and Operation of the SCR-Type NO_x Reduction Plants at the Dürnrohr Power Station in Austria," in 1989 Symposium on Stationary Combustion Nitrogen Oxide Control, Volume 2. Electric Power Research Institute. Palo Alto, California. Report No. GS-6423. July 1989. pp. 7A-1 to 7A-26.

Offen, G.R., D. Eskanazi, M.W. McElroy, and J.S. Maulbetsch, "Stationary Combustion NO_x Control," *JAPCA* 37(7):864-871.

Robie, C.P., and P.A. Ireland (1991), "Technical Feasibility and Cost of Selective Catalytic Reduction (SCR) NO_x Control," GS-7266, Prepared by United Engineers and Constructors, Inc. for the Electric Power Research Institute, Palo Alto, CA, May.

Robie, C.P., P.A. Ireland, and J.E. Chicanowicz. "Technical Feasibility and Economics of SCR NO_x Control in Utility Applications," in 1989 Symposium on Stationary Combustion Nitrogen Oxide Control, Volume 2. Electric Power Research Institute. Palo Alto, California. Report No. GS-6423. July 1989. pp. 6A-105 to 6A-124.

Robie, C.P., P.A. Ireland, and J.E. Chicanowicz. "Technical Feasibility and Cost of SCR for U.S. Utility Application," presented at the 1991 Symposium on Stationary Combustion Nitrogen Oxide Control, Washington, DC, March 25-28, 1991.

Rubin, E.S., J.S. Salmento, J.G. Barrett, C.N. Bloyd, and H.C. Frey, *Modeling and Assessment of Advanced Processes for Integrated Environmental Control of Coal-Fired Power Plants*, prepared by Carnegie-Mellon University for the U.S. Department of Energy, Pittsburgh, Pennsylvania, NTIS DE86014713, July 1986.

Rubin, E.S., J.S. Salmento, H.C. Frey, A. Abu-Baker, and M. Berkenpas, *Modeling of Integrated Environmental Control Systems for Coal-Fired Power Plants*, Final Report, Prepared by Carnegie-Mellon University for the U.S. Department of Energy, Pittsburgh, Pennsylvania, DOE Contract No. DE-AC22-87PC79864, April 1991, 214p.

Schönbucher, B. "Reduction of Nitrogen Oxides from Coal-Fired Power Plants by Using the SCR Process: Experiences in the Federal Republic of Germany with Pilot and Commercial Scale $DeNO_x$ Plants," in 1989 Symposium on Stationary Combustion Nitrogen Oxide Control, Volume 2. Electric Power Research Institute. Palo Alto, California. Report No. GS-6423. July 1989. pp. 6A-1 to 6A-17.

Shiomoto, G.H., and L.J. Muzio, "Selective Catalytic Reduction for Coal-Fired Power Plants: Pilot Plant Results," Prepared by KVB, Inc. for the Electric Power Research Institute, Palo Alto, CA, Report No. CS-4386, April 1986.

U.S. Department of Energy, "Clean Coal Technology Demonstration Program: Program Update 1991", DOE/FE-0247P, February 1992.

6. Air Preheater

This section describes the performance and economic algorithms for the air preheater. Figure 6-1 shows a schematic of the air preheater. The purpose of the air preheater is to heat the combustion air entering the boiler by cooling the flue gas exiting the boiler. Typically, there is a significant amount of leakage between the inlet boiler air and the outlet flue gas. The model assumes that the mixing due to the leakage air occurs independently of the heat transfer across the heat exchanger. This allows separate consideration of the effect of the leakage air and the characteristics of the heat exchanger. The heat exchanger is assumed to be a counterflow type.

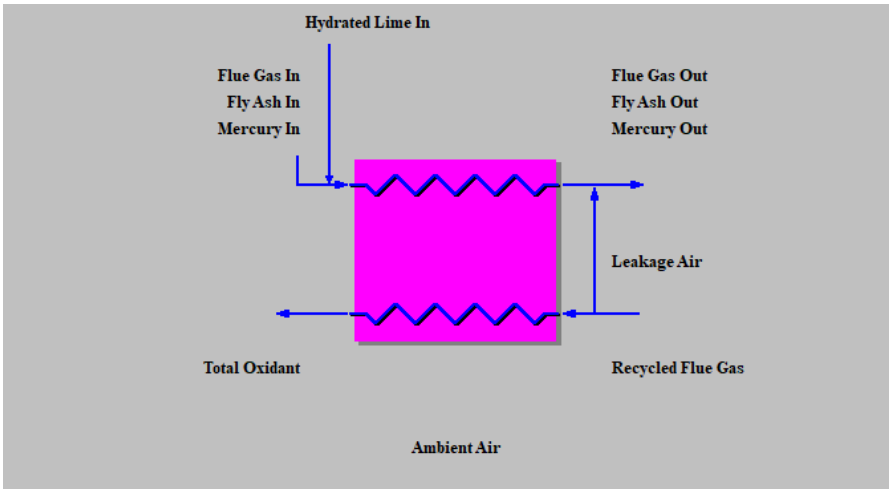

Figure 6-1. Schematic Diagram of Air Preheater

The air preheater algorithms must calculate the performance of the air preheater for a power plant with and without pollution control equipment so that the effects of adding pollution control equipment can be determined. When the term "original" or "design" is used to describe a parameter, it signifies that the parameter is determined for a power plant without pollution control equipment. The term "modified" or "actual" signifies that the parameter is determined for a power plant with pollution control equipment. The purpose of the air preheater model is to calculate

- the design "uncorrected" air preheater temperature for the boiler efficiency algorithm
- the original amount of heat transferred by the air preheater
- the original size of the air preheater
- the actual "uncorrected" air preheater temperature
- the actual amount of heat transferred by the air preheater
- the difference in the amount of energy captured by the air preheater due to the addition of pollution control equipment
- the new size of the air preheater if requested

- the additional capital cost for a larger air preheater if requested

The "uncorrected" flue gas temperature, $T_{unc,orig}$, can be determined from an energy balance of the streams "leak", "fgaphi" and "fgapho" shown in Figure 6-1. This energy balance is shown below, where the temperature of the flue gas exiting the air preheater, $T_{fgapho,orig}$, and the leakage air temperature, $T_{leak,orig}$, are known.

$$\sum_{j=1}^{9}\left(m_{leak,j,orig}\,h_j\left(T_{leak,orig}\right)+m_{fgap\,hi,j,orig}\,h_j\left(T_{unc,orig}\right)\right)=\sum_{j=1}^{9}m_{fgap\,ho,j,orig}\,h_j\left(T_{fgap\,ho,orig}\right)$$

Stream "fgapho" is equal to the sum of streams "leak" and "fgaphi". Therefore, the energy balance can be rearranged as follows:

$$\sum_{j=1}^{9}m_{fgap\,hi,j,orig}\left(h_j\left(T_{unc,orig}\right)-hj\left(T_{fgap\,ho,orig}\right)\right)$$
$$=\sum_{j=1}^{9}m_{leak,j,orig}\left(h_j\left(T_{fgap\,ho,orig}\right)-h_j\left(T_{leak,orig}\right)\right)$$

The temperature difference between $T_{fgapho,orig}$ and $T_{unc,orig}$ is usually less than 40°F, so the left-hand side of this equation can be estimated by the average heat capacity times the temperature difference between $T_{unc,orig}$ and $T_{fgapho,orig}$. The average heat capacity is estimated between $T_{fgapho,orig}$ and $T_{fgapho,orig}$ + 40°F. Therefore, $T_{unc,orig}$ is determined by

$$T_{unc,orig}=\frac{\sum_{j=1}^{9}m_{leak,j,orig}\left(h_j\left(T_{fgap\,ho,orig}\right)-h_j\left(T_{leak,orig}\right)\right)}{Cp_{fgap\,hi,avg,orig}}+T_{fgap\,ho,orig}$$

Where

$$CP_{unc,avg,orig}=\frac{\sum_{j=1}^{9}m_{fgap\,hi,j,orig}\left(h_j\left(T_{fgap\,ho,orig}+40\right)-h_j\left(T_{fgap\,ho,orig}\right)\right)}{40}$$

The amount of energy transferred from the flue gas to the combustion air for a power plant without pollution control equipment is

$$CP_{unc,avg,orig}=\frac{\sum_{j=1}^{9}m_{fgap\,hi,j,orig}\left(h_j\left(T_{fgap\,ho,orig}+40\right)-h_j\left(T_{fgap\,ho,orig}\right)\right)}{40}$$

The temperature of the combustion air exiting the air preheater is typically less than 535°F. It can be estimated by

$$T_{apho,orig}=\frac{Q_{aph,orig}}{2000M_{fuel}Cp_{apho,avg,orig}}+T_{fdfan,orig}$$

Where

$$Cp_{ap\,ho,avg,orig}=\frac{\sum_{j=1}^{9}m_{ap\,ho,j,orig}\left(h_j\left(985\right)-h_j\left(T_{fdfan,orig}\right)\right)}{985-T_{fdfan,orig}}$$

The size of the air preheater is estimated by the quantity UA, where U is the overall heat transfer coefficient and A is the surface area. For a given heat exchanger, the heat transfer can be estimated by the equation below, where the subscripts "i" and "o" represent "in" and "out" and "h" and "c" represent "hot" and "cold" respectively (10).

$$Q = \frac{UA\left[\left(T_{h,i} - T_{c,o}\right) - \left(T_{h,o} - T_{c,i}\right)\right]}{1n\dfrac{\left|T_{h,i} - T_{c,o}\right|}{\left|T_{h,o} - T_{c,i}\right|}}$$

Solving the above equation for UA for the original air preheater. Substituting the appropriate subscripts yields (6.1)

$$UA_{aph,orig} = \frac{Q_{aph,orig}}{\left(T_{fgaphi,orig} - T_{apho,orig}\right) - \left(T_{unc,orig} - T_{fdfan,orig}\right)} 1n\left(\frac{T_{fgaphi,orig} - T_{apho,orig}}{T_{unc,orig} - T_{fdfan,orig}}\right)$$

Certain pollution control equipment, such as the copper oxide and NOXSO processes, significantly change the composition and temperature of the flue gas entering the air preheater. These changes may increase or decrease the amount of energy captured by the air preheater or change the exit temperature of the flue gas exiting the air preheater. Two cases can be considered. The first (or base) case is using the original air preheater without modifications. The alternative is to resize the air preheater so that additional energy can be captured by the air preheater.

For the base case, the original air preheater is used so its size is fixed and the overall heat transfer coefficient is assumed to be constant. Therefore, the known values are

- flue gas flow rate, m_{fgaphi} and inlet temperature, T_{fgaphi}
- combustion air flow rate, m_{apho} and inlet temperature, $T_{fdfan,orig}$
- leakage air flow rate, $m_{leak,orig}$ and inlet temperature, $T_{leak,orig}$
- the product of the overall heat transfer coefficient and surface area, UA

It should be noted that m_{apho}, m_{fgaphi} and T_{fgaphi} are known, but their values may be different from their value for the original power plant without pollution control equipment.

The output parameters are the energy transferred across the air preheater, Q_{aph}, the flue gas exit temperature, T_{fgapho}, the "uncorrected" flue gas temperature, T_{unc} and the combustion air exit temperature, T_{apho}. To simplify the algorithms the average heat capacity of the flue gas entering the air preheater and the combustion air exiting the air preheater is determined.

$$Cp_{apho,avg} = \frac{\sum_{j=1}^{9} m_{apho,j}\left(h_j\left(T_{fgaphi} - 100\right) - h_j\left(T_{fdfan,orig}\right)\right)}{T_{fgaphi} - 100 - T_{fdfan,orig}}$$

$$Cp_{fgaphi,avg} = \frac{\sum_{j=1}^{9} m_{fgaphi,j}\left(h_j\left(T_{fgaphi}\right) - h_j\left(T_{fgapho,input}\right)\right)}{T_{fgaphi} - T_{fgapho,input}}$$

The variable $T_{fgapho,input}$ is the new flue gas exit temperature when the air preheater is resized. It is used for the base case as a matter of convenience to determine the average heat capacity of the flue gas. Once the average heat capacities are calculated, the "uncorrected" flue gas temperature, T_{fgapho}, is determined using the *effectiveness-NTU* method. The effectiveness, ε, is the ratio of the actual heat transfer rate for the heat exchanger to the maximum heat transfer rate.

$$\varepsilon = \frac{Q}{Q_{max}} = \frac{Cp_h\left(T_{h,i} - T_{h,o}\right)}{Cp_{min}\left(T_{h,i} - T_{c,i}\right)} \quad (6.2)$$

The subscript "min" indicates the stream with the lower heat capacity, while the subscript "max" indicates the stream with the higher heat capacity. For a counterflow heat exchanger with both fluids unmixed, the effectiveness can be approximated with the following relation.

$$\varepsilon = \frac{1 - \exp\left[-\mathrm{NTU}\left(1 - \frac{\mathrm{Cp}_{\min}}{\mathrm{Cp}_{\max}}\right)\right]}{1 - \frac{\mathrm{Cp}_{\min}}{\mathrm{Cp}_{\max}} \exp\left[-\mathrm{NTU}\left(1 - \frac{\mathrm{Cp}_{\min}}{\mathrm{Cp}_{\max}}\right)\right]} \tag{6.3}$$

In fossil fuel fired power plants, the hot fluid stream (flue gas) is significantly larger than the cold fluid stream. Therefore, the hot fluid stream has a greater heat capacity rate than the cold fluid. Equations (6.2) and (6.3) can be solved for $T_{h,o}$ by substituting C_c for C_{min} and C_h for C_{max} and eliminating ε.

$$\mathrm{T}_{\mathrm{h,o}} = \mathrm{T}_{\mathrm{h,i}} - \left(\mathrm{T}_{\mathrm{h,i}} - \mathrm{T}_{\mathrm{c,i}}\right) \frac{1 - \exp\left[-\mathrm{NTU}\left(1 - \frac{\mathrm{Cp}_{\min}}{\mathrm{Cp}_{\max}}\right)\right]}{\frac{\mathrm{Cp}_{\mathrm{h}}}{\mathrm{Cp}_{\mathrm{e}}} - \exp\left[-\mathrm{NTU}\left(1 - \frac{\mathrm{Cp}_{\min}}{\mathrm{Cp}_{\max}}\right)\right]} \tag{6.4}$$

The number of transfer units (NTU) is a dimensionless parameter in heat exchanger analysis and is

$$\mathrm{NTU} = \frac{\mathrm{UA}}{\mathrm{Cp}_{\min}}$$

Since UA is known, the term in the exponential of Equation (6.4) can be replaced by

$$\mathrm{d} = -\mathrm{NTU}\left(1 - \frac{\mathrm{Cp}_{\mathrm{c}}}{\mathrm{Cp}_{\mathrm{h}}}\right) = \frac{-\mathrm{UA}}{\mathrm{Cp}_{\mathrm{c}}}\left(1 - \frac{\mathrm{Cp}_{\mathrm{c}}}{\mathrm{Cp}_{\mathrm{h}}}\right) = \mathrm{UA}\left(\mathrm{Cp}_{\mathrm{h}}^{-1} - \mathrm{Cp}_{\mathrm{c}}^{-1}\right)$$

Therefore, Equation (6.4) can be written as

$$\mathrm{T}_{\mathrm{h,o}} = \mathrm{T}_{\mathrm{h,i}} - \left(\mathrm{T}_{\mathrm{h,i}} - \mathrm{T}_{\mathrm{c,i}}\right) \frac{1 - \mathrm{e}^{\mathrm{d}}}{\frac{\mathrm{Cp}_{\mathrm{h}}}{\mathrm{Cp}_{\mathrm{c}}} - \mathrm{e}^{\mathrm{d}}}$$

Substituting the appropriate subscripts for the air preheater into the above equations yields

$$\mathrm{T}_{\mathrm{unc}} = \mathrm{T}_{\mathrm{fgaphi}} - \left(\mathrm{T}_{\mathrm{fgaphi}} - \mathrm{T}_{\mathrm{fdfan}}\right) \frac{1 - \mathrm{e}^{\mathrm{d}}}{\frac{\mathrm{Cp}_{\mathrm{fgaphi,avg}}}{\mathrm{Cp}_{\mathrm{apho,avg}}} - \mathrm{e}^{\mathrm{d}}}$$

$$\mathrm{d} = \mathrm{UA}_{\mathrm{aph,orig}}\left(\mathrm{Cp}_{\mathrm{fgaphi,avg}}^{-1} - \mathrm{Cp}_{\mathrm{apho,avg}}^{-1}\right)$$

Once the "uncorrected" flue gas temperature is determined the flue gas and combustion temperatures exiting the air preheater and the heat transfer across the air preheater can be determined.

$$Cp_{leak,avg} = \frac{\sum_{j=1}^{9} m_{leak,j}\left(h_j(T_{unc}) - h_j\left(T_{leak,orig}\right)\right)}{T_{unc} - T_{leak,orig}}$$

$$\mathrm{T}_{\mathrm{fgapho}} = \frac{\mathrm{Cp}_{\mathrm{leak,avg}}\mathrm{T}_{\mathrm{leak,orig}} + \mathrm{Cp}_{\mathrm{fgaphi,avg}}\mathrm{T}_{\mathrm{unc}}}{\mathrm{Cp}_{\mathrm{leak,avg}} + \mathrm{Cp}_{\mathrm{fgaphi,avg}}}$$

$$Q_{aph} = Cp_{fgaphi,avg}\left(T_{fgaphi} - T_{unc}\right)$$

$$T_{apho} = \frac{Q_{aph}}{Cp_{apho,avg}} + T_{fdfan,orig}$$

For the resize case, the air preheater is resized so that the flue gas has an exit temperature of $T_{fgapho,input}$. Therefore, the known values are

- flue gas flow rate, m_{fgaphi} and inlet temperature, T_{fgaphi}
- combustion air flow rate, m_{fgapho} and inlet temperature, $T_{fdfan,orig}$
- leakage air flow rate, $m_{leak,orig}$ and inlet temperature, $T_{leak,orig}$
- the flue gas exit temperature, $T_{fgapho,input}$

The output parameters are the energy transferred across the air preheater, Qaph, the "uncorrected" flue gas temperature, T_{fgapho} and the combustion air exit temperature, T_{fgapho} and the air preheater size, UA. Since $T_{fgapho,input}$ is specified, the "uncorrected" flue gas temperature is

$$T_{unc} = \frac{\sum_{j=1}^{9} m_{leak,j,orig}\left(h_j\left(T_{fgap\,ho,input}\right) - h_j\left(T_{fgap\,ho,input}\right)\right)}{Cp_{fgap\,hi,avg}} + T_{fgap\,ho,input}$$

With the "uncorrected" flue gas temperature, the flue gas and combustion temperatures exiting the air preheater and the heat transfer across the air preheater can be determined. The flue gas exit temperature, T_{fgapho}, should be very close to $T_{fgapho,input}$.

$$T_{fgapho} = \frac{Cp_{leak,avg}T_{leak,orig} + Cp_{fgaphi,avg}T_{unc}}{Cp_{leak,avg} + Cp_{fgaphi,avg}}$$

$$Q_{aph} = Cp_{fgaphi,avg}\left(T_{fgaphi} - T_{unc}\right)$$

$$T_{apho} = \frac{Q_{aph}}{Cp_{apho,avg}} + T_{fdfan,orig}$$

Once all the exit temperatures are determined, the new air preheater size, UA_{aph}, can be determined with

$$T_{apho} = \frac{Q_{aph}}{\left(T_{fgaphi} - T_{apho}\right) - \left(T_{unc} - T_{fdfan,orig}\right)} \ln\left(\frac{T_{fgaphi} - T_{apho}}{T_{unc} - T_{fdfan,orig}}\right)$$

Once the new size is determined, the additional capital cost in millions of current dollars can be estimated by

$$Cap_{aph} = 2.6x10^{3}\left(UA_{aph}^{0.6} - UA_{aph,orig}^{0.6}\right)\frac{C_{idx}}{C_{idx,1984}}$$

For either the base case or the resize case, the difference in the energy transfer across the air preheater can be determined by

$$Q_{aph,delta} = Q_{aph} - Q_{aph,orig}$$

This difference in the energy transfer is an energy credit and how it affects the economics of the power plant is discussed in Section 2.5.

7. Electrostatic Precipitator

7.1. Introduction

This chapter describes the development of analytical models for the performance and costs of high-performance particulate control technologies, focusing on electrostatic precipitators. Special attention is paid to developing models which can be used to estimate costs for systems whose performance is up to a factor of three below the present NSPS standards of 0.03 lb/MMBtu. Typically, the cost models relate the capital costs and the operating and maintenance (O&M) costs to process parameters and the costs of labor and materials. The capital cost models are anchored to a base capital cost for a specific size unit and adjusted according to the actual or design parameters. The performance models are constructed to estimate the process parameters for a desired level of emissions control. The primary motivation for these models is to estimate the costs of complying with environmental standards on a basis which reflects recent advances in control technology. Finally, we incorporate the uncertainties in various process parameters and inputs costs so as to allow a more rational and robust basis for comparing different technologies.

The development of the performance and cost models for electrostatic precipitators is discussed, followed by a numerical example which illustrates the use of these new models.

7.2. Background

ESPs have long been the work horse of particulate collection at coal-fired power plants. A large number of electrostatic precipitators were installed in power plants in the 1950s and 60s when 30-40% stack plume opacity was considered adequate. However, these ESP's were inadequate as the regulations in the 70s forced utilities to move to low sulfur coals with high resistivity ash. As a result it was not unusual for coal-fired power plants to suffer reductions in capacity due to excessive stack opacity. However, since the 80s due to a tremendous improvement in the technology, ESPs have demonstrated performance that is at least as good as modern-day fabric filters. Older vintage ESPs (of 50s and 60s) performed at 0.1 lbs/MBtu for high sulfur coals. The ESPs in the 80s are almost twice the size[1] of the older ones (400-450 SCA today) and have demonstrated outlet emissions consistently well below 0.1 lbs/MBtu. In the utility industry (Kumar & Feldman, 1994), (Mastropietro, 1994a), the improved performance of ESPs has reduced the emissions of particulate matter from 0.1 lbs/MBtu to 0.01 lbs/MBtu over the last 15 years. In applications in the chemical industry (Kumar & Feldman, 1994), ESPs with SCA of 550-650 have been used in pulp and paper industry (outlet emissions of 0.006 lbs/MBtu) and SCA of 800 has been used in refineries with outlet emissions as low as 0.003 lbs/MBtu. Therefore, it is quite clear that properly sized ESPs are capable of achieving low particulate emissions that are below the 1979 NSPS standard of 0.03 lbs/MBtu.

In the next section, we describe updated performance models for sizing electrostatic precipitators. The process parameters for ESPs which affect the capital cost and O&M costs are explicated. Cost models parametrized by design parameters are then developed. Finally, we provide a numerical example to illustrate these cost models.

7.3. ESP Performance Models

ESPs consist of a series of parallel plates with rows of electrodes in between them and carry a high voltage of opposite polarity. As the particle laden flue gas enters the unit, the particles are charged by the electrodes and are attracted to the plates. At controlled intervals the plates are "rapped" which shakes the dust to a hopper below. However, some of the dust is reentrained, and is carried to the next zone or out of the stack. Most ESPs use rigid collecting plates with shielded air pockets ("baffles") through which ash falls into the hoppers after rapping. Collecting plate auxiliaries include inlet and outlet gas ducts, electrode frames, rappers, supporting framework, dust hoppers, and a protective outer shell. The discharge electrodes provide the corona. In most industrial applications a negative corona is used since its voltage-current characteristics are superior to those of a positive corona. The discharge electrodes are wires with diameters of typically 0.1-0.15 inches and are hung from a support frame with weights at the bottom. The dry dust is collected in hoppers which are usually of a pyramidal shape.

7.3.1. Ash Resistivity

The issue of proper sizing for electrostatic precipitation involves particle charging, particle collection, and removal of collected dust (Edgar, 1983; Oglesby & Nichols, 1978). In this section, we characterize the different parameters which affect electrostatic precipitation and sizing. The general equation used for describing the relationship between ESP size and collection efficiency is the so-called Deutsch-Andersen equation shown below:

$$\eta = 1 - \exp\left(-\frac{A}{V}w\right) \qquad (7\text{-}1)$$

where

η = collector removal efficiency

A = collector area, ft^2

V = volumetric flue gas flow rate, 1000 acfm

w = electrical migration velocity, 1000 ft/min

SCA = specific collection area, A/V

The specific collection area, SCA, is used as the sizing parameter for ESPs. The electrical migration velocity (also called precipitation rate parameter), w, is a critical parameter since it relates the removal efficiency to electrostatic precipitation. The most important factor that determines the electrical migration velocity is the *coal ash resistivity*. The resistivity in turn is a function of three main factors: (1) the flue gas composition, (2) ash composition, and (3) the temperature of the ash in ESP. The Bickelhaupt resistivity algorithms are commonly used to predict resistivity (Bickelhaupt, 1986; Bickelhaupt & Altman, 1984). The algorithms are based on a resistivity-reciprocal absolute temperature curve which is derived from three separate effects discussed below.

1. Volume resistivity, ρ_v, can be described as the resistivity of flyash excluding the influence of flue gas composition. Ash composition, temperature, and physical characteristics of the particulate layer principally affect it.
2. Surface resistivity, ρ_s, results from the interaction of ash surface with adsorbed water vapor. Ash composition, gas temperature, gas moisture concentration and physical characteristics of ash affect it.
3. Acid resistivity, ρ_a, represents the conduction mechanism associated with adsorbed sulfuric acid vapor. It is affected by the sulfur content of coal.

The overall resistivity (ρ_{vsa}) is calculated by treating these individual resistances in parallel and is provided in the equation below:

$$p_{vsa} = \frac{p_a \times p_v \times p_s}{p_a \times p_v + p_v \times p_s + p_a \times p_s} \qquad (7\text{-}2)$$

We have implemented this algorithm for calculating coal ash resistivity in IECM and is shown in "Analytica Model Code for Ash Resistivity" on page 134. However, there is some discrepancy in the predictions of this model and values used in industrial practice especially for western coals (Mastropietro, 1994b; Sloat, 1994). As shown in Table 7-1, we introduce correction factors (Mastropietro, 1994b) for the Bickelhaupt models where appropriate. "Coal and Ash Analysis" on page 138 provides an ultimate analysis and the coal ash composition for each coal type (based on literature).

Table 7-1. Coal Resistivity

Coal Type*	Industry Experience	Bickelhaupt algorithm	Correction factors
App.MS	E8-E10	1.3E9	1
WPCU	E9 - E10	7.6E10	1
Ill#6	E8 - E10	3E8	1
NDL	E8 - E10	3E8	1
WPRB (low) (high)	E9 - E11 E13	9E10 (low) 2E12(high)	1 (low) 10 (high)
App.LS	E12	1.2E12	1

* The coals used for comparison have the following attributes or properties:

App.MS = Appalachian Medium Sulfur (12.7 KBtu/lb. 2% S, 8% ash)

App.LS = Appalachian Low Sulfur (12.2 KBtu/lb, 0.5% S, 11.4% ash)

WPCU = Wasatch Plateau (Central Utah) (11.24 KBtu/lb, 0.6% S, 11% ash)

Ill#6 = East Central Illinois #6 (10.1 KBtu/lb, 4% S, 16% ash)

NDL = North Dakota Lignite (6.6 KBtu/lb, 0.7% S, 7.8 % ash)

WPRB = Wyoming Powder River Basin, (8.0 KBtu/lb, 0.5% S, 6.4% ash) the Na_2O content in ash varies 0.1-0.5%, 0.5% corresponds to low resistivity and 0.1% to high resistivity

7.3.2. Effective Migration Velocity

The next step in developing performance models involves correlating the total resistivity ρ_{sva} to the electrical migration velocity *w*. It is possible to develop a theoretical model which relates *w* to resistivity, which involves solving for the electric field and current density in the gas space between the collecting plates. This requires numerically solving for a set of partial differential equations which describe the electric field in between the plates (McLean, 1988; Oglesby & Nichols, 1978; White, 1977). Various computer-based theoretical models have been developed which represent in greater detail the electrical properties of ash and its particle size distribution (Lawless & Altman, 1989; Lawless & Plaks, 1989). However, in practice, such idealized calculations often do not match experimental data well due to non-uniformities in gas flow distribution, gas sneakage, and rapping reentrainment. Moreover, it is desirable, especially in preliminary design, to have models that are relatively simple to use. In this report, we derive correlations between *w* and resistivity ρ_{sva} by deriving "effective" values for *w* corresponding to empirical data for *SCA* values for different coals and different emission limits. A modified version of the Deutsch equation, discussed below, is used to derive the effective values for *w*. These values are then correlated to the coal ash resistivity derived from the corrected Bickelhaupt algorithms.

The Deutsch-Anderson Equation (see (7-1)) is accurate only up to 95% removal efficiencies. Various empirical models have been developed to describe the "tailing off" of the efficiency curve at higher efficiencies ($\eta > 95\%$). One such empirically based performance model that has found widespread use and is able to effectively describe the efficiency curve for high *A/V* values was developed by White (White, 1977) and is provided in the following equation:

$$\eta = 1 - \exp\left(-\frac{A}{V} w_k \right)^k \qquad (7\text{-}3)$$

This equation is the so-called modified Deutsch equation. Typically, a value of $k \approx 0.6$ (Mastropietro, 1994b) is used in industrial practice today. In Table 7-2, typical *SCA* values for different removal efficiencies and coals are provided. The modified Deutsch equation (7-3) is used to derive the values for precipitation rate parameter w_k (column 5) corresponding to two sets of empirical SCA values. It is important to remember that when we use the modified-Deutsch equation (7-3), the rate parameter w_k ceases to have a physical interpretation (such as precipitation velocity for Equation (7-2)) and only provides a way to parameterize the effect of resistivity.

Table 7-2. Estimation of w_k

Coal	η %	SCA[1]	w_k[1]	SCA[2]	w_k[2]	W_k (aver)
App. MS	98 99.4 99.8	205 295 415	0.0474 0.0515 0.0506	175 270 370	0.0555 0.0563 0.0568	0.053
WPCU	98.7 99.6 99.87	255 385 520	0.0453 0.0448 0.0452	285 425 575	0.0406 0.0406 0.0409	0.043
Ill #6	99.2 99.76 99.92	220 320 425	0.0627 0.0625 0.0622	230 335 440	0.06 0.0597 0.06	0.061
NDL	98.9 99.68 99.89	220 310 420	0.056 0.0556 0.0583	230 335 440	0.0535 0.0515 0.0556	0.055
WPRB (low resist)	98 99.5 99.8	280 405 550	0.0347 0.0398 0.0382			0.037
WPRB (high resist)	98 99.5 99.8			540 835 1055	0.018 0.0193 0.0199	0.019
App.LS	98.65 99.6 99.87	320 490 665	0.0356 0.0352 0.0353	355 540 735	0.0321 0.0319 0.032	0.034

[1] SCA values are based on typical values suggested by vendors (Gaikwad & Sloat, 1992). SCA units are shown in ft^2/1000 acfm and drift velocity in 1000 ft/min.

[2] SCA values used by Research-Cottrell (Mastropietro, 1994b). SCA units are shown in ft^2/1000 acfm and drift velocity in 1000 ft/min

The effective values calculated for w_k and the corresponding resistivities for each coal type (shown in Table 7-2) are summarized in Table 7-3.

Table 7-3. Summary of Resistivity and w_k

Coal	Resistivity (ohm-cm)	$W_{k\ 1000\ ft/min}$
App.MS	1.3E9	0.053
WPCU	7.6E10	0.043
Ill #6	3E8	0.0612
NDL	3E8	0.055
WPRB (low)	9E10	0.037
WPRB (high)	2E13	0.019
App.LS	1.2E12	0.034

We now derive a regression model to develop a functional relation between resistivity and the parameter w_k. We find that a log-linear relationship (resistivity on log-scale) provides an excellent fit for the data presented in Table 7-3. A regression analysis conducted in *Splus* presented in "Regression Analysis for w_k" on page 138 indicates that the log-linear relationship provides a R^2 =0.96. The functional relation between these two parameters is provided in Equation (7-4).

$$w_k = 0.1232972 - 0.003323934 \times \ln(\rho_{vsa}) \qquad (7\text{-}4)$$

This relationship can be used to estimate w_k for any given coal.

In summary, the new IECM performance models for cold-side ESPs are used as follows:

1. For a given coal, use the corrected-Bickelhaupt algorithm to calculate the resistivity, ρ_{vsa} of the flyash produced in the boiler. The resistivity depends on the coal ash composition, sulfur content, flue gas temperature, and moisture content.
2. Using Equation (7-4) and the resistivity, determine the parameter w_k.
3. Finally for a given emission limit (i.e. removal efficiency), determine the sizing parameter SCA using the modified-Deutsch equation (7-3).

Note that all the models developed in this section estimate the SCA values for a minimal spacing of 12 inches between plates.

7.3.3. Default Ash Composition

The new performance models implemented in IECM for cold-side ESPs requires as input coal ash composition, sulfur content, flue gas temperature, and moisture content. The coal ash composition needs to be specified with respect to the following ten constituents: SiO_2, Al_2O_3, Fe_2O_3, CaO, MgO, Na_2O, K_2O, TiO_2, P_2O_5, SO_3. In many cases, this information may not be readily available to the model user. We have developed a capability in IECM to pick default coal types for ash composition based on coal rank and sulfur content. Table 7-4 describes the rules used to pick default ash composition.

Table 7-4. Default Ash Composition

Coal Rank	Classification	Default Ash Composition
Lignite	NDL	NDL
Sub-Bituminous	WPRB	WPRB
Bituminous	App.MS, App.LS, Ill#6, WPCU	If %S < 1.5% then App.LS else App.MS

For example, if the model user does not have readily available the ash composition of the coal, but knows the rank to be bituminous and sulfur content to be less than 1.5% then IECM uses this information to pick App.LS coal as a default for ash composition.

7.4. ESP Cost Models

The cost models for ESPs include both capital costs and operating and maintenance (O&M) costs. These models follow the economic premises for cost development and breakdown developed by EPRI (Gaikwad & Sloat, 1992). The cost areas used are shown in Table 7-5.

Table 7-5. ESP Process Areas

Process Area	Description
10	Collectors
20	Ductwork
30	Fly Ash Handling System
40	Differential Cost

The models developed in this report are based on data provided in two EPRI reports (Gaikwad & Sloat, 1992; Scheck, Mora, Belba, & Horney, 1985) and reflect price quotes from equipment vendors. In this section, we will first present the methodological basis used for model development.

7.4.1. Capital Cost Models

The major design parameters which can significantly impact the total system capital cost are *gas flow volume* (which depends on the generating unit size), *SCA*, the collecting plate area per transformer-rectifier (T-R) set and the spacing between collector plates. All calculations below are based on a default spacing of 12 inches. However, as the spacing between plates increases (as is the case with most modern ESPs), the SCA required also increases and this scaling is a simple ratio as shown in Equation (7-5).

$$\frac{SCA}{SCA'} = \frac{D_{plates}}{D_{plates}'} \qquad (7\text{-}5)$$

where

SCA' = SCA required for base case spacing, say 12 inches

D'_{plates} = default spacing between plates, i.e. 12 inches

The data used to choose different vectors of the design parameters are shown in Table 7-6. (Scheck, et al., 1985).

Table 7-6. Experimental Design

Case	Size in MW	SCA ft^2/1000 acfm	Area per T-R set (ft^2/T-R set)
Base	500	400	23750
1	250	400	23750
2	1000	400	23750
3	500	250	29700
4	500	800	23750
5	500	400	31700
6	500	400	19000
Range	250-1000	250-800	19000-31700

The costs for each vector of parameters in Table 7-6, broken down by process area is provided in Table 7-7, based on a 1985 EPRI study (Scheck, et al., 1985). Note that this cost data is used to develop scaling models and actual numbers are not important.

Table 7-7. Capital Costs in $/kW, 1982 dollars

Process Area	Case 1	Case 2	Case 3	Case 4	Case 5	Case 6	Base Case
10	34.60	29.71	20.68	55.98	29.65	33.99	32.06
20	0.88	0.85	1.00	1.01	1.01	1.01	1.01
30	8.82	4.99	5.17	8.40	5.71	6.79	6.25
40	0.74	0.74	0.74	0.75	0.74	0.74	0.74
Total	45.04	36.29	27.59	66.14	37.11	42.53	40.06

The mathematical model to describe the sensitivity of cost models to parameter variations is normalized against the cost for the base case. The general form of the cost model for each process area is as shown below:

$$N_{C,a} = \frac{N_{C,r}(8{,}760\ hr/yr)c_f}{t_r} \qquad (7\text{-}6)$$

where

PC_i = process area capital, $

PC_i' = process area capital, base case, $

G = inlet gas flow, acfm

G' = inlet gas flow, base case, acfm

$N_{c,r} = 1 \text{ or } N_c$ = collecting area per set, base case AT-R

AT-R = collecting area per set, ft^2/set

SIL = ash rate to silo, tons/hr

SIL' = ash rate to silo, base case

Based on the cost data presented in Table 7-7, the exponents of the model in Equation (7-6) is estimated and presented in Table 7-8. Note that it is important to identify the cases which vary only one parameter from the base case since these allow direct estimation of the exponents. Note also that although the cost numbers in Table 7-7 are in $/kW, total $ need to be used in the model. Since the mathematical model is multiplicative, the exponents derived in Table 7-8 are independent of the base case used.[1]

Table 7-8. Exponents for Equation (7-6)

Area	*f*	*a*	*b*	*c*
10	0.89	0.81	0.266	0
20	0	0	0	0
30	0.59	0.34	0.34	0.1
40	0	0	0	0

In Table 7-8, some of the exponents have been chosen to be zero. This is because the variations for these process areas are not expected to influence cost. Also note that these values for exponents have been averaged over several cases of available data. Due to the small size of the data set, no statistical analysis has been conducted. The exponents derived in Table 7-8 have been verified against some cost data collected more recently for unit sizes ranging from 125-500 MW (Gaikwad & Sloat, 1992), therefore the cost model can be used for the range 125-1000 MW.

The total capital requirement for ESPs is calculated as shown in Table 7-9. This includes the direct process capital costs and indirect costs associated with ESPs.

Table 7-9. Total Capital Requirement

Particulate Collector	PC_{10}
Ductwork	PC_{20}
Flyash Handling	PC_{30}
ID fans	PC_{30}
Total Process Capital	$PC=PC_{10}+PC_{20}+PC_{30}+PC_{40}$
General facilities	0.01 PC
Eng. & Home Office Fees	0.05 PC
Process Contingency	0.05 PC
Project Contingency	0.2 PC
Total Plant Cost	TPC=1.31 PC
Total Plant Investment (including AFUDC)	TPI=1.063 TPC (3 years)
Preproduction Cost	0.002 TPI
Inventory Capital	0.005 TPC
Total Capital Requirement	TCR=1.002 TPI +0.005 TPC

7.4.2. O&M Cost Models

The O&M costs for ESPs consists of fixed costs and variable costs. The fixed operating cost consists of labor, maintenance labor, material, and administrative labor. A mathematical model for the fixed cost is provided by Equation (7-7).

$$\begin{aligned} FOM &= FOM_{labor} + FOM_{maint} + FOM_{admin} \\ FOM_{labor} &= labor \times N_{labor} \times 40\ (hrs/week) \times 52\ (weeks/yr) \\ FOM_{maint} &= 0.08 \times A_{esp} + 0.0134 \times C_{20} + 0.07 \times C_{30} + 0.025 \times C_{40} \\ FOM_{admin} &= 0.3 \times (FOM_{labor} + 0.4 \times FOM_{maint}) \end{aligned} \qquad (7\text{-}7)$$

where

FOM = fixed operating cost, M$/yr

FOM_{labor} = operating labor, M$/yr

$FOM_{maint.}$ = maintenance material costs, M$/yr, the coefficients based on EPRI TAG manuals

FOM_{admin} = administrative costs (assumed to be 30% of total labor costs) M$/yr, note that 40% of $FOM_{maint.}$ are assumed to be labor costs

A_{esp} = total collector area, ft^2

labor = labor rate, $/hour

N_{labor} = number of laborers at 40 hrs/week

C_i = capital for process area *i (20,30,40)*

Notice that the model has been developed analytically except that the dependence on unit size is based on process area costs.

Table 7-10. O&M costs in 1990 $/kW-yr

O&M	125 MW	250 MW	500 MW
Ash	2.23	2.23	2.23
Power	1.41	1.31	1.23

Table 7-10 provides the variation in fixed and variable costs as a function of plant size (assuming a capacity factor of 65%). The variable cost includes the power cost and ash disposal cost. The ash disposal cost is proportional to the ash generated. The power costs are calculated based on the T-R set power and the other auxiliary power requirements. The variable operating cost is given by

$$\begin{aligned} \text{VOM} &= \text{VOM}_{\text{ash}} + \text{VOM}_{\text{power}} \\ \text{VOM}_{\text{ash}} &= cf \times C_{ash} \times 8760 \times T \\ \text{VOM}_{\text{power}} &= cf \times C_{power} \times 8760 \times \{TR' \times \left(\frac{G}{G'}\right) + AR' \times \left(\frac{G}{G'}\right)^{q}\} \end{aligned} \qquad (7\text{-}8)$$

where G, G/ are as before and

VOM = variable operating costs, M$/yr

VOM_{ash} = ash disposal costs, M$/yr

VOM_{power} = power costs (includes T-R power and auxiliary power due to pressure drop, etc.), M$/yr

cf = capacity factor

T = ash disposal rate, tons/hr

C_{ash} = ash disposal cost, $/ton, (default 10.24)

C_{power} = power cost, cents/KWh, (5.54 c/kWh)

TR' = T-R set power as a function of efficiency, as shown in Equation (7-9)

AR' = Auxiliary power other than T-R set (includes energy penalty for pressure drop), 522 kW base case

q = 0.65, exponent derived from data in Table 7-9

Notice that Equation (7-8) is such that the base case cannot be changed arbitrarily. The T-R set power consumption is a function of removal efficiency and is given by Equation (7-9).

$$TR' = A \times \left(1 - \frac{\eta}{100}\right)^{r} \qquad (7\text{-}9)$$

where

A = constant in T-R set power

η = particle removal efficiency

r = exponent in Equation (7-9)

The values of constants A, r were determined based on quotes from various vendors (Gaikwad & Sloat, 1992), and are provided in Table 7-11.

Table 7-11. Parameters for Equation (7-9)

Coal	A	r
App.MS	78	-0.375
WPCU	81	-0.371
Ill.#6	95	-0.34
NDL	108	-0.353
WPRB (low)	102	-0.36
WPRB (high)	57	-0.39
App.LS	67	-0.40

7.4.3. A Numerical Example

We will use a base case of unit size 250 MW (0.95 Macfm), with a SCA of400 ft^2/acfm, 23750 ft^2/per T-R set, using Appalachian Medium Sulfur coal (ash content 8%, ash rate to silo =10.44 tons/hr). We estimate the cost of a unit with the following design parameters:

Size = 500 MW net(1.9 Macfm), SCA = 415 ft^2/acfm,

30000 ft^2/per T-R set, Capacity factor = 65%,

Emission limit = 0.01 lb/MMBtu (99.86%), Ash disposal rate = 10.441 tons/hr

7.4.3.1. Capital Costs

$$PC_{10} = 8.53 \times \left(\frac{1.9}{0.95}\right)^{0.89} \times \left(\frac{415}{400}\right)^{0.81} \times \left(\frac{30000}{23750}\right)^{0.266} = 21.86M\$$$

$$PC_{20} = 0.835M\$$$

$$PC_{30} = 2.0825 \times \left(\frac{1.9}{0.95}\right)^{0.59} \times \left(\frac{415}{400}\right)^{0.34} \times \left(\frac{30000}{23750}\right)^{0.34} \times \left(\frac{10.44}{5.22}\right)^{0.1} = 3.68M\$$$

$$PC_{40} = 0.19M\$$$

Total Process Capital (PC) = 26.6 M$
General Facilities = 0.26 M$
Engg. & Home Office = 0.96 M$
Process Contingenc y = 1.33 M$
Project Contingenc y = 5.2 M$
Total Plant Cost (TPC) = 34.47 M$
TPI = 36.64 M$
Preproduction costs = 0.07 M$
Inventory Capital = 0.18 M$
Total Capital Requiremen t = 36.89 M$($ 73.78/kW)

7.4.3.2. Fixed Costs

$$\text{FOM} = \text{FOM}_{\text{labor}} + \text{FOM}_{\text{maint}} + \text{FOM}_{\text{admin}} = 0.53 \text{ M\$/yr}$$

$$\text{FOM}_{\text{labor}} = \text{labor} \times N_{\text{labor}} \times 40 \text{ (hrs/week)} \times 52 \text{ (weeks/yr)} = 0.12 \text{ M\$/yr}$$

$$\text{FOM}_{\text{maint}} = 0.08 \times C_{10} + 0.0134 \times C_{20} + 0.07 \times C_{30} + 0.025 \times C_{40} = 0.33 \text{ M\$/yr}$$

$$\text{FOM}_{\text{admin}} = 0.3 \times (\text{FOM}_{\text{labor}} + 0.4 \times 0.32) = 0.076 \text{ M\$/yr}$$

7.4.3.3. Variable Costs

$$\text{VOM}_{\text{ash}} = \frac{0.65}{1\times10^{6}} \times 10.24 \times 8760 \times 10.44 = 0.61\ \text{M\$/yr}$$

$$\text{VOM}_{\text{power}} = \frac{0.65}{1\times10^{6}} \times 0.0554 \times 8760 \times \{916.8 \times \left(\frac{1.9}{0.95}\right) + 522 \times \left(\frac{1.9}{0.95}\right)^{0.65}\} = 0.84\ \text{M\$/yr}$$

$$\text{VOM} = 1.45\ \text{M\$/yr}$$

7.5. Analytica Model Code for Ash Resistivity

We provide a listing of the Analytica model code for ash resistivity as implemented in the IECM.

```
Model resistivity
                          Description: Model for ash resistivity based on
                          Bickelhaupt's PB86-178126
                          Author: jk3v
Model volume_r
                          description: model for volume resistivity
                          author: jk3v
variable lina
                          units: atomic concentration in %
                          description: the atomic conc. of lithium plus sodium,
                          based on PB86-178126, appendix A, pg A-15
                          definition:
                          ashchar_atom[coalash_index='Na2O',coalindex=coals]
variable fe
                          units: atomic concentration in %
                          description: the atomic conc. of iron in ash, pg A-15
                          definition:
                          ashchar_atom[coalash_index='Fe2O3',coalindex=coals]
variable mgca
                          units: atomic conc. in wt. %
                          description: the atomic conc. of magnesium plus
                          calcium, based on PB86-178126, appendix A, pg A-15
                          definition:
                          ashchar_atom[coalash_index='MgO',coalindex=coals]+ash
                          char_atom[coalash_index='CaO',coalindex=coals]
function rv1(x,y,z:numeric)
                          description: log(vol. resistivity) at 1000/T(K)=1.6,
                          E=2 kV/cm, pg. 6-6, eq.2
                          definition: 8.9434-1.8916*logten(x)-
                          0.9696*logten(y)+1.237*(logten(z)-logten(2.5))
function rv2(x,y,z,E:numeric)
```

```
                        description: log(vol. resistivity) at 1000/T(K)=1.6,
                        E=12 kV/cm, pg. 6-6, eq.3
                        definition:rv1(x,y,z)+(E-2)*(-0.03)
variable Iv
                        units: log(ohm-cm)
                        description: the line intercept of rv vs 1/T, pg. 6-
                        6, eq. 4
                        definition: rv2(lina,fe,mgca,12)-4334.5/625
function rv(temp:numeric)
                        units: log(ohm-cm)
                        description: vol. resistivity at any T, E=12 kV/cm
                        definition: iv + 4334.5/temp
close volume_r
Model surface_r
                        description: model for surface resistivity
                        author: jk3v
function rs1(x:numeric)
                        units: log(ohm-cm)
                        description: surface resist. at 1000/T(K)=2.6,
                        E=2kV/cm, water conc.(Cw)=9%
                        definition: 10.7737 - 2.2334*logten(x)
function rs2(cw:numeric)
                        units: log(ohm-cm)
                        description: surface resist. at 1000/T(K)=2.6,
                        E=2kV/cm,any Cw
                        definition: rs1(lina)+(cw-9.0)*(-0.1280)
function rs3(cw,z:numeric)
                        units: log(ohm-cm)
                        description: surface resist. adjusted for mgca conc.,
                        at 1000/T(K)=2.6, E=2kV/cm,any Cw
                        definition: if mgca > 10 then rs2(cw)+0.56-0.056*z
                        else rs2(cw)
function rs4(cw,z,E:numeric)
                        units: log(ohm-cm)
                        description: surface resist. adjusted for E
                        definition: rs3(cw,z)+(E-2)*(-0.03)
function rs0(cw:numeric)
                        units: log(ohm-cm)
                        description: intercept for rs
```

```
                          definition:
                          rs4(cw,mgca,12)+logten(exp(1))*7.3895*10^(-
                          4)*exp(2.3033*10^3/385)*cw
function rs(cw,temp:numeric)
                          units: log(ohm-cm)
                          description: surface resist. as function of design
                          water conc.(cw) and temperature
                          definition: rs0(cw)-logten(exp(1))*7.3895*10^(-
                          4)*exp(2.3033*10^3/temp)*cw
close surface_r
function rvs1(cw,temp)
                          units: ohm-cm
                          description: surface and volume resistivities
                          calculated as parallel resistances, E=12kv/cm
                          definition:
                          10^(rv(temp)+rs(cw,temp))/(10^rv(temp)+10^rs(cw,temp)
                          )
model acid_r
                          description: model for acid resistivity
                          author: jk3v
variable rvs2
                          units: ohm-cm
                          description: vol/surface resistivity at
                          1000/T(K)=2.4, E=12kV/cm
                          definition: logten(rvs1(10,1000/2.4))+(-8)*(-0.03)
variable Ia1
                          units: log(ohm-cm)
                          description: intercept for ra1 based on mgca, fe
                          conc.
                          definition: if mgca < 5 and fe < 1 then 2.6354 else
                          0.2915
variable ra1
                          units: log(ohm-cm)
                          description: acid resist. at 4ppm SO3, 10% H2O, 417K,
                          4kV/cm
                          definition: ia1 + 0.7669*rvs2
variable sa
                          units:
                          description: coefficient for ra2
                          definition: if mgca < 5 and fe < 1 then -5.0 else -
                          2.0502
variable ia2
```

```
                        units
                        description: intercept for ra2
                        definition: ra1 - sa*logten(4)
function ra2(ca:numeric)
                        units: log(ohm-cm)
                        description: acid resist. at 4kV/cm,10%H2O, 417K, and
                        any ca
                        definition: ia2 + sa*logten(ca)
Index acid_i
                        description: index for sa1 based on so3 conc.
                        definition: ['1','2','3']
variable atom_i
                        description: index for sa1 based on lina, mgca, and
                        fe conc.
                        definition: ['1','2','3']
variable acid_v
                        description: value of sa1 index based on so3 conc.
                        definition: if so3ppm(esp_gasin) < 2.75 then '1' else
                        if so3ppm(esp_gasin) > 6.5 then '3' else '2'
variable atom_v
                        description: value of sa1 based on mgca etc conc.
                        definition: if lina > 1 and mgca > 5 then '1' else if
                        fe < 1 and mgca < 3 then '2' else '3'
variable sa1
                        description: slope of line denoting acid resistivity
                        vs 1/T
                        definition: table(atom_i,acid_i)(-4.74, -4.85, -4.85,
                        -28.39, -28.39, -28.39, -8.67, -9.71, -10.59)
function ia3(ca:numeric)
                        description: line intercept for ra3
                        definition: ra2(ca) -sa1[atom_i=atom_v,
                        acid_i=acid_v]*2.4
function ra3(ca,temp)
                        units: log(ohm-cm)
                        description: acid resist. for any T, Ca and E=4kV/cm
                        definition: ia3(ca) + sa1[atom_i=atom_v,
                        acid_i=acid_v]*1000/temp
function ra(ca,temp)
                        units: ohm-cm
                        description: acid resist. for all ca, temp
```

```
                        definition: 10^(1.95 + 0.76*ra3(ca,temp))
close acid_r
Close resistivity
```

7.6. Coal and Ash Analysis

Table 7-12. Ultimate Analysis for Coals

	App.MS	WPCU	Ill#6	NDL	WPRB	App.LS
HHV	12.7K	11.24K	10.1K	6600	8020	12.2K
Carbon	0.697	0.642	0.575	0.397	0.48	0.67
Hydrogen	0.049	0.046	0.037	0.027	0.034	0.047
Oxygen	0.081	0.058	0.08	0.114	0.11	0.078
Chlorine	0	100u	1m	200u	300u	0
Sulfur	0.02	5.8m	0.04	6.8m	4.8m	5.5m
Nitrogen	0.013	0.0116	9m	6m	6.2m	0.013
Ash	0.08	0.11	0.16	0.078	0.064	0.114
Moisture	0.06	0.754	0.12	0.37	0.3	0.07

Table 7-13. Ash Analysis for Coals

	App.MS	WPCU	Ill#6	NDL	WPRB	App.LS
SiO2	46.2	53.5	45	31.5	36.85	61
Al2O3	27.7	17.3	18	10.8	17.84	30
Fe2O3	17.2	4.5	20	13.4	5.36	2.9
CaO	3.4	10.7	7	25	26.59	0.91
MgO	0.8	2.4	1	7.1	5.48	0.76
Na2O	0.5	1.48	0.6	6.3	0.58	0.38
K2O	1.5	1.11	1.9	0.6	0.47	1.49
TiO2	1	0.7	1	0.2	1.28	0.09
P2O5	0.6	0.27	0.2	0.1	0.93	0.08
S03	1.1	7.04	3.5	4.6	3	0.2

7.7. Regression Analysis for w_k

The regression analysis for Equation (7-4) on page 128 was done using *Splus*. The analysis is presented here.

```
> data<-data.frame(wk,logr)
> data.fit<-lm(wk~logr,data)
> summary(data.fit)

Call: lm(formula = wk ~ logr, data = data)
Residuals:
 1 2 3 4 5 6 7
```

```
 -0.000486 0.003 0.002653 -0.003347 -0.00244 -0.002527 0.003147

Coefficients:
 Value Std. Error t value Pr(>|t|)
(Intercept) 0.1230 0.0073 16.7695 0.0000
 logr -0.0033 0.0003 -11.0365 0.0001

Residual standard error: 0.003153 on 5 degrees of freedom
Multiple R-Squared: 0.9606
F-statistic: 121.8 on 1 and 5 degrees of freedom, the p-value is 0.0001063

> coefficients(data.fit)
 (Intercept) logr
 0.1230496 -0.003314819
```

7.8. References

Bickelhaupt, R. E. (1986). Fly Ash Resistivity Prediction Improvement with Emphasis on Sulfur Trioxide. No. EPA-600/7-86-010). EPA, Washington, DC.

Bickelhaupt, R. E., & Altman, R. F. (1984). A Method for Predicting the Effective Volume Resistivity of a Sodium Depleted Fly Ash Layer. JAPCA, 34, 832.

Edgar, T. F. (1983). Coal Processing and Pollution Control. Houston, TX: Gulf Publishing Co.

Gaikwad, R. P., & Sloat, D. G. (1992). Economic Evaluation of Particulate Control Technologies No. EPRI TR-100748). Electric Power Research Institute.

Kumar, K. S., & Feldman, P. L. (1994). Electrostatic Precipitators versus Fabric Filters: Fact versus Fiction. In Electrostatic Precipitators versus Fabric Filters: A symposium and Debate, . Crystal City, VA: ICAC.

Lawless, P. A., & Altman, R. F. (1989). An Integrated Electrostatic Precipitator Model for Microcomputers. In Proceedings: Eighth Particulate Control Symposium, Vol. 1: Electrostatic Precipitators, 1 (pp. 12-1:15). San Diego, CA: EPRI.

Lawless, P. A., & Plaks, N. (1989). An Advanced Microcomputer Model for Electrostatic Precipitators. In Proceedings: Eighth Particulate Control Symposium, Vol. 1: Electrostatic Precipitators, 1 (pp. 13-1:14). San Diego, CA: EPRI.

Mastropietro, R. A. (1994a). Achieving Low Particulate Emissions with Electrostatic Precipitators. In Electrostatic Precipitators versus Fabric Filters: Fact versus Fiction, Crystal City, VA: ICAC.

Mastropietro, R. A. (1994b). Performance models for low emission ESPs. In Research-Cottrell.

McLean, K. J. (1988). Electrostatic Precipitators. IEE Proceedings, 135, Pt. A(6), 341-61.

Oglesby, J. S., & Nichols, G. B. (1978). Electrostatic Precipitation. New York, NY: Marcel Dekker Inc.

Scheck, R. W., Mora, R. H., Belba, V. H., & Horney, F. A. (1985). Economics of Fabric Filters and Electrostatic Precipitators No. EPRI CS-4083). Electric Power Research Institute.

Sloat, D. G. (1994). Coal Ash Resistivity. In Sargent & Lundy.

White, H. J. (1977). Electrostatic Precipitation of Fly Ash. JAPCA, 27(3), 206.

8. Fabric Filter

8.1. Introduction

This chapter describes the development of analytical models for the performance and costs of high-performance particulate control technologies, focusing on fabric filters. Special attention is paid to developing models which can be used to estimate costs for systems whose performance is up to a factor of three below the present NSPS standards of 0.03 lb/MMBtu. Typically, the cost models relate the capital costs and the operating and maintenance (O&M) costs to process parameters and the costs of labor and materials. The capital cost models are anchored to a base capital cost for a specific size unit and adjusted according to the actual or design parameters. The performance models are constructed to estimate the process parameters for a desired level of emissions control. The primary motivation for these models is to estimate the costs of complying with environmental standards on a basis which reflects recent advances in control technology. Finally, we incorporate the uncertainties in various process parameters and inputs costs so as to allow a more rational and robust basis for comparing different technologies.

The initial development of the performance and cost models for fabric filters is discussed followed by a numerical example which illustrates the use of these new models. The next quarterly report will provide a similar update of the IECM electrostatic precipitator models, plus a brief discussion of the comparative advantages of different particulate control.

8.2. Fabric Filters for Electric Utilities

Fabric filters have been very effective in achieving the 1979 NSPS limits for coal-fired power plants. As a result, over 100 baghouses associated with 20,000 MW of generating capacity are in operation in the U.S. utility industry (Cushing, Bush, & Synder, 1990; Kumar & Feldman, 1994; Puille, 1985). These units routinely perform at efficiencies above 99.9% and produce clear stack plumes with less than 1% opacity. These fabric filters have been in operation with pulverized coal-fired boilers of various designs including some which are installed on fluidized bed combustion boilers. Operating experience in the U.S. has been predominantly with reverse gas cleaning (about 90%) with low air-to-cloth ratio baghouses. Bag failure rate has stabilized at about 1% per year through the 1980s and four-year bag life is now fairly common. In particular, there has been virtually no reduction in boiler availability due to baghouse malfunction since any target compartment can be brought off-line for baghouse replacement.

In this chapter, we will first discuss the important design parameters for fabric filters and their effects on capital and O&M costs. The design parameters are dependent on the bag cleaning method and this will be explicated. Cost models parameterized by design parameters are developed, along with a numerical example to illustrate the cost models.

8.3. Fabric Filter Design

Fabric filters are essentially huge vacuum cleaners consisting of a large number of long tubular filter bags arranged in parallel flow paths. As the ash-laden flue gas passes through these filters, almost all of the particulate matter is removed. Ash that accumulates on the bags is removed periodically by cleaning. For properly designed fabric filters, the size of the system is independent of the removal efficiency. Thus, efficiency can be improved without an associated increase in

capital costs. The issue of a proper design is characterized by a number of parameters which we now discuss in some detail. We also provide the default operating values used in the industry today with an estimate of uncertainty to bound the variation observed in practice (Belba, Grubb, & Chang, 1992; Carr & Smith, 1984; Cushing, et al., 1990; Scheck, Mora, Belba, & Horney, 1985; Sloat, Gaikwad, & Chang, 1993).

There are various bag cleaning techniques that are used and this influences other process parameters in a non-trivial way. There are four available bag cleaning methods:

1. Reverse Gas Cleaning (RG): This is an off-line bag cleaning technique in which an auxiliary fan forces a relatively gentle flow of filtered flue gas backwards through the bags causing them to partially collapse and dislodge the dustcake. Over 90% of the U.S. utility baghouses use reverse-gas cleaning.
2. Reverse Gas/sonic cleaning (RG/S): A variation of RG in which low frequency pneumatic horns sound simultaneously with the flow of reverse gas to add energy to the dustcake removal process.
3. Shake/Deflate Cleaning (S/D): A method for offline cleaning. The bags are mechanically shaken immediately after or while a small quantity of filtered gas is forced back to relax the bags. The amount of filtered gas used is smaller than that used in RG cleaning.
4. Pulse-Jet Cleaning (PJ): A method for on-line cleaning in which pulses of compressed air are blown down inside and through the bags to remove dustcake while the bags are filtering flue gas. Wire support cages are used to prevent bag collapse during filtration and ash is collected outside of the bags.

The choice of the bag cleaning method is usually based on the type of coal being used (hence the filterability of the ash) and the historical experience with filtering the particular kind of ash. The choice of the bag cleaning method is a design decision and for the purposes of our models we assume that this is specified by the user. While reverse gas cleaning has been dominant in the past, studies have shown that it is not as effective as other methods in achieving low capital and O&M costs (Scheck, et al., 1985). RG/S and S/D impart more cleaning energy to the bags which results in thinner dustcakes and lower pressure drop. Such systems also can be at higher air-to-cloth (A/C) ratios, reducing costs. It appears that more recently, RG/S is emerging as a method of choice for full-scale, low A/C ratio utility baghouses on pulverized coal-fired boilers (Cushing, et al., 1990).

The most critical parameter in the operation of a baghouse is the relative system size which is characterized in terms of air-to-cloth ratio, defined as the volumetric flow rate of flue gas divided by the total bag cloth area. This ratio has the units of acfm/ft^2. The A/C ratio is determined based on the bag cleaning method, which controls the residual quantity of the material remaining on the bags. This in turn affects the resistance to gas flow and determines the pressure drop. Utility baghouses typically use A/C ratios of 1.5-4.0 acfm/ft^2 (net-net)[1] depending on the bag cleaning method. The cost of a baghouse is determined by the unit size which in turn depends on the gross A/C ratio and the volumetric flow rate. Given that the A/C ratio is the primary determinant of the unit size, and hence the capital and operating costs, it is desirable to operate at the highest A/C ratio that comfortably meets the performance specifications. Table 8-1 provides the typical values used for A/C ratio for various baghouse types based on industry experience (Belba, et al., 1992; Bustard, Cushing, & Chang, 1992; Cushing, et al., 1990; Puille, 1985; Sloat, et al., 1993).

Baghouse pressure drop is caused by pressure losses in gas flow as it moves through the bag fabric and dustcake. The pressure drop is usually measured in inches of water gauge or column (iwg or iwc) and is a measure of the energy required to move flue gas through the baghouse structure and bags. Flange-to-flange pressure drop is the pressure difference measured between the baghouse inlet and outlet flanges. It is the sum of ductwork and tubesheet pressure drops. Tubesheet pressure drop is measured across the tubesheet in a single compartment and consists largely of the pressure drop across the dustcake. Tubesheet pressure drop is the largest component of the flange-to-flange pressure drop and is useful since it can be controlled by the operator. However, it is the flange-to-flange pressure drop that is used in terms of a unit's energy consumption during operation and is used for sizing the ID fan. Baghouses are generally designed for a flange-to-flange pressure drop of about 6 -8 in. H_2O regardless of the cleaning method as a result of constraints from induced draft fans, ductwork stiffening, and other design details. Typical values for tubesheet pressure drop for given values of A/C ratios based on industry experience are also provided in Table 8-1.

Table 8-1. Typical Fabric Filter Design Parameters

Baghouse Type	A/C Ratio net-net (acfm/ft^2)	Average tubesheet ΔP (in. H_2O)	Average Bag Life (years)
Reverse Gas	1.7 -2.0	3 x (A/C) +/- 20%	3-5
Reverse Gas Sonic	1.7 -2.0	2.5 x (A/C) +/- 20%	3-5
Shake-Deflate	2.5 - 3.0	2 x (A/C) +/- 15%	2-4
Pulse Jet	4.0 - 4.5	1.3 x (A/C) +/- 50%	2-4

U.S. utilities largely use woven fiberglass bag fabric because of high flue gas temperatures. Fiberglass can withstand temperatures up to 500 F and can be textured to control dustcake formation. But it is also susceptible to abrasion wear. The choice of the bag fabric affects the cost of the bag. Bags generally fall into two size categories: 30-36 ft in length and 1 ft in diameter, and 20 -22 ft in length and 8 in. in diameter. Bag life is generally not an issue (except for manufacturing defects and improper installation) and is usually between 3-5 years. All these parameters influence both the capital and operating costs. Once again, for the purposes of the models developed here these parameters are treated as design variables to be specified by the user. The effect of these choices on the cost of the baghouse has been modeled.

8.4. Cost Models for Fabric Filters

The cost models for the four types of fabric filters are developed for both capital costs and operation and maintenance (O&M) costs. These models follow the economic premises for cost development and breakdown developed by EPRI. The capital costs are developed on a process area by process area basis and the O&M are developed to reflect the fixed and the variable operating costs. The cost areas are shown in Table 8-2.

Table 8-2. Process Areas for Fabric Filter cost Models

Process Area	Description
10	Collectors
20	Ductwork
30	Fly Ash Handling System
40	Differential Cost

The models developed in this report are based on price quotes from equipment vendors obtained for EPRI (Gaikwad & Sloat, 1992; Scheck, et al., 1985). The main difference in our treatment of these costs is that we have developed cost models parametrized by operating design parameters on a process area basis. In contrast, the EPRI models use aggregate costs (such as total capital requirement) for the development of parametrized models. In this subsection, we first present the methodological basis used for model development and then present the cost models.

In the development of cost models, we have treated the Reverse-Gas, Reverse Gas/Sonic and the Shake-Deflate baghouses as one class of systems and the Pulse-Jet fabric filter separately as another class. Engineering experience suggests that the difference in the economics between RG, RG/S, and SD baghouses can be treated parametrically through the operating design parameters A/C, ΔP, and bag life (Scheck, et al., 1985). This implies that the difference in costs between an RG baghouse and an RG/S baghouse is largely accounted by the difference in the design parameters and can be described by one set of cost models. The cost models for Pulse-Jet baghouses have been developed separately since it is a new technology and there is not sufficient experience to treat it parametrically in the context of the RG models.

The major design parameters which can significantly impact the total system cost of the fabric filter are *gas flow volume* (which depends on the generating unit size), *A/C ratio*, the *flange-to-flange pressure drop* in the baghouse, *bag life* and the *bag fabric* that is used for filtering. The costs of baghouses for different unit sizes and with variations in the above parameters are reflected in the models. The sensitivity of baghouse costs to variations in these parameters is analyzed to parameterize the cost models. We will now discuss in detail the experimental design and development the cost models for each system of baghouses separately.

8.4.1. Reverse Gas Systems

The experimental design used to choose different vectors of the design parameters for capital cost estimation (Scheck, et al., 1985) is shown in Table 8-3.

Table 8-3. Range of Model Design Parameters

Case	Size in MW (acfm)	A/C Ratio (gross) cfm/ft^2	Bags per Compartment (No. of Compartments)
Base	500 MW (1.9 M)	2.0	360 (28)
1	250 MW (0.95 M)	2.0	360 (14)
2	1000 MW (3.8 M)	2.0	360 (56)
3	500 MW (1.9M)	1.6	396 (32)
4	500 MW (1.9M)	3.6	396 (14)
5	500 MW (1.9M)	2.0	648 (16)
6	500 MW (1.9M)	2.0	252 (40)
Range	250-1000 MW	1.6-3.6	252-648

The costs for each vector of parameters in Table 8-3, broken down by process area is provided in Table 8-4 based on a 1984 EPRI study (Scheck, et al. 1984). These costs are used only to obtain an exponential scaling factor for each process area. The actual cost-models are based on 1990 dollars.

Table 8-4. Process Area Capital Costs Used for Scaling Parameter Estimation (1982 $/kW)

Process Area	Case 1	Case 2	Case 3	Case 4	Case 5	Case 6	Base Case
10	39.51	32.51	43.23	22.16	32.87	37.84	35.86
20	0.85	0.60	0.71	0.72	0.71	0.71	0.71
30	8.90	4.75	6.45	5.24	5.26	6.73	6.01
40	1.85	1.85	1.50	4.02	4.02	1.85	1.85
Total	51.11	39.71	51.89	32.14	40.69	47.13	44.43

The mathematical model to describe the sensitivity of cost models to parameter variations is normalized against the cost for the base case. The general form of the cost model for each process area is as shown below:

$$\frac{PC_i}{PC_i{}'} = \left(\frac{G}{G'}\right)^f \times \left(\frac{A/C'}{A/C}\right)^a \times \left(\frac{B'}{B}\right)^b \times \left(\frac{SIL}{SIL'}\right)^c \qquad (8\text{-}1)$$

where

PC_i = process area capital, 1990 $

PC_i' = process area capital, base case, 1990 $

G = inlet gas flow, acfm

G′ = inlet gas flow, base case, acfm

A/C = air-to-cloth ratio, acfm/ft2

A/C′ = air-to-cloth ratio, base case, acfm/ft2

B = bags per compartment

B′ = bags per compartment, base case

SIL = ash rate to silo, tons/hr

$SIL^{/}$ = ash rate to silo, base case, tons/hr

Based on the cost data presented in Table 8-4, the exponents of the model in Equation (8-1) are estimated and presented in Table 8-5. Note that it is important to identify the cases which vary only one parameter from the base case since these allow direct estimation of the exponents. Note also that although the cost numbers in Table 8-4 are in $/kW, total dollar needs to be used in the model. Since the mathematical model is multiplicative, the exponents derived in Table 8-5 are independent of the base case used.[1] The actual base costs used in the model are based on more recent EPRI studies for a 250 MW plant, although these costs are not significantly different from those reported in earlier studies.

Table 8-5. Model Scaling Factors

Area	*f*	*A*	*b*	*c*
10	0.86	0.84	0.15	0
20	0.75	0	0	0
30	0.55	0.29	0.275	0.083
40	0	0	0	0

In Table 8-5, some of the exponents have been chosen to be zero. This is because the variations for these process areas are not expected to influence cost. Also note that these values for exponents have been averaged over several cases of available data. Due to the small size of the data set, no statistical analysis has been conducted. The exponents derived in Table 8-5 have been verified against cost data collected more recently for unit sizes ranging from 125-500 MW (Gaikwad & Sloat, 1992); therefore, the cost model can be used for the range 125-1000 MW.

The total capital requirement for a reverse gas baghouse is calculated as shown in Table 8-6. This includes the direct process capital costs and indirect costs associated with reverse baghouses.

Table 8-6. Total Capital Requirement

Component	Cost
Particulate Collector	PC_{10}
Ductwork	PC_{20}
Flyash Handling	PC_{30}
ID fans	PC_{40}
Total Process Capital	$PC=PC_{10}+PC_{20}+PC_{30}+PC_{40}$
General Facilities *	0.10 PC
Eng. & Home Office Fees *	0.05 PC
Process Contingency *	0.05 PC
Project Contingency *	0.2 PC
Total Plant Cost *	TPC=1.31 PC
Total Plant Investment (including AFUDC) *	TPI=1.063 TPC (3 years)
Preproduction Cost *	0.002 TPI
Inventory Capital *	0.005 TPC
Total Capital Requirement *	TCR=1.002 TPI +0.005 TPC
* These items are based on model default values for indirect cost factors. The IECM allows these factors to be changed by the user.	

The O&M costs for the reverse-air baghouse consists of the fixed costs and the variable costs. The fixed operating cost consists of labor, maintenance labor, material, filter bags, and administrative labor. A mathematical model for the fixed cost is parametrized on unit size, the A/C ratio, bag cost and bag life and is provided by Equation (8-2).

$$\frac{FOM}{FOM'} = \left(\frac{G}{G'}\right)^{s} + \frac{N_{bags}}{10^{6}} \times \left(\frac{BC}{BF}\right) \times \left(\frac{G}{G'}\right) \times \left(\frac{A/C'}{A/C}\right) \qquad (8\text{-}2)$$

where G, G/, A/C, A/C/ are as defined in Equation (8-1), and

FOM = fixed operating cost, M$

FOM/ = fixed operating cost, base case (0.455 M$)

G = flue gas flow rate

G/ = flue gas flow rate, base case (0.95 Macfm)

A/C = air-to-cloth ratio, acfm/ft^2

A/C = air-to-cloth ratio, base case (2.0 acfm/ft^2)

BC = bag cost, $

BF = bag life, years

N_{bags} = numbers of bags in baghouse (360 x 14 default)

s = 0.48, exponent developed from data in Table 8-6.

Notice that the model has been developed largely analytically except that the dependence on unit size is based on data in Table 8-7 which is based on quotes from vendors (Gaikwad & Sloat, 1992). *Note that Equation* (8-2) *is such that the base case cannot be changed arbitrarily*.

Table 8-7. Data Used for Scaling Parameter Estimation of O&M Costs ($/kW-yr)

O&M	125MW	250MW	500MW
Fixed	2.80	1.82	1.36
Ash Disposal	2.23	2.23	2.23
Power	1.82	1.69	1.61

The variable cost includes the power cost and ash disposal cost. The ash disposal cost is proportional to the ash generated. The power costs are calculated based on the ID fan power required to overcome the expected pressure drop across the baghouse and the other auxiliary power requirements. The variable operating cost is given by

$$VOM = cf \times [C_{ash} \times 8760 \times A + C_{power} \times 8760 \times (135 \times \Delta P \times \left(\frac{G}{G'}\right) + P_{aux} \times \left(\frac{G}{G'}\right)^{t})] \qquad (8\text{-}3)$$

where G, G/ are as before and

VOM = variable operating costs, 1990 $

cf = capacity factor

A = ash disposal rate, tons/hr

C_{ash} = ash disposal cost, $/ton, (default = $10.24/ton)

C_{power} = power cost, cents/kWh

P_{aux} = auxiliary power requirement (323 kW)

ΔP = flange to flange pressure drop, inches of H_2O (7.5in)

t = 0.65, exponent derived from data in Table 8-6

Note: Once again, Equation (8-3) *is such that the base case cannot be changed arbitrarily.*

8.4.1.1. A Numerical Example

We will use a base case of unit size 250 MW (0.95 Macfm), with a A/C ratio of 2 acfm/ft^2, with 360 bags/compartment, 14 compartments, using Appalachian Medium Sulfur coal (ash content 8%, ash rate to silo =10.44 tons/hr). We estimate the cost in 1990 dollars of a unit with the following design parameters:

Size = 500 MW (1.9 Macfm), A/C = 2 acfm/ft2,

396 bags/compartment, 32 compartments,

Bag life = 4 years, bag cost =$ 80/bag

Capacity factor =65%, flange-to-flange pressure drop = 7.5 in. H2O

Emission limit = 0.01 lb/MMBtu (99.86%), Ash disposal rate = 10.441 tons/hr

Capital Costs ($1990)

$$PC_{10} = 10.21 \times \left(\frac{1.9}{0.95}\right)^{0.86} \times \left(\frac{2}{1.6}\right)^{0.81} \times \left(\frac{360}{396}\right)^{0.15} = 21.89 M\$$$

$$PC_{20} = 0.3325 \times \left(\frac{1.9}{0.95}\right)^{0.75} = 0.56 M\$$$

$$PC_{30} = 2.06 \times \left(\frac{1.9}{0.95}\right)^{0.55} \times \left(\frac{2}{1.6}\right)^{0.29} \times \left(\frac{360}{396}\right)^{0.275} \times \left(\frac{10.44}{5.22}\right)^{0.083} = 3.32 M\$$$

$$PC_{40} = 0.19 M\$$$

$$PC = 21.89 + 0.56 + 3.32 + 0.19 = 25.96 M\$$$

General Facilities = 0.26 M$
Engg. & Home = 1.9 M$
Proc. Contingenc y = 1.9 M$
Proj. Contingenc y = 5.2 M$
TPC = 35.21 M$
TPI = 37.43 M$
Preproduction cost = 0.075 M$
Inventory capital = 0.176 M$
Total Capital Req = 37.68 M$ ($75.4/kW)

Fixed Costs

$$FOM = 0.455 \times \left(\frac{1.9}{0.95}\right)^{0.48} + \frac{396 \times 14}{1 \times 10^6} \times \left(\frac{80}{4}\right) \times \left(\frac{1.9}{0.95}\right) \times \left(\frac{2}{1.6}\right) = 0.91 M\$/yr$$

Variable Costs

$$VOM = 0.65 \times \left(\frac{10.24 \times 8760 \times 10.441}{1 \times 10^6} + \frac{0.0554 \times 8760}{1 \times 10^6} \right) \times \left[135 \times 7.5 \times \left(\frac{1.9}{0.95} \right) + 323 \times \left(\frac{1.9}{0.95} \right) \right]$$

$$= 2.22 M\$ / yr$$

8.4.2. Pulse-Jet Systems

The experimental design used to choose different vectors of design parameters for capital costs are shown in Table 8-8. However, since Pulse-Jet fabric filters are evaluated with three different levels of pressure jets (low, intermediate, and high pressure) this design is used three times, once for each pressure level.

Table 8-8. Design Parameters for Pulse-Jet Systems

Case	Size in MW (M acfm)	A/C Ratio (gross) acfm/ft^2	Bag length (feet)
Base	250 (0.9)	4	20
1	125 (0.475)	4	20
2	500 (1.9)	4	20
3	250 (0.9)	3	20
4	250 (0.9)	6	20
5	250 (0.9)	4	15
6	250 (0.9)	4	25
Range	125 - 500	3-6	15 -25

The costs for each vector of parameters in Table 8-8 broken down by process area is based on recent EPRI data for low, intermediate, and high-pressure Pulse-Jet fabric filters (Gaikwad & Sloat, 1992).

The mathematical model to describe the sensitivity of the cost models to parameter variations again is normalized against the cost for the base case. The generalized form of the model for each process area is shown below:

$$\frac{PC_i}{PC_i^/} = \left(\frac{G}{G^/} \right)^j \times \left(\frac{A/C^/}{A/C} \right)^k \times \left(\frac{BL^/}{BL} \right)^l \times \left(\frac{BC}{BC^/} \right)^m \times \left(\frac{SIL}{SIL^/} \right)^i \qquad (8\text{-}4)$$

where

PC_i = process area capital, M$

$PC_i^/$ = process area capital, base case, M$

G = inlet gas flow, acfm

$G^/$ = inlet gas flow, base case, acfm

A/C = air-to-cloth ratio, acfm/ft^2

$A/C^/$ = air-to-cloth ratio, base case, acfm/ft^2

BL = bag length, feet

$BL^/$ = bag length, base case, feet

BC = bag cost $/bag

$BC^{/}$ = bag cost, base case, $/bag

SIL = ash rate to silo, tons/hr

$SIL^{/}$ = ash rate to silo, base case, tons/hr

i,j,k,l,m = exponents derived from data

The estimated exponents of the model in Equation (8-4) are presented in Table 8-9. The model is once again independent of the base case used.

Table 8-9. Exponents for Equation (8-4)

Area	*j*	*k*	*l*	*m*	*i*
10	0.85	0.72	0.44	0.15	0
20	0	0	0	0	0
30	0.56	0.12	0.10	0	0.13
40	0	0	0	0	0

In Table 8-9 some of the exponents are chosen to be zero since they do not influence the capital costs. All exponents for the process area 40 are chosen zero since the slight variation in cost is not consistent with the economics of scale. Moreover, the cost of process area 40 is less than 5% of the total process cost.

As with reverse gas baghouses, the O&M costs for pulse-jet baghouses consists of fixed and variable costs. The fixed operating costs consist of labor, maintenance labor, material, filter bags, and administrative labor. The mathematical model for the fixed costs is parametrized on unit size, A/C ratio, bag cost and bag life shown in Equation (8-5).

$$\frac{FOM}{FOM^{/}} = \left(\frac{F}{F^{/}}\right)^{u} + \frac{N_{bags}}{10^{6}} \times \left(\frac{BC}{BF}\right) \times \left(\frac{G}{G^{/}}\right) \times \left(\frac{A/C^{/}}{A/C}\right) \qquad (8\text{-}5)$$

where F, $F^{/}$, A/C, $A/C^{/}$ are as defined in Equation (8-1), and

FOM = fixed operating cost, M$

$FOM^{/}$ = fixed operating cost, base case,0.6325 M$

G = flue gas flow rate

$G^{/}$ = flue gas flow rate, base case, 0.95 Macfm

A/C = air-to-cloth ratio, acfm/ft2

A/C = air-to-cloth ratio, base case, 2 acfm/ft^2

BC = bag cost, $, (default $80)

BF = bag life, years, (default 3 years)

N_{bags} = numbers of bags in baghouse, (default 9050)

u = 0.63 exponent developed from data in Table 8-9.

This model has been developed largely analytically, however, the dependence on unit size is based on data in Table 8-10. (Gaikwad & Sloat, 1992).

Table 8-10. Relative O&M costs Used for Scaling Factor Estimation (in $/kW-yr)

O&M	125 MW	250 MW	500 MW
Fixed	3.45	2.53	2.07
Ash	2.23	2.23	2.23
Power	2.06	1.96	1.88

The variable costs, as before, includes power cost and ash disposal costs. The variable operating cost is given by Equation (8-6):

$$VOM = cf \times \left(\begin{array}{l} C_{ash} \times 8760 \times A + C_{power} \times 8760 \\ \times \left[135 \times \Delta P \times \left(\frac{G}{G'} \right) + P_{aux} \times \left(\frac{G}{G'} \right)^{w} \right] \end{array} \right) \qquad (8\text{-}6)$$

where F, F/ are as before and

VOM = variable operating costs, $

cf = capacity factor

A = ash disposal rate, tons/hr

C_{ash} = ash disposal cost, $/ton

C_{power} = power cost, cents/KWh (default 5.54)

P_{aux} = auxiliary power requirement, 742 kW

ΔP = flange to flange pressure drop, inches of H2O

w = 0.85, exponent derived from data in Table 8-10

Notice once again that Equation (8-6) *is such that the base case cannot be changed arbitrarily*

8.4.2.1. A Numerical Example for Pulse-Jet Baghouses

We will estimate the capital and operating costs for a pulse-jet baghouse for the same design parameters as used in the example for reverse-gas baghouses. (Refer to Table 8-6 for indirect costs).

Capital Costs (1990 $)

$$PC_{10} = 5.925 \times \left(\frac{1.9}{0.95} \right)^{0.85} \times \left(\frac{4}{3} \right)^{0.72} \times \left(\frac{20}{15} \right)^{0.44} = 14.9M\$$$

$$PC_{20} = 0.375M\$$$

$$PC_{30} = 2.155 \times \left(\frac{1.9}{0.95} \right)^{0.56} \times \left(\frac{4}{3} \right)^{0.12} \times \left(\frac{20}{15} \right)^{0.1} \times \left(\frac{10.44}{5.22} \right)^{0.13} = 3.70M\$$$

$$PC_{40} = 0.19M\$$$

Total Process Capital (PC) = 19.165 M$

General Facilities = 0.19 M$

Engg. & Home Office = 0.96 M$

Process Contingency = 1.9 M$

Project Contingency = 3.8 M$

Total Plant Cost (TPC) = 26.0 M$

TPI = 27.65 M$

Preproduction costs = 0.055 M$

Inventory Capital = 0.13 M$

Total Capital Requirement = 27.835 M$ ($55.7/kW)

Fixed Costs

$$FOM = 0.6325 \times \left(\frac{1.9}{0.95}\right)^{0.63} + \frac{360 \times 14}{10^6} \times \left(\frac{80}{4}\right) \times \left(\frac{1.9}{0.95}\right) \times \left(\frac{4}{3}\right)$$

$$= 1.78 M\$ / yr$$

Variable Costs

$$VOM = \frac{0.65}{1 \times 10^6} \times \left(\begin{array}{l} 10.24 \times 8760 \times 10.44 \\ + 0.0554 \times 8760 \times \left[135 \times 6.7 \times \left(\frac{1.9}{0.95}\right) + 742 \times \left(\frac{1.9}{0.95}\right)^{0.85} \right] \end{array} \right)$$

$$= 1.6 M\$ / yr$$

8.5. References

Belba, V. H., Grubb, W. T., & Chang, R. (1992). The Potential of Pulse-Jet Baghouses for Utility Boilers. Part 1: A Worldwide Survey of Users. J. Air Waste Manage. Assoc., 42(2), 209.

Bustard, C. J., Cushing, K. M., & Chang, R. L. (1992). The Potential of Pulse-Jet Baghouses for Utility Boilers. Part 2: Performance of Pulse-Jet Fabric Filter Plants. J. Air Waste Manage. Assoc., 42(9), 1240.

Carr, R. C., & Smith, W. B. (1984). Fabric Filter Technology for Utility Coal-Fired Power Plants: A Series of Articles Reprinted from the "J. of Air Pollution Control Association" No. EPRI CS-3754-SR). Electric Power Research Institute.

Cushing, K. M., Bush, P. V., & Synder, T. R. (1990). Operating history and current status of fabric filters in the utility industry. J. Air Waste Manage. Assoc., 40, 1051.

Gaikwad, R. P., & Sloat, D. G. (1992). Economic Evaluation of Particulate Control Technologies No. EPRI TR-100748). Electric Power Research Institute.

Kumar, K. S., & Feldman, P. L. (1994). Electrostatic Precipitators versus Fabric Filters: Fact versus Fiction. In Electrostatic Precipitators versus Fabric Filters: A Symposium and Debate. Crystal City, VA: ICAC.

Puille, W. (1985). 1985 Update, Operating History and Current Status in the Utility Industry. In Third Conference on Fabric Filter Technology for Coal Fired Power Plants. Scottsdale, AZ:

Scheck, R. W., Mora, R. H., Belba, V. H., & Horney, F. A. (1985). Economics of Fabric Filters and Electrostatic Precipitators No. EPRI CS-4083). Electric Power Research Institute.

Sloat, D. G., Gaikwad, R. P., & Chang, R. L. (1993). The Potential of Pulse-Jet Baghouses for Utility Boilers. Part 3: Comparative Economics of Pulse-Jet Baghouse, Precipitators and Reverse-Gas Baghouses. J. Air Waste Manage. Assoc., 43, 120.

9. Flue Gas Desulfurization

9.1. Background to FGD Models

In this chapter we describe the use of systematic sensitivity analysis and multivariate regression for the development of analytical models for the performance and cost of high-performance wet lime/limestone FGD systems and dry lime sprayer systems. Special attention has been paid to FGD systems whose performance with respect to sulfur removal efficiency lies in the 90-98% range. The cost of using additives such as dibasic acid (DBA) as a design option for achieving high performance is also examined. The cost models developed relates the capital costs and the operating and maintenance costs to input variables describing performance parameters and the costs of labor and materials. Systematic sensitivity analysis is used to select and rank the set of input variables and multivariate regression is used for the development of functional relations between the input variables and costs (outputs). This systematic approach along with engineering judgment is used to develop aggregate models for costing high performance FGD systems. These aggregate models are appropriate in size and form for conducting uncertainty analysis using Monte Carlo methods in the IECM.

The chapter is organized as follows. Section 9.2 below describes the development of new FGD performance models. Based on a review of the literature, some approximate functional relations to describe FGD performance are presented. Section 9.3 on page 173 provides an overview of the methodological approach used to derive capital cost models. Four FGD systems are analyzed: (1) wet limestone with forced oxidation (LSFO), (2) dibasic acid enhanced wet limestone (LS/DBA), (3) a magnesium-enhanced wet lime system, and (4) a spray dryer with lime. The relations for direct process capital cost models are derived for each process area in Section 9.4 on page 179. The effects of different sparing philosophies on the capital cost are also examined. Cost models are then developed for the fixed operating and maintenance costs associated with operating an FGD system in Section 9.5 on page 185. Section 9.6 on page 186 develops models for the variable costs of reagent use, power use, waste disposal, energy consumption etc. Section 9.7 on page 189 provides a numerical example to illustrate the new models.

9.2. FGD Performance Models

In this section we describe the performance models used to provide key parameter inputs to the cost models described later. We begin with a brief survey of FGD performance literature. Based on the literature, approximate functional relations between performance parameters are developed.

The analysis in this chapter is geared towards developing updated performance and cost models for four commercial FGD processes:

1. Limestone with Forced Oxidation (LSFO): A limestone slurry is used in an open spray tower with in-situ oxidation to remove SO_2 and form a gypsum sludge. The main advantages as compared to conventional systems is easier dewatering, more economical disposal of scrubber products, and decreased scaling on tower walls.
2. Limestone with Dibasic Acid Additive (LS/DBA): A modification to LSFO where dibasic acid (DBA) is added to act as a buffer/catalyst in the open spray tower. The main advantages are increased SO_2 removal and decreased liquid to gas ratio.

3. Magnesium Enhanced Lime System: A magnesium sulfite and lime slurry (maglime) is used to remove SO_2 and form a precipitate high in calcium sulfite. The high alkalinity of the maglime slurry allows very high SO_2 removal. However, the reagent cost is also higher and solid waste is not easily disposed.
4. Lime Spray Dryer: An atomized spray of a mixture of lime slurry and recycled solids is brought into contact with the hot flue gas. The water in the slurry evaporates leaving dry reaction products and flyash which drops out of the scrubber. A particulate control device such as a baghouse is also used to remove the rest of the dry products from the flue gas before releasing it. The SO_2 removal efficiency is the total of SO_2 removed in the scrubber and the baghouse.

9.2.1. Wet FGD Performance

This section describes the improvements to the wet flue gas desulfurization (FGD) model since the original model development (1). The quantities that were modified are the reagent composition, water evaporation in the scrubber, flue gas composition exiting scrubber, energy needed for reheat, characterization of the scrubber waste and the capital cost when using lime as a reagent. A schematic diagram of the wet scrubber is shown in Figure 9-1. The diagram shows a configuration with bypass and a reheater. These options are mutually exclusive, since it is not likely that a scrubber would be built with both. So, if there is a bypass, the reheater is not used. Conversely, if there is no bypass, the reheater is used to raise the flue gas temperature to a specified value.

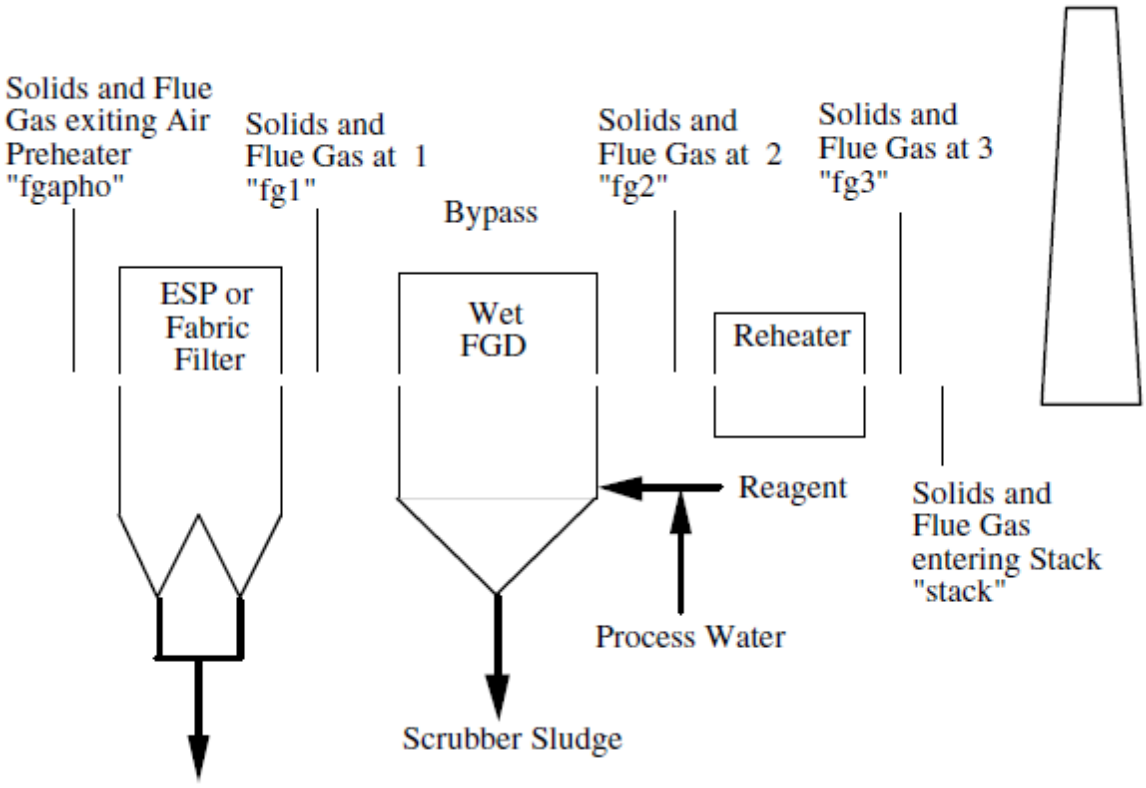

Figure 9-1. Schematic Diagram of the Wet FGD Model

9.2.1.1. Reagent and SO_2 Efficiency

The SO_2 removal efficiency is a key parameter governing the performance of the FGD system. The removal efficiency can either be specified or it can be calculated to meet a desired SO_2 emission standard. The SO_2 removal efficiency, η_{SO2}, based on the emission standard is calculated by

$$\eta_{SO_2,std} = 1 - \frac{2000 ES_{SO_2} M_{fuel} Hhv_{fuel}}{64.06 * 1{,}000{,}000 \left(m_{in,SO2} + m_{in,SO3}\right)}$$

$$\eta_{SO_2,std} = 1 - \frac{ES_{SO_2} M_{fuel} Hhv_{fuel}}{64.06 * 500 \left(m_{in,SO2} + m_{in,SO3}\right)} \qquad (9.1)$$

The wet FGD system has an option to allow bypassing of some flue gas around the scrubber. This option may lower the cost of the wet FGD system if the efficiency calculated by Equation (9.1) is not very high. When the bypass option is chosen the scrubber operates at its maximum removal efficiency, $\eta_{SO2,max}$, provided the amount of bypass is greater than the minimum bypass specified by the user, Byp_{min}. Since the bypass does not affect the total amount of sulfur removed, the moles of sulfur removed by the scrubber are determined from the Equation (9.1).

$$\text{if} \left(1 - \frac{\eta_{SO_2,std}}{\eta_{SO_2,max}}\right) \bullet Byp_{min} \quad \text{then} \quad Byp = 1 - \frac{\eta_{SO_2,std}}{\eta_{SO_2,max}} \;\; ; \;\; \eta_{SO_2} = \eta_{SO_2,max}$$

$$\text{else} \quad Byp = 0.0 \;\; ; \;\; \eta_{SO_2} = \eta_{SO_2,std}$$

$$m_{rem,S} = \eta_{SO_2,std} \left(m_{in,SO_2} + m_{in,SO_3}\right)$$

The reagent for the wet scrubber can be either lime or limestone. The reagent purity, R_{purity}, and moisture content, W_{reag}, must be specified. Any remaining material is considered inert. The molar stoichiometry, σ, (moles of calcium required per mole of sulfur removed) must be specified. The default values for the molar stoichiometry are 1.15 and 1.05 for limestone and lime, respectively. With the molar stoichiometry, the mass flow rate of reagent is calculated by

$$M_{reag} = \frac{100.09 M_{rem,s} \sigma}{2000 R_{purity}} \text{ for } CaCO_3 \;\; ; \;\; M_{reag} = \frac{56.08 M_{rem,s} \sigma}{2000 R_{purity}} \text{ for CaO}$$

9.2.1.2. Water Balance

Makeup water to the FGD system is required principally to offset evaporative losses in the scrubber. The mass of water evaporated in the FGD system is determined by an energy balance assuming adiabatic conditions and neglecting the solid mass flow rates in the scrubber. With these assumptions, the sensible energy released by the flue gas entering the scrubber has to equal the energy needed to evaporate the water evaporated and raise it to the exit temperature. The equation for the energy balance is shown by Equation (9.2) for a scrubber without bypass[17]. The function, $Cp'_{in,avg}$ is the average specific heat of the flue gas between the inlet temperature and the T_{exit}. The function, Δh, is the energy needed to raise the makeup water to saturated steam at T_{exit}.

$$CP'_{in,avg}(T_{in}, T_{exit})(T_{in} - T_{exit}) \sum_{j=1}^{9} \dot{m}_{in,j} = \dot{W}_{evp} \Delta h(T_{exit}) \qquad (9.2)$$

$T_{in} = T_{fg1} + \Delta T_{idfan}$

The temperature T_{in} is higher than $T_{in,}$ since the induce draft fan raises the inlet temperature by ΔT_{idfan}. The induced draft fan is assumed to be located between the scrubber and the particulate collector. The flue gas is assumed to behave as an ideal mixture, so the molar fraction of water in the flue gas is equal to the parcel pressure of water divided by the total pressure of the flue gas. Since the flue gas is saturated when it exits the scrubber, the amount of water evaporated is

17 Bypassing flue gas around the scrubber does not change the exit temperature, but it does change the amount of water evaporated. For these reasons, the bypass variable is excluded from the derivation of the flue gas exit temperature. Once the exit temperature is determined, the amount of evaporated water can be determined for the scrubber with bypass.

constrained by the saturation pressure of the water in the flue gas at the exit temperature. Since the change in the flue gas' total molar flow rate caused by the chemical equations is very small, the water evaporation constraint is show in Equation (9.3).

$$\frac{P_{sat}(T_{exit})}{P_{atm} + P_{g,exit}} = \frac{\bar{W}_{evp} + m_{in,H_2O}}{\bar{W}_{evp} + \sum_{j=1}^{9} \bar{m}_{in,j}} \tag{9.3}$$

Equations (9.2) and (9.3) represent two non-linear equations in two unknowns, T_{exit} and $\bar{W}_{evp}$. These two equations can be turned into a quadratic equation of $\bar{W}_{evp}$, provided the P_{2sat} and Δh are linear functions of the exit temperature and $Cp'_{in,avg}$ is constant. Figure 9-2 shows the typical variation in the average specific heat between 300°F and the exit temperature. The flue gas for Figure 9-2 is from an Illinois #6 coal and the average specific heat is determined using the enthalpy functions. The initial estimate of the average specific heat, $Cp'_{in,avg}$, is determined by guessing the exit temperature.

$$Cp'_{in,avg}(T_{in}, T_{guess}) = \frac{\sum_{j=1}^{9} m_{in,j}\left(h_j(T_{in}) - h_j(T_{guess})\right)}{(T_{in} - T_{guess})\sum_{j=1}^{9} m_{in,j}}$$

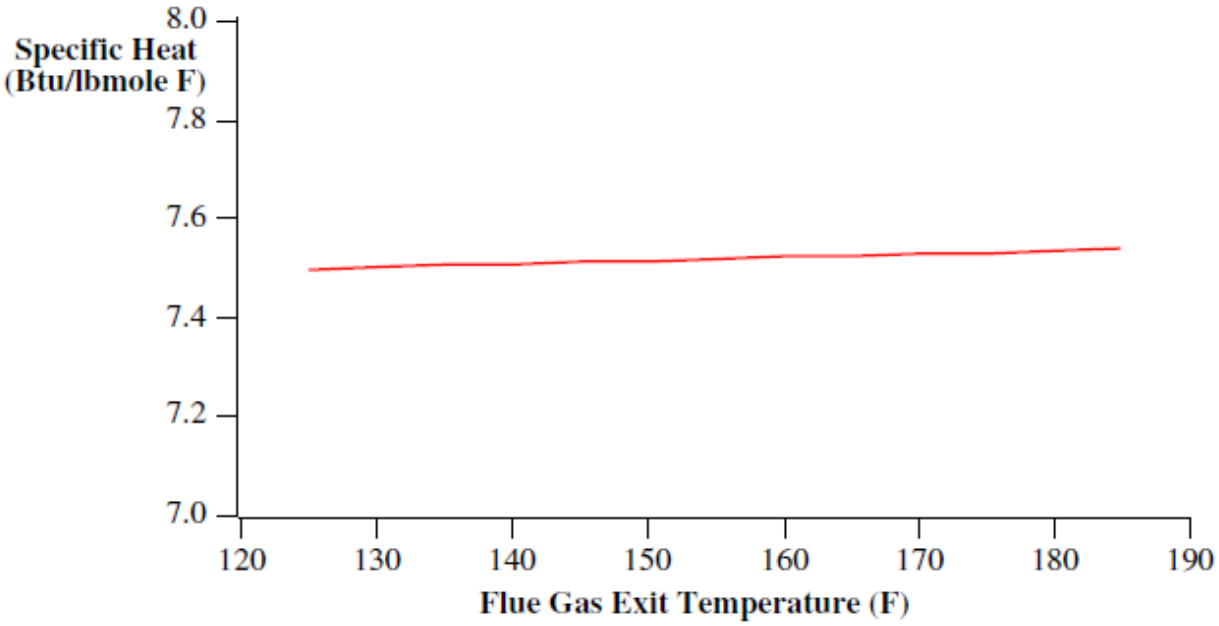

Figure 9-2. Flue Gas Specific Heat versus Exit Temperature

The linear equation, (9.4), for energy absorbed by the evaporating water was determined from a linear regression of the enthalpy of saturated steam minus the enthalpy of saturated water at 120°F, between 125°F and 185°F (10). Figure 9-3 shows the enthalpy difference between saturated steam versus saturated water at 120°F. It was found that the amount of water evaporated is not sensitive to the inlet water temperature, so the inlet water temperature is assumed to be 120°F. The correlation coefficient for the linear regression was greater than 99%.

$$\Delta h(T) = 7.3660\ T_F + 17{,}593.7 \tag{9.4}$$

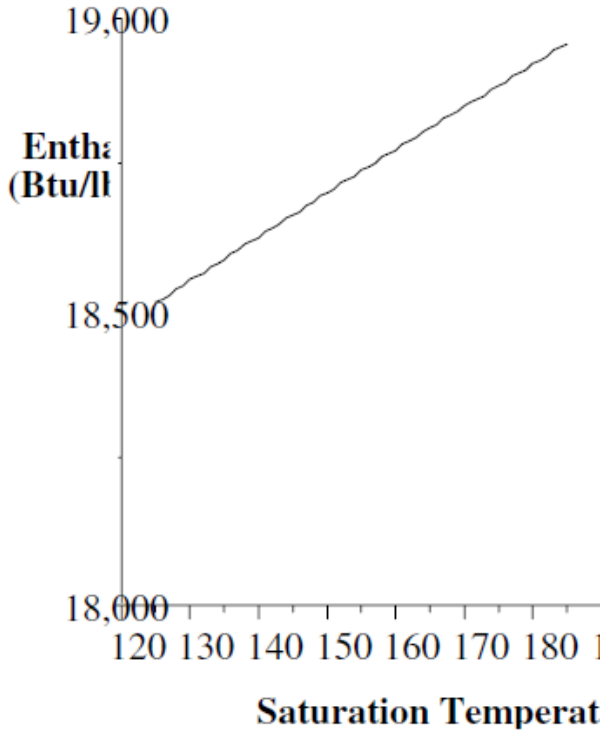

Figure 9-3. Enthalpy Difference between Saturated Steam and Saturated Water at 120°F

The saturation pressure of water versus temperature is shown in Figure 9-4 (11). Because of the curvature of the data and the sensitivity of Equation (9.3) to the saturation pressure, this data was fitted to a piecewise line between 125 and 185°F, (9.5). The correlation coefficient was greater than 99% for each segment.

$$P_{sat}(T_F) = A_{sat}\, T_F + B_{sat} \qquad (9.5)$$

where

$A_{sat} = 59.5475x10^{-3}$, $B_{sat} = -5.5087$ for $125 \bullet T_F \bullet 135$,

$A_{sat} = 74.4615x10^{-3}$, $B_{sat} = -7.5238$ for $135 < T_F \bullet 145$

$A_{sat} = 92.2619x10^{-3}$, $B_{sat} = -10.1068$ for $145 < T_F \bullet 155$

$A_{sat} = 113.333x10^{-3}$, $B_{sat} = -13.3749$ for $155 < T_F \bullet 165$

$A_{sat} = = 138.0782x10^{-3}$, $B_{sat} = -17.4604$ for $165 < T_F \bullet 175$

$A_{sat} = = 166.8782x10^{-3}$, $B_{sat} = -22.5032$ for $175 < T_F \bullet 185$

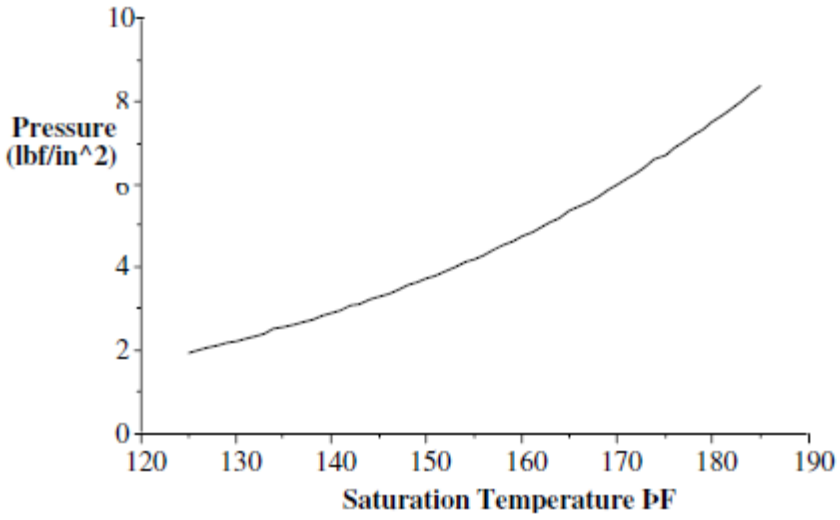

Figure 9-4. Saturation Pressure of Water versus Temperature

Substituting Equations (9.4) and (9.5) into Equations (9.2) and (9.3) and solving for evaporated water yields Equation (9.6). Once the evaporated water is known, the exit temperature can be found by substituting P_{sat} from Equation (9.5) into Equation (9.3) and solving for the exit temperature, (9.7).

$$\dot{W}_{evp} = \frac{-b + \sqrt{b^2 - 4ac}}{2a} \tag{9.6}$$

where

$a = 7.366\,(-B_{sat} + 1) + 17{,}593.7A_{sat}$

$$b = \left(Cp'_{in,avg}\left(T_{in}, T_{guess}\right)\left(-A_{sat}T_{in} - B_{sat} + 1\right) - 7.366B_{sat} + 17{,}593A_{sat}\right)\sum_{j=1}^{9} m_{in,j}$$

$+7.366\dot{m}_{in,H_2O}$

$$c = \left(m_{fg1,H_2O} + \left(-A_{sat}T_{in} - B_{sat}\right)\sum_{j=1}^{9} m_{fg1,j}\right) Cp'_{fg1,avg}\left(T_{in}, T_{guess}\right)\sum_{j=1}^{9} m_{fg1,j}$$

$$T_{exit} = \frac{\dot{W}_{evp} + \bar{m}_{in,H_2O}}{A_{sat}\left(\bar{W}_{evp} + \sum_{j=1}^{9}\dot{m}_{in,j}\right)} - \frac{B_{sat}}{A_{sat}}$$

(9.7)

Since a single linear equation for the saturation pressure does not represent the data, the solution of the quadratic equation for the evaporated water depends on the slope and intercept of Equation (9.5), that are functions of the exit temperature. To eliminate this cyclic dependency, the procedure shown below is used. It has been found that the temperature converges to within a degree and the evaporated water to within one percent on step five.

1. Determine $\dot{W}_{evp,1}$ from (9.6) assuming an exit temperature of 155°F

2. Determine $T_{exit,1}$ from (9.7) with $\dot{W}_{evp,1}$

3. Determine $\dot{W}_{evp,2}$ with $T_{exit,1}$

4. Determine T_{exit} with $\dot{W}_{evp,1}$

5. Determine $\dot{W}_{evp}$ from (9.6) times (1 - Byp) with T_{exit}

Figure 9-5 shows evaporated water based on Equations (9.2), (9.3) and the iterative procedure shown above for an Illinois #6 coal, an inlet temperature of 314°F and gauge pressure of 4" of water. The graph indicates that the iterative solution is very accurate.

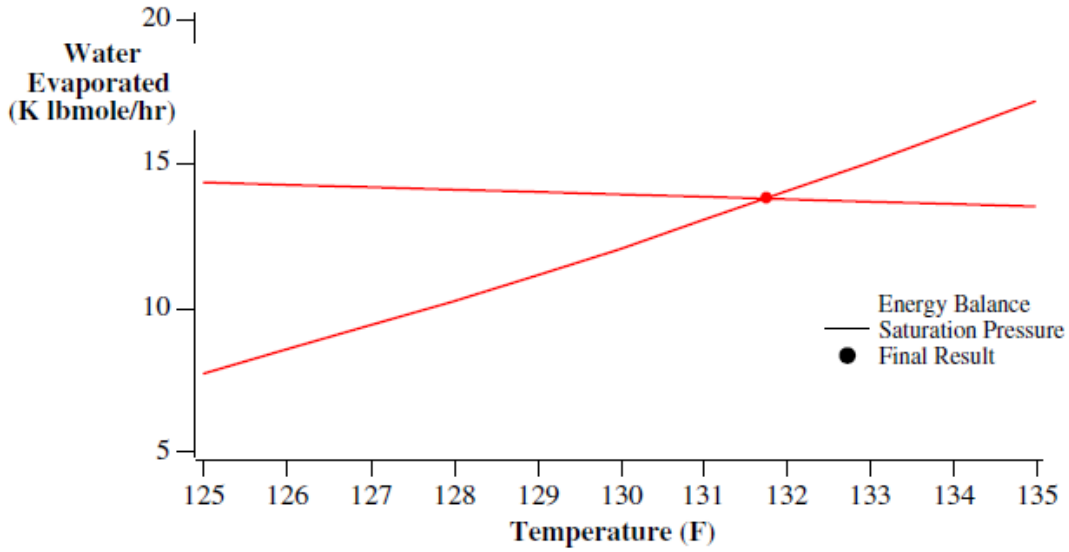

Figure 9-5. Evaporated Water versus Temperature

9.2.1.3. Flue Gas Composition and Reheat

The composition of the flue gas changes in the scrubber. The two most significant changes are the reduction in the sulfur dioxide content and the increase in the moisture content. The sulfur dioxide and sulfur trioxide are removed from the flue gas by a complex set of chemical reactions. These chemical reactions have been greatly simplified in the IECM and are shown below.

$$0.5H_2O + SO_2 + CaCO_3 \text{ --> } CaSO_3 \bullet 0.5H_2O + CO_2$$

$$2H_2O + 0.5O_2 + SO_2 + CaCO_3 \text{ --> } CaSO_4 \bullet 2H_2O + CO_2$$

$$0.5H_2O + SO_3 + CaCO_3 \text{ --> } CaSO_3 \bullet 0.5H_2O + CO_2 + 0.5O_2$$

$$2H_2O + SO_3 + CaCO_3 \text{ --> } CaSO_4 \bullet 2H_2O + CO_2 \qquad (9.8)$$

$$0.5H_2O + SO_2 + CaO \text{ --> } CaSO_3 \bullet 0.5H_2O$$

$$2H_2O + 0.5O_2 + SO_2 + CaO \text{ --> } CaSO_4 \bullet 2H_2O$$

$$0.5H_2O + SO_3 + CaO \text{ --> } CaSO_3 \bullet 0.5H_2O + 0.5O_2$$

$$2H_2O + SO_3 + CaO \text{ --> } CaSO_4 \bullet 2H_2O$$

Using these chemical reactions, the composition of the flue gas exiting the scrubber can be determined from a molar balance and is shown below. It is assumed that the oxygen needed to oxidize the calcium sulfite to calcium sulfate is taken from the flue gas. In practice this oxygen may be supplied by blowing air through the sludge outside the scrubber vessel. It is assumed that the water needed to hydrate the scrubber sludge comes directly from the makeup slurry and

does not reduce the moisture content of the flue gas. The symbol Ox represents the fraction of calcium sulfite oxidized to calcium sulfate.

$$\dot{m}_{exit,j} = (1 - Byp)\dot{m}_{in,j} \quad \text{for } j = N_2, CO, NO, NO_2$$

$$m_{exit,O_2} = (1 - Byp)m_{in,O_2} + (0.5(1 - Ox)M_{in,SO_3} - 0.5\,Ox\,m_{in,SO_2})\eta_{SO_2,std}$$

$$\dot{m}_{exit,H_2O} = (1 - Byp)\dot{m}_{in,H_2O} + \dot{W}_{evp}$$

$$\dot{m}_{exit,CO_2} = (1 - Byp)\dot{m}_{in,CO_2} + (m_{rem,S} \text{ if reagent} = CaCO_3)$$

$$m_{exit,SO_2} = (1 - Byp)m_{in,SO_2} - m_{in,SO_2}\eta_{SO_2,std}$$

$$\dot{m}_{exit,SO_3} = (1 - Byp)m_{in,SO_3} - m_{inSO_3}\eta_{SO_3,std}$$

The flue gas exiting the scrubber contains water droplets that the demister has not removed. These droplets evaporate either in the reheater or after the flue gas is remixed with the bypassed flue gas. These droplets are assumed to be a fraction, W_{demis}, of the evaporated water:

$$\dot{m}_{stack,j} = \dot{m}_{exit,j} + Byp\,\dot{m}_{in,j} \quad \text{for all j except } H_2O$$

$$\dot{m}_{stack,H_2O} = \dot{m}_{exit,H_2O} + Byp\,\dot{m}_{in,H_2O} + W_{demis}\,\dot{W}_{evp}$$

The flue gas exiting the scrubber is either remixed with the bypass flue gas or it passes through a reheater. Therefore, the flue gas temperature entering the stack is either the average temperature of the bypass flue gas and the flue gas exiting the scrubber or the exit temperature of the reheater. The exit temperature of the reheater is an input parameter, $T_{stack,input}$. The energy needed to raise the flue gas temperature to T_{stack} is the sum of the sensible energy of the flue gas and the energy needed to evaporate the water droplets and raise their temperature to T_{stack}.

If no bypass, then

$T_{stack} = T_{stack,input}$

$$E_{wetfgd} = W_{demis}\,\dot{W}_{evp}(7.366T_{stack} + 17593.7) + \sum_{j=1}^{9} \dot{m}_{in,j}\left(h_j(T_{stack}) - h_j(T_{exit})\right)$$

else

$T_{stack} = Byp\ T_{in} + (1 - Byp)\ T_{exit}$

$E_{wetfgd} = 0$

9.2.1.4. Waste Stream Composition

A major environmental flow stream emanating from a wet FGD system is the stream of wet solids. Two model options affect the mass flow rate of wet solids. The user specifies either a forced oxidation FGD system producing a gypsum waste or a natural oxidation FGD system that produces a wet sludge. The basic chemistry for these two options is shown in Equation (9.8). The difference in the composition and mass flow rates of FGD waste depends on the extent of oxidation of calcium sulfite to sulfate, Ox and the extent of dewatering of the final product, W_{sludge}. Other constituents of the FGD solids stream include unreacted reagent (that depends on the molar stoichiometry), inert materials introduced with the reagent (as dictated by the level of reagent purity) and flyash that has been removed by the scrubber (that depends on the particulate removal efficiency, η_{TSP}). The mass flow rates of the component are shown below.

$$M_{sludge,j} = (1 - Byp)\eta_{TSP} M_{in,j} \quad \text{for } j = \text{Ash, } CaSO_4$$

$$\dot{M}_{sludge,CaO} = (1 - Byp)\eta_{TSP}\dot{M}_{in,CaO} + \left(\frac{56.08(\sigma - 1)\dot{m}_{rem,S}}{2000} \text{ if reagent} = CaO\right)$$

$$\dot{M}_{sludge,CaCO_3} = (1 - Byp)\eta_{TSP}\dot{M}_{in,CaCO_3} + \left(\frac{100.09(\sigma - 1)\dot{m}_{rem,S}}{2000} \text{ if reagent} = CaCO_3\right)$$

$$\dot{M}_{sludge,CaSO_3 \bullet 0.5H_2O} = (1 - Byp)\eta_{TSP}\dot{M}_{in,CaO_3 \bullet 0.5H_2O} + \frac{129.14(1 - Ox)m_{rem,S}}{2000}$$

$$\dot{M}_{sludge,CaSO_4 \bullet 2H_2O} = (1 - Byp)\eta_{TSP}\dot{M}_{in,CaSO_4 \bullet 2H_2O} + \frac{172.17Ox\,\dot{m}_{rem,S}}{2000}$$

$$\dot{M}_{sludge,Misc} = (1 - Byp)\eta_{TSP}\dot{M}_{in,Misc} + (1 - R_{purity} - W_{reag})M_{reag}$$

$$\dot{M}_{sludge,H_2O} = \left(\frac{1}{W_{sludge}} - 1\right)\sum_{j=1}^{8} \dot{M}_{sludge,j} \quad \text{for all j except } H_2O$$

9.2.1.5. Economics Algorithm

The economic algorithm for the wet scrubber has remained unchanged except two items. The first is that the single indirect charge factor originally employed for capital cost estimates has been split into its component categories following the nomenclature used by the Tennessee Valley Authority (TVA), author of the basic FGD cost model. The second change is in the direct capital cost for reagent handling. If lime is used as the reagent, the direct capital cost of reagent handling is the same as the algorithm used for a spray dryer (1). If limestone is used, the algorithm remains unchanged. The direct capital cost of reagent handling is shown below.

If Reagent = $CaCO_3$

$$DC_{reag} = \left(\text{If } \dot{M}_{reag} < 18 \text{ Then } 0.1323\dot{M}_{reag} + 2.859 \text{ else } 0.07288\dot{M}_{reag} + 5.393\right)\frac{C_{idx}}{C_{idx,1981}} \text{ else}$$

$$DC_{reag} = \left(\text{If } \dot{M}_{reag} < 2 \text{ Then } 0.2997\dot{M}_{reag} + 1.546 \text{ else } 0.1986\dot{M}_{reag} + 2.042\right)\frac{C_{idx}}{C_{idx,1981}}$$

9.2.2. Wet Limestone FGD Systems

Advanced wet limestone FGD systems are now designed to achieve SO_2 removal efficiencies in excess of 95%. The single loop countercurrent spray tower is the most commonly used device for the removal of SO_2. The design of spray towers for high efficiency without additives is achieved by using high liquid-to-gas (L/G) ratios and improving gas/liquid contact by spray nozzle design (Bhat, et al., 1993; Rader & Bakke, 1991) On the other hand, organic acids such as dibasic acid or adipic acid are added as buffers to improve performance (Blythe, et al., 1993; Moser & Owens, 1990; Smolenski, et al., 1993; Stevens, et al., 1993) In this section, brief descriptions and approximate relations for high performance LSFO and LS/DBA systems are provided. The approximate relations are gleaned from the literature to reflect U.S. experience with high performance wet limestone FGD systems (Benson, 1993; Dene, et al., 1991; Johnson, 1993; Klingspor, 1993; Laslow, 1993; Moser & Owens, 1990; Noblett Jr., et al., 1990; Noblett Jr., 1993; Rader, 1993; Rader & Bakke, 1991; Smolenski, et al., 1993; Stevens, et al., 1993; Stevens, et al., 1991; Weilert, 1993; Weilert &

Ratliff, 1990). The paragraph below provides some background (Corbett, et al., 1977; Noblett Jr., et al., 1990) for the scrubbing process, which is useful in understanding the bases for the relations, provided later.

The removal of SO_2 from flue gas in a lime/limestone scrubber depends on a gas-liquid-solid mass transfer process. The sulfur dioxide is transferred from the flue gas to the slurry liquid in the scrubber and subsequently precipitated as calcium salts. In this section we provide a very brief discussion of the key factors that affect the SO_2 removal efficiency from a theoretical standpoint. Against this backdrop we examine empirical data, which reflects the recent experience with high efficiency scrubbers, and develop an approximate response surface parameterized on the key variables.

The basis for the analysis of vapor-liquid mass transfer phenomena is the two-film theory in which the total resistance to mass transfer is expressed as the sum of individual resistances in the vapor and liquid phases near the interface. Based on expressions for molar flux in the gas and liquid films and assuming that the liquid-vapor interface is at equilibrium (Corbett, et al., 1977; Mehta & Rochelle, 1983; Rochelle, 1981; Rochelle, 1981), the overall mass transfer coefficient is written as:

$$K_g = \left(\frac{1}{k_g} + \frac{H}{e \times k_l} \right)^{-1} \qquad (9\text{-}1)$$

where k_g (mole/cm^2-sec-atm) and k_l (cm/sec) are individual gas and liquid phase mass transfer coefficients, H is a physical constant (atm/mol-liter) from Henry's Law and e is an enhancement factor to account for chemical reactions that permit SO_2 to diffuse through the liquid film as sulfite or bisulfite ions rather than as undissociated SO_2 (Chang and Rochelle 1980). The amount of SO_2 transferred from gas phase per unit time is the integral of the molar flux and the interfacial area for mass transfer. This leads to an expression for SO_2 removal efficiency as shown in Equation (9-2):

$$\eta_{SO_2} = 1 - \exp\left(- \frac{K_g \times a \times P \times V}{G} \right) \qquad (9\text{-}2)$$

where

a = interfacial mass transfer area per unit volume

V = scrubber volume

P = total pressure in scrubber

G = molar gas flow rate

K_g = mass transfer coefficient

The interfacial area is determined by the contractor design, gas distribution in the scrubber and the gas and liquid flow rates (or residence time in the scrubber). V/G is the residence time of flue gas in the scrubber and it depends on superficial velocity and size of the scrubber. The mass transfer coefficient, K_g is influenced by process variables. Any process variable which affects the physical or chemical properties of the two films may affect K_g. The individual mass transfer coefficients k_g and k_l describe the diffusion rates across two hypothetically stagnant films. In the following paragraphs we discuss the effect of various process parameters on the SO_2 removal efficiency and develop a response surface using the exponential form. All the relations developed in this section are based on a log-linear approximation, as suggested by Equation (9-1), and are developed as follows:

$$RTU = -\ln(1 - \eta_{SO2})$$
$$RTU = a + \sum_i b_i \times x_i \qquad (9\text{-}3)$$

where a and b_i parameters which represent the linear slope of the effect of process parameters x_i.

L/G is a key variable since it affects SO_2 removal by increasing the available liquid phase alkalinity and the interfacial mass transfer area. Increasing the L/G ratio brings more alkaline materials into the scrubber per mole of SO_2 scrubbed thus decreasing the liquid film mass transfer resistance and improving the SO_2 removal. This effect is magnified by an associated increase in the interfacial mass transfer area which improves efficiency. Industry practice is based on a log-

linear relation between η_{SO_2} and L/G ratio (Benson, 1993; Bhat, et al., 1993; Dene, et al., 1991; Klingspor, 1993; Rader, 1993). Typical values for η_{SO_2} and L/G are provided in Table 9-1.

Table 9-1. Typical Values for SO_2 Removal and L/G.

η_{SO_2}	L/G(gpm/Kacfm)
90%	90
95%	130

Based on the values in the table above, an approximate relation[18] between sulfur removal efficiency and L/G is:

$$\eta_{SO_2} = 1 - \exp\{-(0.725 + 0.0175 \times L/G)\} \qquad (9\text{-}4)$$

where L/G is measured in gpm/1000 acfm. The effect of lime/limestone scrubbing chemistry on SO_2 removal can be understood by considering the mass transfer resistance from the gas and liquid film separately.

9.2.2.1. Liquid Film Limited Mass Transfer

Limestone systems are generally at least partially liquid film mass transfer limited. The liquid film mass transfer resistance is a strong function of liquid phase alkalinity. When SO_2 is absorbed by an aqueous scrubbing liquor, sulfurous acid is formed. Increasing the liquid phase or solid phase concentrations of alkaline materials (such as $CaCO_3$, $CaSO_3$, Mg^{++}) increases the liquid phase alkalinity which in turn improves SO_2 removal efficiency. Increasing the liquid phase alkalinity decreases the Henry's Law constant which in turn decreases the mass transfer resistance $H/(e\,k_l)$. The enhancement factor depends on the inlet SO_2 concentration and it decreases with increasing SO_2 concentrations thus increasing the mass transfer resistance. The k_l portion of the mass transfer resistance is a function of the hydraulics of the scrubber and depends on gas distribution and the geometry of scrubber.

Increasing the limestone stoichiometry (ϕ) improves liquid phase alkalinity and SO_2 removal. However, the effect saturates and little improvement in SO_2 removal is observed over 1.1. Limestone utilization varies inversely with the pH and is a critical factor for the operating costs of SO_2 scrubbing. Most modern scrubbers are designed for high utilization of about 95% or higher. Therefore, stoichiometry affects the performance in opposite ways. A detailed quantification of the effect of stoichiometry on pH is not straightforward and needs the development of process simulators (Agrawal & Rochelle, 1993; Noblett Jr., et al., 1990). It is possible to get an approximate idea of how SO_2 removal is affected by pH and in turn by ϕ based on empirical data (Klingspor, 1993; Noblett Jr., et al., 1990; Rader, 1993; Stevens, et al., 1991) as shown in Table 9-2 below:

Table 9-2. Stoichiometry and Alkalinity Approximations

η_{SO2}	pH	ϕ
90%	5.3	1.03
95%	6.0	1.1

Based on these numbers a linear approximation for the effect of stoichiometry can be represented by an additional term in Equation (9-4) as follows:

$$\eta_{SO2} = 1 - \exp\{-[0.725 + 0.0175 \times L/G + (10.0 \times \phi - 10.3)]\} \qquad (9\text{-}5)$$

Notice that the effect of stoichiometry is represented as an increase in SO_2 removal due to an increase in pH (caused by increasing ϕ) over the default value of 5.3.

An increase in the inlet SO_2 concentrations beyond 1000 ppm decreases the enhancement factor e which in turn increases the mass transfer resistance. The enhancement factor is a function of gas and solution composition (Chang & Rochelle,

[18] All relations developed in this section are based on a wet limestone/lime FGD tower with four spray headers per tower. The default process parameters are as follows: pH=5.3, ϕ=1.03, L/G=90, inlet SO2=1750 ppm (2.6% S coal), Cl =25,000 ppm (in the slurry) and superficial velocity in tower=10 fps.

1983) which affects the conversion of SO_2 to bisulfite. Typical values of SO_2 removal for different inlet SO_2 concentrations are provided in Table 9-3 based on industry experience (Moser & Owens, 1990; Noblett Jr., et al., 1990; Stevens, et al., 1991).

Table 9-3. Inlet SO_2 Concentration

η_{SO_2}	**SO_2 ppm**
90%	2000 (2.8% S)
84%	4000 (4% S)

This can be represented by an additional term in Equation (9-5), which accounts for the loss of removal efficiency as the inlet SO_2 concentration increases over 2000 ppm.

$$\eta_{SO2} = 1 - \exp\begin{Bmatrix} -[0.725 + 0.0175 \times L/G + (10.0 \times \phi - 10.3) \\ -2.5 \times 10^{-4}(SO_2 - 2000)] \end{Bmatrix} \quad (9\text{-}6)$$

Similarly, calcium chloride accumulation in the slurry leads to a decrease in SO_2 removal. Chloride accumulation suppresses the desirable effects of alkali salts by permitting their accumulation as chloride salts rather than sulfate salts. The effect of accumulated Cl concentrations in the scrubber slurry on the SO_2 removal based on industry experience (Klingspor, 1993; Moser & Owens, 1990; Noblett Jr., et al., 1990; Rader, 1993; Stevens, et al., 1991) is provided in Table 9-4.

Table 9-4. Calcium Chloride Accumulation

η_{SO_2}	**Cl ppm**
86%	10000
80%	80000

This is represented by a term which represents the loss in removal efficiency as the chloride concentration in slurry increases above 25,000 ppm.

$$\eta_{SO2} = 1 - \exp\begin{Bmatrix} -[0.725 + 0.0175 \times L/G + (10.0 \times \phi - 10.3) \\ -2.5 \times 10^{-4}(SO_2 - 2000) + 5.14 \times 10^{-6}(Cl - 25000)] \end{Bmatrix} \quad (9\text{-}7)$$

Addition of organic acids such as adipic, glutiric, and succinct acids to the scrubber slurry improves SO_2 removal efficiency. These acids are usually stronger than sulfurous acid and weaker than carbonic acid. This provides a buffering effect. First it assists limestone dissolution by lowering carbonate ion backpressure and hence more alkalinity in form of bicarbonate enters the scrubber in soluble form. Moreover, since sulfurous acid is a stronger acid, the organic acid ion acts as a base in SO_2 sorption. Dibasic acid (a mixture of) has been found to be the most effective organic acid for use as an additive in commercial scale scrubbers. This improves SO_2 removal and typically every 500 ppm addition of organic acids in the slurry improves SO_2 removal that is comparable to increasing the L/G by 30 gpm/Kacfm in a normal pH operating range of 5.3-5.8 (Blythe, et al., 1993; Rader & Bakke, 1991; Smolenski, et al., 1993; Stevens, et al., 1993). This simple approximation can be represented as follows:

$$\eta_{SO2} = 1 - \exp\begin{Bmatrix} -[0.725 + 0.0175 \times L/G + (10.0 \times \phi - 10.3) \\ -2.5 \times 10^{-4}(SO_2 - 2000) + 5.14 \times 10^{-6}(Cl - 25000) \\ +0.00042 \times DBA] \end{Bmatrix} \quad (9\text{-}8)$$

where DBA represents the concentration (in ppm) of dibasic acid in the slurry. Figure 9-6 plots the sensitivity of SO_2 removal efficiency (η) to the reagent stoichiometry (ϕ) and the liquid to gas ratio (L/G) holding the SO_2, Cl and DBA concentration constant.

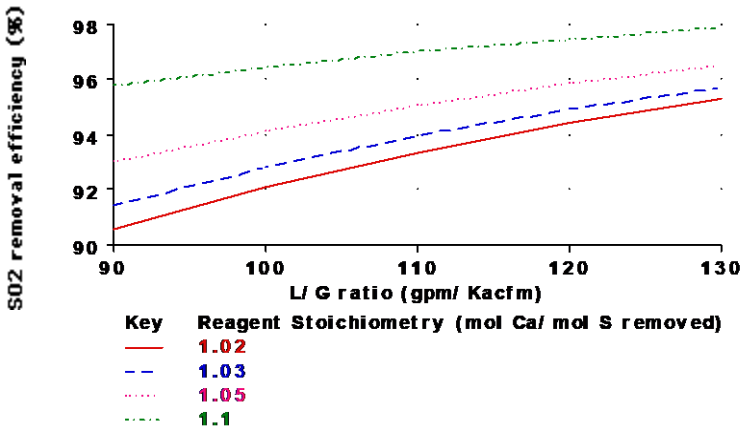

Figure 9-6. IECM performance model for Wet Limestone FGD (with Forced oxidation). Constant parameter value for this case are [SO_2]=1260 ppm, [Cl]= 32360 ppm, and [DBA]=0 ppm.

Figure 9-7 plots sensitivity of SO_2 removal efficiency (η) to the DBA concentration and the liquid to gas ratio (L/G) holding the SO_2, Cl and ϕ constant.

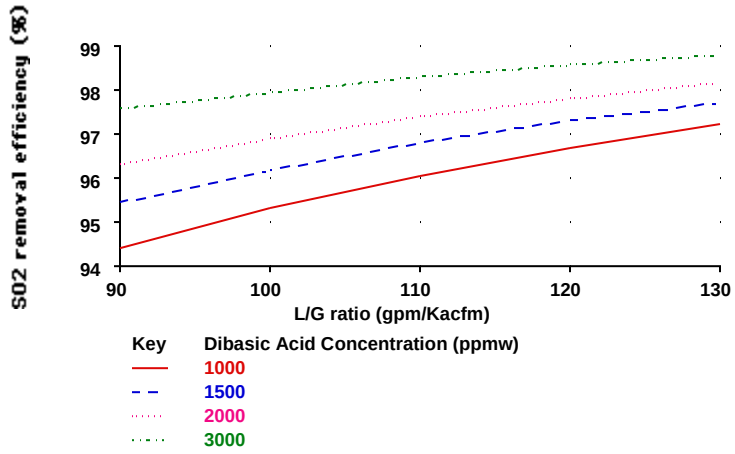

Figure 9-7. IECM performance model for Wet Limestone FGD (with Forced oxidation). Constant parameter value for this case are [SO_2]=1260 ppm, [Cl]= 32360 ppm, and ϕ =1.03.

9.2.2.2. Gas Film Limited

Systems with low inlet SO_2 concentrations are gas film limited, since the liquid phase alkalinity is sufficient to neutralize the dissolved SO_2. For gas film limited case the removal efficiency is largely determined by the contactor design and the L/G ratio; it is not affected by the liquid phase alkalinity. The SO_2 concentration at which the liquid film resistance becomes large enough to be comparable to the gas film resistance depends on the liquid phase alkalinity and L/G ratio. For typical limestone systems with L/G in the 90-130 gpm/Kacfm interval and with a pH between 5.3-5.8 the transition is in the 500-1000 ppm range. Therefore, for inlet SO_2 concentrations below 1000 ppm, the SO_2 removal can be treated as being gas film limited and the relation given in Equation (9-1) without the effects of liquid phase alkalinity can be used for determining SO_2 removal.

9.2.3. Wet Lime FGD System

Magnesium lime systems are also gas film limited. Maglime systems have abundant liquid phase alkalinity since lime has a higher solubility than limestone and magnesium species (usually about 2-4% by weight) provides additional liquid phase alkalinity. Hence the availability of liquid phase alkalinity does not impose any resistance in the absorption of SO_2 and the mass transfer coefficient K_g is based solely on the gas film resistance for inlet SO_2 concentrations from 500-5000

ppm. Typical values for η_{SO_2} and L/G for maglime systems are provided in Table 9-5 (Benson, 1993; Benson, et al., 1991; Johnson, 1993).

Table 9-5. L/G for Mg-Lime

η_{SO_2}	L/G(gpm/Kacfm)
95%	40
98%	56

Based on these values an approximate relation between sulfur removal efficiency and L/G is:

$$\eta_{SO_2} = 1 - \exp\{-(0.2 + 0.07 \times L/G)\}$$

where L/G is measured in gpm/1000 acfm. Figure 9-8 graphs the sensitivity of this model with the removal efficiency versus the L/G ratio for Mg-Lime systems.

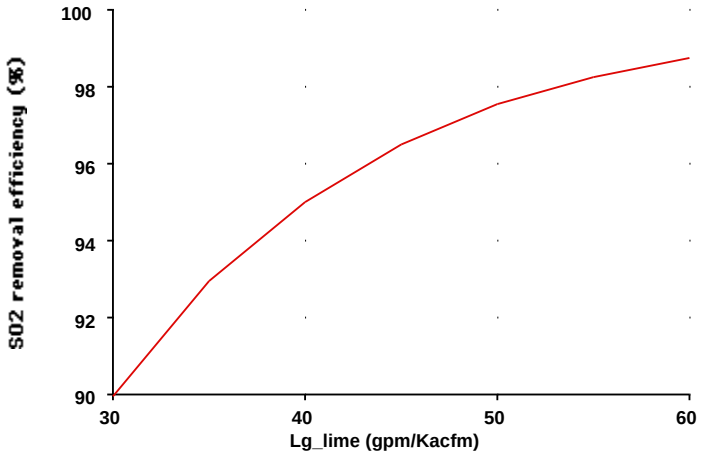

Figure 9-8. IECM performance model for Wet Mg-Lime FGD

9.2.4. Spray Dryer Performance

This section describes improvements to the lime spray dryer performance model relative to the previous report (1). The areas that were modified are the reagent composition, water evaporation in the spray dryer, flue gas composition exiting spray dryer, energy needed for reheat and characterization of the scrubber waste. A schematic diagram of the spray dryer is shown in Figure 9-4. The diagram shows a configuration with bypass and a reheater. These options are mutually exclusive, since it is not likely that a spray dryer would be built with both. If there is a bypass, the reheater is not used. Conversely, if there is no bypass, the reheater is used to raise the flue gas temperature to a specified value.

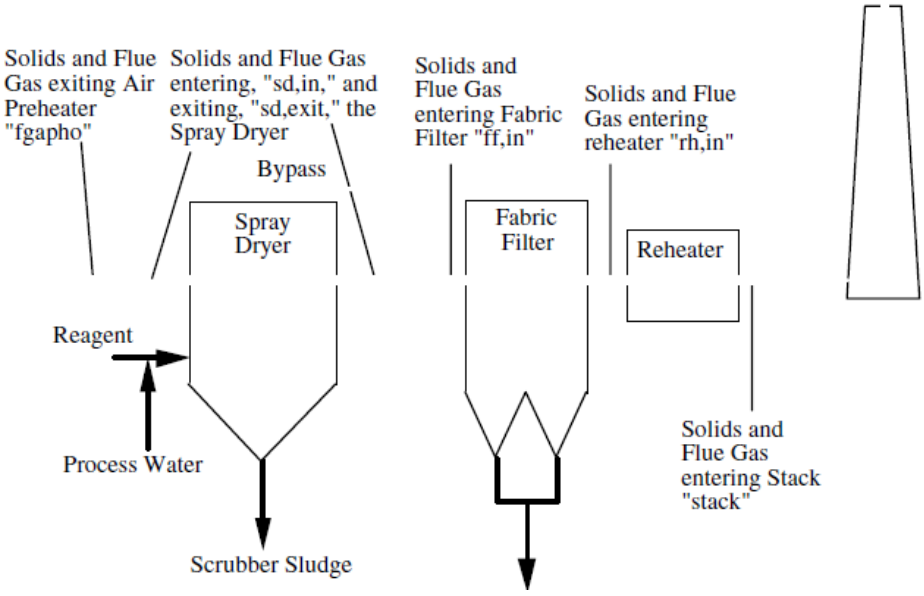

Figure 9-4: Schematic Diagram of the Spray Dryer FGD Model

9.2.4.1. Reagent and SO_2 Efficiency

The SO_2 removal efficiency is a key parameter governing the performance of the spray dryer system. The removal efficiency can either be specified or it can be calculated to meet a desired SO_2 emission standard. The SO_2 removal efficiency, η_{SO2}, based on the emission standard is the same as Equation (9.1) shown in Section 9.2.

The spray dryer system has an option to allow bypassing of some flue gas around the scrubber. This option may lower the cost of the spray dryer system if the efficiency calculated by Equation (9.9) is not very high. When the bypass option is chosen the amount of bypass is based on either the spray dryer operating at its maximum efficiency, $\eta_{SO2,max}$, or the flue gas temperature entering the stack. No bypass will be used if the amount of bypass is less than the minimum bypass specified by the user, Byp_{min}. If the user wants the bypass to be based on the maximum efficiency of the spray dryer then Equation (9.9) is used.

$$\text{if } \left(1-\frac{\eta_{SO_2,std}}{\eta_{SO_2,max}}\right) > Byp_{min} \text{ then } Byp = 1-\frac{\eta_{SO_2,std}}{\eta_{SO_2,max}};\ \eta_{SO_2}=\eta_{SO_2,max}$$

$$\text{else} \qquad (9.9)$$

$$Byp = 0.0\ ;\ \eta_{SO_2}=\eta_{SO_2,std}$$

The user may desire to have the bypass based on a desired stack temperature, $T_{stack,input}$. With this option, a bypass is only allowed if the bypass is greater than the minimum, Byp_{min}, and less than the amount determined by Equation (9.9). The induced draft fan is located after the fabric filter (that is. after the gases remix) and raises the temperature of the flue gas by a user-specified amount, T_{idfan}. The flue gas exiting the spray dryer and the flue gas bypassed around the spray dryer are assumed to have the same specific heat; therefore, Equation (9.10) is used if the user wants the bypass to be based on the $T_{stack,input}$. The inlet temperature, T_{in}, equals the temperature exiting the air preheater, T_{fgapho}, while the exit temperature, T_{2exit}, is determined in the next section.

$$\text{If } Byp_{min} < \frac{T_{stack,input} - T_{idfan} - T_{sd,exit}}{T_{fgap\,ho} - T_{sd,exit}}\ , < \left(1-\frac{\eta_{SO_2,std}}{\eta_{SO_2,max}}\right) \text{ then}$$

(9.10)

$$Byp = \frac{T_{stack,input} - T_{idfan} - T_{sd,exit}}{T_{fgapho} - T_{sd,exit}} \; ; \; \eta_{SO_2} = \frac{\eta_{SO_2,std}}{1 - Byp}$$

else

$$Byp = 0.0 \; ; \; \eta_{SO_2} = \eta_{SO_2,std}$$

The flue gas that is not bypassed and the moles of sulfur removed by the scrubber are determined by

$$m_{sd,in,j} = (1 - Byp) m_{fgapho,j}$$

$$m_{rem,S} = \eta_{SO_2} \left(m_{sd,in,SO_2} + M_{sd,in,SO_3} \right)$$

The reagent for the spray dryer is lime. The reagent purity, R_{purity} and moisture content, W_{reag}, must be specified. Any remaining material is considered inert. The molar stoichiometry, σ, (moles of calcium required per mole of sulfur into the system) is a function of the SO_2 removal efficiency and the approach to saturation temperature (1). With the molar stoichiometry, the mass flow rate of reagent can be determined.

$$\sigma_{sd} = \exp(3.322 \, \eta_{SO2} + 0.025 \, \Delta T_{sat} - 2.900) \quad (9.11)$$

$$M_{reag} = \frac{56.08 \left(m_{sd,in,SO_2} + M_{sd,in,SO_3} \right) \sigma_{sd}}{2000 R_{purity}} \eta_{SO_2} \quad (9.12)$$

9.2.4.2. Water Balance

Makeup water to the spray dryer system is required principally to offset evaporative losses in the scrubber. The mass of water evaporated in the spray dryer system is determined by an energy balance assuming adiabatic conditions and neglecting the solid mass flow rates in the system. With these assumptions, the sensible energy released by the flue gas entering the scrubber has to equal the energy needed to evaporate the water evaporated and raise it to the exit temperature. This is identical with the wet scrubber, except that the flue gas exiting the spray dryer is not saturated. The user specifies an approach to saturation temperature, ΔT_{sat}, which is a measure of how close the flue gas is to being saturated. The procedure for the spray dryer is identical with the algorithm shown in Section 2.5, except steps 4 and 5[19]. Once the saturation temperature, T_{sat}, of the flue gas is determined, the approach to saturation temperature is added to find the exit temperature. The evaporated water is determined with Equation (2.20), shown below, as follows:

1. Determine $\dot{W}_{evp,1}$ from (9.6) assuming an exit temperature of 155˚F
2. Determine $T_{sat,1}$ from (9.7) with $\dot{W}_{evp,1}$
3. Determine $\dot{W}_{evp,2}$ with $T_{exit,1}$
4. Determine T_{sat} with $\dot{W}_{evp,1}$, then $T_{exit} = T_{sat} + \Delta T_{sat}$.
5. Determine $\dot{W}_{evp}$ from (9.13)[20]

---

19 An additional assumption is needed for the spray dryer which is that the enthalpy of the water in the flue gas is approximately equal to the enthalpy of saturated steam at the same temperature.

20 Bypassing flue gas around the scrubber does not change the exit temperature, but it does change the amount of water evaporated. For these reasons, the bypass variable is excluded from the derivation of the flue gas exit temperature. Once the exit temperature is determined, the amount of evaporated water can be determined for the spray dryer with bypass.

$$\dot{W}_{evp} = \frac{(1 - Byp)\sum_{j=1}^{9} m_{sd,in,j}\left(h_j\left(T_{fgap\ ho}\right) - h_j\left(T_{sd,exit}\right)\right)}{7.366T_{sd,exit} + 17{,}593.7} \tag{9.13}$$

9.2.4.3. Flue Gas Composition and Reheat

The composition of the flue gas changes in the spray dryer. The two most significant changes are the reduction in the sulfur dioxide content and the increase in the moisture content. The sulfur dioxide and sulfur trioxide are removed from the flue gas by a complex set of chemical reactions. These chemical reactions have been greatly simplified in the IECM and are shown below:

$$\begin{aligned} &SO_2 + CaO + 0.5H_2O \text{ --> } CaSO_3{\bullet}0.5H_2O \\ &SO_2 + CaO + 2H_2O + 0.5O_2 \text{ --> } CaSO_4{\bullet}2H_2O \\ &SO_3 + CaO + 0.5H_2O \text{ --> } CaSO_3{\bullet}0.5H_2O + 0.5O_2 \\ &SO_3 + CaO + 2H_2O \text{ --> } CaSO_4{\bullet}2H_2O \end{aligned} \tag{9.14}$$

Using these chemical reactions, the composition of the flue gas exiting the scrubber can be determined from a molar balance and is shown below. It is assumed that the oxygen needed to oxidize the calcium sulfite to calcium sulfate is taken from the flue gas. In practice this oxygen may be supplied by blowing air through the sludge outside the scrubber vessel. It is assumed that the water needed to hydrate the scrubber sludge comes directly from the makeup slurry and does not reduce the moisture content of the flue gas. The symbol Ox represents the fraction of calcium sulfite oxidized to calcium sulfate.

$$\dot{m}_{sd,exit,j} = \dot{m}_{sd,in,j} \quad \text{for } j = N_2, CO_2, CO, NO, NO_2$$

$$\dot{m}_{sd,exit,O_2} = \dot{m}_{sd,in,O_2} + \left(0.5(1-Ox)m_{sd,inSO_3} - 0.5Ox\,\dot{m}_{sd,in,SO_2}\right)\eta_{SO_2}$$

$$\dot{m}_{sd,exit,H_2O} = \dot{m}_{sd,in,H_2O} + \dot{W}_{evp}$$

$$\dot{m}_{sd,exit,SO_2} = m_{sd,in,SO_2} - \dot{m}_{sd,in,SO_2}\eta_{SO_2}$$

$$m_{sd,exit,SO_3} = m_{sd,in,SO_3} - m_{sd,inSO_3}\eta_{SO_3}$$

After the spray dryer there are two options depending if a bypass is used. The first is that the flue gas is remixed with the bypassed flue gas before going into the fabric filter. After the fabric filter the flue gas temperature is raised by the induced draft fan before entering the stack. The second is that the flue gas passes through the fabric filter and induced draft fan before going into the reheater. After exiting the reheater the flue gas enters the stack. For either case, the flue gas composition and temperature do not change in the fabric filter. The equations governing the flue gas temperature and composition for the bypass case are shown below.

$$\dot{m}_{ff,in,j} = \dot{m}_{sd,exit,j} + Byp\,\dot{m}_{fgapho,j} \tag{9.15}$$

$$T_{ff,in} = Byp\ T_{fgapho} + (1 - Byp)\ T_{sd,exit} \tag{9.16}$$

$$\dot{m}_{stack,in,j} = m_{ff,in,j} \tag{9.17}$$

$$T_{stack} = T_{ff,in} + \Delta T_{idfan} \tag{9.18}$$

$$E_{dryfgd} = 0 \tag{9.19}$$

The equations governing the flue gas temperature and composition for the reheater case are shown below. The exit temperature of the reheater is an input parameter, $T_{stack,input}$. The energy needed to raise the flue gas temperature to T_{stack} is the sensible energy of the flue gas.

$$\dot{m}_{stack,in,j} = m_{ff,in,j} = \dot{m}_{rh,in,j} = \dot{m}_{ff,in,j} = \dot{m}_{sd,exit,j} \quad (9.20)$$

$$T_{ff,in} = T_{sd,exit} \quad (9.21)$$

$$T_{rh,in} = T_{ff,in} + \Delta T_{idfan} \quad (9.22)$$

$$T_{stack} = T_{stack,input} \quad (9.23)$$

$$E_{dryfgd} = \sum_{j=1}^{9} \dot{m}_{rh,in,j} \left(h_j(T_{stack}) - h_j(T_{rh,in}) \right) \quad (9.24)$$

9.2.4.4. Waste Stream Composition

A major environmental flow stream emanating from a spray dryer system is the stream of dry waste solids. The basic chemistry for the creation of these solids is shown in Equation (9.14). The difference in the composition and mass flow rates of spray dryer waste depends on the extent of oxidation of calcium sulfite to sulfate, Ox. Other constituents of the spray dryer solids stream include unreacted reagent (that depends on the molar stoichiometry), inert materials introduced with the reagent (as dictated by the level of reagent purity) and flyash. The total mass flow rate of the solids created in the spray dryer and the flyash entering the spray dryer is shown below.

$$M_{sd,total,j} = M_{sd,in,j} \quad \text{for } j = \text{Ash}, CaCO_3, CaSO_4$$

$$\dot{M}_{sd,total,CaO} = \dot{M}_{sd,in,CaO} + \left(\frac{56.8\left[\sigma\left(m_{sd,in,SO_2} + m_{sd,in,SO_3}\right) - m_{rem,S}\right]}{2000} \right)$$

$$\dot{M}_{sd,total,CaSO_3 \bullet 0.5H_2O} = \dot{M}_{sd,in,CaSO_3 \bullet 0.5H_2O} + \frac{129.14(1-Ox)\dot{m}_{rem,S}}{2000}$$

$$\dot{M}_{sd,total,CaSO_4 \bullet 2H_2O} = \dot{M}_{sd,in,CaSO_4 \bullet 2H_2O} + \frac{172.17Ox\, m_{rem,S}}{2000}$$

$$\dot{M}_{sd,total,Misc} = \dot{M}_{sd,in,Misc} + \left(1 - R_{purity} - W_{reag}\right) M_{reag}$$

The total solids in the spray dryer either exit with the flue gas or drop out the bottom of the spray dryer. The removal efficiency, η_{TSP}, of the solids is an input parameter, that specifies what fraction of the total solids exit out the bottom. The solids that exit with the flue gas remix with the flyash bypassed around the spray dryer (if present) before entering the fabric filter. After the fabric filter removes most of the solids, the solids from the spray dryer and fabric filter are remixed before being disposed.

$$\dot{M}_{sd,bottom,j} = \eta_{TSP} \dot{M}_{sd,total,j}$$

$$\dot{M}_{sd,exit,j} = (1 - \eta_{TSP}) \dot{M}_{sd,total,j}$$

$$\dot{M}_{ff,in,j} = Byp \dot{M}_{fgapho,j} + \dot{M}_{sd,exit,j}$$

9.2.4.5. Economics Algorithm

The economic algorithm for the spray dryer has remained unchanged except one item. The single indirect charge factor for capital cost has been split into different categories of indirect charges following the nomenclature of the TVA.

9.2.5. Lime Spray Dryer System

Spray dryer scrubbers are sometimes used as an alternative to wet scrubbing since they provide simpler waste disposal and can be installed with lower capital costs. In a typical system, hot flue gas is contacted with finely atomized aqueous solution in the spray dryer. Dry products leave the spray dryer and are removed from the gas in a baghouse. The liquid phase consists of an aqueous slurry of slaked lime. The sulfur dioxide in the flue gas is absorbed into the droplets, which simultaneously evaporate on contact with the hot flue gas. Although some moisture still remains in the flue gas solids which later promotes further removal of SO_2 in the fabric filter. The total SO_2 removal is the sum of the removal in the dryer and the baghouse. In this subsection, we develop empirical relations to describe the total SO_2 removal (Blythe, et al., 1985; Blythe, et al., 1991; Brown & Felsvang, 1991).

The main process parameters that affect the SO2 removal efficiency are (Brown & Felsvang, 1991; Jozewicz & Rochelle, 1984):

1. Inlet SO_2 concentration,
2. Reagent ratio[21], (ϕ)
3. Calcium chloride concentrations in the liquid slurry (*Cl*),
4. Inlet flue gas temperature (T_{in}), and
5. Approach temperature to the adiabatic saturation temperature of the flue gas at outlet (ΔT).

Increase in the reagent ratio increases the alkalinity in the liquid phase, which improves the SO_2 removal. Effects of inlet SO_2 concentrations are similar to those in wet FGD systems. Low inlet SO_2 concentrations (< 1000 ppm) lead to gas film limited mass transfer and medium to high inlet SO_2 concentration leads to comparable contributions from both gas and liquid film resistance. As a result, we develop different response surfaces to describe the removal efficiency for low and high inlet SO_2 concentrations. Increasing the inlet temperature allows more water to be added to the spray dryer to achieve the same approach temperature. This in turn leads to a higher recycle ratio and increased mass transfer area thus improving the removal efficiency.

In order to understand the effect of the other parameters one has to consider the heat transfer characteristics of the spray dryer. The evaporation time, *t*, for a given droplet is also the time available for a droplet to absorb SO_2. As the approach to saturation temperature increases, the evaporation time decreases thereby decreasing removal efficiency. The addition of chlorides in the slurry improves the SO_2 removal efficiency of the spray dryer. This is due to the deliquescent properties of chlorides, which helps the droplet to retain water and hence increase the evaporation time. Hence chlorides are often used as additives to reduce the lime consumption. We now develop response surfaces to describe the overall SO_2 removal efficiency in spray dryers using data from pilot studies conducted by EPRI (1985, 1991) and Joy/Niro (Svend, et al. 1983). We use the log-linear form shown in Equation (9-3) to develop these response surfaces.

The reagent ratio is a key process variable and it affects the removal efficiency significantly. Typical value of SO_2 removal for different stoichiometries are presented in Table 9-6.

[21] For spray dryers the reagent ratio is measured as moles of reagent supplied/mole of SO_2 *entering* the scrubber. Note that for wet FGD systems the reagent ratio is measured as moles of reagent/mole of SO_2 *removed*.

Table 9-6. Reagent Stoichiometry

η_{SO_2}	ϕ
80%	0.9
90%	1.1

These values are representative of both low and high inlet SO_2 concentrations. Based on these numbers the log-linear approximation for the effect of reagent ratio is as follows:

$$\eta_{SO2} = 1 - \exp\{-(-1.495 + 3.45 \times \phi)\} \quad (9\text{-}9)$$

This relation can be used for reagent ratios in the range of 0.9-1.8. Now we develop the response surface for low and high SO_2 concentrations separately.

9.2.5.1. Low Inlet SO_2 Concentrations ($\leq$ 1000 ppm)

The data presented in this section was collected against baseline conditions of 1000 ppm inlet SO_2, approach temperature of 20°F, and inlet temperature of 280°F. For low inlet SO_2 concentrations, the inlet temperatures in the range of 280-325°F has been observed to have no effect on the removal efficiency. However, increasing the approach temperature to saturation from 20 to 40°F results in the requirement of higher stoichiometries for the same removal efficiencies as shown in Table 9-7.

Table 9-7. Effect of 40°F Approach Temperature to Saturation

η_{SO_2}	ϕ
80%	1.1
85%	1.3

Averaging the effects of these values an additional term to describe this effect is added to Equation (9-6) as follows:

$$\eta_{SO2} = 1 - \exp\{-[-1.495 + 3.45 \times \phi - 0.05 \times (\Delta T - 20)]\}$$

As discussed earlier the deliquescent properties of calcium chloride improves the removal efficiency. A presence in the slurry resulting in 0.6% calcium chloride by weight in solids collected in the fabric filter results in higher removal efficiencies for the same stoichiometry as shown in Table 9-8.

Table 9-8. Effect of 0.6% Calcium Chloride

η_{SO_2}	ϕ
90%	1.0
95%	1.2

Averaging the effects based on these values can be accomplished with additional terms being added to Equation (9-7). Thus, the effect of the approach to saturation temperature and calcium chlorides can be described by Equation (9-10):

$$\eta_{SO2} = 1 - \exp\{-[-1.495 + 3.45 \times \phi - 0.05 \times (\Delta T - 20) + 0.58 \times Cl]\} \quad (9\text{-}10)$$

This is the final form of the response surface for low SO_2 inlet concentrations.

9.2.5.2. Medium to High SO_2 Concentrations (> 1000 ppm)

The data presented in this section was collected against baseline conditions of the following values: 2000 ppm inlet SO_2, approach temperature of 20°F, and inlet temperature of 325°F. For inlet SO_2 concentrations greater than 1000 ppm, the removal efficiency increases with increases in inlet temperatures from 280-325°F. Decreasing the inlet temperature to 280°F decreases the removal efficiency to 80% for a given stoichiometry of 1.1. This effect is represented by an additional term to Equation (9-9) as follows:

$$\eta_{SO2} = 1 - \exp\{-[-1.495 + 3.45 \times \phi + 0.015 \times (T - 325)]\}$$

The presence of 0.4% by weight of calcium chloride in the fabric filter solids provides an improved efficiency of 90% for a reagent ratio of 1.0. This is described in by an additional term as follows:

$$\eta_{SO2} = 1 - \exp\{-[-1.495 + 3.45 \times \phi + 0.015 \times (T - 325) + 0.86 \times Cl]\}$$

Increasing the approach temperature to 30°F reduces the removal efficiency to 75% for a reagent ratio of 1.05. On the other hand, increasing the inlet SO_2 concentration to 3000 ppm reduces removal efficiency to 80% at a reagent ratio of 1.1. These effects are included as shown below:

$$\eta_{SO2} = 1 - \exp\left\{\begin{matrix} -[-1.495 + 3.45 \times \phi + 0.015 \times (T - 325) + 0.86 \times Cl \\ -0.0007 \times (SO_2 - 2000) + 0.08475 \times (\Delta T - 20)] \end{matrix}\right\}$$

This is the final form of the response surface for high SO_2 inlet concentrations. Figure 9-9 plots the removal efficiency as a function of the inlet flue gas temperature for different stoichiometries.

Figure 9-10 graphs the sensitivity of the removal efficiency as a function of the approach temperature for different stoichiometries.

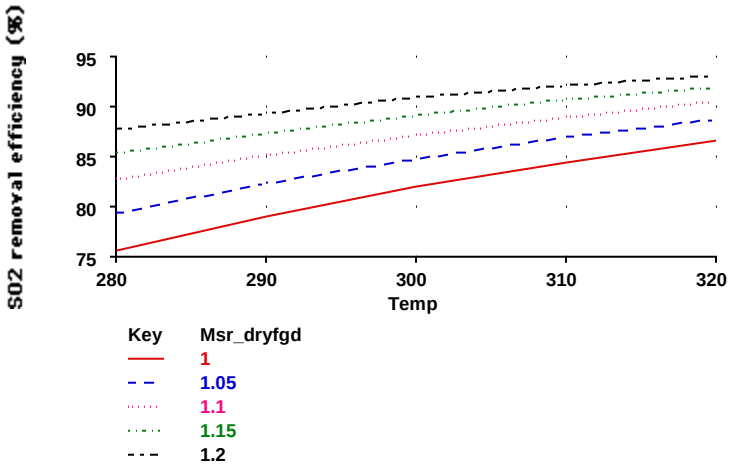

Figure 9-9. IECM performance model for Lime Spray Dryer. Constant parameter value for this case are [Cl]=0.4% wt., [ΔT]=28 F, and [SO_2]= 1260 ppm

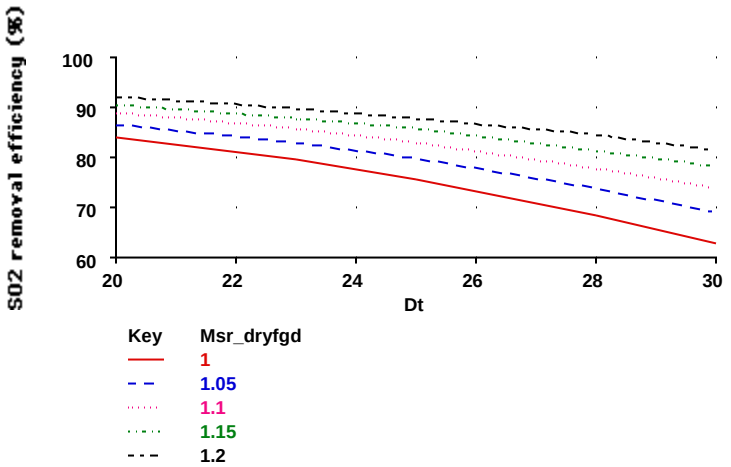

Figure 9-10. IECM performance model for Lime Spray Dryer. Constant parameter value for this case are [Cl]=0.4% wt., [T]=300 F, and [SO_2]= 1260 ppm

9.3. FGD Cost Models

The FGD cost models originally developed for the IECM were derived from a detailed FGD computer program developed in the late 1970s and early 1980s by the Tennessee Valley Authority (TVA). The TVA model was subjected to an extensive set of parametric runs, and the results were used to derive statistical "response surface" models which accurately represented the results of the TVA model in terms of a smaller number of key site-specific plant and design parameters. We follow a similar procedure in developing the new models reported here.

Changes in the design, performance and cost of FGD systems in the mid-to-late 1980s left the TVA model outdated as a basis for performance and cost estimation. The TVA modeling team also was disbanded during this period, and no further updates to the model were made. Instead, the most reliable and widely used estimates of FGD cost came from a new modeling effort sponsored by the Electric Power Research Institute (EPRI). This effort led to the development of a computer model called FGDCOST, which has become the new industry standard in the area. FGDCOST, however, does not contain any FGD performance models (all performance parameters must be supplied by the user); hence, the development of the new performance models described earlier.

The new cost models that we developed were based on results from FGDCOST, a spreadsheet program model developed for EPRI which provides the most up-to-date cost models for fifteen FGD processes (Keeth, et al., 1991). The cost development and breakdown follow the EPRI economic premises. We have augmented FGDCOST to allow for systematic sensitivity analysis with large numbers of input variables. In order to allow the simultaneous variation of many input parameters, the values of the input parameters are read from a lookup table. The values for input variables are generated from sampling probability distributions. These values are imported into the tables. On each execution, the values of all the inputs are read from each row of the table, the corresponding performance parameters are calculated and finally the capital and O&M costs are written along the same row. The output columns can be now exported to other programs for sensitivity analysis and regression modeling. In the following paragraphs we provide a brief outline of the criteria used for designing costs estimates.

Cost is broken down in terms of capital and operating and maintenance costs. We describe in some detail the breakdown of the capital costs estimates. The process parameters that affect operating costs are also outlined.

9.3.1. Capital Costs

Models of capital cost focus first on the process capital requirements of each section of the FGD system. The process facilities costs are then used to determine the other capital costs. These are generally referred to as the indirect capital costs. The bases and items included for each component of the capital estimate is provided in Table 9-9. These standardized components are used throughout all the modules in the IECM and described more fully in the EPRI Technical Assessment Guide.

Table 9-9. Nomenclature for EPRI Cost Estimates

Capital Investment	$/kW
Process Capital (incl. Sales tax)	A (from
General Facilities	B
Eng. & Home Office Fees	C
Project Contingency	D
Process Contingency	E
Total Plant Cost (TPC)	= A + B + C + D + E
Total Cast Expended (TCE)	TPC x Adjust factor*
AFDC (Allowance for Funds During Construction)	F
Total Plant Investment (TPI)	= TCE + F
Royalty Allowance	G
Preproduction Costs	H

Inventory Capital	I
Initial Catalyst and Chemicals	J
Land	K
Total Capital Required (TCR)	TPI + G + H + I + J + K
* Adjustment Factor for TCE per Table 3-4 of EPRI TAG (P6587-L)	

9.3.1.1. Process Facilities Cost

The process capital estimate is broken down on an area-by-area basis for each process area. The costs areas along with the equipment used in each area are provided in Table 9-10. The equipment size is based on a mass balance for various flue gas species (such as SO_2, NO_x, HC_1, CO_2, N_2) performed by FGDCOST, which is similar to the mass balance calculations in the IECM. The sulfur content of the flue gas is the key variable in costing various aspects of the FGD process. Based on the mass balance, the required size of the various equipment in each process area is determined, which is then used to determine costs. The capital costs are also affected by the sparing philosophy for the absorber towers. The sum of the capital cost for all process areas provides the total process facilities cost.

Table 9-10. Cost Areas for Process Capital Breakdown (Source: EPRI)

Area	Description
10	Reagent Feed System
20	SO_2 Removal System
30	Flue Gas System
40	Regeneration System
50	By-product System
60	Solids Handling System
70	General Support Area
80	Miscellaneous Equipment

10 Reagent Feed System – all equipment required for storage, handling and preparation of raw materials, reagents, and additives used in each process.

20 SO_2 Removal System – equipment required for SO_2 scrubbing, such as the absorption tower, recirculation pumps and other associated equipment.

30 Flue Gas System – duct work and fans required for flue gas distribution to the SO_2 scrubbing system, plus gas reheat as required.

40 Regeneration System – specific to regenerable reagent systems, equipment used to regenerate spent absorbent for return to the process, plus any preconditioning system for SO_2 or H_2S off-gas.

50 By-Product System – production equipment for salable process by-products and storage facilities for the final products.

60 Solids Handling System – equipment required for fixation, treatment, and transportation of all sludge/dry solids materials produced by each scrubbing process.

70 General Support Area – additional equipment required to support FGD system operation such as makeup water and instrument air.

80 Miscellaneous Equipment – This area will include plant modifications necessitated by the addition of the FGD system. Also included are costs for electrical equipment tie-ins and other associated systems.

9.3.1.2. Other Capital Costs:

Besides the process capital costs, a series of additional indirect costs are included in the IECM cost models. Following the EPRI format, these are represented as simple parameters whose values are user-specified. Their relationship to each other and to the direct facilities cost are shown in Table 9-9.

General Facilities: The general facilities costs include roads, office buildings, shops, laboratories etc. A cost factor (f_{gf}) of 5 - 20% of the process capital cost is used to evaluate this cost. A cost factor of f_{gf}=10% is used as default value in the FGDCOST models.

Engineering & Home Office Fees: An estimate of engineering, home office overhead and fees is included in capital costs estimates. A cost factor (f_{eho}) of about 10 -15% is used to estimate this expense. FGDCOST uses a value of f_{eho}=10% of the process facilities cost.

Project Contingency: Project contingency costs covers additional equipment and other costs that would arise from a more detailed design. Project contingency factors (f_{cproj}) range from 10 - 20% of process capital costs. An average value of about 15% is used in FGDCOST.

Process Contingency: A process contingency is applied to a new technology in an attempt to quantify the design uncertainty and the cost of a commercial scale system. The contingency factor (f_{cproc}) can range from 2-50% of the process capital costs. For FGD processes a contingency factor of 2% is used.

Total Plant Cost: The total plant cost (tpc) is the sum of process capital, general facilities, engineering and home office fees, and contingencies.

Total Cash Expended: The total cash expended is an estimate of the cash expected to be spent during the construction duration of the FGD system. This estimate accounts only for the escalation of costs up to the date of expenditure.

Allowance for Funds During Construction (AFUDC): The schedule for engineering procurement and construction is assumed to be two years for installation. For example, for an escalation of 5% a year, the total plant costs is multiplied by 0.0548 to calculate the allowance for interest expenses during a two-year construction period. The IECM has general function which calculates the escalation costs given the escalation rate and the time for installation.

Total Plant Investment: The total plant investment is the sum of the total cash expended and the allowance for interest during construction.

Royalty Allowance: Royalties paid are 0.5% of the process capital.

Preproduction Costs: Preproduction costs are intended to cover operator training, equipment checkout, major changes in plant equipment, extra maintenance, and inefficient use of materials during plant startup. It is a sum of one-month fixed operating costs, one-month variable operating costs at full capacity and 2% of the total plant investment.

Inventory Capital: The inventory costs include the expense of raw materials and other consumables based on a 100% capacity operation for 60 days.

Land: FGD system land requirements include the plant site area and disposal area. Land has not been included as a line item.

Total Capital Requirement: The total capital requirement is calculated as the total of all the costs enumerated above.

9.3.1.3. Operating & Maintenance Costs

Operating costs for FGD systems are separated into fixed and variable operating costs. Fixed costs include operating and maintenance labor, maintenance materials and administrative/support labor. Various factors based on EPRI premises are used to estimate these costs many of which are based on capital cost estimates. Variable operating costs include consumables such as fuel, water, power, chemicals, and solids disposal. Table 9-11 provides the operating cost criteria used. The fixed and variable O&M costs depend on the feed rate of reagent, sludge disposal costs, power for pumping, labor and other operations. Table 9-12 provides the default process design criteria used in our models.

Table 9-11. Criteria for Calculating Operating Costs

Fixed Operating Costs	Units	Rate
Operating Labor	Man-hrs	$20.00 (Jan. 1990)
Maintenance Labor – Slurry Handling	$/yr	3.2% of Process Capital
Maintenance Labor – Liquid Handling	$/yr	1.2% of Process Capital
Maintenance Material – Slurry Handling	$/yr	4.8% of Process Capital
Maintenance Material – Liquid Handling	$/yr	1.8% of Process Capital
Administrative & Support Labor	$/yr	30% of O&M Labor

Variable Operating Costs	Units	Jan 1990 $/Unit	Add'l Freight $/ton	30-Yr Level Factor	30-Yr Level $/Unit
Fuel Oil (#6)	gal	0.41	Incl	1.613	0.66
Raw Water	1000 gal	0.60	Incl	1.613	0.97
Cooling Water	1000 gal	0.16	Incl	1.613	0.26
Power	kWh	0.05	Incl	1.668	0.08
Methane	1000 ft^3	3.00	Incl	1.668	5.00
Lime	ton	55.00	Incl	1.613	88.72
Limestone	ton	15.00	Incl	1.613	24.20
Soda Ash	ton	93.00	43.00	1.613	219.37
Magnesia	ton	232.00	135.00	1.613	591.97
Ammonia	ton	145.00	5.50	1.613	242.76
Sulfur Emulsion	ton	220.00	Incl	1.613	354.86
Dibasic Acid	ton	360.00	Incl	1.613	580.68
Formic Acid	ton	800.00	20.00	1.613	1322.66
Allied Catalyst	ton	2500.00	45.00	1.613	4105.09
Claus Catalyst	ton	1000.00	Incl	1.613	1613.00
Disposal Charges					
Dry Solids (lined)	ton (dry)	9.29	Incl	1.613	14.98
Fly Ash (unlined)	ton (dry)	8.00	Incl	1.613	12.90
Sludge (truck to lined landfill))	ton (dry)	9.25	Incl	1.613	14.92
Sludge (truck to unlined landfill)	ton (dry)	8.15	Incl	1.613	13.15
Sludge (ponded)	ton (dry)	6.00	Incl	1.613	9.68
Gypsum (pumped and stacked)	ton (dry)	4.75	Incl	1.613	7.66
Condensate	1000 lb	0.77	Incl	1.613	1.24
Steam					
0 – 70 psia	1000 lb	2.85	Incl	1.668	4.75
70 – 250 psia	1000 lb	3.50	Incl	1.668	5.84
250 – 400 psia	1000 lb	5.30	Incl	1.668	8.84
By-Product Credit					
Sulfur	Long ton	90.00	Incl	1.613	145.17
Sulfuric Acid	ton	50.00	Incl	1.613	80.65
Liquid Sulfur Dioxide	ton	230.00	Incl	1.613	371.00
Gypsum	ton	2.00	Incl	1.613	3.23

NOTE:
1000 gal = 3.785 m^3 , short ton = 0.9072 long ton, 1000 ft^3 = 28.32 m^3,
1000 lb = 453.6 kg

Table 9-12. Description of Default Criteria used in the Model

Variable name	Units	Description	Default Value
Gas	Kacfm	flue gas flow rate	971
MW	106 MW	Net plant capacity	300
L/G	gpm/Kacfm	liquid to gas ratio	90/55/30[a]
%S	%	% sulfur in coal by weight	2.6% 1750 ppm
Stoichiometry (ϕ)		moles of Ca per mole of SO_2 removed	1.03/1.02/ 1.1[b]
labor	$/hr	FGD operating labor rate	20
reag	$/ton	reagent ($CaCO_3$/CaO) cost	15/55[d]
solid	$/ton	sludge disposal cost	8.15
stack	$/ton	sludge disposal - stacking cost	4.75
power	mills/kWh	power cost	50
steam	$/1000 lbs	steam cost	3.5
waterf	$/1000 gallons	fresh water cost	0.6
Waterc	$/1000 gallons	cooling water cost	0.16
DBA_{ppm}*	ppm	scrubber slurry DBA concentration	1500
DBA_{feed}*	lbs DBA/ton SO_2 removed	DBA feed rate	20
DBA_{cost}[C]	$/ton	DBA additive cost	360
?P	inches of H_2O	total system pressure drop	10
?T	°F	temperature increase of scrubbed flue gas due to reheat	25

a the default values are: 90 gpm/Kacfm for LSFO and 55 gpm/Kacfm for LSDBA and 30 for Mg-lime System for a 90% removal efficiency.

B the stoichiometry for limestone systems is 1.03, for lime systems is 1.02, and for lime spray dryer is 1.1(note that for lime spray dryer the reported stoichiometry is moles of Ca per mole of inlet SO_2).

C these input variables for LS/DBA only

d limestone cost is 15 and lime cost is 55 $/ton

9.3.2. The Methodological Approach

Response surface construction is the central objective of the sensitivity analysis techniques presented in this section. Sensitivity analysis seeks to identify the set of input variables that have significant effect on the model output and to rank order them according to the magnitude of their effects. Once the relevant variables are identified regression methods can be used to develop adequate response surface replacements for the models. Subsequently probability distributions on the input variables can be used in conjunction with the response surface to derive the probability distributions of the model outputs. In this section, we briefly describe the use of Latin hypercube sampling (LHS) (Iman, et al., 1980) along with partial rank correlation coefficients (PRCC) to examine the influence of individual variables on the model output (Iman, et al., 1981a; Iman, et al., 1981b). Finally, the use of regression analysis with log-linear transformations for developing response surfaces is described (Ang & Tang, 1975; Draper & Smith, 1966; Neter, et al., 1983).

9.3.2.1. Sampling and Ranking Methods

In order to perform sensitivity analysis, it is necessary to obtain model output for various values of input variables. Latin hypercube sampling is used to select values for input variables. The LHS technique to select *n* different values from *k*

different input variables operates in the following manner. For each variable, the range is divided into *n* non-overlapping intervals of equal probability. One value from each interval is selected at random with respect to the probability density in the interval. The *n* values for variable x_1 are paired at random with the *n* values of x_2 and these *n* pairs are paired at random with *n* values of x_3 and so on to generate *n* k-tuples. This is the Latin hypercube sample used as input to the model. The model is then exercised at each of these *n* input values to generate *n* *l*-tuples for *l* output variables of interest. This data set of *n* *k*-tuples of input values and *n* *l*-tuple of output values forms the basis for the rest of the analysis.

The importance of an input variable is derived by assessing its influence on the output variable. For linear relationships this can be assessed by the use of partial correlation coefficients (PCC) which measure the correlation between an input and output variable when the effects of all the other variables is removed. For nonlinear relations it becomes more difficult to assess the importance of individual variables. However, if the model output is a monotonic function of the input then it is possible to linearize the relationship by using rank transformations on the input and output values. A rank transformation involves replacing each value of a variable by its rank. Now the partial correlation coefficient on the rank transformed variables (PRCC) can be used to assess the importance of the input variables.

9.3.2.2. Regression Analysis

Once the important input variables are chosen, multivariate linear regression approaches can be used with the data set to construct response surfaces. If *k* input variables are chosen as relevant, a linear regression model is written as:

$$y_i = a + b_1 x_1 + b_2 x_2 + \ldots + b_k x_k + \varepsilon$$

where, ε is an error term which represents the variance in y_i unexplained by the model. The linear fit is obtained by selecting *a*, b_i so as to minimize the sum of squares between the model predictions and the data for y_i. Often the relationships between input and output variables are nonlinear. In this case it is often possible to use some data transformation to linearize the relationship. A commonly used transformation for exponential nonlinearities is the logarithm transform. Therefore, an exponential relationship such as:

$$y_i = a \times x_1^{b_1} \times x_2^{b_2} \ldots \times x_k^{b_k}$$

is transformed to:

$$\ln(y_i) = \ln(a) + b_1 \ln(x_1) + \ldots + b_k \ln(x_k)$$

which has a linear relationship.

Common statistical tests are used to determine the adequacy of the regression model. The most common measure is the coefficient of multiple correlation (R^2) which is a ratio of the variation explained by the regression to the total variation in y_i. Values of R^2 near 1 represent good fits. R^2 however is not a sufficient measure of the goodness of fit of a model. The *t*-statistic is used to test if the partial regression coefficients *a*, b_i are significantly different from zero. Moreover, an *F*-statistic can be used to check if any of the partial correlation coefficients are different from zero. This statistic provides an idea of the lack of fit of a regression model as a whole. However, for large R^2 values this test is not informative. Standard error of a regression model provides an estimate of the variance in the residual errors for y_i. This can be used to compare across regression models (in terms of functional forms) and to conduct the Kolmogorov-Smirnov test to evaluate if the errors ε are normally distributed. The normality assumption underlies most of the statistical tests used. Most statistical packages provide utilities for regression analysis and the statistical tests outlined in this section. The regression analysis for this work was done using *Splus* on the Andrew network (Becker, et al., 1988).

9.3.2.3. Analysis & Results

In the following sections we present the sensitivity analysis conducted with the FGDCOST model and provide response surface algorithms for capital costs and O&M costs based on results from FGD cost. A set of input variables is chosen and Latin hypercube sampling is used to generate a sample of 100 values for each variable using a uniform distribution for the given range. A Fortran77 package was used to generate the samples (Iman 81a). These samples are then imported into the sensitivity analysis module in FGDCOST and the model exercised to generate corresponding output values for capital and O&M costs. The data set consisting of the input samples and the corresponding output samples is used for response surface generation. PRCC, a Fortran77 package, is used to compute the partial rank correlation coefficients between the input and output variables. Note that linear relations are monotonic, hence a rank transformation does not

affect the order of importance of the input variables. Using these coefficients the relevant variables for regression modeling are gleaned. *Splus* is used to generate regression models for capital and O&M costs.

9.4. FGD Capital Cost Models

In this section we present the response surface models for capital cost derived from applying the method outlined in the previous section to FGDCOST. The results are very robust and provide excellent reduced form models for capital costs parameterized on a few operating parameters (no more than four to five). The accuracy is within 5% of FGDCOST, which is well within the 20% uncertainty associated with FGDCOST. The standard error of the regression models are explicitly included in the IECM as an additional uncertainty in the costs (they are usually very small, about 1%).

In the following subsection we present the capital cost models by process areas for each of the four technologies outlined in the introduction. The format used for presenting the results is as follows. For each technology, the results of the PRCC analysis are presented in tabular form. Based on the results of this analysis, the most important variables for explaining the variation in the capital costs are identified. Usually the first four or five variables are chosen. Subsequently, regression models for each process area parameterized on these few important variables are presented.

Usually, the main variables which effect the process capital costs are flue gas flow rate (Kacfm), SO_2 the inlet SO_2 concentration in flue gas (ppm), L/G ratio (gpm/Kacfm), and stoichiometry. The capital costs are calculated in millions of dollars It is known from prior engineering experience that the relation between the capital costs and the input variables is exponential, hence we use logarithmic transformations on the variables and conduct a linear regression of the transformed variables. The general form of the regression model is the same for all process areas and is presented below.

$$\log(C_i) = a_i + b_i \times \log(\text{gas}) + c_i \times \log(SO_2)$$

$$+ d_i \times \log(L/G) + e_i \times \log(\phi)$$

$$i \in (10, 20, 30, 60, 70, 80)$$

where C_i is the process facilities cost of each area (denoted by the numbers 10,20,30,60,70,80) in millions of 1990 dollars. The coefficients and the significance of explanatory variables differ by process area. In the following sections we present the coefficients for each of the process areas based on a regression analysis using *Splus*.

9.4.1. Wet Limestone with Forced Oxidation

A PRCC analysis of the data set for LSFO was performed. Based on this analysis the input variables are ranked in order of importance in Table 9-13.

Table 9-13. PRCC Analysis for Limestone Forced Oxidation

		Process Capital	
Variables	**Range**	**PRCC**	**Rank**
flue gas(Kacfm) (MW equivalent)	625-3350 (300-1000)	-0.992	1
L/G(gal/Kacfm)	90-130	0.336	4
SO_2(inlet SO_2 ppm)	0.5-5.0	0.806	3
stoichiometry	1.01-1.15	0.856	2
labor rate($/hr)	15-25	0.018	10
reagent cost($/ton)	10-20	-0.066	7
solid disposal	5-10	-0.161	5
power cost(mills/kwh)	40-60	-0.03	9
steam cost($/Klbs)	3-4	0.10	6
water ($/Klbs)	0.5-0.75	-0.059	8

Now we present the development of regression models using the variables identified from the PRCC analysis. The main variables that affect the process capital costs are flue gas flow rate (Kacfm), SO_2 the inlet SO_2 concentration in flue gas (ppm), L/G ratio (gpm/Kacfm), and stoichiometry (ϕ). The capital costs are expressed in millions of dollars (1990 M$) for all process areas. The coefficients for the regression model are provided in Table 9-14. Recall that the models estimates $\log(C_i)$. Figure 9-11 graphs the sensitivity of the cost models for different coals and sizes. The y-axis plot the normalized cost ($/kW) as a function of size (MW gross) for different coals.

Table 9-14. Regression Coefficients for LSFO

Wet Limestone with Forced Oxidation						
Variables	**Area 10**	**Area 20**	**Area 30**	**Area 60**	**Area 70**	**Area 80**
intercept (a_i)	5.532139	5.199094	4.967549	3.728971	5.29923	5.118347
log(gas) - b_i	0.2047287	0.5526016	0.5968993	0.3751297	0.0963776	0.2987416
log(SO_2) - c_i	0.1998244	0.0171820	-	0.3600074	-	-0.0070039
log(L/G) - d_i	0.064419	0.1531021	-	0.0984928	0.01744453	-
log(ϕ) - e_i	0.297487	-	-	0.2896275	0.0639004	-0.4110633
R2	0.96	0.998	0.997	0.96	0.97	0.999

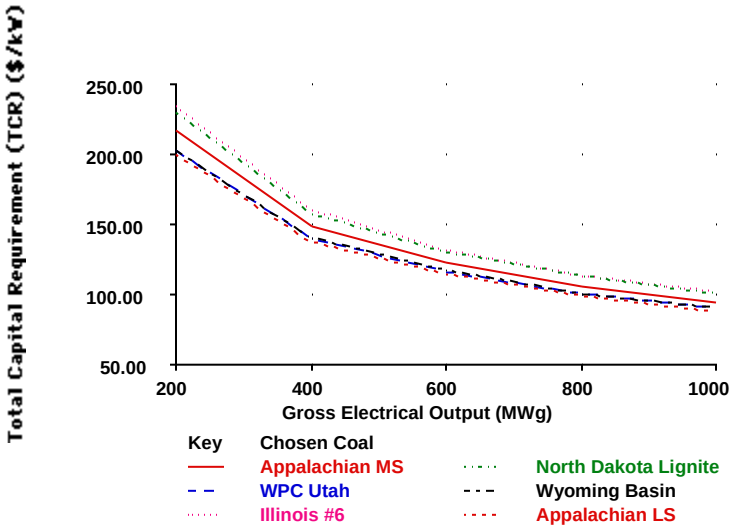

Figure 9-11. IECM cost model for LSFO with $\phi = 1.03$

9.4.2. Wet Limestone with Additives

The PRCC analysis for the LS/DBA system was performed. Based on this analysis the input variables are rank ordered in terms of the magnitude of their influence on the costs in Table 9-15:

Table 9-15. PRCC analysis for Wet Limestone with Dibasic Acid

		Capital Costs	
Variables	**Range**	**PRCC**	**Rank**
Flue gas(Kacfm) Size (MW)	625-3350 (300-1000)	-0.991	1
L/G(gpm/Kacfm)	50-90	0.293	4
%S(weight)	0.5-5.0	0.803	3

Stoichiometry	1.01-1.15	0.852	2
labor rate($/hr)	15-25	0.071	9
reagent cost($/ton)	10-20	-0.031	11
solid disposal	5-10	-0.173	6
power cost(mills/kwh)	40-60	0.056	10
steam cost($/Klbs)	3-4	0.192	5
water fresh($/Klbs)	0.5-0.75	-0.073	8
DBA ppm	1-2K	0	12
DBA feed (lbs/ton of SO_2)	15-25	-0.147	7
DBA cost($/ton)	300-400	0	12

Now we present the development of regression models using the variables identified by the PRCC analysis. The regression analysis is parallel to the one presented for LSFO with a data set that is different, i.e. generated using a cost model for LS/DBA. The main variables which affect the process capital costs (expressed in 1990 M$) are flue gas flow rate (Kacfm), SO_2 in inlet flue gas, L/G ratio (gpm/Kacfm), and stoichiometry (ϕ). Note that the range of L/G for LS/DBA is between 60-90. Once again using logarithmic transformations, linear regressions are used for each process area. We provide highlights for each process area in Table 9-16. Figure 9-12 graphs the sensitivity of the normalized cost ($/kW) for different coals and sizes (MW gross).

Table 9-16. Regression Coefficients for Wet Limestone with DBA

Wet Limestone with DBA						
Model Parameter	**Area 10**	**Area 20**	**Area 30**	**Area 60**	**Area 70**	**Area 80**
intercept (a_i)	5.656823	5.283843	4.967474	3.914778	5.33193	5.118347
log(gas) - b_i	0.2116698	0.5487767	0.5969214	0.3830471	0.0932564	0.2987416
log(SO_2) - c_i	0.1965567	0.0182601	-	0.3528121	0.0033284	-0.0070039
log(L/G) - d_i	-	0.1124185	-	-	-	-
log(ϕ) - e_i	0.3971839	-	-	0.6173974	0.0825347	-0.4110633
R2	0.96	0.998	0.997	0.95	0.98	0.999

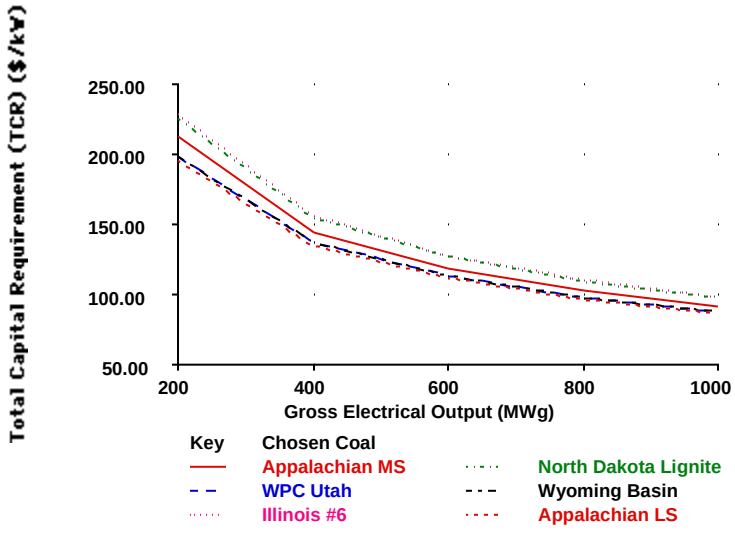

Figure 9-12. IECM cost model for Wet Limestone FGD with 1500 ppm of DBA as additive

9.4.3. Magnesium-Enhanced Lime System

A PRCC analysis of the data set for Mg-Lime system was performed. Based on this analysis the input variables are ranked in order of importance in Table 9-17.

Table 9-17. PRCC Analysis for Mg-Lime

		Process Capital	
Variables	**Range**	**PRCC**	**Rank**
flue gas(Kacfm) (MW equivalent)	625-3350 (300-1000)	-0.986	1
L/G(gal/Kacfm)	30-56	0.149	4
SO_2(inlet SO_2 ppm)	0.5-5.0	0.890	2
Stoichiometry	1.01-1.15	0.801	3
labor rate($/hr)	15-25	0.13	6
reagent cost($/ton)	50-60	-0.069	8
solid disposal	5-10	-0.133	5
power cost(mills/kwh)	40-60	-0.051	10
steam cost($/Klbs)	3-4	0.064	9
water ($/Klbs)	0.5-0.75	-0.097	7

Now we present the development of regression models using the variables identified from the PRCC analysis. The main variables which affect the process capital costs are flue gas flow rate (Kacfm), SO_2 the inlet SO_2 concentration in flue gas (ppm), L/G ratio (gpm/Kacfm), and stoichiometry. The highlights are presented in Table 9-18. Figure 9-13 graphs the sensitivity of the normalized cost ($/kW) for different coals and sizes (MW gross).

Table 9-18. Regression Coefficients for Process Facilities Capital Cost

Wet Limestone with Mg-Lime						
	Area 10	**Area 20**	**Area 30**	**Area 60**	**Area 70**	**Area 80**
intercept (a_i)	4.18205	5.343637	4.985706	3.805031	5.406733	5.118347
log(gas) - b_i	0.4287465	0.5571364	0.5965417	0.4408358	0.0859990	0.2987416
log(SO_2) - c_i	0.3973585	-0.0031376	-0.0057330	0.4067988	-0.0042571	-0.0070039
log(L/G) - d_i	-	0.0865696	-	-	-	-
log(ϕ) - e_i	-	-	-	-	0.0711735	-0.4110633
R2	0.96	0.999	0.999	0.97	0.98	0.999

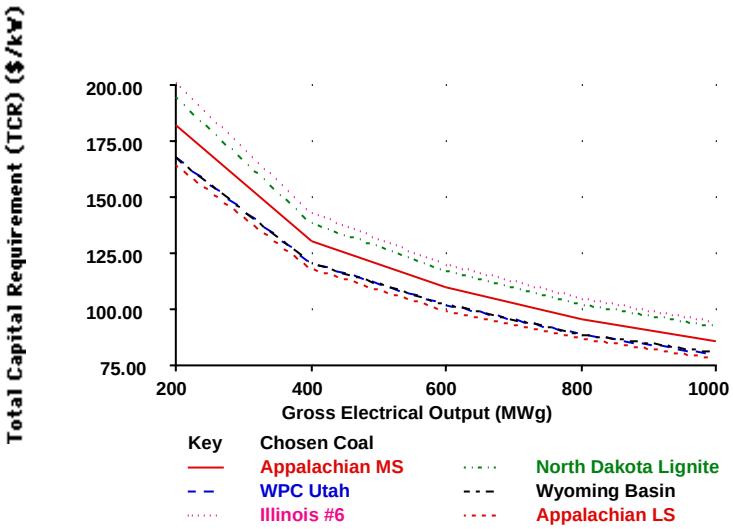

Figure 9-13. IECM cost model for Mg-enhanced Lime FGD with ϕ = 1.02

9.4.4. Lime Spray Dryer

A PRCC analysis of the data set for the Lime Spray Dryer was performed. Based on this analysis the input variables are ranked in order of importance in the table below. Note however, that some of the key operating parameters are different for the Lime Spray Dryer. The water entering with the slurry spray vaporizes and the flue gas (along with the fly ash) carries the dried reaction products. These particles are then removed in the baghouse (downstream of the FGD) and a portion of the collected solids is recycled back to the absorber. The amount of recycle (lb of dry solids recycled/lb of lime added) is based on the sulfur content of the flue gas. The total slurry that is recycled to the absorber (gpm) depends on the recycle ratio (rr), stoichiometric ratio (ϕ) and the flue gas flow rate (gas). In order to determine the gpm we need to solve the process flowsheet of the LSD iteratively. In order to avoid this computational burden for the IECM we have developed a regression equation for the slurry flow rate as a function the recycle ratio, stoichiometry and the flue gas flow rate as shown below.

$$\log(\text{gpm}) = -0.9312959 + 0.9959784 \times \log(\text{gas}) - 0.03043575 \times \log(\text{rr}) + 0.09146684 \times \log(\phi)$$

with R^2=0.994. The operating parameter gpm is used in the PRCC analysis (Table 9-19) and the regression analysis (instead of the equivalent L/G used for other technologies). The coefficients of the regression analysis are in Table 9-20.

Table 9-19. PRCC Analysis for Lime Spray Dryer

		Process Capital	
Variables	**Range**	**PRCC**	**Rank**
flue gas (Kacfm) (MW equivalent)	625-3350 (300-1000)	-0.602	2
Stoichiometry(ϕ)	1.1-1.8	0.325	3
SO_2(inlet SO_2 ppm)	500-3500	0.827	1
gpm	70-400	0.151	5
labor rate($/hr)	15-25	0.061	9
reagent cost($/ton)	50-60	0.121	6
solid disposal	5-10	0.043	10
power cost(mills/kwh)	40-60	-0.165	4

steam cost($/Klbs)	3-4	0.084	8
water ($/Klbs)	0.5-0.75	0.106	7

Now we present the development of regression models using the variables identified from the PRCC analysis. The main variables which effect the process capital costs are flue gas flow rate (Kacfm), SO_2 the inlet SO_2 concentration in flue gas (ppm), L/G ratio (gpm/Kacfm), and stoichiometry. The highlights are presented in Table 9-20. Figure 9-14 graphs the sensitivity of the normalized cost ($/kW) for the lime spray dryer for different sizes (MW gross) and coals.

Table 9-20. Regression Coefficients for Lime Spray Dryer

Lime Spray Dryer						
Model Parameters	**Area 10**	**Area 20**	**Area 30**	**Area 60**	**Area 70**	**Area 80**
intercept (a_i)	-1.187585	-1.391273	-1.154033	-1.742325	-0.3249075	-0.9106584
log(gas) - b_i	-0.3133721	0.8549951	0.6044183	-	-	0.300299
log(SO_2) - c_i	0.386108	-	-	0.4840697	-0.0089210	-0.0052555
gpm - d_i	0.7677725	-0.0009575	-	0.00161753	0.00016397	-
log(ϕ) - e_i	0.3871053	-	-	-	-0.0177219	-
R2	0.97	0.97	0.998	0.95	0.98	0.9999

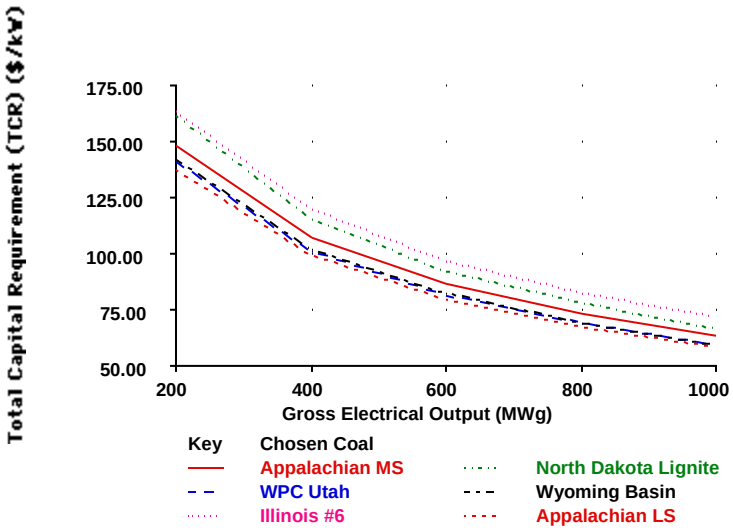

Figure 9-14. IECM cost model for Lime Spray Dryer for $\phi = 1.1$

9.4.5. Sparing Philosophy

The models developed in the previous subsections are based on the assumption of two operating absorber towers (each rated at 50% of the plant capacity, with a maximum of 650MW) and one spare absorber tower. With the recent development of advanced absorber towers of near 100% reliability it is possible to eliminate the spare tower and reduce capital costs significantly (no significant changes in variable costs). Another approach to reducing capital cost exploits the economy of scale by using single absorber towers of large capacity. In this subsection we develop scaling factors to estimate the reduction in capital costs for different FGD systems by changing the sparing philosophy. Note that in all the factors developed below, the scaling factors are derived by a regression of the capital cost of various sparing philosophies against the capital cost of the default system, i.e. an FGD with two operating towers and one spare absorber.

In order to estimate the reduction in capital costs from eliminating the spare tower, we set the number of spare towers in FGDCOST to zero and exercise the model for various values of input for the relevant variables such as flue gas flow rate

(*gas*), SO_2 in flue gas, L/G, and stoichiometry (ϕ). The capital costs for system with no spares (C') is then regressed against the capital cost for the system with one spare tower (C) and correlation coefficient (s_i) of this regression provides us with the scaling factor we desire:

$$C_i^{/} = s_i \times C_i,\ i \in (20, 30)$$

where C_i is the process area (denoted by 20, 30) cost. The capital cost of the SO_2 removal system (includes absorber towers) and the flue gas system (includes piping to absorber towers) is affected by the sparing philosophy. We present results for those process areas whose capital cost is affected in Table 9-21. The columns under "Zero Sparing" characterize the reduction in capital cost by dropping the spare absorber. The columns under "One Absorber" characterize the reduction in capital cost by reducing the number of absorbers from two (rated @50% each) to one (rated @100% of capacity).

Table 9-21. Regression Coefficients for Different Sparing Philosophies

System	Zero Sparing		One Absorber	
	Area 20	Area 30	Area 20	Area 30
LSFO	0.7306793	0.943658	0.5818281	0.9449641
LSFO with DBA	0.7213572	0.9436423	0.5692575	0.9316498
Mg-Lime	0.6926448	0.9437713	0.525391	0.9316498
Lime Spray Dryer	0.7114379	0.8002883	0.5126236	0.64543523

9.5. Fixed O&M Costs

The O&M costs for FGD consists of fixed costs and variable costs. The fixed operating cost consists of labor, maintenance labor, material, and administrative labor. A mathematical model for the fixed cost is provided below.

$$FOM = FOM_{labor} + FOM_{maint} + FOM_{admin}$$

$$FOM_{labor} = labor \times N_{labor} \times 40\ (hrs/week) \times 52\ (weeks/yr)$$

$$FOM_{maint} = \sum_i \left(f_{maint}\right)_i \times TPC_i \text{ where i = process area}$$

$$FOM_{admin} = f_{admin} \times (FOM_{labor} + f_{maintlab} \times FOM_{maint})$$

where

FOM = fixed operating and maintenance cost, M$/yr

FOM_{labor} = operating labor, M$/yr

FOM_{maint} = maintenance material costs, M$/yr, (coefficients based on EPRI TAG, the fraction $f_{maintlab}$ of these costs are allocated to maintenance labor and rest to maintenance material).

FOM_{admin} = administrative costs, M$/yr (calculated as the fraction f_{2admin} of total labor costs)

TPC_i = total process capital for each process area, (10,20,30,40, 50,60)

N = total number of laborers (per week)

labor = labor rate ($/hr)

Figure 9-15 provides the levelized fixed costs (mills/kWh) as a function of size (MW gross) for different coals for wet limestone FGD systems. Similar sensitivity analysis can be conducted for other technologies.

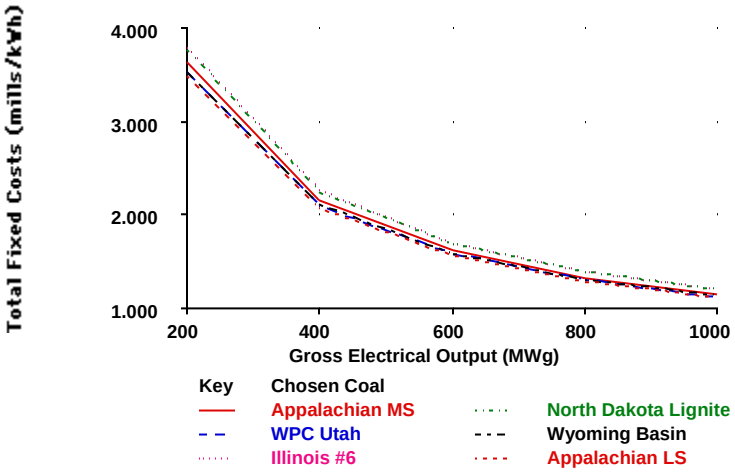

Figure 9-15. Fixed costs for all Wet Limestone FGD systems for 90% SO_2 removal, and default stoichiometry ϕ =1.03

9.6. Variable O&M Costs

Variable operating costs include consumables such as reagents, additives, water, power, steam for reheat and the continuous costs related to solid disposal. The variable operating costs can be usually calculated directly based on engineering principles. In this section we outline the formulations based on basic engineering principles for the calculation of variables costs. We then characterize the parameters that are specific to the different FGD technologies. The total variable cost (in M$) is given as:

$$\text{varcost} = \text{rcost} + \text{scost} + \text{dbacost} + \text{pcost} + \text{stcost} + \text{wcost}$$

where,

rcost	=	reagent consumption, M$/yr
scost	=	solid disposal cost, M$/yr
dbacost	=	cost of dibasic acid feed, M$/yr
pcost	=	power consumption, M$/yr
stcost	=	steam consumption, M$/yr
wcost	=	makeup water cost, M$/yr

9.6.1. Reagent Cost

The total amount of reagent usage cost (rcost, M$/yr) depends on the total amount of reagent used and the cost of the reagent (reag, $/ton). The amount of reagent used (M_{reag} tons/yr) depends on the reactive species in flue gas (gas_i lbmole/yr), sulfur removal efficiency (η_{SO2}), the plant capacity factor, and the stochiometric ratio (ϕ). Therefore, the model to calculate the total cost of reagent (rcost) used is:

$$\text{rcost} = \text{reag} \times \text{M}_{\text{reag}}$$

$$\text{M}_{\text{reag}} = \frac{1}{2000}\left(\sum_i (\eta_i \times \phi_i \times \text{gas}_i \times \text{r}_i) \times \text{MW}_{\text{CaCO}_3} \times \text{cf} \times 8766\right) / \text{R}_{\text{purity}}$$

where

i	$\in$	(SO_2, SO_3, HCl)
r_i	=	moles of reagent required per mole of species, I

r_i $\in$ (1, 1, ½)

MW_{CaCO_3} = molecular weight of $CaCO_3$

R_{purity} = reagent purity (weight fraction of $CaCO_3$)

9.6.2. Solid Waste Disposal Costs

The solid waste disposal cost (scost, M$/yr) depends on the amount of solid waste and the unit cost of disposal (disposal, in $/ton). The amount of solid waste produced depends on the amount of reactive species scrubbed from the flue gas ($M_{disposal}$ tons/yr), the total amount of inerts in the slurry (M_{inerts}, tons/yr) and the amount of unused reagent in the slurry ($M_{unused\ reagent}$, tons/yr). Therefore, the model to calculate the total cost of waste disposal (scost) is:

$$s_{cost} = disposal \times \left(M_{disposal} + M_{inerts} + M_{unused\ reag}\right)$$

$$M_{disposal} = \frac{1}{2000} \times \sum_i \left(\eta_i \times \phi_i \times gas_i \times r_i\right) \times MW_i \times cf \times 8766$$

$$M_{inerts} = \frac{M_{reag}}{2000} \times \left(1 - R_{purity}\right) \times cf \times 8766$$

$$M_{unused\ reag} = \frac{1}{2000} \times \sum_{-} \frac{\left(\eta_i \times gas_i \times r_i \times (\phi_i - 1)\right) \times M_{CaCO_3}}{R_{purity}} \times cf \times 8766$$

where,

i $\in$ (SO_2, SO_3, HCl)

r_i = moles of reagent required per mole of species

r_i $\in$ (1, 1, ½)

$$MW_i = \begin{cases} \left(MW_{CaSO_4 \bullet 2H_2O}, MW_{CaSO_4 \bullet 2H_2O}, MW_{CaCl_2}\right) \text{Limestone System} \\ \left(MW_{CaSO_3 \bullet 5H_2O}, MW_{CaSO_3 \bullet 5H_2O}, MW_{CaCl_2}\right) \text{Lime System} \end{cases}$$

9.6.3. Power Costs

The power costs (pcost, M$/yr) depends on the unit cost of power (power, $/MWh), and power consumption in the reagent handling (P_{20}, MW) and flue gas handling systems (P_{30}, MW). Slurry is injected into the absorber towers at four levels to remove SO_2 and a pump serves each level. The power consumption for these pumps is proportional to the amount of slurry being pumped (Q, gallons/hr) and the total dynamic head required. Similarly, the power consumption for the I.D. fans to overcome the flow resistance (or equivalent pressure drop) of the absorber towers and ducts to the chimney is proportional to the total flue gas flow rate and the pressure drop. The total power consumption (P_{total}, MW) is given by:

$$p\cos t = power \times P_{total} \times cf \times 8766$$

$$P_{total} = P_{20} + P_{30}$$

$$P_{20} = \rho \times Q \times H / \eta_{pump}$$

$$P_{30} = 0.12 \times 10^{-6} \times gas \times \Delta p / \eta_{fan}$$

where,

ρ = density of slurry (lb/gallon)

H	=	total dynamic head (ft)
gas	=	flue gas flow rate (acfm)
Δp	=	total pressure drop (inches of water)
Q	=	flow rate (gallons/hr = L/G x gas x 60 or gpm x 60)
η_{fans}	=	fan efficiency (fraction)
η_{fans}	=	pumping efficiency (fraction)

The power consumption due to I.D. fans (P_{30}) is easily calculated by assuming an efficiency for the centrifugal fans (usually 60-70%). The constant factor ($0.12x10^6$) is a conversion factor which provides power required in MW. The total dynamic head (H) and slurry density (ρ) are not easily available in the specification of FGD systems. In order to minimize the data requirements of the model we have developed a regression model which provides a proportionality constant for the slurry pumps by aggregating the head and density as a fraction of the slurry flow rate as follows:

$$P_{30} = k_t \times Q + c, \quad t \in (\text{LSFO, LS/DBA, Mg - Lime, LSD})$$

The units for k_t are in lb-ft/gallons and value reported in the table below includes the conversion factor for changing to MW. The constant c is in MW. The regression coefficients for the different technologies is provided in Table 9-22.

Table 9-22. Regression Coefficients for Power

Technology	LSFO	LS/DBA	Mg-Lime	LSD
k_t	3.6165x10-5	3.8234x10-5	3.2456x10-5	9.99x10-5
c	-	-	0.21	-
R2	0.99	0.98	0.99	0.9

9.6.4. Steam Costs

The saturated gas exiting the absorbers at approximately 127°F is reheated to 152°F using steam heat. The steam cost (stcost, M$/yr) of reheating depends on the cost of electricity, heat rate, and the energy required (E_{reqd}, Btu/hr) to reheat the flue gas. The energy required is calculated as the change in enthalpy of the flue gas (ΔH_{127}^{152}) and the heat of vaporization for the water removed (?H_{vapor}). IECM calculates all the necessary thermodynamic relationships and properties.

$$E_{reqd} = \Delta H_{127}^{152} + \Delta H_{vapor}$$

The cost of reheating is calculated by estimating the cost of the equivalent electricity that could have been generated if the steam had not been used for reheating:

$$\text{stcost} = E_{reqd}/\text{hr} \times \text{power} \times \text{cf} \times 8766$$

where *hr* is the steam cycle heat rate (Btu/kWh) and *power* is the cost of electricity ($/kWh).

9.6.5. DBA Costs

For systems that use organic acid additives (LS/DBA), the cost of replacing DBA which degrades on a yearly basis (dbacost, M$/yr) depends on the replacement cost of Dibasic Acid (C_{DBA}, $/ton), and the amount of DBA degradation (F_{DBA}, tons/yr), which depends on the amount of SO_2 removed (M_{SO2}, tons/yr) and the degradation of DBA per ton of SO_2 removed (D_{DBA}, lb of DBA/ton of SO_2 removed). This is characterized as follows:

$$\text{dbacost} = C_{DBA} \times F_{DBA}$$

$$M_{SO_2} = \frac{1}{2000} \times (\eta_{SO_2} \times \text{gas}_{SO_2} \times M_{SO_2}) \times \text{cf} \times 8766$$

$$F_{DBA} = \frac{1}{2000} \times D_{DBA} \times T_{SO_2} \times \text{cf} \times 8766$$

9.6.6. Water Costs

Water from the scrubbing slurry is lost due to evaporation in the scrubber. The water costs pertain to the supply needed to replenish this loss. The water cost (wcost, M$/yr) depends on the cost of fresh water (waterf, $/Kgallons), and the total amount of water used (Wtotal, Kgallons). The water costs are characterized as:

$$\text{wcost} = \text{waterf}/1000 \times W_{total}$$

$$W_{total} = W_{MW} \times 60 \times MW_{gross} \times \text{hoursannua l}$$

where W_{MW} is the water consumed (gallons/min) per MW gross. This consumption differs for different technologies. Nominal values used for model development are shown in Table 9-23.

Table 9-23. Water Consumption for FGD Systems

Technology	LSFO	LS/DBA	Mg-Lime	LSD
W_{MW} (gpm/MW)	0.098	0.098	1.08	-

Figure 9-16 graphs the total levelized variable O&M costs (mills/kWh) as a function of size (MW gross) and coal type for Wet Limestone FGD. Similar analysis can be conducted for different technologies.

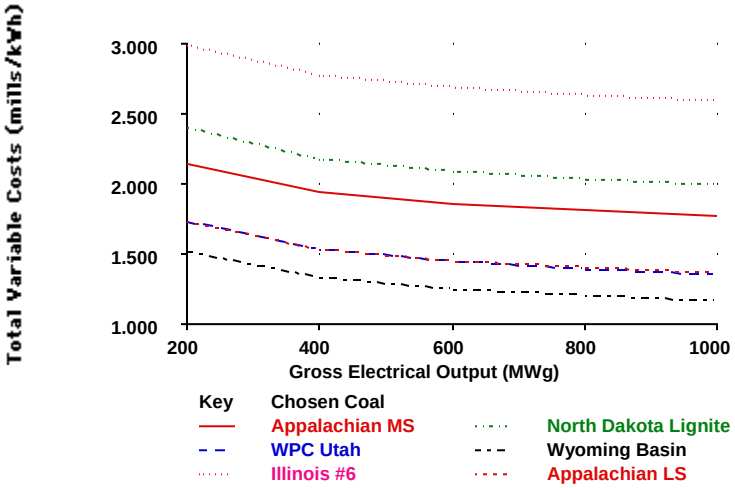

Figure 9-16. Variable costs for all Wet Limestone FGD systems for 90% SO_2 removal, and default stoichiometry $\phi = 1.03$

9.7. A Numerical Example

In this section we provide an illustrative example which uses the models developed above to calculate the capital and O&M costs for a given set of inputs. We compute costs for the limestone forced oxidation (LSFO) FGD system. A plant of gross capacity of 330 MW (300 net) which uses a medium sulfur Appalachian coal (2.13% sulfur and 0.07% chlorine) and operates at 65% capacity factor, yielding 5698 hours/yr of operation. We design the FGD system for a SO_2 removal efficiency of 95% with a stochiometric ratio of 1.03. The base case assumes 2 absorber towers and 1 spare tower. We use Equation (9-8) to evaluate the L/G ratio as shown.

$$0.95 = 1 - \exp\left\{\begin{array}{l} -(0.725 + 0.0175 \times L/G + (10.0 \times 1.03 - 10.3) \\ -2.5 \times 10^{-4}(1260 - 2000) + 5.14 \times 10^{-6}(27900 - 25000)) \end{array}\right\}$$

$$\Rightarrow L/G = 120 \text{ gpm/Kacfm}$$

The operating parameters of the power plant are calculated using IECM and are provided in Table 9-24.

Table 9-24. IECM Operating Parameter Values

Operating parameters	Variable name	Value
flue gas flow rate, Kacfm	Gas	1064 Kacfm
SO_2 inlet concentration, SO_2, ppm	SO_2	1260 ppm
Chloride conc. in slurry stream, Cl, ppm	Cl	27900 ppm
L/G ratio, gpm/Kacfm	L/G	120 gpm/Kacfm

9.7.1. Capital Cost

The calculation of process facilities capital is based on the regression coefficients in Table 9-19. The template for such calculations is provided in Table 9-25.

Table 9-25. Example Calculation of Process Capital Costs (1990 $)

Wet Limestone with Forced Oxidation						
Variables	**Area 10**	**Area 20**	**Area 30**	**Area 60**	**Area 70**	**Area 80**
(a_i)	5.532139	5.199094	4.967549	3.728971	5.29923	5.11835
b_i x log(gas)	0.6197	1.673	1.807	1.136	0.2918	0.9043
c_i x log(SO_2)	0.6185	0.05318	-	1.114	-	-0.0217
d_i x log(L/G)	0.134	0.3184	-	0.2048	0.03627	-
e_i x log(ϕ)	3.819m	-	-	3.718m	820.3u	-5.277m
sum(variables)	6.908	7.243	6.774	6.187	5.628	5.996
C_i (M$)	8.094	17.52	5.949	1.54	0.425	0.99

The total process facilities cost is the sum over all process areas.

$$PFC = \sum_i C_i = 34.52 \text{ M\$ (1990)}$$

$$= 34.86 \text{ M\$ (1993)}$$

The IECM uses chemical engineering cost indices to provide the cost indexed by other years. The typical default year that is used in IECM is 1993, hence we scale the costs to this year and conduct all subsequent calculations in 1993 dollars. Note that a cost index of 1.01 has been used to provide all numbers in 1993 dollars. The indirect costs are calculated as fractions of the process capital based on Table 9-9 and Table 9-10. The calculations based on this are shown in Table 9-26.

Table 9-26. Capital Cost Summary (1993 $)

Capital Investment	M$	$/kW
Process Facilities Capital $\sum_i C_i$	34.86	116.6
General Facilities (10%)	3.486	11.66
Eng. & Home Office Fees(10%)	3.486	11.66
Project Contingency (15%)	5.229	17.49
Process Contingency (2%)	0.6972	2.333
Total Plant Cost	47.76	159.8
Total Cash Expended (Adjust Factor=1)	47.76	159.8
AFDUC (Adjust Factor=0.0548)	1.156	3.867
Total Plant Investment (TPI)	48.91	163.7
Royalty Allowance (0.5%)	0.1743	0.5831
Preproduction costs	1.621	5.416
Inventory Capital	0.1647	0.5509
Total Capital Requirement	50.87	169.9

9.7.2. Fixed O&M Costs

The calculations for fixed operating costs are provided using the following default values for model parameters:

N = 32 (total number of laborers, per week)

labor = 21.87 $/hr (labor rate)

f_{maint} = (0.04,0.06,0.02,0.04,0.015,0.015)

f_{admin} = 30%

$f_{maintlab}$ = 40%

$$\begin{aligned} FOM_{labor} &= 21.87 \times 32 \times 40\ (\text{hrs/week}) \times 52\ (\text{weeks/yr}) \\ &= 1.44\ \text{M\$/yr} \\ FOM_{maint} &= 0.04 \times TPC_{10} + 0.06 \times TPC_{20} + 0.02 \times TPC_{30} \\ &\quad + 0.04 \times TPC_{60} + 0.015 \times TPC_{70} + 0.015 \times TPC_{80} \end{aligned}$$

Th $= 2.182$ M$/yr

$$\begin{aligned} FOM_{admin} &= 0.3 \times (FOM_{labor} + 0.4 \times FOM_{maint}) \\ &= 0.694\ \text{M\$/yr} \\ FOM &= FOM_{labor} + FOM_{maint} + FOM_{admin} \\ &= 4.32\ \text{M\$/yr}\ (14.42\ \text{\$/kW - yr}) \end{aligned}$$

9.7.3. Variable O&M Costs

The calculations for variable operating costs are providing using the following default values for model parameters:

η = 95% (SO_2 removal efficiency)

ϕ = 1.03 (reagent stoichiometry)

gas_{SO2} = 140.8 (lb moles/hr, IECM calculation)

gas_{SO3} = 1.63 (lb moles/hr, IECM calculation)

gas_{HCl} = 8.67 (lb moles/hr, IECM calculation)

ΔH_{127}^{152} = 19.7 MBtu/hr (IECM calculation)

ΔH_{vapor} = 1.24 MBtu/hr (IECM calculation)

reag = 15 $/ton (reagent cost)

cf = 65% (capacity factor)

R_{purity} = 94% (reagent purity, wt. fraction)

MW_{CaCO_3} = 100 (molecular weight)

$MW_{CaSO_4 \bullet 2H_2O}$ =172 (molecular weight)

MW_{CaCl_2} = 112 (molecular weight)

9.7.3.1. Reagent Cost

This calculation is

$$T_{reag} = \frac{1}{2000}\left(\sum_i \begin{Bmatrix} (0.95\times 1.03\times 140.8\,(SO_2)\times 1) + \\ (0.95\times 1.0\times 1.63\,(SO_3)\times 1) + \\ (0.95\times 1.0\times 8.67\,(HCl)\times 0.5) \end{Bmatrix} \times 100\times 5698\right) / 0.94$$

$$= 44.26K$$

$$rcost = 15.15\times T_{reag} = 0.671\ M\$$$

9.7.3.2. Solid Waste Disposal Costs

This calculation is:

$$M_{disposal} = \frac{1}{2000}\times\left(\sum_i \begin{Bmatrix} (0.9\times 1.03\times 140.8\,(SO_2)\times 1\times 172) + \\ (0.9\times 1.0\times 1.63\,(SO_3)\times 1\times 172) + \\ (0.9\times 1.0\times 8.67\,(HCl)\times 0.5\times 112) \end{Bmatrix} \times 5698\right)$$

$$= 69.63K\ (tons/yr)$$

$$M_{inerts} = 44.26K\times(1-0.94)/2000$$

$$= 3.365K\ (tons/yr)$$

$$M_{unused\ reagent} = \frac{1}{2000}\times\left(\sum_i \begin{Bmatrix} (0.9\times(1.03-1)\times 140.8\,(SO_2)\times 1) + \\ (0.9\times(1.0-1.0)\times 1.63\,(SO_3)\times 1) + \\ (0.9\times(1.0-1.0)1.0\times 8.67\,(HCl)\times 0.5) \end{Bmatrix} \times 100\times 5698\right) / 0.94$$

$$= 1.238\ K\ (tons/yr)$$

$$scost = 8.15\times\left(M_{disposal} + M_{inerts} + M_{unused\ reagent}\right)$$

$$= 0.605\ M\$$$

9.7.3.3. Power Costs

This calculation is:

$$P_{20} = 3.62 \times 10^{-5} \times 120 \times 1064 + 0 = 3.34 \text{ MW}$$

$$P_{30} = 0.12 \times 10^{-6} \times 1064 \times 10/0.5 = 2.56 \text{ MW}$$

$$P_{total} = P_{20} + P_{30} = 5.73 \text{ MW}$$

$$\text{pcost} = 43.45 \times P_{total} \times 5698 = 1.78 \text{ M\$}$$

9.7.3.4. Steam Costs

This calculation is:

$$E_{reqd} = 19.7 \ (\Delta H_{127}^{152}, \text{MBtu/hr}) + 1.24 \ (\Delta H_{vapor}, \text{MBtu/hr})$$

$$= 20.94 \text{ (MBtu/hr)}$$

$$\text{stcost} = 20.94 \times 1\text{K}/7880 \times 43.45 \times 5698 = 0.665 \text{ M\$}$$

9.7.3.5. Water Costs

This calculation is:

$$W_{total} = 0.098 \times 330 \times 60 \times 5698 = 11.06 \text{ Kgallons/year}$$

$$\text{wcost} = 0.7 \text{ (\$/K gallons)} \times W_{total}$$

$$= 7721 \text{ \$/yr } (4.53 \times 10^{-3} \text{ mills/kWh})$$

9.7.3.6. Total Variable Operating Costs

The total variable costs (mills/kWh) are derived as the sum of the reagent, solid waste disposal, power and steam costs as follows:

$$\text{fixcost} = 4.32 \text{ M\$}$$

$$\text{varcost} = 0.671 + 0.605 + 1.78 + 0.665 + 0.0077 = 3.724 \text{ M\$}$$

$$\text{totalcost} = 8.04 \text{ M\$ } (4.735 \text{ mills/kWh})$$

9.7.4. Sparing Options

	Zero Sparing		One Absorber	
	Area 20	**Area 30**	**Area 20**	**Area 30**
LSFO	12.93 (17.69)	5.67 (6.01)	10.29 (17.69)	5.678 (6.01)

The numbers in (brackets) are capital costs for 2 towers and 1 spare (base case assumption) and are provided for comparison.

9.8. References

Agrawal, R. S., & Rochelle, G. T. (1993). Chemistry of Limestone Scrubbing. In SO_2 Control Symposium, Boston, MA.

Ang, A. H., & Tang, W. H. (1975). *Probability Concepts in Engineering Planning and Design*. New York: John Wiley & Sons.

Becker, R. A., Chambers, J. M., & Wilks, A. R. (1988). *The New S Language*. Pacific Grove, CA: Wadsworth & Brooks/Cole.

Benson, L. (1993). Wet Lime/Limestone Performance Modeling. In Radian Corp., Texas.

Benson, L., Hicks, R., & Johnson, H. (1991). Advanced Mg-Enhanced SO_2 and NO_x Control Pilot Plant. In SO_2 Control Symposium, Washington, DC.

Bhat, P. A., Johnson, D. W., & Jankura, B. J. (1993). Results of Babcock & Wilcox Limestone Wet FGD Pilot Program at EPRI's High Sulfur Test Center. In SO_2 Control Symposium. Boston, MA.

Blythe, G. M., Burke, J. M., Lewis, D. L., & Thompson, C. (1985). *Field Evaluation of Utility Spray Dryer* No. CS-3954). EPRI.

Blythe, G. M., Lepovitz, L. R., & Thompson, C. M. (1991). *Evaluation of a 2.5MW Spray Dryer/Fabric Filter SO_2 Removal System* No. GS-7449). EPRI.

Blythe, G. M., Phillips, J. L., & Slater, T. (1993). Results of High Efficiency SO_2 Removal Testing at the Southwestern Electric Power Company's Henry W. Pirkey Station. In SO_2 Control Symposium, Boston, MA.

Brown, B., & Felsvang, K. (1991). High SO_2 Removal Dry FGD Systems. In SO_2 Control Symposium, Washington, DC.

Chang, C.-S., & Rochelle, G. T. (1983). Mass Transfer Enhanced by Equilibrium Reactions. *Ind. Eng. Chem. Fund.*, **21**, 379-385.

Corbett, W. E., Hargrove, O. W., & Merrill, R. S. (1977). *A Summary of Effects of Important Chemical Variables upon the Performance of Lime/Limestone Wet Scrubbing Systems.* No. FP-639). Radian Corporation.

Dene, C. E., Boward, W. L., Noblett, J. G., & Keeth, R. J. (1991). Development of Advanced Retrofit FGD Designs. In SO_2 Control Symposium, Washington, DC.

Draper, N. R., & Smith, H. (1966). *Applied Regression Analysis*. New York: John Wiley & Sons.

Iman, R. L., Davenport, J. M., & Zeigler, D. K. (1980). *Latin Hypercube Sampling (A Program User's Guide).* No. SAND79-1473). Sandia National Laboratories.

Iman, R. L., Helton, J. C., & Campbell, J. E. (1981a). An Approach to Sensitivity Analysis of Computer Models: Part I - Introduction, Input Variable Selection and Preliminary Variable Assessment. *Journal of Quality Technology*, **13**(3), 174-183.

Iman, R. L., Helton, J. C., & Campbell, J. E. (1981b). An Approach to Sensitivity Analysis of Computer Models: Part II - Ranking of Input Variables, Response Surface Validation, Distribution Effect and Technique Synopsis. *Journal of Quality Technology*, **13**(4), 232-40.

Johnson, H. (1993). Advanced Mg-Enhanced Wet FGDs. In

Jozewicz, W., & Rochelle, G. T. (1984). Modeling of SO_2 Removal by Spray Dryers. In Pittsburgh Coal Technology Conference, Pittsburgh, PA.

Keeth, R. J., Baker, D. L., Tracy, P. E., Ogden, G. E., & Ireland, P. A. (1991). *Economic Evaluation of Flue Gas Desulfurization Systems* No. GS-7193, Research Project 1610-6.). EPRI, Palo Alto, CA.

Klingspor, J. (1993). Wet Limestone Modeling. In ABB Environmental Systems.

Laslow, D. (1993). Wet Lime/Limestone Performance Modeling. In General Electric, Connecticut.

Mehta, R. R., & Rochelle, G. T. (1983). Modeling of SO_2 Removal and Limestone Utilization in Slurry Scrubbing with Forced Oxidation. In AIChE National Meeting, Houston, TX.

Moser, R. E., & Owens, D. R. (1990). Overview on the Use of Additives in Wet FGD Systems. In SO_2 Control Symposium, New Orleans, LA.

Neter, J., Wasserman, W., & Kutner, M. H. (1983). *Applied Linear Regression*. Homewood, ILL: R.D. Irwin.

Noblett Jr., G. E., DeKraker, D. P., & Moser, R. E. (1990). FGDPRISM, EPRI's FGD Process Model -- Recent Applications. In SO_2 Control Symposium, New Orleans, LA.

Noblett Jr., G. E., Hebets, M. J., & Moser, R. E. (1990). EPRI's FGD Process Model (FGDPRISM). In 1990 SO_2 Control Symposium, Washington, DC.

Noblett Jr., J. (1993). Wet Lime/Limestone Performance Modeling. In Radian Corp., Texas.

Rader, P. (1993). Wet Limestone Modeling. In ABB Environmental Systems.

Rader, P. C., & Bakke, E. (1991). Incorporating Full-Scale Experience into Advanced Limestone Wet FGD Designs. In 1991 SO_2 Control Symposium, Washington, DC.

Rochelle, G. T. (1981). Appendix A: Chemistry of Limestone Scrubbing. In R. H. Borgwardt (Eds.), *Limestone FGD Scrubbers: Users Handbook* EPA.

Rochelle, G. T. (1981). Appendix B: Operational Factors of Limestone Scrubbing. In R. H. Borgwardt (Eds.), *Limestone FGD Scrubbers: Users Handbook* EPA.

Smolenski, J., Phillips, J. L., Epsenscheid, A. P., & Shires, T. M. (1993). High Efficiency SO_2 Removal Tests at Tampa Electric Company's Big Bend Unit 4. In SO_2 Control Symposium, Boston, MA.

Stevens, G. E., Horton, W. M., Hargrove, O. W., & Owens, D. R. (1993). Evaluation of High SO_2 Removal Efficiency Upgrade Options: EPRI High Sulfur Test Center. In SO_2 Control Symposium, Boston, MA.

Stevens, G. E., Sitkiewitz, S. S., Phillips, J. L., & Owens, D. R. (1991). Results of High SO_2 Removal Efficiency Tests at EPRI's High Sulfur Test Center. In SO_2 Control Symposium, Washington, DC.

Weilert, C. (1993). Wet Lime/Limestone Performance Modeling. In Burns and McDonnell, Missouri.

Weilert, C. V., & Ratliff, J. (1990). Development and Use of Site-Specific FGD System Performance and Economic Models. In SO_2 Control Symposium, New Orleans, LA: EPRI/EPA.

10. Carbon Injection

10.1. Background

In December 2000, EPA announced its intention to regulate mercury (Hg) emissions from coal-fired power plants under the air toxics provisions of the Clean Air Act Amendments (CAAA) of 1990. Coal-fired power plants are the largest industrial source of airborne mercury accounting for about one-third of U.S. anthropogenic emissions.

Recent legislative proposals for multi-pollutant controls including mercury also have been put forth in the U.S. Congress. Most policy proposals would establish national emission caps and allow emissions trading to minimize overall cost. Recent Congressional bills would require mercury reductions to a level of 90% below the 1997 level. While none of these multi-pollutant proposals have yet gained widespread Congressional support, they are nonetheless suggestive of the kinds of requirements that could be imposed on coal-fired power plants in the future.

10.2. Emission Control Options

In general, the methods available to reduce or eliminate power plant emissions of mercury include: (1) switching to a cleaner fuel containing less of the undesirable constituent; (2) installing control technology to reduce or eliminate emissions; (3) improving power generation efficiency to reduce emissions per kilowatt-hour generated; (4) switching to a power generation technology with lower or no emissions; and (5) generating less electricity by reducing demand or by reducing the load factor of "dirtier" plants. The effect of these methods is summarized in Table 10-1.

Table 10-1. Power plant operations affecting mercury emissions

Power Plant Config and Operations Strategy	**Effect on Mercury Emissions**	
	Oxidized Mercury	**Elemental Mercury**
Conv. Coal Cleaning	Decrease (highly coal specific)	
Electrostatic Precipitator	Some decrease	Some decrease
Fabric Filter	Some decrease	Greater decrease
Wet SO_2 Scrubber	Decrease	No Effect
Spray Dryer/Fabric Filter	Some decrease	Limited decrease
Carbon Adsorption System	Decrease (based on pilot-scale studies)	

The choice of a control strategy is typically dominated by the cost of alternative options. For existing coal-fired plants, coal switching and/or the installation of control technology historically have been the preferred approaches to environmental compliance for criteria air pollutants (SO_2, NO_x and particulates). For most existing plants, the most promising emission control option for reducing mercury emissions is activated carbon injection (ACI). This involves the injection of powdered activated carbon into the flue gas upstream of the particulate control device. Activated carbon is a specialized form of carbon produced by pyrolyzing coal or various hard, vegetative materials (e.g., wood) to remove volatile material. The technology has been proven in municipal waste combustors but has not been directly scaled to utility flue gas applications. Mercury is adsorbed onto the sorbent and is then removed along with the fly ash in the fabric filter or electrostatic precipitator (ESP).

Moderate removal of mercury is accomplished by ash alone. Circulating the ash in a fluidized bed has been shown to enhance the removal of mercury, particularly with the addition of activated carbon to the circulating fluidized bed[1, 2]. An additional benefit of circulating fluidized beds is the ability to add other sorbents to reduce acid gases[3].

Once fuel is combusted, mercury can be identified in primarily two chemical states: elemental (Hg^0) and oxidized (Hg^{+2}). The ability of environmental control systems to capture the mercury is dependent on the forms of mercury in the flue gas. The data collected by EPA's ICR shows that wet scrubbers effectively remove oxidized mercury from the flue gas but are ineffective at removing elemental mercury. Efforts to convert the elemental mercury to an oxidized state using catalysts, such as those used in an SCR to reduce NO_x emissions, have resulted in higher capture rates of mercury in scrubbers[4].

10.3. Mercury Emission Controls

Mercury control technologies, such as sorbent injection, have not yet been installed commercially at coal-fired power plants. However, data from smaller-scale tests indicate that mercury capture efficiency may be strongly affected by temperature, coal properties, and interactions with other environmental control systems. In the sorbent injection process, fine solids such as activated carbon are injected into the flue gas to adsorb or interact with gaseous mercury species. The adsorbed solids are then collected in a downstream particulate collector such as an electrostatic precipitator or fabric filter.

For existing coal-fired plants with only a particulate collector such as an ESP (the predominant plant configuration), mercury control is nominally achieved by injecting activated carbon upstream of the ESP. To achieve high levels of mercury control, substantial amounts of carbon injection are required, increasing the load on the particulate collector. Thus, a larger ESP, or a second collector (e.g., a baghouse filter), is needed to achieve allowable particulate emission levels if carbon injection is used for mercury control. The use of water injection to humidify the flue gas can reduce the activated carbon requirement and the associated load on the particulate collection device.

As indicated earlier, the presence of a wet lime or limestone FGD system also reduces emissions of air toxics including mercury. Thus, power plants already equipped with a wet FGD system can achieve mercury emission reductions at substantially lower costs.

For plants burning eastern bituminous coals, limited data from the ICR suggests that the presence of an SCR system together with a wet FGD system can eliminate altogether the need to inject activated carbon while achieving high levels of mercury control. On the other hand, for plants without a wet FGD system, the addition of SCR appears to have little or no effect on mercury capture efficiency. Additional research is clearly needed to better understand these observations.

The particle size of the activated carbon also has been shown to influence the effectiveness of the sorbent injected [5]. Reducing the particle size will potentially increase the mass transfer between the gas and the solids by increasing the interfacial area of the sorbent. However, due to limited available data on particle size effects, the IECM does not currently consider particle size.

10.4. Evaluating Feasibility and Cost

Analyses of competing options for environmental control are typically carried out using computer models to simulate or optimize the electric utility response to new requirements or policy proposals. Figure 10-1 depicts several types of modeling tools that are currently used for analysis. One type of model (to be elaborated in this paper) evaluates emission control options and costs at the level of a single plant or facility. This type of model is able to incorporate a fairly high level of technological detail and site-specific factors, while offering fast turnaround time and minimum data requirements. The plant-level model typically draws upon results of more detailed process-level models and data for individual plant components.

Figure 10-1. A hierarchy of models for policy analysis

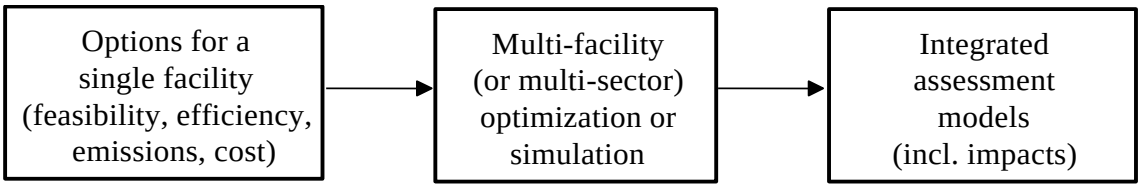

Other models are designed to analyze multiple facilities and multiple time periods. These models are more complex and data intensive. Typically, they treat power plants as aggregates of representative facilities of a given type or class. While these models have less technological detail, they incorporate a wider variety of interactions such as inter-fuel substitutions, energy demand forecasts, electric power dispatching, and macroeconomic impacts. The National Energy Modeling System (NEMS) used by the U.S. Department of Energy (DOE) for its Annual Energy Outlook[6] is an example of this class of model.

Another class of models depicted in Figure 10-1 is integrated assessment (IA) models. These large-scale models link anthropogenic emissions to the environmental consequences and impacts of proposed policy measures. Typical applications of IA models include assessments of acid deposition, ambient ozone concentrations, and atmospheric CO_2 levels. IA models attempt to represent the complex couplings between emissions, atmospheric processes, and resulting impacts at the regional, national or global scale, for time periods ranging from decades to a century or more.

In principle, the different types of modeling and assessment tools shown in Figure 10-1 can draw upon one another to form an overall hierarchy of analytical capabilities able to address a broad spectrum of questions. In the present paper, the emphasis is on the "bottom-up" plant-level model. This perspective is needed to develop a careful understanding of plant-level factors that influence the feasibility and cost of multi-pollutant emission control strategies. It is important that large-scale "top-down" models in turn adequately represent such factors and interactions in their more aggregated representations of power plant technologies.

10.5. The IECM Modeling Framework

The Integrated Environmental Control Model (IECM) developed for the U.S. Department of Energy by Carnegie Mellon University provides plant-level performance, emissions and cost estimates for a variety of environmental control options for coal-fired power plants. The model is built in a modular fashion that allows new technologies to be easily incorporated into the overall framework. A user can then configure and evaluate a particular environmental control system design. Current environmental control options include a variety of conventional and advanced systems for controlling SO_2, NO_x, particulates and mercury emissions for both new and retrofit applications. The IECM framework now is being expanded to incorporate a broader array of power generating systems and carbon management options [7].

10.5.1 Technology Performance Models

The building blocks of the IECM are a set of performance and cost models for individual technologies that can be linked together to configure a user-specified power generating system. Figure 10-2 shows a schematic of the integrated approach, which links the various technology types together. Each technology area represents one or more individual technologies. The process performance models employ mass and energy balances to quantify all system mass flows including environmental emissions. The energy requirements of each technology also are modeled and used to calculate the net efficiency of the overall plant. Details of current models can be found in published papers and reports [8]and the software is publicly available[9]. Typically, each process performance model has approximately 10 to 20 key input parameters, depending upon the complexity and maturity of the technology.

Figure 10-2. Schematic diagram of the IECM technology types

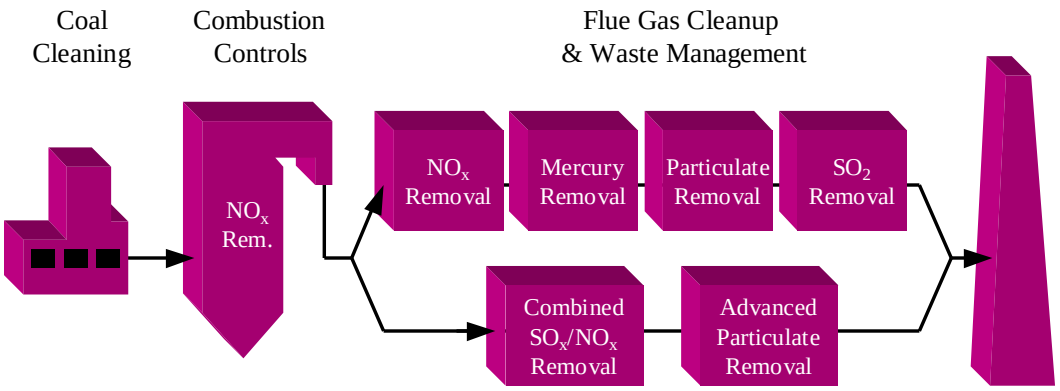

10.5.2 Technology Cost Models

For each technology module in the IECM, associated cost models are developed for total capital cost, variable operating costs, and fixed operating costs. These elements are combined to calculate a total annualized cost based on a consistent set of user-specified financial and lifetime assumptions. Normalized cost results, such as costs per kilowatt (or kilowatt-hour) of net capacity, and the cost per ton of pollutant removed or avoided, also are calculated. Cost models typically have about 20 to 30 parameters per technology, including all indirect cost factors and unit costs.

An important feature of the cost models is that they are explicitly coupled to the process performance models. Thus, capital costs depend on key flowsheet variables such as mass or volumetric flow rates, and important thermodynamic variables such as temperature or pressure. Annual operating and maintenance (O&M) costs also are linked to mass and energy flows derived from the process performance model.

10.5.3 Characterization of Uncertainties

An important feature of the IECM is the capability to rigorously characterize and analyze uncertainties. In addition to conventional deterministic (single-valued) calculations, the IECM allows any or all model input parameters and output results to be quantified probabilistically. This allows the interactive effects of uncertainties in many different parameters to be considered simultaneously.

Stochastic analysis thus provides quantitative insights about the likelihood of various outcomes, allowing users to more rigorously address questions such as:

- What is the likely cost (or cost savings) of a particular emission control strategy relative to other options? What are the potential risks such as shortfalls in performance or overruns in cost?
- Which control methods and technologies are most suitable for a given plant? Are there particular markets or applications that are likely to be most attractive for a given approach?
- Which parameters contribute most to overall uncertainty in performance and cost? What are the potential payoffs from targeted research and development to reduce key uncertainties?

10.5.4 User-Friendly Operation

The IECM was designed to provide sophisticated modeling capabilities with quick turn-around time (seconds per run), transparency, and ease of use. A user-friendly graphical interface provides the capability to configure an analysis, set key parameter values (and their uncertainties), and get results in either probabilistic or deterministic form. A variety of graphical, pictorial, and tabular reports are available via the interface. Figure 10-3 shows several screen shots from the IECM's current graphical user interface.

10.6. Mercury Control Module

Activated carbon injection with the option of water spray injection is the first mercury capture module in the IECM. Version 3.4 of the IECM software was released in May 2001 with the addition of this new module. This technology enhances baseline mercury removal with additional removal to allow flue gas treatment to meet a user-specified emission constraint or percent reduction requirement.

Figure 10-3. Sample screens from the IECM graphical user interface

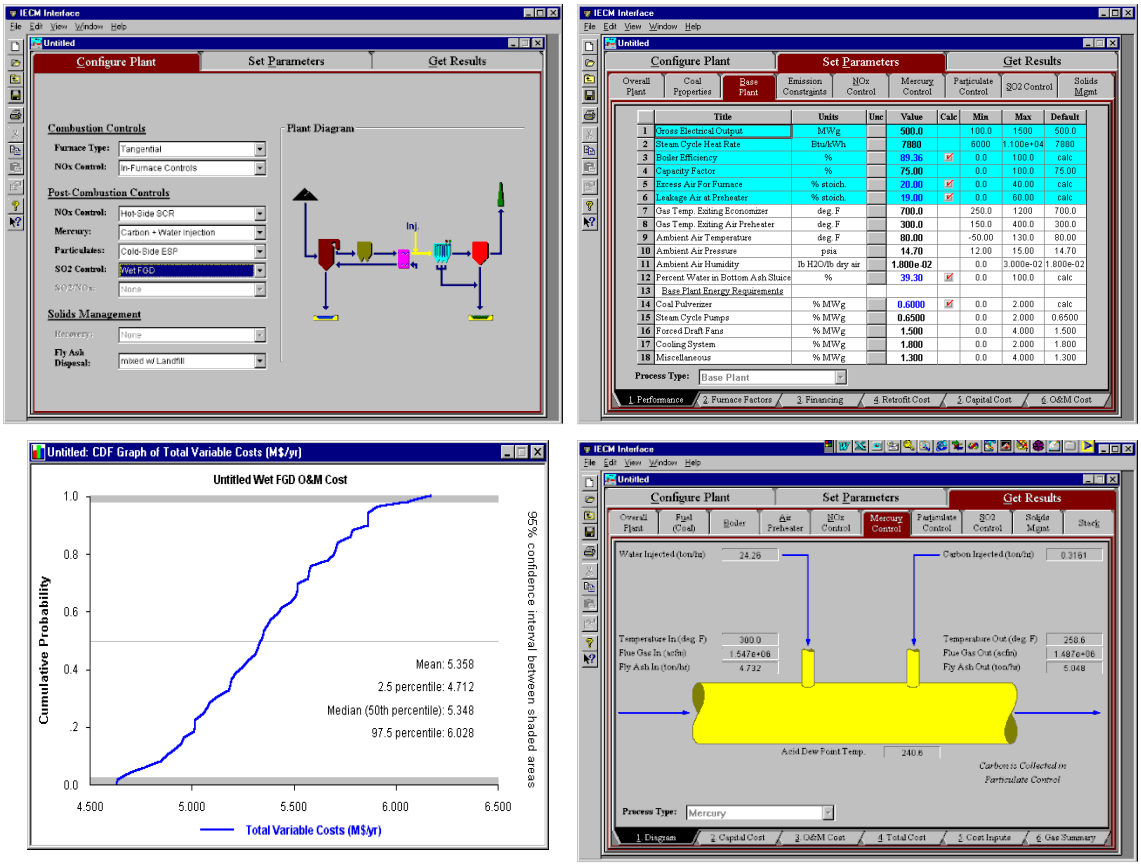

The adsorption of mercury onto the activated carbon sorbent is a physical rather than a chemical process, whose effect increases as the temperature decreases. Spray cooling of the flue gas is an effective method for reducing the temperature of the flue gas stream. In most cases this reduces the amount of sorbent required for mercury capture and therefore the cost of mercury control. Understanding the potential effects of retrofitted controls that affect the baseline removal may further reduce the required sorbent and the total cost of pollution control.

The combination of base level controls and enhanced controls provide a useful approach for evaluating the relative merits of retrofitting a power plant to meet specific emission constraints, while minimizing the overall cost of abatement. As will be shown in the illustrative examples in the next several sections, the uncertainty features of the IECM add a unique dimension to the analysis of mercury control not provided by other models.

10.6.1 Performance Model

The IECM incorporates a dual approach to the removal of mercury in coal-fired power plants. The amount of mercury required for capture is determined by an emission constraint specified by the user. Because mercury is adsorbed in small amounts by bottom ash and fly ash, each abatement technology incorporates a level of mercury capture in the absence of special treatment.

To reach higher levels of mercury capture, an activated carbon injection and optional water spray injection model has been added to the IECM. This additional injection system is referred to from this point as the mercury control module. The mercury control module is assumed to build on (add to) the baseline removal rate.

10.6.2 Mercury Emission Constraint

The level of removal of any flue gas constituent is determined by an emission constraint in the IECM. Nominally, the mercury capture is specified as an overall percentage reduction or removal efficiency. The level of removal refers to the total fraction of mercury that must be removed after the economizer and prior to the stack.

The mass flow rate of mercury emitted into the flue gas is directly proportional to the concentration of mercury in the coal. However, each power plant component between the economizer and the stack contribute to the removal of mercury even without the addition of a mercury module. Each of these baseline removals must first be determined and factored together before consideration of the mercury module. The necessary amounts of activated carbon and water are then calculated so as to remove any additional mercury necessary to meet the emission constraint.

10.6.3 Baseline Mercury Removal

Baseline mercury removal is defined as total removal of mercury without the addition of a carbon injection mercury module. These baseline removals are measured across the inlet and outlet of flue gas abatement technologies designed to remove other constituents in the flue gas, as shown in Equation (11). Examples of these baseline technologies include cold-side ESP, fabric filter, wet lime/limestone FGD, spray dryer, and SCR.

Note that mercury removal efficiency (%) is based on total (oxidized plus elemental) mercury removed from the flue gas and is defined as

$$Mercury\ \ Removal\ \ Efficiency\ \ (\%) = 100 \times \frac{\left(Emission_{in} - Emission_{out}\right)}{Emission_{in}} \qquad (11)$$

Measurements of mercury concentration in coal and removal efficiency across various flue gas cleanup systems were performed at coal-fired power plants as part of the ICR program initiated by EPA. The ICR results show that the removal is dependent on multiple factors such as coal type, temperature, and flue gas control device design. The ICR results for 1999 are summarized in Table 10-2.

Table 10-2. Summary of mercury in coal-fired power plants in 1999 (ICR data[10])

Parameter	Median	Range (min – max)
Mercury content in coal		
Bituminous	0.12 ppm	0.01 – 0.45
Subbituminous	0.10 ppm	0.02 – 0.36
Lignite	0.22 ppm	0.02 – 0.42
Oxidized Mercury at Economizer		
Bituminous	70%	7 - 100
Subbituminous & Lignite	25%	3 - 88
Baseline removal in particulate collectors		
Boiler (total)	7%	0 - 10
Cold-side ESP (total)	31%	0 - 87
Spray Dryer & Fabric Filter (total)	39%	0 - 100
Mercury removed in wet FGD		
Elemental	0%	
Oxidized	100%	
Elemental Mercury Oxidized in an SCR	35%	

The “Range” column in Table 10-2 shows the high degree of uncertainty in the ICR data. This reduces the confidence in results based only on the median or nominal values typically used for analysis. Inclusion of the data ranges will be shown later to demonstrate the effect of uncertainty.

The forms of mercury present in the flue gas affect the adsorption of mercury on fly ash. Tests indicate that elemental mercury is adsorbed at a lower rate than oxidized mercury. The measurements in Table 10-2 indicate that mercury speciation can be changed by catalytic oxidation in an SCR unit, shifting the speciation from elemental to oxidized. Thus, the presence of a selective catalytic reduction system (SCR) in the IECM results in a 35% shift of the elemental mercury to oxidized mercury.

The IECM incorporates the median mercury parameters shown in Table 10-2 to report the expected total removal of mercury. Due to the effects of coal type on the oxidation state of mercury, the combination of technologies affects total mercury removal. Table 10-3 shows a summary of the total mercury removal for various combinations of coal rank and abatement technologies using the nominal values alone.

Table 10-3. Baseline mercury removal for various plant configurations

Technology	Baseline Mercury Removal (%)		
	Bituminous	Subbituminous	Lignite
ESP	31.0	31.0	31.0
SCR + ESP	31.0	31.0	31.0
ESP + FGD	79.3	48.3	48.3
SCR + ESP + FGD	96.2	54.3	54.3
SD + FF	39.0	39.0	39.0
SCR + SD + FF	39.0	39.0	39.0

10.6.4 Activated Carbon Injection Model

The relationship between the rate of AC injected for a given mercury removal efficiency is very important. The removal that is necessary to meet the constraint depends on the baseline mercury removal, the temperature of the flue gas and the type of coal fired in the boiler. The AC injection rate, flue gas temperature, and mercury removal efficiency were measured in pilot-scale tests and fitted to the form of Equation (1) with curve-fit parameters *a*, *b*, and *c*. Equation (12) can be used to calculate the AC injection rate (lb/10^6 acfm) needed to achieve a specified mercury removal efficiency (%) for the control technology of interest at a particular temperature.

$$Mercury\ Removal\ Efficiency(\%) = 100 - \frac{Baseline\ Removal\ (\%)\ \times\ a}{\left[ACInjection\left(lb/10^6\ acfm\right) + b\right]^{c}} \qquad (12)$$

For each technology for which pilot-scale test data were available, separate correlations of mercury removal efficiency and AC injection rate were determined for bituminous and subbituminous coals. These coals are predominantly used at utility boilers and, therefore, were chosen for the mercury module. Table 10-4 gives the coefficients derived from a facility burning an eastern bituminous coal.

Table 10-4. Regression coefficients used in Equation (12) for eastern bituminous coal

Parameter	225 °F	250 °F	275 °F
a	128.73	373.55	1143.2
b	1.4293	3.7206	11.485
c	1	1	1
R^2	0.99	0.85	0.89

The data and regression curves are shown together for the three temperature ranges in Figure 10-4. Carbon injection rates associated with other temperatures are interpolated from the injection rates of the adjacent temperature curves at the same removal efficiency.

The regression model depicted in Figure 10-4 has several important limitations that contribute uncertainty to any results obtained by using Equation (12):

- The lack of available full-scale data
- The lack of carbon injection rates for mercury removals in the 80-95% range (dotted region)

- Flue gas conditions (SO_3 and H_2O) to safely achieve a 225ºF temperature are very unlikely

Figure 10-4. Mercury removal across an ESP for various operating temperatures (Eastern bituminous coal; 31% baseline mercury capture)

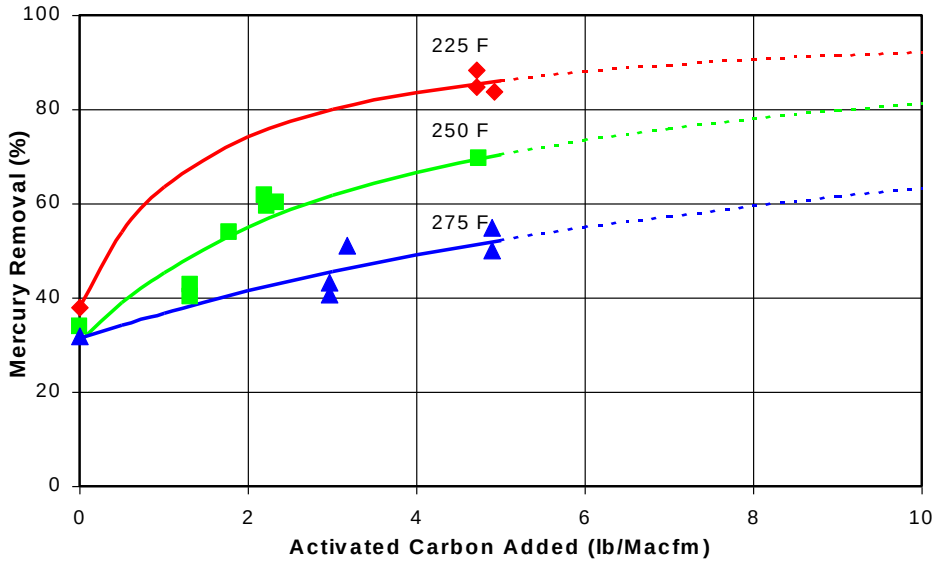

Substantial uncertainty results particularly in the mercury removal regions associated with activated carbon injection rates greater than 5 lb/Macfm.

10.6.5 Flue Gas Humidification Model

The IECM includes the option of humidifying the flue gas to lower its temperature and thus reduce the ACI requirement for a given level of mercury removal. The difference between the operating flue gas temperature and the approach to saturation temperature determines the amount of water injected into the flue gas. All calculations are based on the thermodynamic properties and state of the flue gas. If the operating temperature is above the approach temperature, the flue gas temperature is cooled to the user-specified approach above the dew point (nominally 18°F). The dew point is a function of the SO_3 and H_2O content in the flue gas and the pressure of the flue gas. Because of the effect of SO_3 concentration, high sulfur coals limit the amount of water than can be injected and subsequently require higher injection rates of activated carbon.

10.6.6 Illustrative Example

Here we define a base case power plant configuration to illustrate the effects of retrofit options added, coal switching, and the associated uncertainty in these and other default values. For the sections to follow, a coal-fired power plant burning a low sulfur eastern bituminous coal with a cold-side ESP is chosen as a base case. Table 10-5 shows the important input parameters defined in the IECM to describe this base case.

Table 10-5. Base case IECM input parameters used in the illustrative example

Coal Parameters	Value
Heating value (Btu/lb)	14,220
Sulfur content (%)	0.6
Ash content (%)	3.8
Moisture content (%)	2.2

Other Parameters	Value
Gross Plant Size (MW)	500
Steam Cycle HR (Btu/kWh)	7880
APH Exit Temperature (F)	300
Percent of SO_x as SO_3 (%)	0.8
Mercury Removal (%)	90

The effectiveness of activated carbon in mercury capture is inversely proportional to the flue gas temperature. As water is added to the flue gas, the temperature decreases. As shown in Figure 10-4, this reduces the amount of AC injected to achieve the desired mercury removal. Figure 10-5 shows the effect of water injection for the base case. The AC injection is decreased from 68 lb/Macfm to 38 lb/Macfm, a reduction of 44 percent. This substantial reduction is possible because of the low sulfur content of the coal and subsequent low concentration of SO_3 in the flue gas.

Figure 10-5. Carbon injection requirement as a function of water spray injection for the case study plant with 90% mercury removal

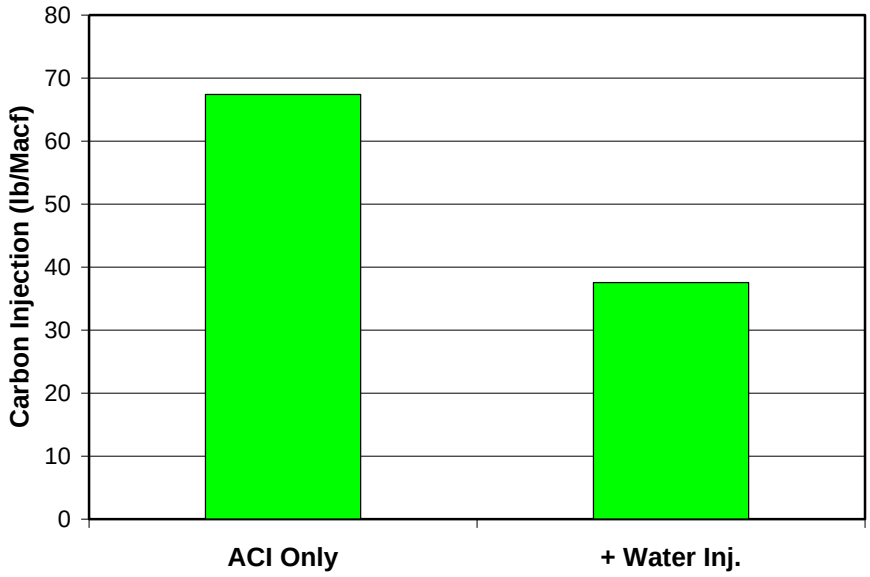

Figure 10-6 adds the effects of additional retrofit technologies. The plant configurations assume water injection to reduce the temperature within 18°F of the acid dew point. Four different coal types are compared: low sulfur bituminous coal (0.6% S), high sulfur bituminous coal (3% S), Wyoming subbituminous coal, and a North Dakota lignite.

Figure 10-6. Carbon injection requirement (with humidification) as a function of coal type and control technology for 90% mercury removal

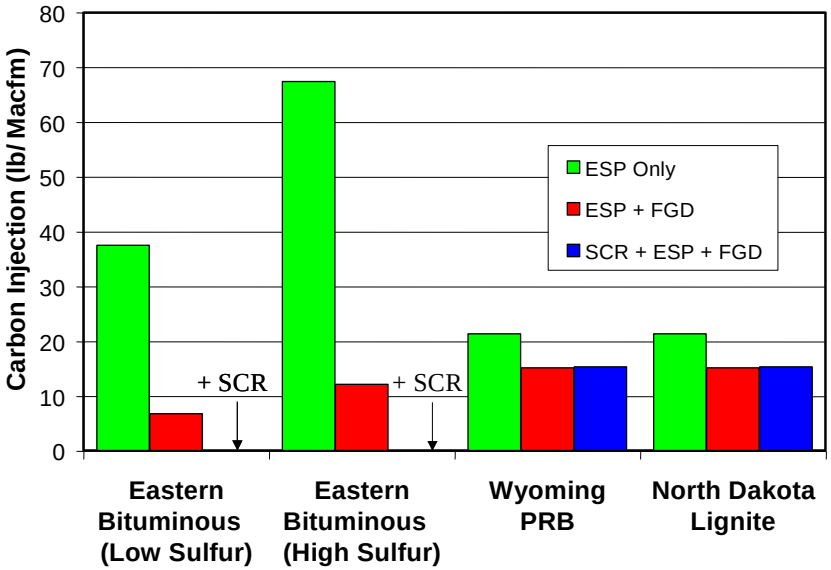

Retrofit technologies compared include a wet limestone FGD and hot-side SCR. The carbon injection flow rates calculated by the IECM are based on the default values given in Table 10-2 and Table 10-5.

The effect of adding FGD and SCR is most dramatic for plants burning bituminous coals. This is due to the high percentage of mercury in the oxidized state and the effectiveness of wet scrubbing in removing the oxidized mercury. Subbituminous and lignite coals do not exhibit the same magnitude of reduced carbon injection although the ACI requirements are much lower to begin with. The addition of an SCR unit to an ESP-FGD system in the case of bituminous coal eliminates the need for activated carbon injection entirely while reducing mercury emissions by nearly 95 percent. For the subbituminous and lignite cases, however, the addition of SCR has no discernable effect on mercury control.

The cost of retrofitting mercury controls is also affected by other multi-pollutant interactions. Consider, for example, an SCR in combination with an ESP or with an ESP plus FGD. Because an SCR converts some SO_2 to SO_3, the ash removal in the ESP is enhanced. However, the additional SO_3 also increases the minimum flue gas temperature for a water plus carbon injection system due to the increased acid dew point temperature. This results in higher activated carbon requirements with higher costs.

10.6.7 Uncertainty Considerations

The ability to characterize uncertainties explicitly is a feature unique to the IECM. Up to one hundred input parameters at a time can be assigned probability distributions. When input parameters are uncertain, an uncertainty distribution for affected results is returned, see Figure 10-7. Such distributions give the *likelihood* of a particular result, in contrast to conventional single-value estimates.

Figure 10-7. Uncertainty of activated carbon injection (base plant)

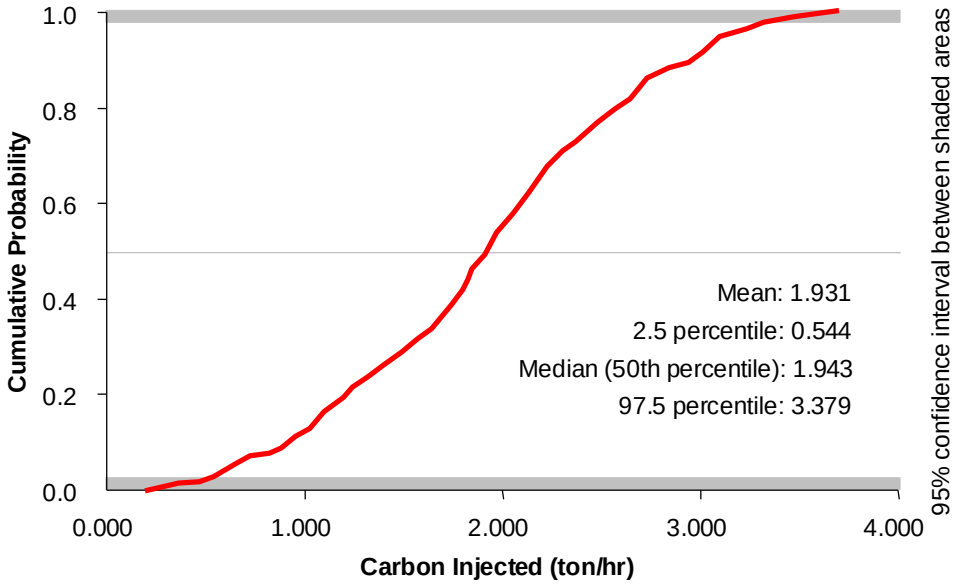

Triangular distributions were assigned to the baseline values shown in Table 10-2, with the end points spanning the ranges shown in Table 10-2. In addition, the approach to acid saturation limit was given a uniform distribution between 18°F and 30°F. The IECM randomly varies each of these uncertain input variables to generate the cumulative probability distribution shown in Figure 10-7. This figure demonstrates the uncertainty in the calculated carbon injection required to achieve 90 percent removal for the base case plant (ESP only). The 95 percent confidence interval spans a six-fold range from 0.54 to 3.38 tons/hr for this case.

As shown earlier in, no activated carbon is necessary for an SCR-ESP-FGD configuration burning bituminous coal based on the nominal values from Table 10-2 and Table 10-5. This represents the deterministic result. However, a probabilistic analysis similar to the one above shows the likelihood of no carbon injection for this case. This is exhibited in Figure 10-8. The results show a 53% chance of not needing carbon injection, but a 47% chance that it will be needed. The

uncertain results also show that the injection required has a 20% chance of being higher than 1-ton year, but will be no high than 2.5 tons per hour.

A hypothetical research program that improves the characterization of the oxidation of mercury and the baseline mercury removal in an ESP can substantially reduce this uncertainty. Assume that the differences between the median and the extreme values shown in Table 10-2 are cut in half as a result of new research. This produces the hypothetical research uncertainty shown in Figure 10-8. This curve shows a 62% probability that no carbon injection will be necessary, and reduces the worst-case scenario to 1.0 ton/hr of carbon injected.

Figure 10-8. Uncertainty of activated carbon injection (base plant with retrofit SCR and FGD)

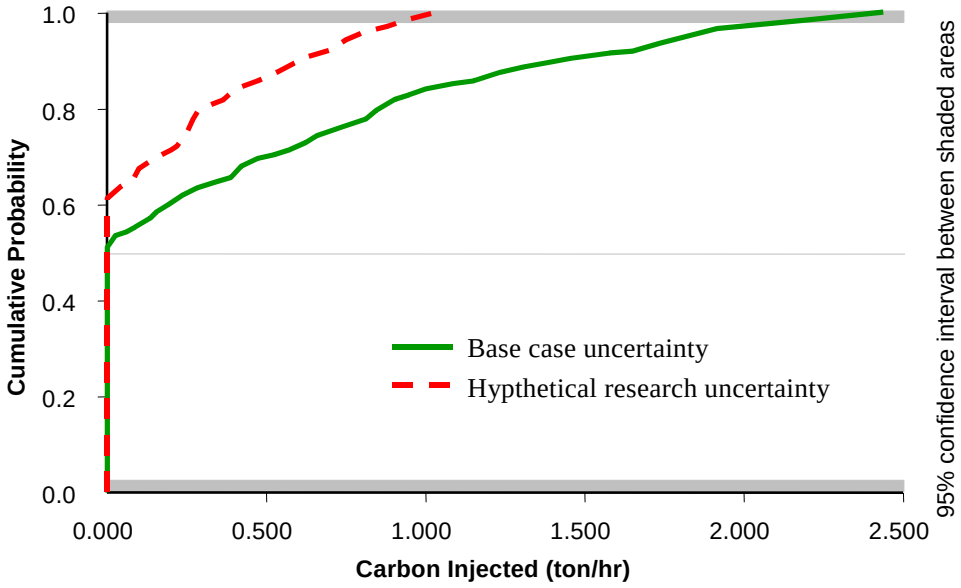

10.6.8 Economic Model

The cost of installing and operating an activated carbon injection system to remove mercury depends on a number of factors, such as power plant size, desired mercury removal efficiency, baseline removal efficiency, sorbent cost, sorbent disposal cost, and additional costs of particulate control equipment. To estimate these costs, the amount of sorbent required must first be calculated using the mercury performance module described previously. Most utilities use an ESP for particulate control. The presence of the ACI sorbent in the collected fly ash is assumed not to change the plant's method of disposing the fly ash. The methodology to estimate the cost of this treatment involves the determination of the quantity of sorbent required to achieve a desired mercury removal efficiency and then an estimation of the appropriate size of the injection equipment.

10.6.9 Capital Cost Model

The IECM mercury control costs are based on a recent joint study performed by EPA, DOE/NETL, and Carnegie Mellon University[10]. The capital costs are broken down into seven separate process areas and are described in Table 10-6. The cost of each process area is a function of various stream flows and is summed to provide the total process facilities cost (PFC). Indirect cost factors using the EPRI Technical Assessment Guide (TAG)[11] are then applied to the PFC to give the total capital cost.

The total capital cost of ACI comprises only 20-25 percent of the total cost of the mercury control system. The remainder is composed of the O&M costs described next.

Table 10-6. Carbon injection system capital cost process areas

Process Area	Primary Stream Dependence
Spray Cooling Water	Water spray injection rate
Sorbent Injection	Activated carbon injection rate
Sorbent Recycle‡	Sorbent recycle rate
Additional Ductwork‡	Length of additional ducts
Sorbent Disposal	Activated carbon injection rate
CEMS Upgrade	Net plant capacity
Pulse-Jet Fabric Filter‡	Flue gas flow rate; Air-to-cloth ratio
Process Facility Cost	*(sum of all above)*

‡ These process area costs are not currently used in the IECM.

10.6.10 O&M Cost Model

Table 10-7 shows the unit costs used for the IECM mercury module. The cost of activated carbon is the most important in the overall cost of the mercury removal module. On an annualized basis, it contributes nearly 75 percent of the total cost of the mercury capture technology. It is uncertain how the cost of activated carbon will change in the future in response to new mercury control requirements.

Table 10-7. O&M unit costs for the mercury module ($1999)

Parameter	Unit Cost
Activated Carbon (w/ shipping)	$1,100 / ton
Waste Disposal Cost	$11.44 / ton
Water Cost	$0.70 / ton
Operating Labor Cost	$25.00 / hour

Finally, the cost of waste disposal could increase dramatically if mercury-laden particulates are designated as hazardous wastes. This possibility adds further uncertainty to the cost of mercury capture.

10.6.11 Total Revenue Requirement

Capital costs, direct and indirect, are combined with the O&M costs and levelized over the life of the plant to assess the total revenue required. To illustrate the magnitude of carbon injection costs, the total levelized cost of abatement is shown in Figure 10-9 for the base case plant discussed earlier.

Figure 10-9. Deterministic results for a low-sulfur bituminous coal-fired plant (base case with retrofit technologies added). All costs in constant 1999 dollars.

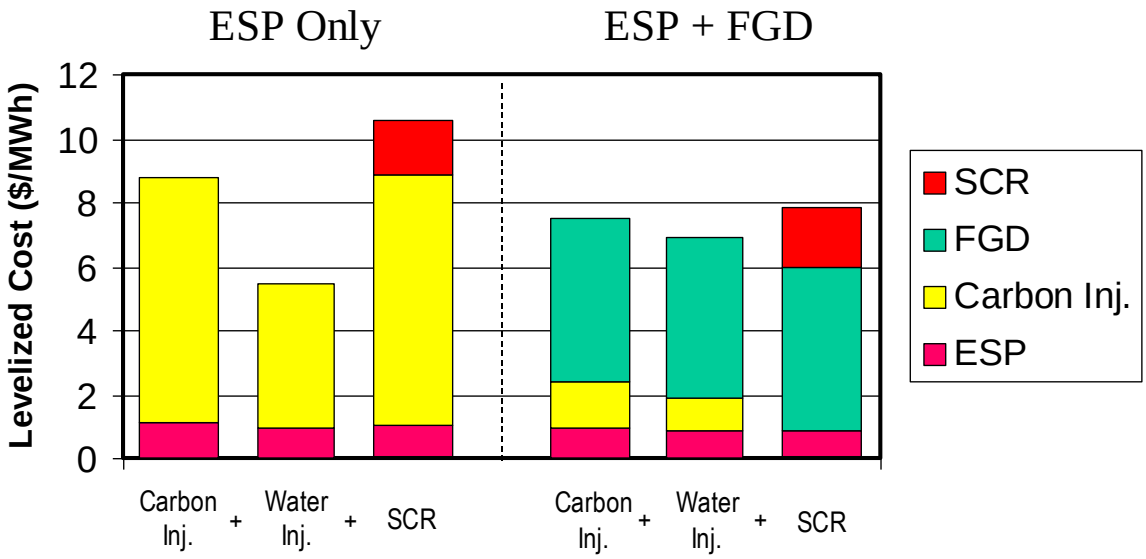

The first bar shows the cost of mercury removal by carbon injection alone. The cost savings by injecting water to cool the flue gas is shown in the second bar, reducing the ACI cost from 7.6 to 4.5 $/MWh. The cost associated with the ESP also decreased slightly due to the reduced disposal flow rate. The third bar indicates that the effect of water injection is negated by the addition of a retrofit SCR system. The oxidation of SO_2 to SO_3 by the SCR catalyst increased the acid dew point sufficiently that water injection was not possible in this case.

The second set of bars considers the case of the base plant with an FGD system. The cost of carbon injection is greatly reduced from the ESP-only example. The addition of an SCR unit eliminates the need for carbon injection (based on the deterministic assumptions). The total cost with SCR is only slightly more than that with ACI in the presence of a wet FGD system.

10.7. Conclusion

The IECM is now capable of integrating mercury control into the existing suite of models that address criteria air pollutants. As demonstrated, the model effectively captures the multi-pollutant interactions that affect plant performance and cost. Additional discussions of multi-pollutant effects are presented elsewhere.[12] The costs of adding mercury control are shown to be dependent on the plant configuration, the flue gas temperature, and the fuel type being burned.

Although the mercury control module presented in this paper is preliminary based on limited data, it represents accurately what is currently known regarding the performance and cost of mercury control systems. As additional studies are performed and results published, the uncertainties in baseline removal and carbon injection system performance and cost will be reduced. Future versions of the IECM will incorporate such results as they become available.

10.8. Acknowledgements

This research was supported by the U.S. Department of Energy's National Energy Technology Laboratory (Contract Number DE-AC21-92MC29094). The authors alone, however, are responsible for the content of this paper.

10.9. References

[1] A Novel High Efficiency Fine Particulate and Mercury Control Device. 1999, Environmental Elements Corporation: Baltimore, MD.

[2] Easom, B.H., et al., Particulate Control Technology for Power Generation. Pollution Engineering, 1999: p. 40-42.

[3] Butz, J.R., et al., Use of Sorbents for Air Toxics Control in a Pilot-Scale COHPAC Baghouse. 92nd Annual Meeting of the Air & Waste Management Association, 1999(99-130).

[4] Richardson, C.F., et al., Enhanced Control of Mercury by Wet FGD Systems. EPRI-DOE-EPA Combined Utility Air Pollution Control Symposium: The MEGA Symposium, 1999. **3**: p. 20-55 - 20-69.

[5] Meserole, F.B., et al., Estimating Electric Utility Mercury Control Costs Using Sorbent Injection. EPRI-DOE-EPA Combined Utility Air Pollution Control Symposium: The MEGA Symposium, 1999. **3**: p. 20-9 - 20-23.

[6] National Energy Modeling System (NEMS). 2000, U.S. Department of Energy: Washington, DC.

[7] Rubin, E.S., A.B. Rao, and M.B. Berkenpas, A Multi-Pollutant Framework for Evaluating CO2 Control Options for Fossil Fuel Power Plants, First National Conference on Carbon Sequestration, U.S. Department of Energy, Washington, DC, 2001.

[8] Rubin, E.S., et al., Integrated Environmental Control Modeling of Coal-Fired Power Systems. Journal of the Air and Waste Management Association, 1997. **47**: p. 1180-1188.

[9] NETL Integrated Environmental Control Model (IECM) version 3.4.5. 2001, Produced by Carnegie Mellon University for the U.S. Department of Energy, National Energy Technology Laboratories: Pittsburgh, PA.

[10] Srivastava, R.K., C.B. Sedman, and J.D. Kilgroe, Performance and Cost of Mercury Emission Control Technology Applications on Electric Utility Boilers. 2000, U.S. Environmental Protection Agency: Office of Research and Development: Research Triangle Park, NC. p. 123.

[11] EPRI, TAG Technical Assessment Guide, Volume 1: Electricity Supply. 1993, Electric Power Research Institute (EPRI): Palo Alto, CA.

[12] Rubin, E.S., et al., Multi-Pollutant Emission Control of Electric Power Plants, Proceedings of the EPA-DOE-EPRI Mega Symposium, August 2001.

11. Region-Specific Cost Factors

11.1. Introduction

Site-specific cost factors are added to the IECM to account for geographic variations relevant to power plant cost estimation.

11.2. Research Method

- Define a set of U.S. geographical regions for plant location (including an *Other Region* for plants outside the contiguous U.S.)
    - **U.S. Midwest Region**: Iowa (IA), Illinois (IL), Indiana (IN), Kentucky (KY), Michigan (MI), Minnesota (MN), Missouri (MO), North Dakota (ND), Nebraska (NE), Ohio (OH), South Dakota (SD), Wisconsin (WI), West Virginia (WV);
    - **U.S. Northeast Region**: Connecticut (CT), Delaware (DE), Massachusetts (MA), Maryland (MD), Maine (ME), New Jersey (NJ), New York (NY), Pennsylvania (PA), Vermont (VT);
    - **U.S. Northwest Region**: Idaho (ID), Montana (MT), Oregon (OR), Washington (WA), Wyoming (WY);
    - **U.S. Southwest Region**: Arizona (AZ), California (CA), Colorado (CO), New Mexico (NM), Nevada (NV), Utah (UT);
    - **Other**: This includes any location not explicitly listed above.

- Create a set of geographic-specific factors added to the IECM as "multipliers" that can be used to adjust the default estimates for plant capital cost as well as annual operating and maintenance (O&M) costs
    - Construction materials cost: the ratio of local construction materials cost to default construction material cost. The construction materials cost is a percent of the process facilities cost (PFC).
    - Construction labor cost: the ratio of local construction labor cost to default construction labor cost. The construction labor cost is a percent of PFC.
    - Construction labor requirement: the ratio of local labor need to default labor need.
    - Seismicity factors (for Equipment+ Material): the ratio of local seismicity to default seismicity, which is applied to the construction equipment and materials.
- Implement these factors in the Graphical User Interface (GUI) and IECM calculations.

11.3. Case Study

Here is the procedure regarding how to conduct a site-specific cost assessment in the IECM:

Step 1: Choose a plant location under *Configure Session*, as shown in Figure 11-1.

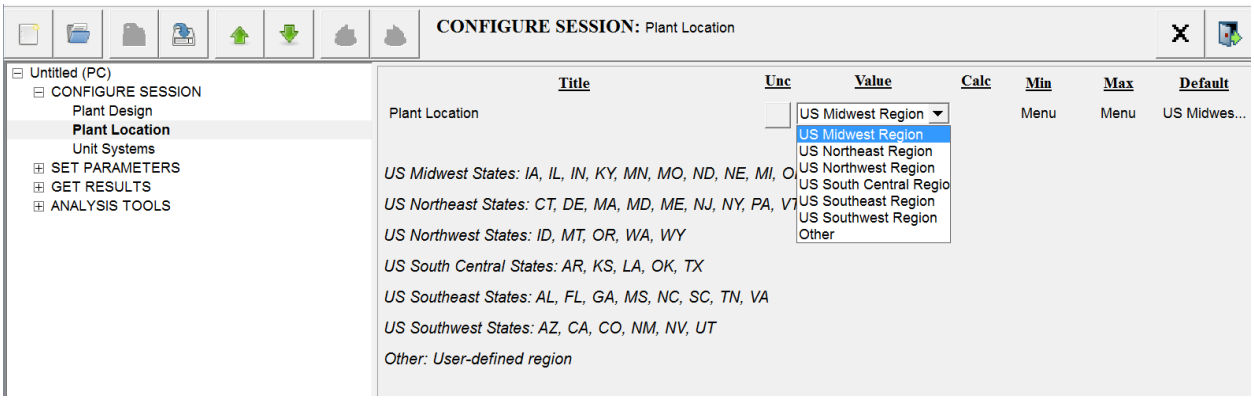

Figure 11-1. Choose a Plant Location under Configure Session

Step 2: Under *Set Parameters* for each major IECM plant component, two new parameters that allocate total Process Facilities Cost (PFC, equivalent to Bare Erected Cost) between equipment cost, materials cost, and construction labor cost, as illustrated below. The Default values of these new parameters are based on the National Energy Technology Laboratory's (NETL) Bituminous Baseline Report (NETL 2013), as shown in Figure 11-2.

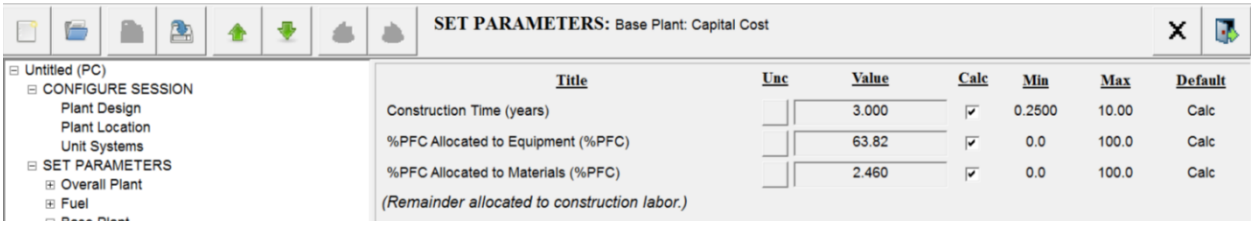

Figure 11-2. Specify Allocations of PFC to Equipment and Materials under Set Parameters

Step 3: Under *Set Parameters*, a new set of region-specific multipliers for capital cost and O&M cost factors, as shown in Figure 11-3.

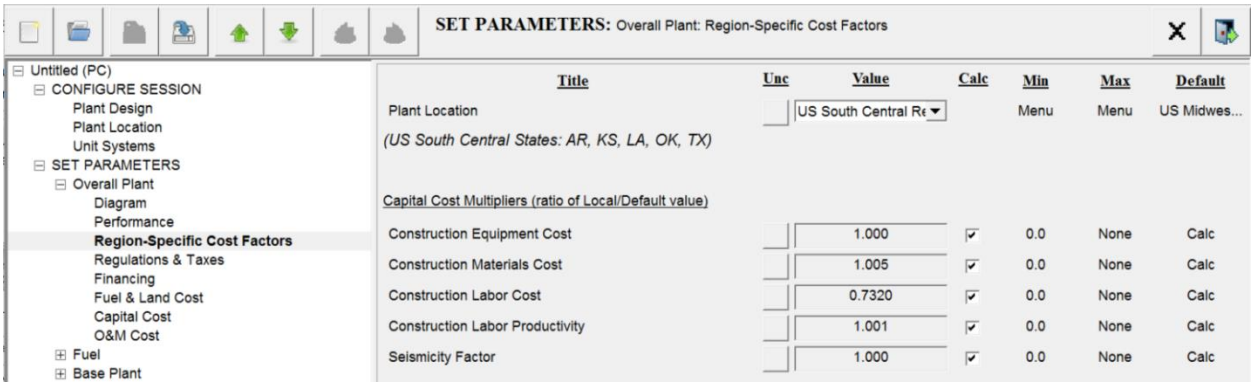

Figure 11-3. Specify Site-Specific Cost Factors under Set Parameters

Step 4: Under *Get Results*, display the *Cost Summary* screen, as shown in Figure 11-4.

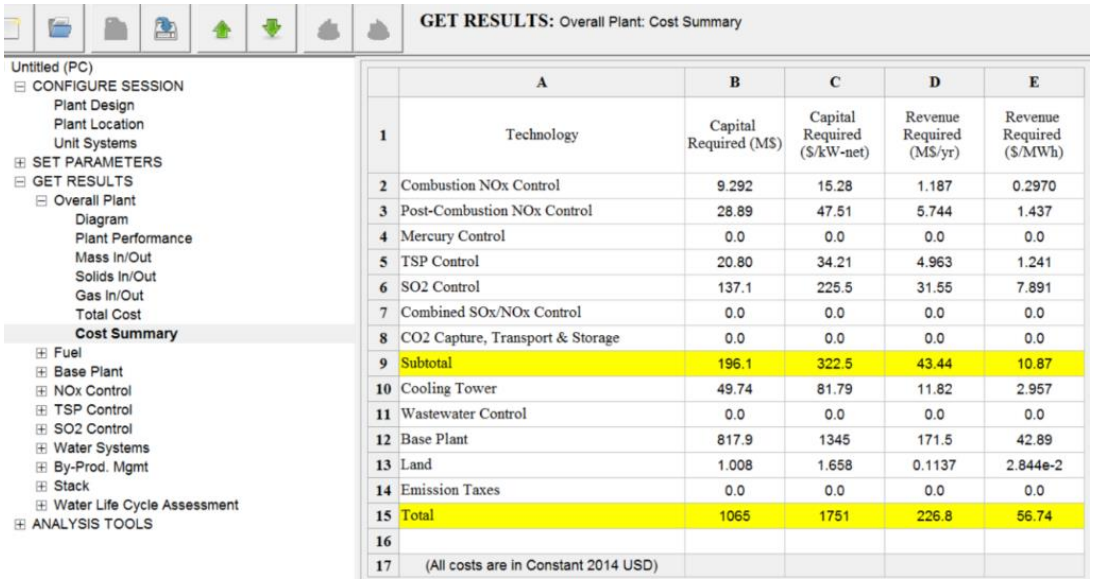

	A	B	C	D	E
1	Technology	Capital Required (M$)	Capital Required ($/kW-net)	Revenue Required (M$/yr)	Revenue Required ($/MWh)
2	Combustion NOx Control	9.292	15.28	1.187	0.2970
3	Post-Combustion NOx Control	28.89	47.51	5.744	1.437
4	Mercury Control	0.0	0.0	0.0	0.0
5	TSP Control	20.80	34.21	4.963	1.241
6	SO2 Control	137.1	225.5	31.55	7.891
7	Combined SOx/NOx Control	0.0	0.0	0.0	0.0
8	CO2 Capture, Transport & Storage	0.0	0.0	0.0	0.0
9	Subtotal	196.1	322.5	43.44	10.87
10	Cooling Tower	49.74	81.79	11.82	2.957
11	Wastewater Control	0.0	0.0	0.0	0.0
12	Base Plant	817.9	1345	171.5	42.89
13	Land	1.008	1.658	0.1137	2.844e-2
14	Emission Taxes	0.0	0.0	0.0	0.0
15	Total	1065	1751	226.8	56.74
16					
17	(All costs are in Constant 2014 USD)				

Figure 11-4. Display Cost Summary Under Get Results

11.4. Reference

National Energy Technology Laboratory. Cost and Performance Baseline for Fossil Energy Plants Volume 1: Bituminous Coal and Natural Gas to Electricity, Revision 2a, September 2013.

12. Appendix: Additional References

ASHRAE Handbook: 1981 Fundamentals (1981). American Society of Heating, Refrigerating and Air-Conditioning Engineers, Inc., Atlanta, GA.

Babcock, G. H. and Wilcox, S. (1978). *Steam/Its Generation and Use*. Babcock and Wilcox Company, New York, NY.

Bloyd, C. N., Molburg, J. C., Rubin, E. S. and Skea, J. F. (1984). *The State Level Advanced Utility Simulation Model Analytical Documentation*, Chapter 5: The Pollution Control Module, U.S. EPA, Research Triangle Park, NC.

Incropera, F. P. and Witt, D. P. D. (1981). *Fundamentals of Heat Transfer*. John Wiley & Sons, New York, NY.

Gibbs, C. W., Eds. (1971). *New Compressed Air and Gas Data*. Ingersol-Rand Co., Phillipsburg.

Molburg, J. C. and Rubin, E.S. (1983). 'Air Pollution Control Costs for Coal-to-Electricity Systems,' *Journal of the Air Pollution Control Association* , **33**.

Singer, J. G. Eds. (1981). *Combustion: Fossil Power Systems*. Combustion Engineering Inc., Windsor, CT.

U.S. Environmental Protection Agency (1982). *Compilation of Air Pollutant Emission Factors*, Third Edition. Research Triangle Park, NC.

13. Glossary of Terms

CAAA – Clean Air Act Amendments

EPA – United States Environmental Protection Agency

ESP – Electrostatic Precipitators

FGD – Flue Gas Desulfurization

ICAC – Institute of Clean Air Companies

LNB – Low-NOx Burners

LNCFS – Low-NOx Concentric Firing Systems

LOI – Loss On Ignition

NESCAUM – Northeast States Coordinated Air Use Management

NSR – Normalized Stoichiometric Ratio

OFA – Overfire Air

OTAG – Ozone Transport Air Group

SCR – Selective Catalytic Reduction

SNCR – Selective Non-Catalytic Reduction

UARG – Utilities Air Regulatory Group